Modulation of the Gut-Liver Axis in Cirrhosis with Activated Carbon

Jane Macnaughtan

PhD Thesis

University College London

Supervisors

Primary Supervisor	Professor Rajiv Jalan Division of Medicine
Secondary Supervisor	Dr. Rajeshwar Mookerjee (Jan 2014- Division of Medicine Professor Alastair Forbes (June 2010-Dec 2013)
Tertiary Supervisor	Dr. Nathan Davies Division of Medicine

I, Jane Macnaughtan confirm that the work presented in this thesis is my own. Where information has been derived from other sources, I confirm that this has been indicated in the thesis.

Dedicated to my parents

Olwen and Harry Macnaughtan

Acknowledgements

To the Liver Failure Group ‘family’, who supported me with this project and who will always remain lifelong friends: Vikram Sharma, Maria Jover, Naina Shah, Rita Garcia Martinez, Abe Habesion, Helen Jones, Rohit Sawhney. To Dr. Junpei Soeda who for teaching me flow cytometry analysis. To Dr. Jude Oben for his guidance and support for the non-alcoholic fatty liver disease studies. To Professor Alastair Forbes, Dr. Nathan Davies and Dr.Raj Mookerjee for their wisdom, support and encouragement throughout the project.

My final thanks and acknowledgement is to my primary supervisor Professor Rajiv Jalan. I wish to thank him for teaching me by example what it means to be a true philosopher of science and for fostering a spirit of intellectual curiosity. I wish to thank him for his foresight to identify this as an important research area which complements my clinical practice and for which I have developed a great passion and enthusiasm. I thank him for developing my skills as a clinician scientist to observe both at the bench and the bedside and the ability to marry these two together. Finally, I wish to thank him for teaching me that everything we do is from patients and for patients and it is to these patients that I give my final word of thanks.

“All disease begins in the gut.” **Hippocrates**

Abstract

Introduction

A substantial body of evidence now exists to implicate bacterial products such as endotoxin in the pathogenesis of cirrhosis and determinants of outcome, most markedly in advanced disease. Strategies to modulate this process clinically are currently limited to antibiotics with the attendant risk of superinfection and resistance. Yaq-001, a new, synthetic non-absorbable carbon, has been shown to exhibit a high adsorptive capacity for bacterial toxins and thus represent a novel strategy to modulate the gut-liver axis.

Methods

Neutrophil function, cytokine profile and endotoxin concentrations were determined in the splanchnic circulation of cirrhotic patients. Gut barrier integrity, innate immune function and microbiome analysis was performed in bile duct ligated (BDL) rats treated with or without oral Yaq-001. Ob/ob and MCD mice were treated with or without Yaq-001. Effects on liver injury, immune function and metabolomic profile were determined.

Results

Portal compartmentalisation of neutrophil dysfunction and endotoxaemia was observed and associated with an anti-inflammatory cytokine profile. In vitro Yaq-001 exhibited a high adsorptive capacity for endotoxin and acetaldehyde without any effect on bacterial growth kinetics. Yaq-001 administration in BDL rats significantly improved organ injury, portal pressure and innate immune profile along the gut-liver

axis. In vivo and in vitro endotoxin sensitivity was improved. Oral Yaq-001 was found to significantly improve liver injury, Kupffer cell function and metabolomic profile in NASH models.

Conclusions

Defects at the gut barrier interface play a key role in driving bacterial translocation rates with preserved integrity of hepatic immune surveillance despite advanced disease. Oral administration of Yaq-001 in models of cirrhosis and NASH is safe and associated with a significant improvement in organ injury, portal pressure, innate immune function and endotoxin sensitivity. These studies suggest Yaq-001 represents a promising new strategy for the management of liver disease.

Contents

List of Figures

Chapter 8 Biological Effects of Oral Administration of Yaq-001 Carbon Therapy in Bile Duct Ligated Rats

List of Tables

List of Abbreviations

Abbreviation	Definition
A	Arterial
ACE	Angiotensin Converting Enzyme
ACLF	Acute-on-Chronic Liver Failure
AJ	Adherens junction
ALD	Alcoholic Liver Disease
ALP	Alkaline Phosphatase
ALT	Alanine Transaminase
AST	Aspartate Aminotransferase
ATP	Adenosine Triphosphate
B/E	Bifidobacteria/Enterobacteriaceae
BDL	Bile Dict Ligation
BMI	Body Mass Index
BPI	Bactericidal permeability increasing protein
CARS	Compensatory anti-inflammatory response syndrome
CBA	Cytometric Bead Array
CCL4	Carbon Tetrachloride
cDNA	Complementary DNA
CDR	Cirrhosis Dysbiosis Ratio
DAPI	4',6-Diamidino-2-Phenylindole, Dihydrochloride
DIH	2-diphenylacetyl-1,3-indandione-1-hydrazone
DMA	Dimethylarginine
DMEM	Dulbecco's modified Eagle's medium
DNA	Deoxyribonucleic acid
ECL	Electrochemiluminescence
EDTA	Ethylenediaminetetraacetic acid
ELISA	Enzyme-linked immunosorbent assay
EM	Electron Microscopy
ESI-MS	Electrospray Ionisation Mass Spectrometry
FACS	Fluorescence-activated cell sorting
FE	Fractional Extraction
FITC	Fluorescein isothiocyanate
fMLP	N-Formylmethionyl-leucyl-phenylalanine
FXR	Farnesoid X receptor
GABA	Gamma-Aminobutyric acid
GFR	Glomerular Filtration Rate
H&E	Haematoxylin and Eosin
HBSS	Hanks' Balanced Salt Solution
HE	Hepatic Encephalopathy
HLA-DR	Human Leukocyte Antigen - antigen D Related
HPLC	High Performance Liquid Chromatography
HVP	Hepatic venous plasma

HVPG	Hepatic Venous Pressure Gradient
IFN	Interferon
IL	Interleukin
IMV	Inferior Mesenteric Vein
iNOS	inducible Nitric Oxide Sythetase
KC	Kupffer cell
LAL	Limulus amebocyte lysate
LBP	Lipopolysaccharide binding protein
LC-MS	Liquid chromatography–mass spectrometry
LGV	Left Gastric Vein
LPS	Lipolysaccharide
MARS	Mixed anti-inflammatory response syndrome
MARS	Molecular Adsorbent Recirculation System
MCD	Methionine Choline Deficient
MELD	Model for End-Stage Liver Disease
MGS	MetaGenomic Species
MLN	Mesenteric Lymph Node
NAFLD	Non-Alcoholic Fatty Liver Disease
NASH	Non-Alcoholic Steatohepatitis
NFkB	nuclear factor kappa-light-chain-enhancer of activated B cells
NLRP6	NOD-like receptor family pyrin domain containing 6
NMR	Nuclear Magnetic Resonance
NO	Nitric Oxide
NOD	Nucleotide-binding oligomerization domain
NPC	Non-Parenchymal Cell
OMD	O-Methyl-Dextrose
PAMP	Pathogen-associated molecular pattern
PBMC	peripheral blood mononuclear cell
PBS	Phosphate Buffered Saline
PBST	Phosphate Buffered Saline with Tween
PCA	Principal Component Analysis
PCR	Polymerase Chain Reaction
PE	Phycoerythrin
PMA	Phorbol myristate acetate
PP	Portal Pressure
PPI	Proton Pump Inhibitor
PV	Portal Vein
PVP	Portal Venous Plasma
RAS	Renin Angiotensin System
RNA	Ribonucleic Acid
ROS	Reactive Oxidant Species
SBP	Spontaneous Bacterial Peritonitis
SD	Standard Deviation
SEM	Standard Error of the Mean

SIF	Simulated intestinal Fluid
SIRS	Systemic Inflammatory Response Syndrome
SMV	Superior Mesenteric Vein
SNS	Sympathetic Nervous System
SV	Splenic Vein
TIPSS	Transjugular Intrahepatic PortoSystemic Stent Shunt
TLR	Toll Like Receptor
TMA	Trimethylamine
TMAO	Trimethylamine Oxidase
TNFα	Tumour Necrosis Factorα
TSB	Tryptone soya broth
TSP	Trimethylsilylpropanoic acid
ZO-1	Zonula occludens-1

Chapter 1

Introduction

1.1 Cirrhosis and Acute-on-Chronic Liver Failure

Cirrhosis is currently the 3rd most common cause of premature death in the United Kingdom with a 400% increase in mortality observed since 1970 (Williams et al, 2014). Exponential rises in incidence of cirrhosis have been observed over the last decade principally due to increasing alcohol consumption and obesity. Mortality occurs typically in the context of an acute decompensating event and may be precipitated by sepsis, alcoholic hepatitis, variceal haemorrhage or even in the absence of a clear precipitating event.

Historically the natural history of patients hospitalized with a complication of cirrhosis has been considered as a single, albeit heterogenous clinical entity following a step-wise progression from compensated to decompensated disease manifest clinically by jaundice, variceal bleeding, ascites, hepatic encephalopathy and infection. Over the last few years, large prospective clinical studies have informed understanding of this group of patients (Gustot et al, 2015; Moreau et al, 2013). This has led to the understanding that in contrast to patients with chronic end-stage liver failure, patients with an acute deterioration in liver function in the context of established cirrhosis have a distinct pathophysiology. This clinical entity is termed acute-on-chronic liver failure (ACLF) and is characterized by a dysregulated systemic inflammatory response with a significantly higher risk of multi-organ failure and mortality. ACLF is an exceptionally dynamic disease entity with variable outcomes. Resolution is seen to occur in approximately 50% of patients, a steady or fluctuating course observed in 30% with deterioration in approximately 20% of patients (Gustot et al, 2015). In

ACLF, organ function is potentially recoverable and therefore interventional strategies to impact on pathogenesis have the potential to reduce mortality.

The pathogenesis of ACLF is incompletely understood. Current data suggests that in patients with cirrhosis, there are two underlying factors that render them susceptible to the deleterious effect of a superimposed insult (Jalan et al, 2012). The first is the underlying cirrhosis and the structural disturbances, portocaval shunting, portal hypertension and metabolic disturbance this entails. ACLF may develop at any stage of disease. The second is the observation of heightened translocation of bacterial and bacterial ligands to the liver and systemic circulation which 'primes' the patient's organs and immune response to the effect of a superimposed secondary insult. The patient therefore responds abnormally to the superimposed insult and this results in multi-organ failure.

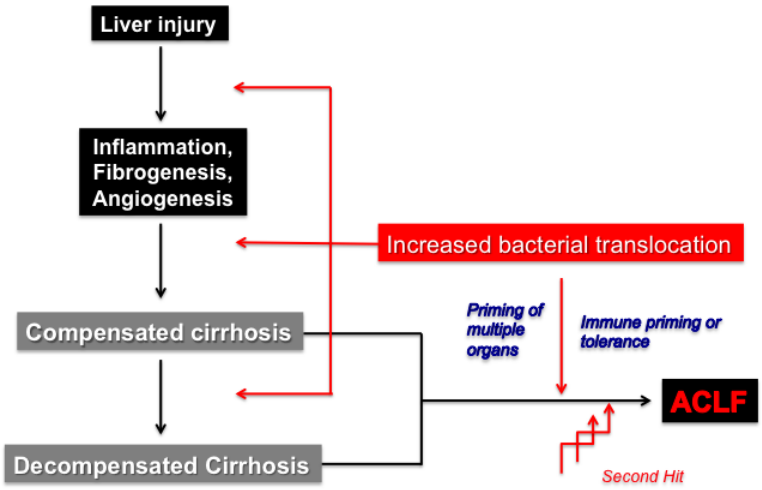

Figure 1.1 Role of bacterial translocation in the natural history of cirrhosis

1.2 Systemic Inflammation; cirrhosis and ACLF

1.2.1 Nature of immunological response in cirrhosis and ACLF

Advanced cirrhosis is characterized by a dysregulated inflammatory response, a central feature of pathogenesis resulting in a heightened propensity to organ injury with functional immunoparesis, which may be responsible for its complications (Albillos et al, 2004; Jalan et al, 2012; Wasmuth et al., 2005). Exposure to bacterial endotoxin may either induce a heightened biological sensitivity to LPS termed priming or a diminished endotoxin sensitivity termed endotoxin tolerance. Factors such as endotoxin dose, duration of exposure will influence the nature of the response. (Morris et al, 2015). There is a growing body of evidence suggestive that both states are observed in cirrhosis but in different stages of disease (Albillos et al, 2004; Wasmuth et al, 2005). The mechanisms of the increased susceptibility to infection are unclear but recent studies suggest that even in patients with compensated cirrhosis, the innate immune response is defective (Tritto et al, 2011).

Models of Immunopathology in ACLF

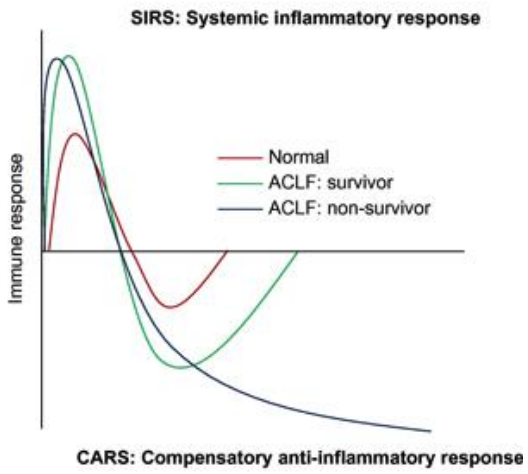

Figure 1.2 Immunopathology of ACLF (Macnaughtan J et al, 2011)

The immunological response in sepsis is multimodal, characterised by an initial pro-inflammatory process (SIRS) followed by a mixed anti-inflammatory response syndrome (MARS) followed by a compensatory anti-inflammatory response syndrome (CARS). The systemic inflammatory response syndrome includes but is not limited to, greater than one of the following clinical manifestations: (1) body temperature > 38°C or < 36°C; (2) heart rate > 90 beats per minute; (3) respiratory rate > 20 breaths per minute, or hyperventilation, as indicated by a $PaCO_2$ of less than 32 mm Hg; and (4) an alteration in leucocyte count either >12,000/ cu mm or< 4,000/cu mm, or the presence of more than 10 per cent immature neutrophils ("bands") (Bone et al, 1992).

The presence of a dysregulated systemic inflammatory response syndrome is a cardinal feature of ACLF and appears to be a key driver promoting the transition from stable cirrhosis to ACLF associated with increased mortality. The presence of SIRS is associated with more severe encephalopathy, renal failure and an increased incidence of bacterial infection (Cordoba et al, 2014; Maiwall et al, 2016; Thabut et al, 2007). SIRS is associated with a hyper-dynamic circulation with low systemic vascular resistance and a low mean arterial pressure resulting in low organ perfusion compounding organ injury. Higher leucocyte counts are associated with more severe grades of ACLF and are predictive of poor outcome (Moreauet al, 2013). Early mortality has been attributed to cytokine storm-mediated events.

Experimental strategies targeting this hyper-inflammatory phase have however been associated with variable outcomes and mortality largely occurring in septic patients who are immune suppressed such as infliximab therapy in alcoholic hepatitis. A case series of single low dose infliximab described an improvement in hepatic and renal haemodynamic status but randomized, placebo-controlled studies have failed to demonstrate an improvement in survival (Mookerjee et al. 2004; Naveau et al, 2004; Spahr et al, 2002). Naveau et al (2004) performed the largest placebo-controlled

randomized study in a cohort of 36 patients evaluating prednisolone and infliximab for the management of severe alcoholic hepatitis. A significant increase in infection and upward trend in mortality was observed in the treatment group and the trial was terminated early as a result. The study was criticized for the high dose of infliximab but highlighted the susceptibility of patients to sepsis and the risks of ablating the pro-inflammatory response. Hotchkiss et al (2009) described that most deaths secondary to sepsis occurred in the prolonged state of immune suppression as a function of immune incompetence at multiple cellular levels. Given the heightened susceptibility to infection in cirrhotic patients, the degree of immune incompetence is much greater.

Features of a compensated anti-inflammatory response syndrome (CARS) may predominate over SIRS in sub-groups of patients with ACLF in particular during later stages of the syndrome. Such patients are immune deficient and prone to nosocomial infection. Berres et al (2009) observed that a reduction in monocyte HLA-DR expression correlated with reductions in interferon gamma concentrations and ICU mortality. Xing et al (2007) observed a pre-dominantly pro-inflammatory cytokine profile in early stage ACLF with increases in IL1β, TNFα and IL-12p70. In late stage ACLF, a predominance of IL10 and reduced surface monocyte HLA-DR expression was observed. In practice, a state of immunological dissonance in ACLF is observed at the level of both cell-mediated and humoral innate immunity. TNFα and IL-6 are both known to be raised in cirrhosis yet elevated levels of IL-10, an anti-inflammatory cytokine, have also been found to be elevated and correlate with endotoxin concentrations and degree of liver failure (Qi et al 2011; Peter et al, 2013). As with sepsis, it is in the state of immune paralysis that many ACLF patients develop organ dysfunction and die.

1.2.2 Innate immunity

1.2.2.1 Neutrophil Dysfunction

Neutrophil function is known to be impaired in cirrhosis both in the context of stable disease (Tritto *et al.* 574-81) or ACLF (Fiuza et al, 2000; Mookerjee et al, 2007). Neutrophils exhibit an activated but dysfunctional phenotype with heightened spontaneous production of reactive oxidant species but diminished phagocytic function, the severity of which predicts mortality in alcoholic cirrhosis patients (Mookerjee et al., 2007). Treatment of patient plasma with endotoxin-removal columns or with anti-CD14 antibodies prevented neutrophil dysfunction, implicating endotoxin in pathogenesis.

Bacterial DNA is also known to have a marked effect on neutrophil function via TLR9 and TLR9-independent pathways (El Kebire et al, 2008). This results in a heightened neutrophil primed state for ROS production and enhanced chemokine expression. Neutrophil TLR9 expression is known to be increased in patients with alcoholic cirrhosis (Stadlbauer et al, 2009).

1.2.2.1 Monocyte/Macrophage Dysfunction

Kupffer cell (KC) and intestinal monocyte/macrophage populations play a key role in immune surveillance directing the initial immune response to gut-derived antigens towards either an appropriate antimicrobial inflammatory response or the induction of tolerance. In liver failure there is diminished reticulo-endothelial activity with reduced elimination of endotoxin (Nakao et al, 1994). This is compounded functionally by portosystemic shunting resulting in enhanced systemic endotoxin exposure and thus diminished immune surveillance. In cirrhosis, portal endotoxin levels are higher due to increased bacterial translocation resulting in priming towards a more activated state. Activated Kupffer cells produce pro-inflammatory cytokines and result in

hepatic stellate cell activation and fibrogenesis. Kupffer cells mediate liver injury by TLR4-mediated mechanisms in alcoholic and non-alcoholic fatty liver disease (Gao et al, 2011; Rivera et al, 2007). Serum and ascitic bacterial DNA positivity in patients with decompensated cirrhosis has been shown to correlate with peritoneal macrophage iNOS and NO levels and enhanced cytokine production (Frances et al, 2004).

A marked increase in the number and activation state of peripheral monocytes has been observed in cirrhotic patients. Albillos et al (2004) demonstrated an increase in the number and activation status of peripheral monocytes in ascitic alcoholic cirrhotic patients. Increased HLA-DR expression and spontaneous and LPS-induced TNFα production was observed. Treatment with norfloxacin normalised monocyte populations and activation phenotype implicating bacterial products in pathogenesis. Further evidence implicates TLR-mediated pathways in pathogenesis. Overexpression of TLR2 but not TLR4 was found on PBMCs of cirrhotic patients (Riordan et al, 2003). TLR2 expression was found to correlate with circulating levels of the pro-inflammatory cytokines TNFα and sTNFα. Despite these observations, constant stimulation of peripheral blood mononuclear cells (PBMC) with endotoxin leads to the development of endotoxin tolerance, characterized by reduced capacity to produce pro-inflammatory cytokines (Granowitz et al, 1993). Indeed a state on monocyte hypo-responsiveness has been demonstrated in more advanced disease in the context of ACLF (Wasmuth et al, 2005). This is evidenced by reduced HLA-DR expression which correlates with reduced interferon-γ and TNF-α production and diminished survival (Berres et al, 2009, Wasmuth et al, 2005).

Dendritic cells play a key role in orchestrating the innate immune response. In health intestinal conditioning of dendritic cell function shapes tolerance and immune response. Dendritic cells dictate the homing potential of recently activated T cells and promote the development of regulatory T cells in the periphery from naïve T cells

(Mann et al, 2013). They also can interact with tight junctions to modulate permeability (Rescigno M et al, 2001). The ability of mesenteric lymph node and Peyer Patch dendritic cells to imprint T cells with gut-homing potential is dependent on retinoic acid (Zeng et al, 2013). In the context of vitamin A-deficiency, the balance is shifted in favour of the generation of Th1 cell responses, an immunological profile observed in the mesenteric lymph nodes of cirrhotic rats (Munoz et al, 411-19). Vitamin A levels are closely linked to the magnitude of IgA responses in the intestine (Stephensen et al, 1996), with vitamin A deficiency leading to reduced levels of IgA and increased rates of sepsis (Wiedermann et al, 1996). Total hepatic Vitamin A and retinol stores are lower in cirrhotic patients than controls and may contribute to the immunological profiles observed in chronic liver disease (Ukleja et al, 2002). Limited clinical data exists regarding dendritic cell function in cirrhotic patients. Tanoue et al (2015) observed enhanced M2 polarisation in monocyte-derived dendritic cells but with a similar capacity for activation and antigen presentation in a small study of 15 patients. Further mechanistic studies are required.

1.2.3 Acquired immunity

Cirrhotic patients are known to have low numbers of naïve and memory T cells with an increased percentage of activated T cells. Cirrhotic patients were shown to have a higher percentage of CD4+ T lymphocytes exhibiting an activated state (as evidenced by expression of CD25 and CD122) (Marquez et al, 2009). It is thought that these activated lymphocytes traffic systemically to result in a systemic inflammatory process. The composition of T lymphocyte populations is also known to be altered in cirrhosis. Polarisation towards a Th1-predominant profile is known to occur within mesenteric lymph nodes (Munoz et al, 2005). Munoz et al (2005) demonstrated an expansion in the Th1 lymphocyte population within the mesenteric lymph nodes of rats with cirrhosis with a resultant increase in IFNγ production. The

hallmark cytokine profile and Th1 polarisation described above was abrogated by the use of norfloxacin suggesting an important role of bacterial translocation in the immune dysfunction of cirrhosis.

Cirrhotic patients also have higher proportion of memory CD4 and CD8+ T cells expressing apoptotic markers showing a commitment to activation-induced death. Most effector memory cells lack the ability to enter the lymph nodes from the blood. Instead they traffic towards inflamed tissue, a task naïve lymphocytes cannot perform. It has been suggested on the basis of these observations that a state of immune exhaustion occurs in cirrhosis which accounts in part for the functional impairment of the adaptive response.

CD4 CD25 high regulatory T cells which play a key role in dampening immunopathological responses have been the subject of much interest. Cirrhotic patients of alcoholic or viral aetiology had higher levels of regulatory T cells with an increase in lipopolysaccharide binding protein indicative of an increased antigenic load suggesting that these T cells permit endotoxaemia (Marquez et al, 2009). Data suggests that chronic antigenic stimulation may result in modulation of the adaptive immune response to induce a state of ‘permissive antigenaemia’. Marquez et al (2009) demonstrated an increase in ‘exhausted’ cytotoxic T cell populations (CD8+CD45RO+CD57+) in cirrhosis with an increase in expression of apoptotic markers (CD95). These immunosenescent cells are known to be unable to proliferate in response to a new antigenic load. Together this data suggests an exhausted adaptive immune response in cirrhosis resulting in tolerance of endotoxaemia.

1.2.4 Other factors modulating immune function

As a consequence of hepatic synthetic dysfunction, complement and C-reactive protein levels are low in cirrhotic patients which further contribute to impaired innate immunity. Secretory immunoglobulin A levels are known to be reduced together with opsonising proteins.

Vitamin D deficiency has been shown to be a common finding amongst patients with chronic liver disease affecting over half of cirrhotic patients and is a near universal finding in patients with ascites (Chinnaratha et al, 2015, Zhang et al, 2012). Low 25-hydroxylated D3 has been shown to be associated with mortality on multivariate analysis of a cohort of 251 cirrhotic patients (Finkelmeier et al, 2015). This affects macrophage function and dendritic cell differentiation and induces the expression of cathelicidin (antimicrobial peptide). Significantly higher expression of vitamin D receptor and LL-37 was observed in patient with spontaneous bacterial peritonitis compared to sterile ascites (Zhang et al, 2012). Effects on lymphocytes include modulation of the T cell receptor, a decrease in Th1/Th17CD4+T cells and cytokines (IL-1, 6, 8, TNFα), T cell homing and IgG production (Semba, 1994).

The concept of neurohumoral regulation of immune function is increasingly recognised. Autonomic dysfunction, in particular a heightened sympathetic drive, is known to be a feature of advanced cirrhosis. Early data suggests this may play an important role in pathogenesis. Non-selective beta-blockade has been shown to be associated with an improvement in survival in ACLF patients and this was associated with a reduction in white cell count (Mookerjee et al, 2016). In a rodent model of cirrhosis chemical sympathectomy prevented translocation of *E..coli* but not *S. aureus* (Worlicek et al 2010).and was associated with increased influx of peritoneal polymorphonuclear cells exhibiting increased phagocytosis. Emerging data in the renal and cardiovascular literature suggests a role for renin-angiotensin system

modulation of immune function, most typically towards a pro-inflammatory phenotype (Crowley & Rudemiller, 2017). Heightened renin-angiotensin system activation is evident in advanced cirrhosis but the mechanistic link with immune pathology is yet to be explored.

1.2.5 Role of bacterial ligands in pathogenesis (TLR pathways)

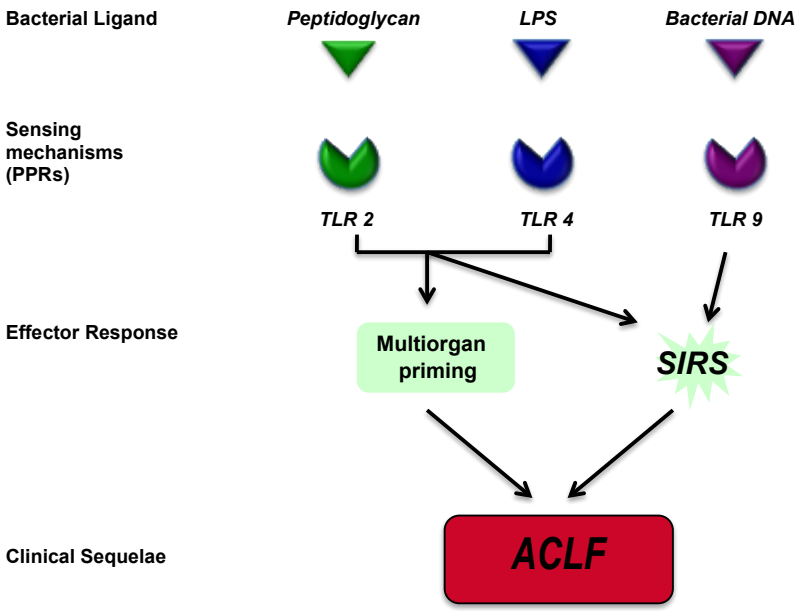

Figure 1.3 Inter-relationship of PAMP-sensing pathways in the pathogenesis of ACLF

The biological effect of bacterial translocation is determined not only by the absolute levels of bacterial product but also the magnitude of downstream sensing pathways. Toll like receptors 2,4 and 9 are responsible for sensing different bacterial ligands: peptidoglycan (TLR2), endotoxin (TLR4), bacterial CpG motifs (TLR9). All three receptors have been implicated in innate immune dysfunction in cirrhosis. Furthermore there is evidence that TLR expression may determine enhanced organ sensitivity to a second pathological 'hit' in ACLF and promote multiple organ failure. Indeed TLR4 expression is upregulated in rodent models of ACLF in which

expression was increased in the kidney, brain and liver. Norfloxacin prevented acute kidney injury in this context suggesting that modulation of gut flora can diminish 'organ priming' to a subsequent endotoxin insult sensed by TLR4 (Shah et al, 2012). In clinical studies TLR2 polymorphisms have been associated with increased susceptibility to SBP infection (Nischalke et al, 2011). Multiple cells types in the liver express TLRs; a necessary and appropriate measure given exposure to the antigenic load of portal venous blood; Hepatocytes (TLR1); Stellate cells, Kupffer cells (TLR2, 3,4); Bile duct epithelium (TLR2, 3,4,5) (Testro & Visvanathan, 2009). Not unsurprisingly, the magnitude of these pathways are critical determinants in the pathogenesis of cirrhosis, in particular with regards to production of cytokines, reactive oxidant species and consequent liver injury. TLR 4 stimulation has been shown to play an important role in fibrogenesis. This was elegantly demonstrated by attenuation of fibrosis in bile duct ligated $TLR4^{-/-}$ mice (Seki et al, 2007).

The nucleotide-binding oligomerization domain (NOD) like receptors also play a role in recognition of pathogenic bacteria and stimulation of the innate immune response. Variants of NOD2 have been also been identified as predictors of culture-positive SBP and survival in cirrhosis (Bruns et al, 2012). Other endotoxin sensing mechanisms include lipopolysaccharide-binding protein (LBP) and Bactericidal/Permeability-increasing protein (BPI) LBP is an endotoxin binding molecule produced by the liver mediating a predominantly pro-inflammatory response, levels of which have been shown to increase with more advanced disease. BPI is also an endotoxin-binding molecule but derived from the primary azurophilic granules of the neutrophil. BPI has a high binding affinity for endotoxin and mediates a pre-dominantly anti-inflammatory response (Balakrishnan et al, 2013). Therefore availability of all of these sensing molecules will determine the magnitude of

biological response to the translocated product. Further work is required to more comprehensively understand these mechanisms.

1.3 The role of alterations in the Gut Barrier interface and bacterial translocation on pathogenesis of cirrhosis and ACLF

1.3.1 Background

The symbiotic relationship that exists between the enteric microflora and human host is integral to health. The microbiome plays a key role in shaping immunological tolerance and contributing to the metabolic status of the host. In liver disease this interaction becomes pathological in nature with evidence of bacterial translocation and consequent immunopathology compounded by deleterious metabolic sequelae. Bacterial translocation is defined as the migration of bacteria or bacterial products from the intestinal lumen to mesenteric lymph nodes or other extra-intestinal organs or sites (Berg & Garlington 1979) and has been demonstrated in cirrhotic patients by a number of methods including mesenteric lymph node culture and detection of bacterial DNA products in serum and ascitic fluid (Gonzalez-Navajas et al, 2007).

The presence of viable bacteria and metabolic or structural components have been shown to be associated with hepatic fibrogenesis (Bilzer M et al 2006), and complications of cirrhosis such as spontaneous bacterial peritonitis (Riordan & Williams 2006), hepatorenal syndrome (Fernandez et al, 2007; Shah et al, 2012), variceal haemorrhage (Thalheimer et al, 2005), hepatic encephalopathy ((Bajaj et al 2012; Riordan & Williams, 2010)), hepatopulmonary syndrome (Sztrymf et al, 2005), and diminished survival (Gonzalez-Navajas et al, 2007). Endotoxaemia has also been implicated in the pathogenesis of both innate and adaptive immune dysfunction (Lin et al, 2007) resulting in a dysregulated systemic inflammatory response

syndrome so central to the pathogenesis of ACLF. Whether these changes are a cause or consequence of advancing liver disease is unclear.

In addition to the immunological sequelae of translocated bacteria and bacterial products, the resident microflora has a key role in metabolism. In fact although the composition of the gut microflora is diverse and subject-specific, its functionality is thought to be homogenous between individuals in health. The metabolic contribution of the microflora to disease pathogenesis is already recognised in chronic liver disease in particular with reference to alcoholic liver disease (Salaspuro, 1996), non-alcoholic fatty liver disease (Tilg, 2010), hepatic encephalopathy (Riordan & Williams, 2010) and portal hypertension (Chu et al, 2000). It is the combined metabolic output of the gut and microflora referred to as the metabiome which is of functional relevance. It is likely that the mucosa-associated bacterial populations have a far greater contribution in this regard than the central intraluminal compartment. Given the central role of translocated bacteria/bacterial products in the pathogenesis of cirrhosis, strategies which target this process have a potential to impact on outcome at all stages of disease.

1.3.2 Mechanisms of Bacterial Translocation

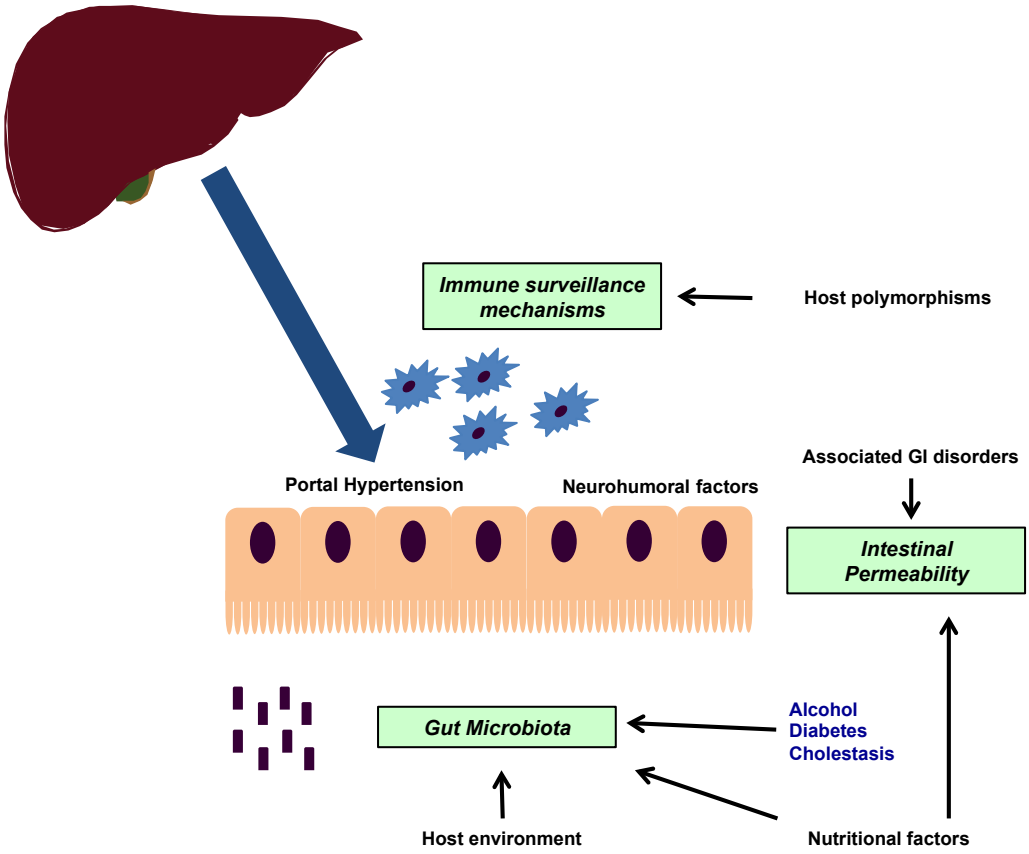

Figure 1.4 Factors determining Bacterial Translocation Rates

Bacterial translocation is defined as the migration of bacteria or bacterial products from the intestinal lumen to mesenteric lymph nodes or other extra-intestinal organs or sites (Berg & Garlington, 1979) and has been demonstrated in cirrhotic patients by a number of methods including mesenteric lymph node culture and detection of bacterial DNA products in serum and ascitic fluid which have been shown to have prognostic significance (González-Navajas et al, 2007). The three principal factors promoting bacterial translocation are intestinal bacterial overgrowth, intestinal permeability, and diminished immune surveillance. Each of these factors has been shown to be more pathologically disturbed with progressive disease.

1.3.3 Intestinal Microbiota

1.3.3.1 How does the microbiota of cirrhosis differ from that of health?

The understanding of the composition of the microbiota has been significantly advanced by the use of newer culture-independent techniques. These have been complemented by metagenomic studies to determine the microbial gene pool and therefore provide key information regarding the collective functionality of the microbiota. Whilst the microbiota plays a key role in the progression to cirrhosis, we will not consider the data for microbiota composition in the pre-cirrhotic context. The nature of the dysbioses of pre-cirrhotic liver disease is complex and typically aetiology-specific.

Dysbiosis has been described in a broad range of liver diseases and its manifestations. In general, clinical studies demonstrate a perturbation in the typical composition of enteric flora in cirrhotic patients with an increase in *enterobacter* and *enterococcus* and a reduction in *bifidobacteria* most marked with advancing disease (Zhao et al, 2004). As with pathological states such as obesity and inflammatory bowel disease, a reduction in microbial phylogenic and metagenomic diversity is observed in patients with cirrhosis compared to healthy controls.

1.3.3.1.1 Data from Phylogenic Studies

Scoring systems, which have been clinically validated to differentiate cirrhosis from health and predictive of disease stage include the cirrhosis dysbiosis ratio (CDR) (Bajaj et al, 2014a) and *Bifidobacteria/Enterobacteriaceae* (B/E) ratio (Lu et al, 2011). Both provide measures of dysbiosis and both have been validated in studies of healthy versus cirrhotic patients. The B/E ratio reflects the ability of the bowel to counteract pathogen colonization, termed colonization resistance. CDR is determined by multitagged pyrosequencing to determine microbiome composition in

cirrhotic patients. Whilst inter-individual species variation was found to be considerable, quantifying the degree of dysbiosis by determining the ratio of autochthonous to non-autochthonous taxa was found to be a consistent and reliable predictor of disease severity. CDR was highest in controls followed by compensated, decompensated cirrhosis, and in-patient cirrhotics, negatively correlating with endotoxin levels (Bajaj JS *et al.* 2014b). In longitudinal studies, CDR remained unchanged in stable outpatient cirrhotics. In contrast, patients who subsequently developed hepatic encephalopathy (HE) exhibited a dynamic change in population towards dysbiosis. Significant differences in the microbiota of cirrhotic patients who went on to develop sepsis compared with uninfected cirrhotics were observed at baseline. CDR was found to be predictive of organ failure and 30 day mortality. These data indicate a strong association between CDR and disease state but whether these are mere associations or whether they are the pathophysiologic basis of disease is unclear.

Chen *et al* (Chen et al, 2015) observed the phylogenetic profiles of the faecal microbiome in cirrhotic patients to be characterized by a relative expansion of pathogenic bacteria such as *enterobacteriaceae* and *streptococcaceae* with a reciprocal reduction in autochthonous bacteria such as *lachnospiraceae*. Similarly, Qin *et al* (Qin et al, 2014) identified an over-representation of *Veillonella* and *Streptococcus* at the expense of *bacteroidetes* and *clostridiales* populations in a cohort of cirrhotic patients. A majority of the patient-enriched species were observed to be of buccal origin suggesting that there is distal migration of pathogenic species from the oropharynx which influences the composition of the downstream bacterial populations.

Author	(n)	Changes in stool	microbiome with cirrhosis
		Increase	**Decrease**
Qin N *et al 2014*	181	*Veillonella*	*Bacteroides*
		Streptococcus	
Bajaj JS et al 2014	244	*Enterobacteriaceae*	*Ruminococcaceae*
		Enterococcaeae	*Lachnospiraceae*
		Staphylococcaeae	*Veillonellaceae*
			Clostridialies XIV
			Porphyromonadaceae
Tuomisto S *et al* 2014	49	*Enterobactericaea*	
Liu J *et al* 2012		*Enterobacteriaceae*	
		Enterococcus	
Chen Y *et al* 2011	60	*Proteobacteria*	*Bacteroides*
		Fusobacteria	*Lachnospiraceae*
		Enterobacteraceae	
		Streptococcaceae	
		Veillonella	
Wei X *et al* 2013	120	*Enterobacteriaceae*	*Bacteroides*
		Veillonella	*Clostridium*
Zhang Z *et al* 2013	77	*Streptococcus*	
		Veillonella	
Kakiyama G *et al* 2013	61	*Enterobacteriaceae*	*Ruminococcaceae*
			Lachnospiraceae
			7α-dehydroxylating bacteria
Bajaj JS *et al* 2012	60	*Enterococcus*	*Megasphaera*
		Veillonella	*Burkholderia*
Bajaj JS *et al* 2012	35	*Enterobacteriaceae*	*Ruminococcaceae*
		Alcaligeneceae	*Lachnospiraceae*
		Fusobacteriaceae	

Table 1.1 Microbiome Composition in Cirrhosis

1.3.3.1.2 Data from Metagenomic studies

Quantitative metagenomic studies by Qin *et al* (2014) revealed over 75,000 genes which differed in abundance between the intestinal microbiome of cirrhotic patients and healthy individuals. A group of 15 bacterial species were identified as potential biomarkers to define a highly accurate patient discrimination index which could be used as a biomarker for cirrhosis. This was subsequently validated in an independent cohort (Qin et al, 2014). Metagenomic species (MGS) were identified based on abundance profiles of bacterial genes associated with disease. Abundance of MGS

enriched in cirrhosis was found to positively correlate with stage of cirrhosis. Conversely an inverse correlation with cirrhosis s severity and MGS enriched in controls was observed. Thus, the pathological signature of disease in cirrhosis may be described at a bacterial genomic level both with regard to gene abundance and functional profile.

1.3.3.2 Clinical relevance of bacterial translocation in cirrhosis

1.3.3.2.1 Hepatic encephalopathy

Gut bacteria contribute to the development of HE by generation of ammonia and promotion of a pro-inflammatory response (Shawcross et al, 2004) and neutrophil dysfunction (Shawcross et al, 2010), both of which are driven by endotoxaemia (Wright et al, 2007). Culture-independent techniques are beginning to further inform understanding of the role of the microbiome in the pathogenesis of hepatic encephalopathy. Studies to date have evaluated the stool microbiome (Bajaj et al 2012a, Bajaj et al, 2014a) in addition to the mucosal adherent populations (Bajaj et al, 2012b) and salivary microbiome (Bajaj et al, 2015). Broadly, reductions in autochthonous and increases in non-autochthonous microbial populations are observed in patients with a current or past history of hepatic encephalopathy. Increases in *enterobacteriaceae* and *enterococcaceae* have been observed in both the stool and salivary microbiome. Indeed, microflora of oral origin were also identified in the stool microbiome in other studies of cirrhosis (Qin et al, 2014) as well as in a cohort of compensated cirrhotics treated with proton pump inhibitors (PPI) (Bajaj et al, 2014c). It may therefore be that disease-specific changes in luminal environment compounded by side effects of PPI therapy may serve to promote colonization of more distal gut with bacteria from the oral microbiome and predispose to an encephalopathic state.

On network analysis, improved cognition and decreased inflammation is observed with autochthonous genera in both cirrhotics with and without hepatic encephalopathy (Bajaj et al, 2012a). Indeed higher *prevotella* representation is associated with prevention of recurrence of hepatic encephalopathy. In contrast, worsening cognition was observed in patients with a higher representation of *alcaligeneceae* and *porphyromonadaceae, veillonellaceae, enterococcus, megasphaera*, and *burkholderia.*

Inflammation plays a key role in pathogenesis of hepatic encephalopathy, frequently driven by gut-derived bacterial ligands (Wright et al, 2007). In the context of hepatic encephalopathy, positive correlation with inflammatory indices was observed with *fusobacteriaceae, veillonellaceae*, *and enterobacteriaceae, enterococcus, megasphaera*, and *burkholderia* (Bajaj et al, 2012a). A negative correlation was observed with *ruminococcaceae* and the relative abundance of *lachnospiraceae* was obviously decreased in ACLF patients with hepatic encephalopathy (Chen et al, 2011). Interestingly, the stool microbiota of cirrhotic patients was more significantly correlated with systemic inflammation as compared to saliva microbiota. This may be a reflection of differential immunogenicity of bacterial ligands derived from these two sites.

Gut bacteria contribute to the development of HE by means of ammoniagenesis and generation of an endotoxin-driven inflammatory response acting synergistically (Butterworth, 2013). The important role of gut bacteria in this process is highlighted by the effects of lactulose and oral antibiotics on lowering gut-derived ammonia and encephalopathic state (table 1.2). Despite improving encephalopathic state, interventions such as rifaximin and lactulose impose only modest changes in microbiome composition (Bajaj et al, 2013a). Rifaximin is associated with a shift in bacterial metabolic phenotype towards a more physiological state (Bajaj et al, 2013a). Bajaj et al (2013) demonstrated that eight weeks of rifaximin therapy in

twenty cirrhotics with minimal HE was associated with only modest changes in microbiome composition (increase in *eubacteriaceae* and decrease in *veillonellaceae*) despite a significant improvement in cognition. This may be explained by an apparent change in linkage of networks centered on *enterobacteriaceae, porphyromonadaceae* and *bacteroidaceae* towards more physiological metabolites. Lactulose withdrawal was found to be associated with a reduction in *faecalibacterium* in two studies. Functionally, *Prevotella* was found to be associated with improved cognition and inflammatory state in patients without HE recurrence.

1.3.3.2.2 Spontaneous bacterial peritonitis

Translocation of enteric bacteria is considered to be the principal underlying mechanism responsible for spontaneous bacterial peritonitis (SBP). The three key factors responsible for promoting bacterial translocation; bacterial overgrowth, increased intestinal permeability and integrity of immune surveillance mechanisms, are important in driving SBP. Of these three factors, bacterial overgrowth is of particular importance in pathogenesis.

SBP rates have been shown to be significantly higher in ascitic patients with evidence of intestinal bacterial overgrowth than without (Morencos et al, 1995). Indeed in experimental models of cirrhosis, bacterial translocation is almost always associated with intestinal bacterial overgrowth. Intestinal bacterial overgrowth rates increase with progressive disease in cirrhosis (Gunnarsdottir et al, 2003; Morencos et al 1995). Delayed intestinal transit time is a key factor driving this process and is more prevalent in patients with a history of SBP (Chang et al 1998). Other intraluminal factors such as presence of alcohol (Bode et al 1984), bile acid profile, nutritional factors and pH will further contribute. Perhaps the most convincing evidence for the association and importance of intestinal bacterial overgrowth and

SBP is the observation that selective intestinal decontamination with non-absorbable antibiotics such as norfloxacin is associated with a significant improval in survival in this context (Fernández et al, 2007).

Factors which promote bacterial overgrowth such as proton pump inhibitor (PPI) therapy have been associated with increased risk of SBP and mortality (Deshpande A et al, 2013; Kwon et al, 2014). The most recent meta-analysis was performed in 2013 by Deshpande et al who evaluated 8 studies (3815 patients) and identified a three-fold increased risk of developing SBP with PPI. A recent prospective study have since been published suggesting no significant correlation (Terg et al, 2015). The heterogeneity in the literature may be a function of the heterogeneity of the patient group and variations in physician practice.

The emergence of multi-resistant organisms and induction of further dysbiotic states such as *Clostridium difficile* colitis is a particular concern in patients on oral antibiotic therapy with SBP. Multiple studies have highlighted the shift in microbial sensitivity patterns in SBP charting a concerning rise in resistant strains and also an increase in gram-positive infections particularly in context of patients receiving quinolone prophylaxis (Alexopoulou et al, 2013).

Finally, integrity of the innate immune response is another important factor promoting SBP. Genome wide association studies have identified polymorphisms in the Toll-like receptor (TLR) 2 and Nucleotide-Binding Oligomerization Domain Containing 2 (NOD2) as risk factors for the development of SBP (Appenrodt B et al 2010; Bruns et al, 2012; Nischalke et al, 2011). Increased intestinal permeability associated with Child Pugh status is also associated with a history of SBP (Scarpellini et al, 2010).

1.3.3.2.3 Portal hypertension and circulatory dysfunction

Splanchnic vasodilatation is a hallmark of advanced cirrhosis. Selective intestinal decontamination is associated with improvement in vascular resistance and reduction in portal pressure suggestive of interplay between these hemodynamic disturbances and the resident microflora (Albillos et al, 2003). Antibiotic prophylaxis in context of variceal bleeding has been shown to be associated with a significant reduction in early re-bleeding rates and transfusion requirements (Hou et al, 2004). Although this was not associated with a significant improvement in survival, it does highlight the important association between gut bacteria and hemodynamic status.

Splanchnic vasodilation is thought to result in part from activation of the local immune system and endothelial dysfunction. Gut bacteria with the propensity to translocate (in particular facultative anaerobes such as *enterobacteraceae*) possess diverse nitric oxide handling mechanisms, which may put them at a competitive advantage under conditions of nitrosative stress (Tiso & Schechter, 2015). Microbial nitric oxide production may further contribute to exacerbating splanchnic vasodilation. Hydrogen sulphide (H_2S) derived from gut bacteria has also been implicated in mediating splanchnic vasodilatation in cirrhosis (Iwakiri, 2007).

Bacterial translocation has also been implicated in the pathogenesis of hepatopulmonary syndrome. Treatment with norfloxacin diminishes the incidence and severity of hepatopulmonary syndrome in cirrhotic rats (Rabiller et al, 2002).

1.3.3.2.4 Acute-on-chronic liver failure (ACLF)

Chen *et al* demonstrated that gut dysbiosis has been shown to be a prognostic determinant in acute-on-chronic liver failure (ACLF) (Chen et al, 2011). Overall microbial diversity and richness were significantly lower in ACLF than in controls with lower abundance of *bacteroidaceae*, *ruminococcaceae*, and *lachnospiraceae*, and

higher abundance of *pasteurellaceae, streptococcaceae,* and *enterecoccaceae*. Interestingly, the gut microbiota was relatively stable in a short term after the onset of ACLF and use of antibiotics only showed moderate impacts on the gut microbiota. Network-analysis comparison showed robust correlations between autochthonous bacteria and inflammatory cytokines. The relative abundance of *pasteurellaceae* and MELD score were found to be independent factors predicting mortality rate. It must be noted however that viral hepatitis was the underlying cause of cirrhosis in the majority of patients in this study. Aetiology-specific factors are likely to impact on microbiome composition. Further studies are required in which other aetiologies are represented.

1.3.3.2.5 Pre-cirrhotic chronic liver disease

Multiple lines of evidence implicate gut-derived bacterial products in the promotion of fibrogenesis in the liver. Endotoxin-induced Kupffer cell activation has been identified as an important event in the induction of hepatic stellate cell activation and fibrosis in alcoholic, non-alcoholic and cholestatic liver injury. Indeed LPS/TLR4 signalling is implicated in disease pathogenesis in alcoholic liver disease, non-alcoholic fatty liver disease, primary sclerosing cholangitis, primary biliary cirrhosis, chronic hepatitis B and C (Mencin, Kluwe & Schwabe, 2009). Modulation of TGF-signalling by a TLR4-MyD88-NFKβ axis provides a novel link between pro-inflammatory and pro-fibrotic pathways (Seki et al, 2007). Mice deficient in TLR4 exhibit significantly attenuated steatohepatitis and fibrosis (Csak et al, 2011). Indeed selective intestinal decontamination with antibiotics results in prevention of hepatic fibrosis after bile-duct ligation, CCL4 treatment or a choline-deficient diet (Zhu et al, 2012). Rifaxamin treatment in bile duct ligated (BDL) mice was also associated with a reduction in portal pressure. Manipulation of the gut flora with probiotic VSL3 results in

attenuation of fibrosis in methionine choline deficient (MCD) mice (Velayudham et al, 2009).

1.3.3.3 Metabolic sequelae of dysbiosis in cirrhosis

1.3.3.3.1 Background

There is a complex, dynamic and pathological metabolic interplay between host and microbiota in cirrhosis, which is incompletely understood. Metagenomic studies suggest that multiple metabolic pathways are over-represented in the microbiome of cirrhotic patients implicating them in either a pathogenic or compensatory role.

Disordered bile salt metabolism is observed in cirrhosis, a finding which is associated with a shift in microbiota composition Ridlon et al, 2014). Cirrhotic patients with hepatitis B were found to have a metagenomic profile characterized by an enrichment in the metabolism of glutathione, gluconeogenesis, branched-chain amino acid, nitrogen, and lipids, with a decrease in the level of aromatic amino acid, bile acid and cell cycle related metabolism (Wei et al, 2013). Qin et al (2014) observed that the microbiome of cirrhotic patients had an over-representation of products of nitrate and ammonia metabolism, de-nitrification, GABA (gamma-aminobutyric acid) synthesis, phosphotransferase systems and amino acid membrane transports.

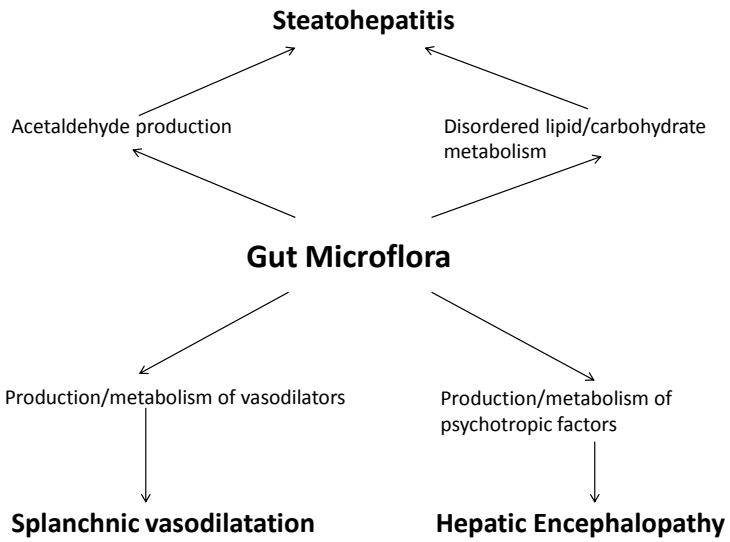

Figure 1.5 Metabolic contributions of the gut microbiome in the pathogenesis of liver disease

1.3.3.3.2 Bile acid metabolism and the microbiome in cirrhosis

Reduced colonic bile salt availability is observed in cirrhosis, with a marked effect on secondary bile salts resulting in a reduction in secondary/primary bile acid ratio (Kakiyama et al, 2013). Low intraluminal bile salt levels are a composite function of progressive cholestasis compounded by a reduction in bile acid production due to hepatic inflammation and an observed increase in expression of ileal bile salt transporters (Ridlon et al, 2013). This metabolic shift is associated with a change in microbiome composition with progressive disease associated with a lower 7α-dehydroxylating bacteria representation and a reciprocal expansion of potentially pathogenic *enterobacteriaceae* (Kakiyama et al, 2013).

Bile acids exert a bacteriostatic effect, in particular in relation to anaerobic bacteria. Administration of conjugated bile acids to cirrhotic rats is associated with a reduction in bacterial overgrowth and translocation (Lorenzo-Zúñiga et al, 2003). 7α-dehydroxylating bacteria have a selection advantage in context of intraluminal bile acids due to their metabolic pathways and bile-tolerance. Without such selection

pressures, the 7α-dehydroxylating bacterial populations collapse, associated functionally with an increase in primary/secondary bile acid ratio due to a reduction in secondary bile acid synthesis (Ridlon et al, 2013). Interestingly, this observed shift in microbiota composition in the context of cirrhosis may be protective to the host in the context of cirrhosis. A reduction in secondary bile acids, which are responsible for membrane instability, may have a beneficial effect on epithelial integrity (Stenman et al, 2013). Furthermore, primary bile acids are more potent FXR (Farnesoid X receptor) agonists with beneficial effect on portal pressure and haemodynamic status and promotion of antimicrobial peptide production (Ridlon et al, 2013).

1.3.3.4 Aetiology-specific changes in microflora

1.3.3.4.1 Alcohol

Small bowel bacterial overgrowth is well documented in patients with chronic alcohol use. Jejunal aspirate culture yielded significant bacterial counts of $>10^5$ colony forming units/ml in 48% of patients with chronic alcohol use compared with 7.6% in a control group (Bode et al, 1984). Coliform organisms were cultured more frequently in the jejunal fluid of alcoholics (55.6%) compared to control (15.4%). Morencos et al established that 30.3% of patients with alcoholic cirrhosis had evidence of bacterial overgrowth (Morencos et al, 1995). The prevalence of small bowel overgrowth increased with Child Pugh score affecting 48.3% of patients with Child Pugh C cirrhosis.

Intraluminal bacteria play an important role in bacterial translocation in chronic alcohol consumption (Ferrier et al, 2006). They are the principal source of alcohol dehydrogenase responsible for the generation of acetaldehyde from ethanol and bacterial overgrowth is a key factor in determining bacterial translocation rates. Acetaldehyde results in mucosal injury thus facilitating translocation.

1.3.3.4.2 Non-alcoholic fatty liver disease

Small intestinal bacterial overgrowth occurs in patients with NAFLD and correlates with the severity of steatosis (Miele et al, 2009; Sabate et al, 2008). Over-representation of firmicutes at the expense of bacteroides has been demonstrated both in clinical studies and in genetically obese mice (Ley et al, 2005). The increase in small intestinal bacterial overgrowth is associated with enhanced TLR-4 expression and production of IL-8 (Shanab et al, 2011). In murine models, a high fat diet has been associated with modulation of the dominant bacterial populations within the commensal bacteria and resulted in a continuous increase in plasma endotoxin (Serino et al, 2012). Endotoxin then contributes to the development of a subclinical inflammatory state and insulin resistance associated with metabolic syndrome by stimulating the release of pro-inflammatory cytokines from the adipose tissue. Endotoxin is thought to be an important co-factor in the development of steatohepatitis in the setting of established steatosis. Animal studies have demonstrated that systemic endotoxaemia results in TNFα-mediated steatohepatitis in genetically obese mice. These mice have an increase in intestinal permeability and portal endotoxaemia which renders hepatic stellate cells more susceptible to endotoxin (Yang et al, 1997). Mice deficient in TLR4 (endotoxin receptor) have significantly attenuated steatohepatitis and fibrosis when fed a methionine choline deficient diet compared to wild type MCD fed controls (Rivera et al, 2007). Recent evidence has also highlighted the importance of the inflammasomes NLRP3 and NLRP6 in negative regulation of disease progression in NAFLD in parallel to TLR-mediated mechanisms (Henao-Mejiaet al, 2012).

Gut bacteria are thought to contribute to the pathogenesis of NASH by increasing gut luminal alcohol production derived from carbohydrate metabolism and subsequently metabolising this to acetaldehyde. Nair *et al* (2001) identified an association of

obesity with high breath ethanol levels, particularly significant in patients with a BMI over 36. Genetically obese mice have also been shown to have higher breath ethanol concentrations than lean mice, an effect significantly attenuated by oral antibiotics implicating gut flora in pathogenesis (Cope, Risby & Diehl 2000). Subsequent metabolism of alcohol by gut bacteria to acetaldehyde with resultant mucosal injury is well documented.

In addition to endogenous generation of ethanol and acetaldehyde, gut bacteria further contribute to liver injury by promoting disordered carbohydrate and lipid metabolism within the gut lumen. The microflora of genetically obese leptin deficient mice have been shown to contain genes encoding enzymes to digest otherwise indigestible polysaccharides, more end products of fermentation such as acetate and butyrate and fewer calories in the faeces of microflora. Transfaunation of the faecal microflora of genetically obese mice to lean mice conferred a significant increase in body fat associated with an increase in calorific extraction from food (Turnbaugh et al, 2006). Germ-free mice have been shown to be resistant to obesity when consuming a Western-style high fat high sugar diet (Rabot et al, 2010). This occurs by two mechanisms both resulting in an increase in fatty acid metabolism. An increase in the activity of adenosine monophosphate-activated protein kinase which determines cellular energy status was observed together with an increase in Fiaf-induced PPAR co-activator expression which results in an upregulation of regulators of mitochondrial fatty acid oxidation. In addition to this action, Fiaf acting as a lipoprotein lipase inhibitor promotes fatty acid uptake.

1.3.3.4.3 Cholestatic Liver disease

Luminal bile salt availability in cholestatic disorders plays a role in bacterial translocation. Bile acids have a bacteriostatic effect, in particular in relation to

anaerobic bacteria. The increased intestinal permeability and morphological disturbance of terminal ileum observed in bile-duct ligated rats was prevented with duodenal administration of bile (Ogata et al, 2003). Supplementation of ursodeoxycholic acid has been shown to be associated with a reduction in bacterial translocation rates in rats after seven days of bile duct ligation (Aldemir et al, 2003). Further studies in bile duct ligated rats have demonstrated that endotoxin levels and rate of positive mesenteric lymph node cultures were reduced following administration of cholic acid, deoxycholic acid or whole bile (Ding et al, 1993).

1.3.4 Intestinal Permeability

1.3.4.1 Evidence for alterations in intestinal permeability in cirrhosis

Increased intestinal permeability has been well documented in chronic liver disease and shown to increase with severity of disease. Increased intestinal permeability has been described using sugar probe-based assays (Zuckerman et al, 2004) and also (51)Cr-EDTA in up to 45% cirrhotic patients compared with 4% controls (Scarpellini et al, 2010). Independent determinants of altered intestinal permeability included alcohol, diabetes, portal hypertension and age. Increased intestinal permeability was significantly associated with severity of liver disease (Child-Pugh Score A-22%, B-39%, C-75%), presence of ascites (60%) and history of spontaneous bacterial peritonitis (100%) (Cariello R *et al.* 2010). Keshavarzian *et al* (1999) demonstrated that increased intestinal permeability and endotoxaemia preceded steatohepatitis suggesting that gut-barrier injury and resultant endotoxaemia are necessary for the development of liver injury. In principle bacteria can traverse the mucosal epithelium via either paracellular or transcellular routes. Paracellular permeability is determined by alterations in the tight junction proteins and transcellular permeability by enterocyte channels and membrane pumps. It is the latter which is thought to be

primarily responsible for bacterial translocation in cirrhosis although data on the integrity of the gut barrier in cirrhosis is conflicting.

The ability of tight junctions to discriminate between and restrict solute based on size varies with location in the intestine as permeability to larger solutes decreases from the crypt to the villus. In addition to the fixed differences, mucosal permeability of many tissues is adaptable and may be regulated in response to extracellular stimuli, such as nutrients, cytokines, bacteria and nitric oxide. The tight junction is the rate limiting step in trans-epithelial transport and therefore the principle determinant of mucosal permeability. At least two routes exist which allows transport across the tight junction. One route termed the leak pathway, allows paracellular transport of large molecules including limited flux of proteins and bacterial endotoxin. The leak pathway does not exhibit charge selectivity. Flux across the leak pathway may be increased by cytokines IFNγ and TNFα. A second pathway characterised by small pores that are thought to be defined by tight junction-associated claudin proteins, which are also the primary determinants of charge selectivity. Active transcellular transport depends on the presence of intact tight junctions. Transcellular transport can activate intracellular signalling events which then regulate the tight junction barrier such as apical Na-nutrient co-transport. This allows passive paracellular absorption of nutrients and water to amplify transcellular nutrient absorption particularly when high luminal concentrations exceed the capacity of apical Na-nutrient co-transporters. The best data are from studies of the effects of alcohol, cirrhosis and role of nutrition and portal hypertension.

Structural abnormalities in intestinal mucosa have been shown to occur in cirrhosis. Bile duct ligated cirrhotic rats were shown to have increased gut permeability with loss of occludin expression and increased endotoxemia in one study whereas the

zona-occludens-1 expression was shown to be normal in another. Morphological abnormalities included a reduction in villus height, mucosal thinning, inflammatory infiltrate with oedema and focal separation and vacuolation of enterocytes (Parks et al 2000). The terminal ileum was most markedly affected. The mechanisms these abnormalities are thought to result from oxidative damage of the intestinal mucosa as evidenced by increased xanthine oxidase activity, altered antioxidant status, increased lipid peroxidation of brush border membranes and abnormal intestinal transport (Schimpl et al, 1996). Inhibition of xanthine oxidase by allopurinol resulted in a reduction in bacterial translocation in bile duct ligated rats (Schimpl et al, 1996). It is unclear however whether increased intestinal permeability is a primary mechanism of bacterial translocation or the result of endotoxin-driven inflammation and/or high NO production which secondarily compromises gut barrier function.

1.3.4.2 Alcohol

Metabolites of alcohol in particular acetaldehyde can directly influence the function of epithelial tight junction and adherens junction proteins leading to an increase in paracellular permeability. Acetaldehyde dose-dependently increases colonic paracellular permeability and has been shown to affect bioavailability of low-molecular weight hydrophilic probes in chronic alcohol fed rodent models. Acetaldehyde is known to disrupt adherens junctions (AJ) within 10 minutes of exposure as evidenced by a redistribution of E-cadherin and β-catenin from the intercellular junctions (Atkinson & Rao 2001). This then results in a redistribution of the tight junction (TJ) proteins occludin and zonula occludens-1 (ZO-1). Disruption of TJ and AJ has been observed in human colonic tissue (Basuroy et al, 2005).

Histologically, alcoholic liver disease is associated with architectural disturbance of the small intestine and abnormal activities of brush border, cellular and membrane enzymes (Bhonchal et al, 2008). These abnormalities are most pronounced within

cirrhotic patients. Acute alcohol intake is associated with increased gastro-duodenal permeability and chronic intake with increased distal small bowel permeability which occurs prior to the development of endotoxaemia and liver injury (Keshavarzian et al, 1999). Alcohol-induced nitric oxide production can influence tubulin function and cytoskeletal dysfunction (Banan et al, 2000) resulting in altered gut barrier function. Data from rodent models of ALD suggests that NO production is responsible for the development of increased intestinal permeability, oxidative stress, endotoxaemia and liver injury (Tang et al, 2009). iNOS inhibitors attenuated these features in this context. Acute administration of alcohol inhibits active intestinal absorption of L-amino acids and reduces the activity of the Na+/K+ ATPase brush border enzymes (necessary for sodium-dependent amino acid uptake) which is further decreased with more advanced liver disease (Beesley 1986). Bala et al (2014) demonstrated that acute alcohol consumption in healthy volunteers was associated with bacterial translocation as evidenced by increased serum endotoxin and bacterial DNA. These abnormalities are most pronounced in cirrhotic patients.

1.3.4.3 Nutritional factors and obesity

Intestinal permeability is increased in patients with NAFLD and its severity correlates with the severity of steatosis (Miele et al, 2009). Genetically obese obob$^{-/-}$ mice display enhanced intestinal permeability leading to increased portal endotoxaemia (Yang et al, 1997).

Glutamine is an important fuel for the enterocytes and its deficiency results in compromised gut barrier integrity due to reduced expression and localisation of tight junction proteins. Supplementation of glutamine in BDL rats at ten days does result in a reduction in BT rates and an improvement in ileal histology (Margaritis et al, 2005). Zinc deficiency is also frequently observed in patients with cirrhosis, and its

supplementation has been shown to result in preservation of intestinal integrity, prevention of endotoxaemia and resultant TNFα production (Mohammad et al, 2012).

1.3.4.4 Portal Hypertension

The interplay between portal hypertension, intestinal permeability and bacterial translocation is complex and incompletely understood. In a large cohort of cirrhotic patients the presence of portal hypertension and ascites was an independent determinant of intestinal permeability in addition to age, alcohol intake and diabetes (Cariello et al, 2010). Gastric permeability was shown to be increased in patients with portal hypertensive gastropathy (Giofre et al, 2000) and TIPS insertion and treatment with propanolol was found to improve intestinal permeability (Senzolo et al, 2009; Xu, Wu & Li, 2002). Importantly, a reduction in hepatic venous pressure gradient by non-selective beta blockers reduced the incidence of spontaneous bacterial peritonitis (Senzolo et al, 2009). It is unclear at present as to whether this is merely a function of portal pressure reduction or an effect on gut transit with associated reduction in bacterial overgrowth.

These observations suggest a causal association with portal hypertension and associated vascular congestion and increased intestinal permeability. Importantly, a reduction in portal pressure by non-selective beta-blockers reduced the incidence of spontaneous bacterial peritonitis (Senzolo et al 2009). It is unclear at present as to whether this is merely a function of portal hypertension or an effect on gut transit with associated reduction in bacterial overgrowth.

1.4 Manipulation of the microbiota as a therapeutic manoeuvre in liver disease

1.4.1 Reducing gut bacterial populations: Antibiotics

Clinically, the strategy of selective intestinal decontamination to diminish gut-derived endotoxemia has been shown to be associated with a reduction in multiple complications of cirrhosis: spontaneous bacterial peritonitis, variceal hemorrhage, hepatic encephalopathy and hepatorenal syndrome (see table 1.2). Selective intestinal decontamination with oral antibiotics remains the primary therapeutic strategy to manipulate the microbiota and thus the natural history of advanced cirrhosis. This highlights the central role of the gut microbiota in determining risk of development of complications of cirrhosis, in particular, organ failure and thus mortality.

Modulation of commensal enteric flora with norfloxacin and rifaximin have been shown to partially reverse the hyperdynamic circulatory state in cirrhotic patients (Miele et al, 2009) and improvement in systemic hemodynamics and HVPG respectively (Giofre et al, 2000), which was associated with improvement in glomerular filtration rate (GFR) and natriuresis. Furthermore, reduction in bacterial translocation with empirical broad-spectrum antibiotic therapy in the context of variceal bleeding has been shown to result in a reduction in re-bleeding and mortality rates (Bernard et al, 1999).

Translocation of enteric bacteria is considered to be the principal underlying mechanism responsible for SBP. Administration of norfloxacin as secondary prophylaxis for SBP has been shown to result in a reduction in the probability of developing SBP significantly (Gines et al 1990) and a reduction in hepatic encephalopathy (Dawson et al 1957; Morgan, Read & Speller, 1982). RIfaximin has been shown to significantly reduce recurrence of hepatic encephalopathy (Bass et al 2010).

Shah *et al* demonstrated that selective intestinal decontamination with a 10 day course of norfloxacin in BDL and LPS-treated BDL rats resulted in a significant

improvement in ALT and creatinine (2012). This improvement in organ injury was associated with a significant attenuation in neutrophil ROS production and systemic TNFα concentrations. Marked reductions in immunostaining for TLR4 and caspase3 were observed in norfloxacin-treated BDL and BDL+LPS rats compared to untreated controls (Shah et al, 2012).

Taken together, these observations demonstrate that manipulation of the microflora with quinolone therapy in a model of cirrhosis and ACLF is associated with significant improvements in organ injury and improvement in innate immune phenotype. Growing concern regarding resistance, super-infection and emergence of greater numbers of gram positive organisms limits the role of oral antibiotics.

1.4.2 Altering Bacterial composition: Probiotics

Probiotic therapy provides an attractive alternative strategy with a preferable safety profile. *In vitro* and animal studies indicate a strong role of probiotics in immunomodulation via modulating dendritic cell function and epithelial barrier function. Available clinical trials of probiotics are summarized in table1.2. The marked heterogeneity of studies particularly in regards to microbial composition and concentration of probiotic, duration of therapy, aetiology and stage of disease limits interpretation of the established literature in particularly with regards to decompensated disease. Given the important contribution of the gut microbiota in the pathogenesis of other complications of cirrhosis, probiotic therapy is likely to have a broader application in the future treatment algorithms of cirrhosis. Further trials are required to established optimal probiotic doses and compositions.

1.4.3 Other potential and emerging approaches

1.4.3.1 Beta-blockers

Use of beta-blockers in cirrhosis have been found to be protective against infection and associated with a lower morbidity and mortality. A meta-analysis by Senzolo et al (2009) described a significant protective effect of beta-blockade against SBP. It has been suggested that this effect may be mediated by modulating intestinal motility, small bowel overgrowth and therefore bacterial translocation rates. The use of these agents is controversial in patients with decompensated cirrhosis and refractory ascites (Ng et al, 2009).

1.4.3.2 Targeting toll-like receptor pathway

TLR pathways have been shown to play a key role in complications of cirrhosis (Bosoi et al, 1995; Shah et al, 2012). Inhibition of the endotoxin receptor TLR4 with antagonist STM-28 has been shown to significantly improve dendritic cell populations in models of cirrhosis (de Oca et al, 2010). Zhu *et al* (2012) demonstrated the central importance of the TLR4 pathway as a mediator of rifaximin-induced reduction in portal pressure, fibrosis, and angiogenesis in a murine model of cirrhosis. Given the central role of TLR pathways in priming organ injury in acute on chronic liver failure, TLR antagonists represent attractive future therapies to improve survival in advanced cirrhosis.

1.4.3.3 Faecal Transplantation

Faecal transplantation is an emerging therapeutic strategy to correct dysbiotic states such as *Clostridium difficile* colitis (Youngster et al, 2014). Transfaunation of stool from animal models of NAFLD and obesity to germ free animals has been shown to confer disease phenotype highlighting the potential of stool transplantation in modulating liver disease (Le Roy et al, 2013). Currently, no data are available but different approaches may be needed for different aetiologies.

Intervention	Endpoint evaluated	(n)	Outcome	Authorship
Selective Intestinal Decontamination				
Norfloxacin vs placebo	SBP recurrence	80	Superiority	Ginés P et al 1990
Norfloxacin vs placebo	SBP, HRS, mortality	68	Positive	Fernández J et al 2007
Norfloxacin vs ceftriaxone	Bacterial infection post- VB	111	Inferiority	Fernández J et al 2006
Norfloxacin vs placebo	Bacterial infection post- VB	119	Positive	Soriano G et al 1992
Norfloxacin	HVPG	16	Negative	Kemp W et al 2009
Rifaximin vs placebo	HE	299	Positive	Bass N et al 2010
Rifaximin	VB/HE/SBP/HRS/Survival	69	Positive	Vlachogiannakos J et al 2013
Rifaximin vs lactulose	Overt HE	58	Yes	Bucci L et al 1993
Rifaximin+lactulose vs lactulose	Overt HE/mortality	120	Superiority	Sharma BC et al 2013
Rifaximin vs lactitol	Acute HE (grade 1-3)	103	Superiority	Mas A et al 2003
Neomycin vs lactulose	Minimal HE	173	Equivalent	Orlandi F et al 1981
Neomycin-sorbitol vs lactulose	Acute PSE	45	Equivalent	Atterbury CE et al 1978
Probiotics				
VSL#3 vs placebo	HVPG	94	Negative	Gupta N et al 2013
Probiotics	Minimal HE	43	Negative	Saji S et al 2011
SF-68 vs lactulose	Minimal HE	40	Superiority	Loguercio C et al 1995
Probiotic	HE	155	Positive	Agrawal A et al 2012
Probiotic	Minimal HE	25	Positive	Bajaj J et al
Probiotic	Overt HE	160	Positive	Lunia MK et al 2014
Probiotic	HE	80	Positive	Mittal VV et al 2011
Probiotic vs placebo	HE	36	Negative	Pereg D et al 2011
E.coli Nissle vs placebo	CP score	39	Negative	Lata J et al 2006
Synbiotic vs FFvs placebo	HE	55	Positive	Liu Q et al 1995
Synbiotic vs placebo	Minimal HE	60	Positive	Malaguarnera M et al 2007
Lactulose				
Lactulose	Minimal HE	40	Yes	Dhiman RK et al 2000
Lactulose	Minimal HE	75	Yes	Watanabe A et al 1997
Lactulose	HE	80	Positive	Mittal VV et al 2011
Lactulose	HE	158	Positive	Agrawal A et al 2012
Lactulose vs lactose	Minimal HE	14	Yes	Horsmans Y et al 1997
Lactulose vs sorbitol	Chronic HE	7	Yes	Elkington SG et al 1969
Lactulose vs lactitol	Acute PSE	40	Equivalent	Heredia D et al 1987
Lactulose vs lactitol	Chronic HE	9	Equivalent	Morgan MY et al 1987

HE = hepatic encephalopathy; SBP = spontaneous bacterial peritonitis; HVPG = hepatic venous pressure gradient; VB = variceal bleeding; HRS = hepatorenal syndrome; CP = Child Pugh score; FOS = fructo-oligosaccharides

Table 1.2 Summary of Interventional Clinical studies to manipulate the microbiome in cirrhosis

1.5 Nanoporous carbons

Selective intestinal decontamination with oral antibiotic therapy is currently the only intervention in clinical practice with proven efficacy to modulate bacterial translocation rates in cirrhosis. Whilst associated with improvements in complications of cirrhosis such as hepatic encephalopathy, hepatorenal syndrome and spontaneous bacterial peritonitis, concerns regarding resistance and superfection limits their role. Novel oral therapeutic strategies to adsorb immunogenic and metabolic bacterial products in the gut therefore remain an unmet clinical need.

Activated carbons have a high adsorptive capacity and surface area. They have been used historically to adsorb a range of drugs and toxic compounds both orally and latterly in context of extracorporeal devices such as the Prismaflex Adsorba haemoperfusion system for severe poisoning (Juurlink et al, 2015) and as part of the MARS liver assist device (Bañares et al, 2013). Developments in synthetic carbon production have facilitated the manufacture of activated carbons of highly tailored porosity. Conventionally manufactured activated carbon is typically microporous (pore diameter <2 nm) with few pores in the mesoporous (2-50 nm) or macroporous (>50 nm) range. AST 120, currently licensed in Japan for oral administration in renal failure, is a typical example of a microporous carbon but remains limited in it's capacity to adsorb larger biologically relevant molecules (Niwa, 2016).

Yaq-001 is a highly adsorbent, pyrolysed spherical carbon synthetically derived from phenolic resin. It has a highly tailored bimodal pore size distribution extending into the larger nanoporous range to allow removal of larger biotoxins in addition to the microporous range with adsorption of smaller targets (Howell et al, 2013). The Yaq-001 carbons have a powerful, non-selective adsorptive capacity with a large surface area.

Given that Yaq-001 had the physical properties appropriate to the adsorption of bacterial toxins and metabolites, we sought to determine the effects of oral carbon therapy in models of cirrhosis, ACLF and non-alcoholic fatty liver disease.

Chapter 2

Hypothesis and Aims

2.1 Hypotheses

2.1.1 Hypothesis 1

The nature of the portal derived innate immune response in cirrhosis is pathologically disturbed and associated with heightened bacterial translocation

2.1.2 Hypothesis 2

The gut barrier interface is pathologically disturbed in bile duct ligated rats and is associated with disturbance of the gut microbiota and innate immune response

2.1.3 Hypothesis 3

Oral administration of Yaq-001 will attenuate organ injury, improve portal pressure and normalise innate immune profile in bile duct ligated rats

2.1.4 Hypothesis 4

Oral administration of Yaq-001 will attenuate organ injury and improve Kupffer cell function in models of non-alcoholic steatohepatitis

2.2 Aims

2.2.1 Characterisation of the portal-derived neutrophil and cytokine profile and association with markers of bacterial translocation

The nature of the portal-derived innate immune response remains poorly described. The aim of this study was to characterize the portal-derived neutrophil, cytokine profile together with markers of bacterial translocation. In so doing, the relative contribution of the gut and liver to the nature of the innate immune response will be described and the degree to which this is associated with markers of bacterial translocation. This data will provide a quantatitive measure of the magnitude of bacterial translocation and the integrity of endotoxin clearance mechanisms in the liver.

2.2.2 Assessment of the integrity of the gut barrier interface and correlation with clinical, immune and pathological characteristics of bile duct ligated rats

Alterations in microbiome, gut barrier integrity and innate immune function have been shown to contribute to bacterial translocation and disease progression in cirrhosis (see figure 2.1). The first aim of this study was to describe each of these three factors in context of the 4 week bile duct ligated rat model. Whilst data does exist describing each of these factors in isolation, concomitant characterization of all three factors in this model system has not been previously described and thus the relative contribution to pathogenesis is incompletely understood.

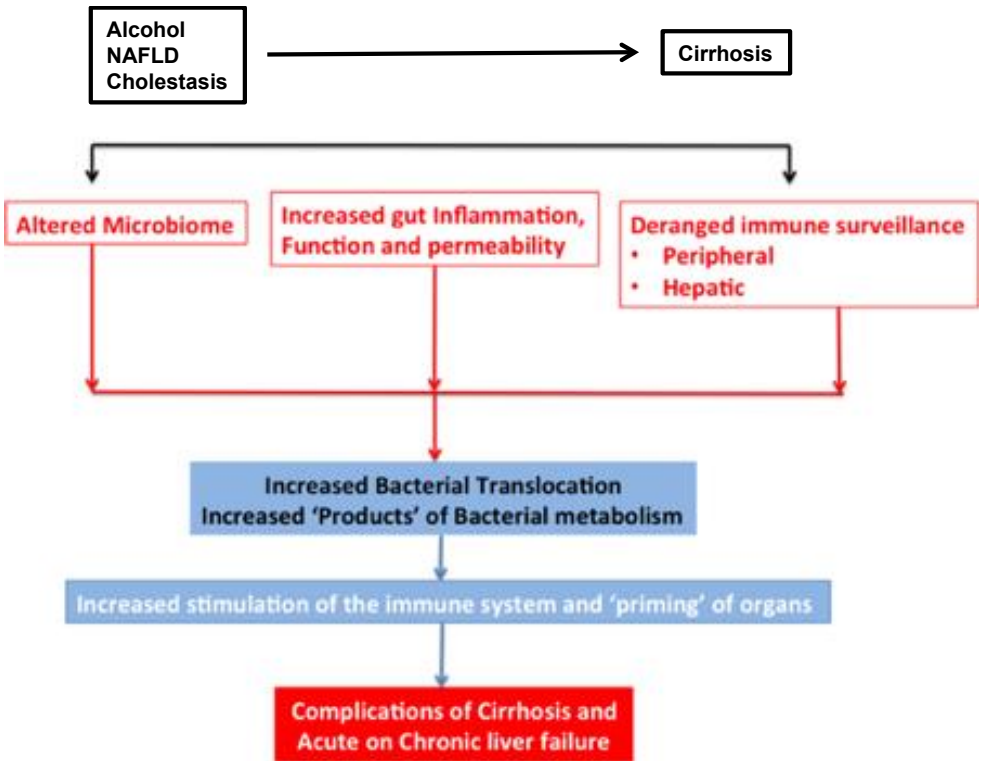

Figure 2.1 Role of bacterial translocation in disease progression in chronic liver disease

2.2.3 Characterisation of functional, immunological and microbiological changes in the gut-liver axis with oral administration of Yaq-001 in bile duct ligated rats

Bacterial products, in particular endotoxin, accelerate disease progression to cirrhosis and play a key role in pathogenesis of decompensated disease and acute-on-chronic liver failure. Yaq-001 activated carbons have been shown in *in vitro* studies to exhibit a high adsorptive capacity for biologically relevant intra-luminal factors such as endotoxin and other bacterial metabolites without exerting an effect on bacterial growth kinetics (unpublished data). The primary hypothesis of this study was that oral administration of Yaq-001 carbons would abrogate disease progression of cirrhosis clinically manifest by a significant improvement in liver biochemistry and improvements in haemodynamic status. A key objective was therefore characterisation of the effects of oral Yaq-001 carbon therapy on each of the three factors which promote bacterial translocation in a 4 week bile duct-ligated rat model of cirrhosis. As the carbons should be retained in the gut due to the bead size, they exert their effect at a local level. In order to determine how this results in a distant biological effect, elements of the gut-liver axis were described.

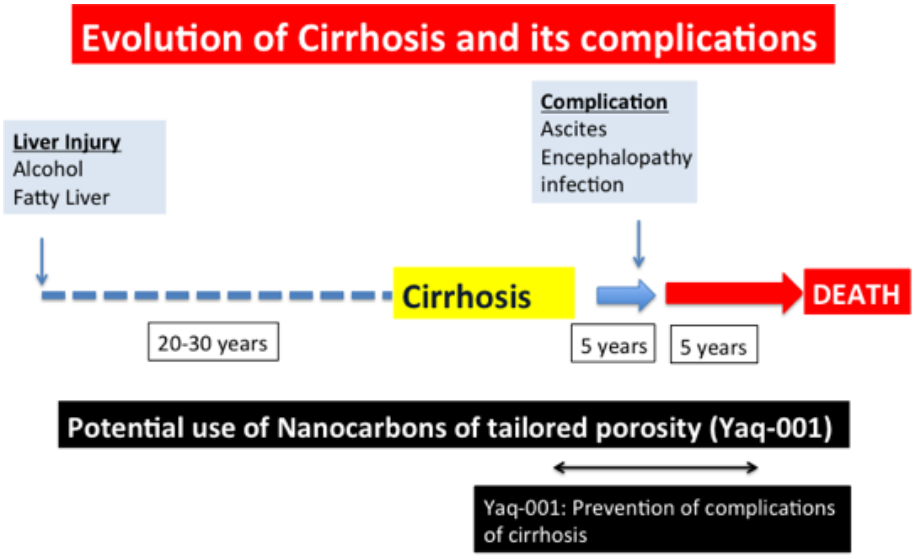

Figure 2.2 Potential role of oral Yaq-001 therapy in prevention of complications of cirrhosis

2.2.4 Characterisation of effects of oral administration Yaq-001 in models of non-alcoholic fatty liver disease

Multiple lines of evidence implicate the gut microbiota in disease pathogenesis of non-alcoholic steatohepatitis. The final aim of the study was to evaluate oral Yaq-001 in models of non-alcoholic fatty liver disease to ascertain whether a similar biological effect was observed in pre-cirrhotic liver disease. The final hypothesis was that oral administration of Yaq-001 results in significant attenuation of liver injury in models of steatohepatitis as evidenced biochemically by alanine transaminase.

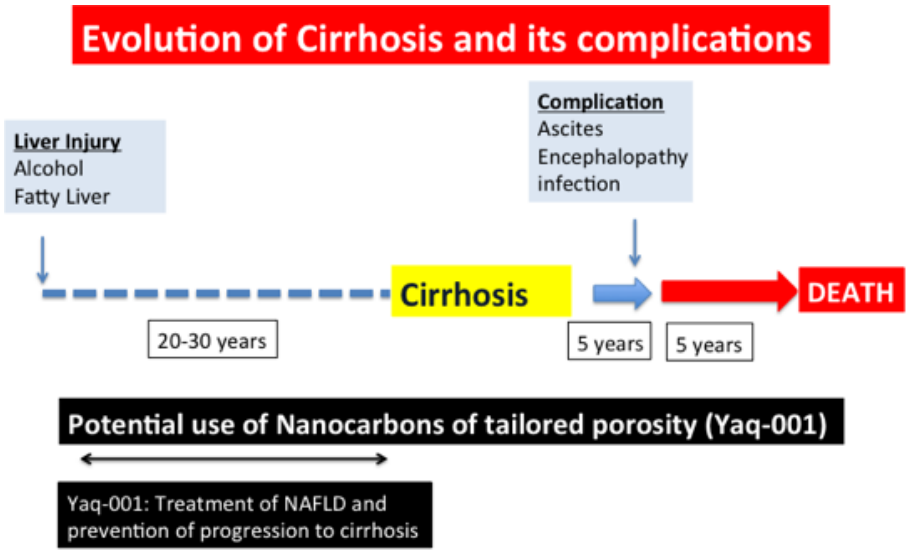

Figure 2.3 Potential role of oral Yaq-001 therapy in prevention of complications of non-alcoholic fatty liver disease

Chapter 3

Methods

3.1 Clinical study

The study was undertaken with the approval of the local research ethics committee and in accordance with the Declaration of Helsinki (1951) of the World Medical Association. The TIPSS procedure was performed by the interventional radiology teams at the University of Edinburgh and University College London and laboratory analysis performed by Dr. Ter Steege and Dr. Vanessa Stadlbauer. Statistical analysis was performed by myself.

3.1.1 Patients

26 patients with alcoholic cirrhosis were studied prior to and 1-hour after TIPSS insertion. Patients were included into the study if they had clinical, biochemical or histological evidence of cirrhosis and were undergoing TIPSS placement indicated for variceal haemorrhage. All patients were haemodynamically stable at the time of TIPSS insertion and informed consent (from the patient) or assent (from next of kin) was obtained. Other exclusion criteria included pregnancy, a diagnosis of diabetes, cardiovascular disease or malignancy.

3.1.2 Patient Management

The patients were managed according to a standardized protocol, and in accordance with the UK guidelines for variceal haemorrhage (Jalan & Hayes, 2000). TIPSS insertion was indicated either because the patient had variceal bleeding refractory to endoscopic therapy or due to recurrent bleeding despite endoscopic therapy. At the

time of TIPSS insertion, the patients were mechanically ventilated following sedation with propofol and paralysed with atracurium besylate (300-600μg/Kg/hr). Routine invasive and electrocardiographic monitoring was performed. Fluid resuscitation and red cell concentrate were administered in guidance with the central venous pressure, mean arterial pressure and the haematocrit. All the patients received broad spectrum prophylactic antibiotics. Blood glucose levels were maintained between 5-7 mmol/l.

3.1.3 Transjugular Intrahepatic Portosystemic Stent Shunt procedure and catheter insertion

A single interventional radiologist on each site performed all the TIPSS procedures using standard techniques. Pre-TIPSS procedure, a femoral artery was cannulated using an 18 gauge needle (Vygon leader company, Ecoven, France). The right internal jugular vein was then punctured and a 10 F sheath (William-Cook, Bjaeverskov, Denmark) introduced. The right or middle hepatic vein was selected using a stiff hydrophilic guide wire (Terumo, Hatagaya, Tokyo, Japan) and a fine stylet was used to puncture a branch of the portal vein.

3.1.4 Blood sampling and Measurements

Blood from the femoral artery (A), hepatic vein (HV) and portal vein (PV) sampled before insertion of the TIPSS. A sub-group of patients underwent further blood sampling of the left gastric vein, splenic vein, superior mesenteric vein and inferior mesenteric vein. An angioplasty balloon catheter was then used to dilate the parenchymal tract prior to stent insertion (10 mm Wallstent, Schneider, Bulach, Switzerland). Portal venous and inferior vena caval pressures were recorded pre- and post-TIPSS insertion and the portal pressure gradient determined (portal venous pressure minus inferior vena caval pressure). One hour after TIPSS insertion blood

was sampled from the following: femoral artery, hepatic vein (not involving TIPSS-shunt) and portal vein.

3.1.5 Calculations

Intestinal and hepatic fractional extraction rates of endotoxin, BPI, LBP, IL-6, IL-10, were calculated according to the following equation using pre-TIPSS plasma levels. The calculation of hepatic fractional extraction assumes a 70% contribution from the hepatic artery and 30% contribution from the portal vein in this patient cohort. Previous data supports this assumption (Bloeman et al, 2010).

Hepatic Fractional Extraction Rate= [Hepatic vein-(0.7xarterial +0.3xportal vein)]/[0.7arterial+ 0.3 portal vein]

Intestinal Fractional Extraction Rate = [Portal vein-arterial]/Arterial

3.1.6 Patient Follow-up

Patients were followed up until death or 240 days post-TIPSS insertion.

3.2 Animal Models

All animal experiments were conducted according to Home Office guidelines under the UK Animals in Scientific Procedures Act 1986. Male Sprague-Dawley rats (body weight 280-300g) and C57B mice (body weight 25g) were used (Charles River Laboratories UK Ltd.). All rats/mice were housed in the unit and given access to standard powdered rodent chow and water, with a light/dark cycle of 12 hours, at a temperature of 19°C to 23°C and humidity of approximately 50%. All animal studies were performed by myself under supervision from Dr. Nathan Davies.

3.2.1 Bile Duct Ligated Rat Model

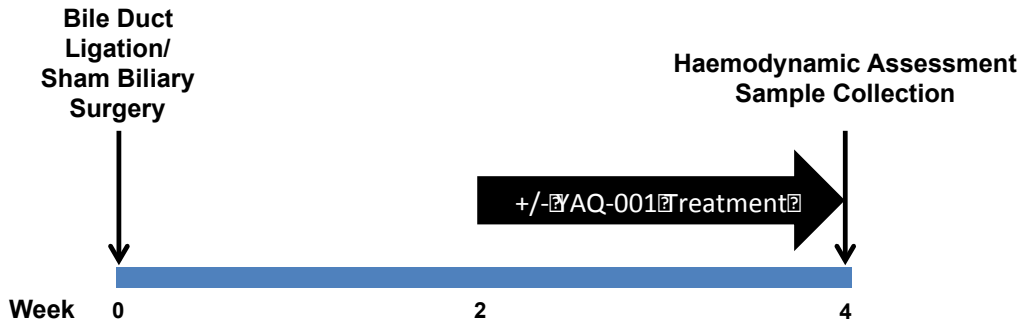

Figure 3.1 Experimental Schedule for Bile Duct Ligated Rat Model

Under halothane anaesthesia male Sprague-Dawley rats underwent bile duct-ligation or sham biliary surgery. Rats were pair-fed powered chow until completion of the experiment at 4-5 weeks from initial surgery. Rats were randomised to receive standard powdered chow or powdered chow supplemented with Yaq-001 carbon therapy (4g/kg body weight/day) two weeks following surgery until the completion of the experiment. Previous studies with AST-120 in bile duct ligated rats had demonstrated tolerability and efficacy with regards to ammonia reduction with a dose of 4g/kg/day. This was therefore the dose selected for this study. The following groups were studied: Sham (n=23), Sham + carbon (n=18), Sham + LPS (n=8), Sham+LPS+carbon (n=10), BDL (n=25), BDL + carbon (n=26), BDL+LPS (n=12), BDL+LPS+carbon (n=10).

Under halothane anaesthesia (5ml/min induction 2ml/min maintenance) an internal carotid catheter (0.96 outer diameter Portex fine-bore polythene tubing, Scientific Laboratory Supplies Ltd., Nottingham, UK) was inserted. The catheter was held in place for the duration of the study by both proximal and distal holding sutures. The catheter was transduced and mean arterial pressure determined. A laparotomy was then performed under sterile conditions and a catheter placed in the portal vein. Arterial and portal venous catheters were transduced. Concomitant arterial and portal

venous plasma was collected aseptically into lithium heparin and EDTA tubes until a state of exsanguination was achieved. 5ml of ice-cold PBS was then perfused into the liver to achieve organ blanching. The liver was extracted and placed in 10ml of ice cold PBS. Plasma was centrifuged at 3,500rpm for 10 minutes at 4°C. The supernatant was transferred immediately to cryotubes and stored at -70°C.

Duodenum, mid-jejunum, terminal ileum and ascending colon was collected and stored in formaline and electron microscopy preservation solution (200mM sodium cacodylate, 4% gluteraldehyde, pH=7.2-4). Histological specimens were collected with no attempt to irrigate or decontaminate the lumen. Samples were also collected from all four sites following decontamination of the lumen and irrigation with saline solution. These samples were transferred immediately to cryotubes and stored at -70°C. Liver, kidney and brain tissue was also collected and stored in formaline and cryotubes and stored at -70°C.

3.2.2 Murine models of Non-Alcoholic Fatty Liver Disease

Samples were collected as previously described for rat studies with the exception of no invasive arterial pressure monitoring.

3.2.2.1 Leptin deficient mice (ob/ob)

Male genetically leptin deficient (ob/ob) mice were randomized to receive standard powdered chow with or without carbon supplementation for four weeks. Heterozygote mice were used as the control population and also randomized to receive standard powdered chow with or without carbon supplementation for four weeks. Carbon supplementation was administered at a dose of 4g/kg body weight per day for four weeks.

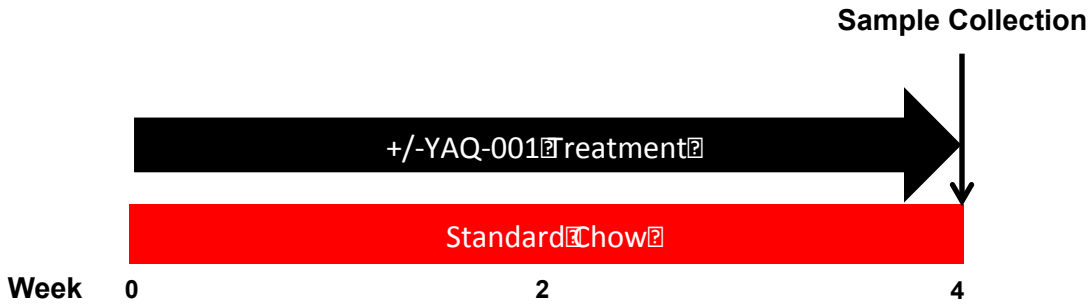

Figure 3.2 Experimental Schedule for Yaq-001 treatment in ob/ob mouse model

3.2.2.2 Methionine Choline Deficient Mice

Male C57/B mice were randomized to receive a diet of control powdered chow or powdered chow deficient in methionine choline (IPS Irradiated Baker Amino Acid Diet without Choline or Methionine (578B – 1811438) for 4 weeks. These feeds were randomized to be supplemented with carbon or not. The carbon was administered at a dose of 0.4g/100g body weight per day. The diet and treatment was continued for 4 weeks.

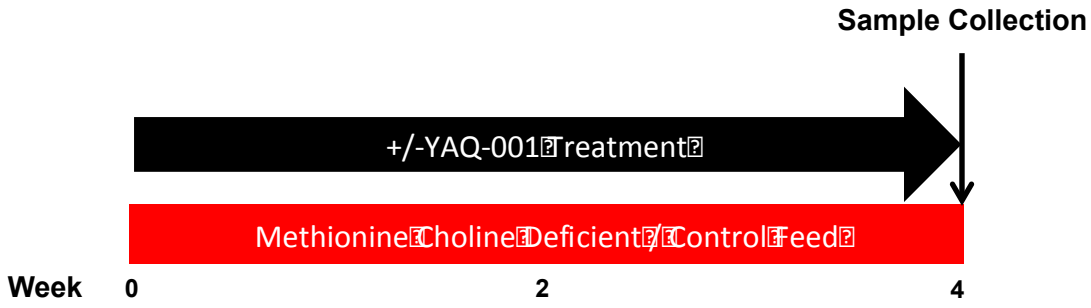

Figure 3.3 Experimental Schedule for Yaq-001 treatment in MCD model

3.3 Cell Culture Experiments

Cell culture experiments were performed by Dr, Isi Ranchal and analysed by myself.

3.3.1 HEK-Blue hTLR4 cells

HEK-Blue hTLR4 cells (HEK-Blue LPS Detection Kit, InvivoGen) were cultured according to the manufacturer's instructions. Cells were cultured in Dulbecco's modified Eagle's medium (DMEM) high-glucose medium supplemented with foetal bovine serum (FBS, 10 %), glutamine (2 mM), 1× Normocin (InvivoGen), and 1× HEK-Blue Selection (InvivoGen). Cell concentration was determined with a cell counter, cells were then diluted in DMEM medium supplemented with FBS (10 %), glutamine (2 mM), 1× Normocin (InvivoGen) and 200 µL of cell suspension (10^5 cells) was added to each well on a 96-well plate. Following 72 hours of incubation (37 °C, 5 % CO2, 95 % humidity), the cells reached 80 % confluency. The supernatant was removed and cell monolayers washed with warm PBS without Ca^{2+} and Mg^{2+}, and incubated for 24 hours in 180 µL DMEM and 20 µL of rat or human plasma. Rat plasma concentrations up to 1:200 rat plasma were evaluated. Lipopolysaccharide (LPS) derived from *Klebsiella pneumoniae* (Sigma-Aldrich; L4268) and LPS from *Salmonella ssp* (Sigma-Aldrich; L6143) at final concentrations of 0.001, 0.01, 0.1, 1, 10, 100 or 1000 ng /mL were then added as a stimulus (10 µL per well), and the cells incubated for 24 hours under the same conditions as above. Following the incubation, the supernatants were collected and 20 µL added to a Quanti-blue reagent assay (200 µL). The plates were incubated in the dark at room temperature and then analyzed using a spectrophotometer (absorbance at 615 nm).

3.3.2 HEK-Blue IL-1β/IL-18 cells

HEK-Blue IL-1β/IL-18 cells containing an IL-1β-sensitive reporter and IL-18-sensitive reporter (InvivoGen, San Diego, CA, USA) were grown at 37°C with 5% CO_2 in Dulbecco's modified Eagle's medium (DMEM) supplemented with 10% (vol/vol) foetal bovine serum (FBS), 4.5 g/L glucose, 2 mM GlutaMAX medium, 100 U/ml penicillin, 100 µg/ml streptomycin (all obtained from Gibco BRL/Life Technologies, London, UK), 100 µg/ml zeocin, 200 µg/ml hygromycin and 100 µg/ml Normocin (InvivoGen). The cells were seeded onto a 96-well plate (200 µL, 5 x 10^5 cells). After 24 hours of incubation at 37°C, supernatant was removed, and cell monolayers were washed with warm PBS without Ca^{2+} and Mg^{2+} and incubated for 24 hours in 180 µL DMEM with 20 µL of rat or human plasma. 40 µl of the cell supernatants were added to each well of a 96-well plate together with 160 µl of QUANTI-Blue (InvivoGen), incubated at 37°C for 60 minutes and measured in an enzyme-linked immunosorbent assay (ELISA) reader at 615 nm to determine the expression levels of reporter genes activated by NF-κB.

Quanti-Blue SEAP (secreted embryonic alkaline phosphatase) Reporter Assay: 20 µl aliquots of cell culture medium were removed and added to plates containing 180 µl of pre-warmed Quanti-Blue detection reagent per well as per manufacturer's instructions. Colour was allowed to develop for 1 h, and absorbance was read at 615 nm in Bio-Tek® microplate reader (Burlington, VT).

Cell Viability and toxicity Assays: Cells were labeled with (3-(4,5-dimethylthiazol-2-yl)-2,5-diphenyltetrazoliumbromide (MTT) for 2 hours followed by dissolution of the violet crystals. Cell viability was determined by measuring the absorbance at 570 nm in a Bio-Tek® microplate reader (Burlington, VT). Cell morphology was assessed at 24 hours under phase-contrast inverted microscopy.

3.4 Immunology Methods

All rodent immunology studies were performed by myself.

3.4.1 Clinical study

3.4.1.1 Neutrophil isolation

4ml of whole blood was layered over 5 ml of Polymorphprep (Axis-Shield), centrifuged for 30 minutes at 400 g at 21°C. Neutrophils were aspirated from the second buffy coat and washed with phosphate buffered saline (PBS, Sigma Aldrich). Total neutrophil cell yield was determined and re-suspended in PBS to produce a cell suspension of $1x10^7$/ml. 50 µL of cell suspension and 50 µL of plasma were used per assay. Viability was tested by Trypan blue exclusion and was over 98%.

3.4.1.2 Neutrophil function

3.4.1.2.1 Phagoburst Assay

The Phagoburst kit (Orpegen Pharma, Heidelberg, Germany) was used to determine the percentage of neutrophils that produce reactive oxidants as previously described (FACS Canto II, BD Bioscience) (Mookerjee RP *et al*, 2007). 20µl of each of the following was added to FACS tubes containing $5x10^5$ neutrophil cell suspension: PBS, pre-cooled unlabelled *E.coli*, fMLP (low control), PMA (high control). The samples were then incubate for 20 minutes at 37°C. 20ul of substrate solution was then added and the samples were incubated at 37°C for 20 minutes. 3ml of lysing solution (reagent F, Phagoburst, Orpegen Pharma) was then added to each sample. The samples were then centrifuged at 1800rpm for 5 minutes at 4°C. The supernatant was then decanted, the samples washed with 3ml of PBS and centrifuged for 5 minutes at 400g at 4°C. The supernatant was then decanted and incubated with anti-CD16-(PE) (Immunotools) for 30 minutes at 4°C in the dark. The samples were immediately analysed using a Beckton Dickinson FACS Canto II flow cytometry machine.

3.4.1.2.2 Phagotest

The Phagotest (Orpegen Pharma) was used to measure phagocytosis by using FITC-labeled opsonized *E. coli* bacteria. 20µl of FITC-labeled E.coli (Phagotest reagent B) was added to FACS tubes containing $5x10^5$ neutrophil cell suspension. The samples were then incubated for 20 minutes at 37°C. Control samples were incubated at 4°C. Samples were then transferred to ice to stop phagocytosis and 100ul of brilliant blue solution (stored on ice) was added to quench the bacteria bound to the surface. 3ml of PBS was then added and samples centrifuged at 400g for 5 minutes at 4°C. The supernatant was then decanted and 3 ml of lysing solution was added to each sample. The samples were then incubated at 21°C for 20 minutes. The samples were centrifuged 1800rpm for 5 minutes at 4°C and supernatant decanted followed by washing with 3ml of PBS and a repeat centrifugation step at 1800rpm for 5 minutes at 4°C. The samples were then incubated for 30 minutes at 4°C in the dark with anti-CD16-(PE) (Immunotools). Following this, samples were washed with PBS, centrifuged at 400g at 4°C, supernatant decanted and cells re-suspended in PBS and immediately analysed using a Beckton Dickinson FACS Canto II flow cytometry machine.

3.4.2 Rodent Studies

3.4.2.1 Sample Preparation

3.4.2.1.1 Isolation of Non-Parenchymal Cell Fraction from Rodent Liver Tissue

Perfused liver tissue was dissected with a scalpel and homogenized in Hanks balanced salt solution (with calcium and magnesium + collagenase 0.01% and DNAse I (0.01%). The homogenate was transferred to a 50ml Falcon tube and incubated at 37°C prior to filtration through a cell strainer (100µm for rat tissue; 70µm

for murine tissue). This was then centrifuged at 30g for 5 minutes at 4°C and the supernatant subsequently centrifuged at 500g for 10 minutes at 4°C. The supernatant was discarded and the pellet re-suspended in PF4 (HBSS with no calcium or magnesium, DNAse I 0.01%, bovine serum albumin (0.25%)) and centrifuged at 500g for 10 minutes at 4°C. The pellet was then re-suspended in 3.9ml of RPMI 1640 and mixed gently with 2.1ml (RPMI and Optiprep 22%). RPMI was then layered on top followed by a 25 minute centrifugation step at 900g without brake at 4°C. The non-parenchymal cells were isolated from the interface, re-suspended in an equivalent volume of PF4 and centrifuged at 2000rpm at 4°C for 10 minutes. The pellet was re-suspended in 5ml of Red Cell Lysis Buffer (BioLegend) and incubated for 5 minutes at 4°C with occasional shaking. The reaction was then stopped by addition of 10 ml of PBS. This was then centrifuged at 500g for 10 minutes at 4ºC, the supernatant discarded and the cells re-suspended in 3ml of culture media. The cells were counted and adjusted to a concentration of 10^7 cells/ml. $1x10^6$ cells were used in all subsequent assays.

3.4.2.1.2 Whole Blood Preparation (Arterial and portal venous)

2ml of blood was collected from portal vein and arterial blood. 40ml of RBC lysis buffer was added to each 2ml sample, vortexed and incubated for 15 minutes at room temperature. Following centrifugation at 450g for 5 minutes the supernatant was discarded and the pellet re-suspended with 1ml of complete culture media (RPMI (Gibco), 10% FBS, 200mM L-Glutamine) .The cell number using the nucleoCounter method and adjusted to $1x10^7$cell/ml.

3.4.2.1.3 Mesenteric Lymph Node Cell Isolation

The resected mesentery was placed on a sterile petri dish filled with ice cold HBSS. All mesenteric lymph nodes were dissected. One lymph node was stored

immediately in RNA later and one in 10% formalin. The remaining mesenteric lymph nodes were placed on a cell strainer (100μm pores) on a 50ml Falcon tube, homogenised and re-suspended in 10ml of ice cold HBSS. The homogenate was then centrifuged at 450xg for 5 minutes at 4ºC, supernatant discarded and the pellet re-suspended in 10ml of FACS buffer. One further passage through the cell strainer was performed and the cell number determined and standardised to a cell concentration of $1x10^7$ cells/ml.

3.4.2.2 Population Studies

3.4.2.2.1 Kupffer Cell Population studies

2ul of Fc blocker (anti-CD32 antibody) was added to 10^6 cells (non-parenchymal cell fraction) and incubated for 5 minutes at 4°C. The cells were then co-incubated with anti-CD163 antibody for 30 minutes at 4°C in the dark**.** The cells were washed with 1ml of FACS buffer, centrifuged and re-suspended in 100μl FACS buffer solution and analysed immediately on a Becton Dickinson LSR II flow cytometer.

3.4.2.2.2 Cell population assay (Portal Venous and Arterial Blood)

2ul of Fc blocker (anti-CD32 antibody) was added to 10^6 cells and incubated for 10 minutes at 4°C. The cells were then co-incubated with the following primary antibodies for 20 minutes at 4°C: PE-CD11b (0.2mg/ml), Alexa647-CD43 (0.5mg/ml), FITC-HIS48 (200ug/ml). After incubation, 2 ml of FACS buffer was added to each tube, centrifuged at 450xg for 5 minutes at 4°C and supernatant discarded. This last step was then repeated with 1ml FACS solution and the pellet re-suspended the pellet in 100ul of FACS buffer. 5ul of DAPI solution was added into the each tube prior to analysis.

3.4.2.2.3 Mesenteric Lymph Node Cell Population Assay

2ul of Fc blocker (anti-CD32 antibody) was added to 10^6 cells and incubated for 5 minutes at 4°C. The cells were then co-incubated with the following primary antibodies and incubated for 30 minutes at 21°C: 0.2ug PE-CD80, 1ug FITC-HIS48, 5ul Alexa647-CD163 (ED2). 1ml of FACS buffer was then added per tube and centrifuged at 450g for 5 minutes at 4ºC. After discarding the supernatant, 100ul of Leucoperm Reagent A was added per tube and incubated for 30 minutes at 21°C. Each tube was then washed with 3ml of FACS buffer, centrifuged and supernatant discarded. The pellet was then re-suspended with 100ul of Reagent B followed by addition of 5ul of biotin conjugated CD68. Following a 30 minute incubation at 4°C, the tubes were washed with 1ml of FACS buffer and then centrifuged at 450g for 5 minutes at 4°C. The pellet was then re-suspended in 100ul of FACS buffer containing 1ul BV650- streptavidin and incubated for 20 minutes at 4°C. Finally 2ml of FACS buffer was added per tube, samples centrifuged at 450g for 5 minutes at 4°C. After discarding the supernatant, each sample was re-suspended with 100ul of FACS buffer.

3.4.2.3 Functional Assays

3.4.2.3.1 Rat Kupffer Cell and Portal Venous ROS studies

20ug/ml of *E.coli* endotoxin was added to 1x 10^6 non-parenchymal cells sample and incubated for 30 minutes at 37°C. ROS inducer at a final concentration of 200-500uM was used as a positive control. The samples were then centrifuged at 500g for 5 minutes and the supernatant discarded. The cells were re-suspended in 5ml of wash buffer, centrifuged at 500g for 5minutes and the supernatant removed. The cells were re-suspended in 500ul of ROS detection solution and incubated for 30 minutes at 37°C in the dark. Following centrifugation, the cells were re-suspended in 100ul of

FACS buffer, Fc blocker added (1:25) and incubated for 10minutes at 4°C**.** Anti-CD163 antibody was added and the cells incubated for 30 minutes at 4°C in the dark (Kupffer cells)**.** The cells were then washed with 1ml of FACS buffer, centrifuged and re-suspended in 100μl FACS buffer solution.

3.4.2.3.2 Murine Kupffer cell ROS studies

ROS inhibitor (N-acetyl-L-cysteine) was added to the negative control samples to achieve a final concentration of 5mM and incubated for 30 minutes. 20ug/ml of LPS was added to the pre-aliquoted cell suspension samples and incubated for 30 minutes at 37°C. For the positive control sample, ROS inducer (pyocyanin) was added to achieve a final concentration of 500uM and incubated for 30 minutes. During the incubation step, the tube was agitated occasionally. The cells were then centrifuged at 500g for 5 minutes and the supernatant discarded. The cells were then re-suspended in 5ml of FACS wash buffer, centrifuged at 500g for 5 minutes and the supernatant removed. The cells were then re-suspended n 500ul ROS detection solution (ENZO life sciences (ENZO cat ENZ-51011)) and incubated for 30 minutes at 37°C in the dark. The cells were then centrifuged the cells, media removed and cells re-suspended in 100ul of FACS buffer. 2μl of anti-mouse CD16/32 (Biolegend 101301:0.5mg/ml) was added and incubated for 10 minutes at 4°C. F4/80 antibody PerCP/Cy5.5 anti-mouse F4/80 clone BM8 (Biolegend 123127; 0.2mg/ml) was then added and incubated for 30 minutes at 4°C in the dark. (Isotype control: PerCP/Cy5.5 Rat IgG2a k Isotype (Biolegend 400531; 0.2mg/ml)). 1ml of FACS wash buffer was then added and the samples centrifuged at 2000rpm. Following one further wash step, the samples were analysed on a BD LSR II Flow Cytometer.

3.4.2.3.3 Kupffer cell phagocytic function

The cells were centrifuged at 500g for 5 minutes at 4ºC and the supernatant discarded. 200ul of latex beads containing media were added to the pellet and incubated at 37°C in the dark for 20 minutes. 5ml of ice cold phosphate buffered saline (PBS) was then added and centrifuged at 2000rpm for 5 minutes at 4ºC. The pellet was then washed with 5ml of cold PBS and centrifuged. Anti-CD32 antibody (Fc blocker) was then added and incubated for 10 minutes at 4°C. Anti-CD163 antibody was then added and incubated for 30 minutes at 4°C in the dark.

3.4.2.3.4 Flow Cytometer Analysis

All samples were kept at 4°C and analysed immediately using a FACS LSR II machine. Data was analysed using FlowJo software.

3.5 Microbiological Methods

Stool 16S sequencing was performed outside the institution. Otherwise all microbiological studies were performed by myself.

3.5.1 Bacterial PCR

3.5.1.1 Bacterial DNA Isolation from Plasma

100µl of fresh or thawed plasma was added to 600µl of chilled Nuclei Lysis Solution and homogenized for 10 seconds**.** This was followed by a 15-30 minute incubation step at 65°C. 3µl of RNase solution was added to the lysate, mixed and incubated for 15-30 minutes at 37°C. The solution was then cooled to room temperature, 200µl of Protein Precipitation Solution added and subsequently chilled on ice for 5 minutes. This was then centrifuged at 13000-16000g for 4 minutes. The supernatant was

transferred to a fresh tube containing 600µl of room temperature isopropanol and mixed gently by inversion. The samples were then centrifuged at 13000-16000g for 1 minute, supernatant removed and 600µl of room temperature 70% ethanol added. Following mixing and a further centrifugation step, the ethanol was aspirated and pellet allowed to air dry for 15 minutes. The DNA was then re-suspended in 100µl of DNA Rehydration Solution overnight at 4°C.

3.5.1.2 DNA Amplification and Sequencing (Plasma samples)

2µl of DNA template was added to a reaction mix containing: 10mmol/L Tris buffer (pH 8.3), 50 mmol/L KCl, 1.5mmol/L MgCl2, 200 mol/L of each deoxynucleoside triphosphate, 50 pmol of primers 5_-AGAGTTTGATCATGGCTCAG-3_ and 5_ACCGCGACTGCTGCTGGCAC-3_, 1.25 U BioTaq (Bioline, London, England) to complete a final volume of 50µl. A 35-cycle PCR was then run in GeneAmp 9700 (Applied Biosystems, Foster City, CA) using the following profile: 94°C for 30 seconds, 55°C for 30 seconds, 72°C for 60 seconds. The total PCR reaction volume was then filtered with QIAquick Spin Columns (QIAquick PCR Purification Kit; QIAGEN) to remove rests of primers. 5mcl of purified products were then analysed by 2% agarose gel electrophoresis and UV visualization. A band of about 540 base pairs was obtained from different bacterial cultures corresponding to the specific amplification of the prokaryotic 16S ribosomal RNA gene.

3.5.1.3 Isolation of DNA from Stool for Pathogen Detection

180–220 mg stool was placed into a 2 ml microcentrifuge tube at 4°C and1.4 ml Buffer ASL (Qiagen) added to each sample. The samples were then vortexed for 60 seconds and the suspension heated to 95°C for 5 minutes. The samples were then vortexed for 15 sseconds, centrifuged at 13000g for 1 minute and 1.2 ml of the supernatant was then pipetted into new 2 ml microcentrifuge tubes.

One InhibitEX Tablet was then added to each sample and vortexed for 60 and the suspension incubated for 1 minute at 21°C following which the samples were centrifuged at full speed for 3 minutes. All of the supernatant was then transferred into a new 1.5 ml microcentrifuge tube and the pellet discarded. These samples were then centrifuged at full speed for 3 minutes. 15 µl proteinase K and subsequently 200 µl Buffer AL (Qiagen) was added to 200 µl of the supernatant, vortexed for 15 seconds and incubated at 70°C for 10 minutes. 200 µl of ethanol (96–100%) was added to the lysate, vortexed and passed through a new QIAamp spin column by means of centrifugation at full speed for 1 minute. 500 µl Buffer AW1 (Qiagen) was added to the lysate and centrifuged at full speed for 1 minute. 500 µl Buffer AW2 (Qiagen) was subsequently added to the lysate and centrifuged at full speed for 3 minutes. 200 µl Buffer AE (Qiagen) was then added directly onto the QIAamp membrane, incubated for 1 min at room temperature, then centrifuged at full speed for 1 minute. The samples were then stored at –20°C prior to determination of DNA concentration by spectrophotometry (Nanodrop).

3.5.1.4 Sequence-based microbiota composition determination

DNA was extracted from 200 mg of faecal material /animal. Total DNA was extracted initially with bead-beating step and the QIAamp DNA stool mini kit (Qiagen, West Sussex, UK). Universal 16SrRNA primers, forward primer F1 (5′-AYTGGGYDTAAAGNG) and four reverse primers R1 (5′-TACCRGGGTHTCTAATCC), R2 (5′-TACCAGAGTATCTAATTC), R3 (5′-CTACDSRGGTMTCTAATC) and R4 (5′-TACNVGGGTATCTAATC) were used for Taq-based PCR amplification. Sequencing was performed on a Roche 454 GS-FLX using Titanium chemistry by the Teagasc 454 Sequencing Platform (Teagasc, Fermoy, Ireland). The reads were quality trimmed, clustered, aligned and checked for

chimeras (Qiime). The reads for the major phyla were averaged for each group and expressed as a percentage of the total number of reads for that particular group.

3.5.2 Endotoxin measurement

The chromogenic limulus amoebocyte lysate (LAL) kinetic assay (Charles River Laboratories) was used for the detection of endotoxin. Portal venous plasma (100mcl) was diluted 1:10 with endotoxin-free water and incubated at 75°C for 30 minutes. 100mcl of sample and 100mcl of LAL reagent were mixed in a 96-well plate and analysed at 405nm with spectrophotometer using the Endoscan V software. Results are expressed as EU/ml.

3.5.3 Mesenteric Lymph Node Culture

Mesenteric Lymph nodes were isolated and prepared as previously described. Blood agar plates were inoculated with mesenteric lymph node homogenate and incubated at 37°C for 48 hours following which the culture positivity was determined.

3.6 Histological analysis

All histological analysis was performed by myself. Mr. Ray Moss supervised acquisition of electron microscopy images.

3.6.1 Light microscopy

Liver tissue was processed in accordance with standard protocol and Haematoxylin and Eosin together with Sirius Red staining was performed.

3.6.1.1 Haematoxylin and Eosin Staining

Sections were deparaffinised and rehydrated as follows: 3 x 5 minutes Xylene (blot excess xylene before going into ethanol) 3 x 5 minutes 100% ethanol; 1 x 5 minutes 95% ethanol; 1 x 5 minutes 80% ethanol; 1 x 5 minutes deionized H2O.
Haematoxalin staining was performed as follows: 1 x 5 minutes Haematoxalin. Rinse deionized water, 1 x 5minutes Tap water (to allow stain to develop), Dip 8- 12x (fast) Acid ethanol (1 ml concentrated HCl + 400 ml 70% ethanol), Rinse 2 x 1minute Tap water, Rinse 1 x 2 minutes Deionized water. Eosin staining and dehydration:1 x 30 seconds Eosin, 3 x 5 minutes 95% ethanol, 3 x 5 minutes 100% ethanol, 3 x 15 minutes Xylene. Slides were dried overnight in the hood.

3.6.1.2 Sirius Red staining

Picro-Sirius Red mixture is prepared as follows (10ml 1% aqueous Sirius Red F3B, 90ml Saturated aqueous picric acid). Mix together and add excess picric acid crystals to ensure saturation. Stand solution for 24 hours before use. Take the sections to water (Xylene x 3: 3 mins, IMS x 3: 1 min). Treat sections with freshly filtered picro-sirius mixture for 8 minutes. Rinse directly in 100% IMS (74 OP). Dehydrate, clear and mount. (IMS x 3: 1 min, Xylene x 3: 1 min)
Sirius red staining was quantified using computer assisted digital image analysis. Collagen proportionate area was determined using Zeiss KS300 image analysis software.

3.6.2 Electron microscopy

The tissue was drop-fixed in sodium cacodylate buffer at room temperature and dehydrated through increasing concentrations of alcohol (50-100%) prior to embedding in Spurr's resin (Agar Scientific). 80-100nm sections were cut, stained with 2 % aqueous uranyl acetate and subsequently Sato's lead stain for 20 minutes

each prior to viewing with a Hitachi 7100 transmission electron microscope at 75 kV. Images were captured using a column-mounted CCD camera (Gatan) (1024x1024 pixels).

3.6 Biochemical Analysis

Bile acid analysis was conducted at King's College tertiary biochemistry unit and mass spectroscopy analysis performed by colleagues at the Institute of Child Health. All other biochemical analysis was perfomed by myself.

3.6.1 COBAS

250mcl of lithium heparin anti-coagulated plasma was analysed using an automated biochemical analyser (COBAS, Roche Diagnostics, UK) for the following: bilirubin, ALT, AST, alkaline phosphatase, albumin, urea, creatinine, calcium, phosphate, glucose.

3.6.2 Bile acid Analysis

250 µl of plasma was added to 800 µl of protein precipitation reagent containing acetonitrile and internal standards, vortexed for 30 seconds and centrifuged for 10 minutes at 13000rpm. 900 µl of the supernatant was then dried with compressed air in a 60ºC heated block. The samples were then reconstituted in 250 µl of 50:50 mixture of mobile phases A and B and transferred to a glass HPLC injection vial and 10 µl injected into the LC-MS/MS system. Samples were resolved using a Supelco Analytical, Ascentis Express C18 fused core column (15 cm x 4.6 mm, 2.7 µm, SigmaAldrich) on a Jasco high pressure liquid chromatography (HPLC) system by reverse phase HPLC using mobile phases A: methanol and B: water each with 5nM ammonium acetate and 0.012% (v/v) formic acid. The Jasco HPLC system is coupled to an Applied Biosystems API 3200 triple stage quadrupole mass

spectrometer operated with electrospray ionisation source in negative ionisation mode followed by detection by multiple reaction monitoring.

3.6.3 Lactulose/Rhamnose Test

3.6.3.1 General

Intestinal permeability assays were conducted 1 day prior to completion of the experiment. Animals were placed in metabolic cages for overnight acclimatisation. Baseline urine samples were collected in cryotubes and stored at -70°C. 0.6ml of a solution of lactulose (277mM), L(+)-Rhamnose (10mM) and 3-methyl-o- pyranose (2.0mM) was then administered by gavage and urine collected for the subsequent 5 hours. Urine samples were analysed using mass spectroscopy to determine urinary excretion of lactulose, rhamnose and 6-0-methy-glucose. Animals were returned back to their group cages for re-acclimatisation and fasted prior to termination.

3.6.3.2 Electro-Spray Ionization Mass Spectrometry (ESI-MS)

ESI-MS was performed using a LTQ Orbitrap XL mass spectrometer (Thermo Fischer Scientific, USA). A 1:10 serial dilution was prepared for 3-OMD, lactulose and rhamnose in 70:30 acetonitrile and water (LC-MS grade) (Sigma Aldrich, UK). 0.2µl of formic acid was added to each sample. Samples of µM concentration were then analysed by direct injection to check for detection limits. Urine samples were prepared in a 1:50 dilution with acetonitrile following a centrifuged for 5 minutes centrifugation step at 4000g prior to analysis. Samples and standards were transferred to appropriated labeled glass vials and placed in the autosampler to be analysed.

3.7 Protein Expression

Western blot analysis and cytokine bead array was performed by myself.

3.7.1 Protein Extraction Methods

300micg duodenal tissue was homogenized in TRIS buffer 50 mM, pH 7.4. 20 uL of protease inhibitor cocktail (Sigma) was added. The samples were then centrifuged for 59 min at 12000 rpm supernatant collected. 1 □l of DM buffer was added per 100 ul of solution. Protein content was then determined using the Biuret method. Serial dilutions of Human Serum Albumin were prepared as follows: 50 mg/mL, 25 mg/mL, 12.5 mg/mL, 6.25 mg/mL, 3.125 mg/mL, 1.5625 mg/mL, 0.781 mg/mL. 15 ul of standard was added to 1 mL of Biuret solution (0.75g g Cu $SO_{4,}$ 3 g Na K tartrate, 25 g NaOH in 500 mL of distilled water) and incubated for 1 hour at room temperature. Protein concentrations were then determined using Agilant 8453.

Stock Sample Solution was prepared to achieve a protein concentration of 80ug/80ul with NuPAGE sample buffer (20mcl) and reducing agent. Samples were heated for 10 min at 70^{o}C. 15mcl of samples was then loaded into 4-12 % Bis Tris Gel with 10mcl of standard used. The gel was then run for 40-60 minutes at 120V. The samples were then transferred to a membrane for 1 hour at 30V at room temperature. Transfer efficiency was then determined using Ponceau Red stain. The membrane was then washed 3 times in PBST and blocked for 1 hour with 30 ml 5% milk in PBST. The membrane was then co-incubated with 2% milk in TPBS with primary antibody at a concentration of x overnight at 4ºC. The membrane was then washed 4 times with PBST for 5 minutes and co-incubated with secondary antibody for 1 hour. The membrane was then washed a further 4 times with PBST for 5 minutes and developed using a standard ECL kit. Protein expression was determined by optical densitometry and quantified.

3.7.2 Tight junction protein expression

3.7.2.1 Western Analysis of Connexin-43/iNOS/eNOS/ZO-1/Claudin 3

Sample Solution (80ug/80ul) was added to 20 ul of NuPAGE Sample Buffer and reducing agent with water added up to 80 ul. Samples were heated for 10 minutes at 70 ^{o}C. 15 uL of sample was loaded per well into a 4-12% Bis Tris running gel (NuPAGE Novex Bis/Tris Mini Gel) and running buffer added. The gel was then run at V for 40 minutes. The proteins were then transferred to the membrane (Transfer buffer: 25ml Transfer Buffer Invitrogen Nu PAGE x20; 375 mL distilled water; 100ml methanol 20%). The transfer stage is for 1 hour at 30V at room temperature. Protein transfer efficiency was determined with staining with Ponceau Red (1-2ml). The membrane was subsequently washed 3 times for 15 minutes with PBST. The membrane was then co-incubated for one hour at room temperature with 30 ml 5% milk in TPBS. The membrane was then incubated overnight with the primary antibody at 4ºC (20ml of 2% milk with TPBS and 1:500 of 1st antibody). The membrane was then washed 4 times for 5 minutes with TPBS. The membrane was then co-incubated with 20ml of secondary antibody 1:1000 in TPBS for 1 hour and washed another 4 times for 5 minutes with TPBS. The enhanced chemiluminescence (ECL) Western Blotting System (Amersham ECL Prime GE Healthcare Life Sciences) was used to develop the images. The membranes were exposed to the film for 2-5 minutes and subsequently emersed in developing solution (30-45 seconds), fixer solution (1minute with agitation) and finally washed with water. The films were then scanned and optical density determined with digital image analysis software.

3.7.3 Cytokine Studies

3.7.3.1 Clinical studies

Plasma levels of IL-10 and IL-6 were determined using commercially available ELISA assays in accordance with manufacturers instructions (R and D Biosystems).

3.7.3.2 Rodent Studies

Portal venous TNFα, IL-4, IL-10 levels were determined using the BD™ Cytometric Bead Array (CBA) kit. 50μL of the mixed capture beads were added to each assay well of a pre-wetted plate. 50 μL of standard or sample was then added to the assay wells. The plate was agitated for 5 minutes using a digital shaker at 500 RPM and the plate incubated for 1 hour at room temperature. 50 μL of mixed PE detection reagent was then added to each assay well. The plate was then agitated for 5 minutes using a digital shaker at 500 RPM and incubated at room temperature for 2 hours. The plate was vacuum aspirated until the wells were drained. 150μL of wash buffer was added to each assay well. The plate was then agitated on a digital shaker at 500 RPM for 5 minutes to resuspend the beads. The samples were then analysed by flow cytometry and data analysed using FACS Diva software.

3.8 Gene Expression

Gene expression studies were performed by Esther Putzjens.

3.8.1 RNA extraction from terminal ileal tissue

2 ml microcentrifuge tubes containing one 5mm stainless steel bead and one 7mm stainless steel bead were kept on dry ice for at least 15 minutes. 50 mg of frozen tissue was then transferred to the precooled tubes and incubated for another 15 minutes on dry ice. The tubes were then placed into the insert of the TissueLyser LT

Adapter, and incubate at room temperature for 2 minutes. 700 µl QIAzol Lysis Reagent was then added to each tube. The tubes were then transferred to the TissueLyser LT Adapter and homogenised at 50Hz for 8 minutes. The tube containing the homogenate was then placed at room temperature (15–25°C) for 5 minutes.140 µl chloroform was then added to each tube containing the homogenate and capped securely and agitated vigorously for 15 seconds. The homogenate was then placed on the bench top at room temperature for 2–3 minutes. The tubes were then centrifuged for 15 minutes at 12,000 g at 4°C. The upper aqueous phase was then transferred to a new collection tube and 1.5 volumes of 100% ethanol added and mixed. 700 µl of the sample was then pipetted into a spin column in a 2 ml collection tube. The tubes were then centrifuged at 10,000 rpm for 15 seconds at room temperature and the flow-through discarded. This last step was repeated with remaining sample. 700 µl Buffer RWT (RNeasy mini kit) was added to the spin column and centrifuged for 15 seconds at 10,000 rpm and the flow-through discarded. 500 µl of Buffer RPE (RNeasy Mini kit) was then added to the spin column and centrifuged for 15 seconds at 10,000 rpm and the flow-through discarded. A further 500 µl of Buffer RPE was added to the spin column and centrifuged for 2 minutes at 10,000 rpm. 50 µl of RNase-free water was the pipetted directly onto the RNeasy Mini spin column membrane and the tube centrifuged for 1 minute at 10,000 rpm. The RNA quality and yield was then determined using Nanodrop technology.

3.8.2 Quantitative PCR

cDNA synthesis (iScript cDNA Synthesis Kit, BioRad). QPCR was conducted on MyIQ real time PCR system (BioRad) with primer pairs as per manufacturers protocol.

Gene	Forward	Reverse

Gapdh	5'-TGCACCACCAACTGCTTAGC-3'	5'-GGCATGGACTGTGGTCATGAG-3'
Actb	5'-AGAGGGAAATCGTGCGTGAC-3'	5'-CGATAGTGATGACCTGACCGT-3'
Lyz2	5´-CTGTCCATACATCTCTGCTG-3´	5´-ACAGTGAGAAAGAGACAGAGTG-3´
Rd5	5´-GAAGACACTTGTCCTCCTTTCTG-3´	5´-TGTTGCAGATCCCCATAATGCCT-3´
Defa8	5´-GAAGACTCTTGTCCTCCTCTCTG-3´	5´-AATAGACCTGGACGACAGGACC-3´
Tnfa	5'-CTCACACTCAGATCATCTTCTC-3'	5'-TGGTATGAAATGGCAAATCGG-3'

3.9 ^{1}Nuclear Magnetic Resonance Spectroscopy

^{1}NMR spectroscopy and analysis was performed by myself under the supervision of Dr. Jane Cox.

400µl of urine were mixed with 200µl of 0.2 M phosphate/TSP buffer, pH 7.4 and centrifuged at 13000 rpm for 10 minutes. 550µl of supernatant was then transferred into a 5 mm tube and maintained at 4°C until analysis. Analysis was performed using a JEOL ECP 500 nuclear magnetic resonance spectrometer at MRC Harwell. Data was acquired at 25°C using a pulse-collect sequence with water pre-saturation. Urinary NMR spectra were acquired at 298K from using a JEOL ECP 500 MHz NMR spectrometer (JEOL Ltd, Tokyo, Japan). A standard pulse-collect sequence with water presaturation was used to acquire the NMR data. The spectral width was 15 ppm, pulse angle 90°, acquisition time 4.36 s and relaxation delay 3 s. 32K data points were acquired per collect and 64 transients were summated. The receiver gain was constant for all samples. The resulting free induction decay was zero filled and multiplied by an exponential function corresponding to 0.3 Hz line broadening prior to Fourier Transformation. The NMR spectra were manually phased using the JEOL Delta.

3.10 Carbon Adsorption studies

Carbon adsorption studies were performed by Dr. Susi Sandeman.

3.10.1 Cytokine adsorption by carbon beads from plasma

Human recombinant IL-6 and TNFα (BD Biosciences, Oxford, UK) was added to defrosted fresh frozen plasma (National Blood Service, London, UK) at a final concentration of 1000 pg/ml and 300 pg/ml respectively. 1ml of phosphate buffered saline (PBS) was added to 0.02g of carbon beads and incubated at 37°C for 2 hours. The samples were then centrifuged at 2000 g, supernatant removed and 800 µl of spiked plasma was added to each carbon and incubated at 37°C. Negative controls of non-spiked plasma and positive control with no carbon beads were also included. At timed intervals (5, 45, and 90 minutes) the samples were centrifuged at 2000 g and 150 µL aliquots removed. They were then stored at -20℃ prior to ELISA analysis to determine cytokine concentration (BD Biosciences, Oxford, UK) according to manufacturer's instructions.

3.10.2 Carbon Adsorption of TNFα from simulated intestinal fluid

Different weights of carbon bead (0.001-0.005 g) were incubated with 1 ml of SIF (Sigma 53757) for 2 hours. Following centrifugation at 8000 rpm for 3 minutes, the supernatant was removed and SIF spiked with 10 ng/ml of recombinant TNFα added. Following 24 hour incubation at 37° C at 90 rpm, samples were centrifuged at 8000 rpm for 3 minutes and supernatant collected and stored at −20° C. The samples were diluted in assay diluent prior to measurement of TNFα concentration by ELISA in accordance with the manufacturer's instructions (BD Biosciences).

3.11.3 Carbon Endotoxin Adsorption Kinetics

TE8 test carbon beads underwent dry heat sterilisation at 250° C for three hours. Carbons were pre-wetted with simulated intestinal fluid (Sigma-Aldrich) (22mM

Sodium hydroxide, 50mM Potassium phosphate) . SIF was prepared to the United States Pharmacopoeia 26 recipe without pancreatin and using endotoxin-free reagent water. E coli 055:B5 endotoxin standard solution was prepared at a concentration of 200 EU ml−1 in SIF. SIF was then aspirated from the carbons and endotoxin spiked SIF added to each test carbon (10 ml/gram of carbon). Test samples and positive controls without carbon were incubated at 37° C. 450 µl of sample was removed at time points 0, 15, 30, 45 and 60 minutes and the endotoxin concentration of each sample was calculated using the limulus amebocyte lysate (LAL) endosafe endochrome-K test (Charles River Laboratories UK) and Tecan Sunrise incubating plate reader with endoscan-V software as described.

3.10.4 Carbon Acetaldehyde Adsorption Kinetics

Different weights of carbon bead (0.001-0.005 g) were incubated with 1 ml of simulated intestinal fluid (Sigma-Aldrich) (22mM Sodium hydroxide, 50mM Potassium phosphate) at 37°C for 2 hours. A 7.2 mM spike (0.1 g/ml) of acetaldehyde was added at 4° C. Eppendorfs were then centrifuged (8000 rpm for 3 minutes) at a range of time intervals up to 30 minutes following addition of acetaldehyde spike. Acetaldehyde adsorption was measured using a derivatisation method with 2-diphenylacetyl-1,3-indandione-1-hydrazone (DIH) and HPLC analysis.

3.10.5 Determination of the Effect of Direct Contact Incubation of Test Carbon on Bacterial Metabolism

Yaq-001 carbon beads were dry heat sterilised in glass universal bottles for 2 hours at 80° C. 1 ml of phosphate buffered saline (PBS) was added to 0.1 g of Yaq-001 and incubated at 37° C for 1 hour at 120 rpm. Tryptone soya broth (TSB) was inoculated with Staphylococcus aureus (NCTC 6571) or Escherichia coli (NCTC 10418) and incubated overnight at 37° C at 120 rpm. Following centrifugation, the pellet was re-suspended in 1 ml PBS and the absorbance of the suspension

measured at 540 nm. The suspension concentration was adjusted to give a value of 0.5 and this dilution factor was then used to prepare a bacterial suspension in TSB. Serial dilutions of E coli suspension were prepared and inoculated onto agar plates. 1 ml of inoculum was added to each material and incubated at 37° C at 120 rpm. At timed intervals of 30 minutes, 2 and 6 hours, 100 µl of bacterial suspension was removed from each sample and placed into the wells of a 96 well plate. Samples were lysed and analysed for ATP content as a measure of cell metabolism using the BacTiter-Glo microbial cell viability assay (Promega).

3.10.6 Determination of the Effect of Carbon Leachate on Bacterial Metabolism

Yaq-001 carbon beads were dry heat sterilised in glass universal bottles for 2 hours at 120° C. 2 ml of phosphate buffered saline (PBS) was added to each 0.2 g of material and samples were incubated for 24 hours at 37° C at 120 rpm. TSB was inoculated with Bacillus subtilis or Escherichia coli (NCTC 10418) and incubated overnight at 37° C at 120 rpm. Following centrifugation, the pellet was re-suspended in TSB to achieve a final approximate concentration of 1×109 bacteria/ml. 100 µl of TSB, 100 µl of inoculum and 100 µl of extract were added in a 100 well Bioscreen plate. Bacterial growth was determined with a Bioscreen turbidometric analyser at 540 nm for 72 hours.

3.11 Statistical Analysis

One-way ANOVA and MANOVA tests were performed using SPSS version 24 with post-hoc analysis (Tukey test). Descriptive variables analysed were as follows: Arterial neutrophil ROS pre-TIPSS, Arterial neutrophil ROS post-TIPSS portal pressure, hepatic venous neutrophil ROS, portal venous neutrophil ROS, arterial LPS pre-TIPSS, arterial LPS post-TIPSS, hepatic venous LPS, portal venous LPS, arterial IL-10, hepatic venous IL-10, portal venous IL-10, arterial IL-6, hepatic venous IL-6, portal venous IL-6, creatinine, albumin, bilirubin, prothrombin time, INR, portal

pressure gradient pre-TIPSS insertion, portal pressure gradient post-TIPSS insertion, mortality, MELD score, encephalopathy.

Prior to statistical analysis, all NMR spectra were baseline corrected to a 4th degree polynomial, zero filled by a factor of 2 and referenced with the TSP peak set to 0.00 ppm using KIA version 9.0 (Bio-Rad, Philadelphia, USA). NMR spectral resonances were assigned according to previously described methods.

The resonances attributable to residual water and urea (δ 4.6– 6.4 ppm) were excluded from further analysis. NMR spectra were normalised to the total spectral integral in the range δ =0.2–10 ppm (excluding 4.6– 6.4 ppm). NMR spectra were bucketed (total buckets 603) using the Intelligent Bucketing algorithm and mean centred. Principal Components Analysis (PCA) was used as an unsupervised method for data visualisation and outlier identification and performed using BioRad KnowItAll software.

All other statistical analysis was performed using Graph Prism Version 7.0. Parametric (paired t-test, Pearson) and non-parametric (Mann Whitney, Spearman) analyses were performed as appropriate. Significance was considered present at $p<0.05$.

Chapter 4

TIPSS Study

4.1 Introduction

A substantial body of evidence exists to implicate gut-derived bacterial ligands, in particular endotoxin, in the promotion of a dysregulated inflammatory response central to the pathogenesis of many complications of cirrhosis, in particular, ACLF. Manipulation of gut bacterial flora with oral norfloxacin has been associated with an improvement in neutrophil function, improvement in vascular resistance and reduction in portal pressure. Higher systemic endotoxin levels have been observed in cirrhotic patients with decompensated disease compared to compensated controls.

Several questions remain however regarding the underlying mechanisms of bacterial translocation. These include the relative contribution of compromised gut barrier integrity and defective hepatic immune surveillance to the development of systemic endotoxaemia. In order to answer this question, arterial, portal and hepatic venous blood was sampled in patients undergoing TIPSS (transjugular intrahepatic portosystemic shunt) insertion indicated for refractory variceal haemorrhage and neutrophil function, cytokine concentrations and markers of bacterial translocation determined.

4.2 Aims

The first aim of this study was to determine relative endotoxin concentrations within different splanchnic territories and characterise the associated neutrophil response and cytokine concentrations. The second aim was to determine whether the early effects of artificial portosystemic shunting with TIPSS insertion on systemic endotoxin concentrations and neutrophil function. The final aim was to ascertain whether these parameters were associated with clinically relevant end-points, in particular, ACLF, mortality and portal pressure.

4.3 Results

4.3.1 Patient Characteristics

Patient Characteristics	Mean ± SEM
n	29
Age (yrs)	51.66 ± 2.50
M:F	16:13
Weight (kg)	56.93 ± 3.00
Aetiology	
Alcohol	26
Autoimmune Hepatitis	2
Primary Sclerosing Cholangitis	1
MELD score	21.48 ± 1.29
Ascites present (%)	66
Encephalopathic grade	1.55 ± 0.17
Albumin (g/dL)	27.48 ± 0.78
Bilirubin (μmol/L)	107.90 ± 14.85
INR	1.80 ± 0.09
Creatinine (μmol/L)	118.40 ± 12.92
PPG pre-TIPSS (mm Hg)	21.07 ± 1.04
PPG post-TIPSS (mm Hg)	9.52 + 0.32

Table 4.1 Patient Characteristics Pre-TIPSS insertion

Twenty-nine patients underwent TIPSS insertion indicated for variceal haemorrhage refractory to standard endoscopic therapy. The mean age was 51.66±2.50 years with a male:female ratio of 16:13. The mean MELD score was MELD score 21.48±1.29 and ascites was found to be present in 66% patients. Mean encephalopathic grade was 1.55±0.17. The predominant aetiology of underlying cirrhosis was alcohol in 26 patients. Two patients had a diagnosis of autoimmune hepatitis and one Primary Sclerosing Cholangitis. Mean laboratory values were as follows: albumin 27.48±0.78 g/dL, bilirubin 107.90±14.85 μmol/L, INR 1.80+0.09, Creatinine 118.40± 2.92 μmol/L. Mean portal pressure gradient pre-TIPSS was 21.07±1.04 mm Hg. Mean portal pressure gradient post-TIPSS insertion was 9.52±0.32 mm Hg.

4.3.2 Endotoxin studies

Mean endotoxin concentrations in the portal vein and hepatic vein pre-TIPSS insertion were 0.22±0.02 and 0.04±0.02 EU/ml respectively (p<0.0001). The pre-TIPSS trans-intestinal (TI) fractional extraction (FE) rate was 2.7±0.7 indicative of net intestinal endotoxin generation. Conversely, negative fraction extraction rates of -0.79 were observed across the liver consistent with endotoxin clearance. TIPSS insertion resulted in a significant increase in arterial endotoxin levels from 0.08 ±0.02 to 0.19±0.02 EU/ml (p=0.0001).

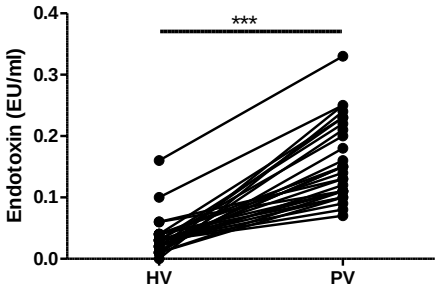

(a)

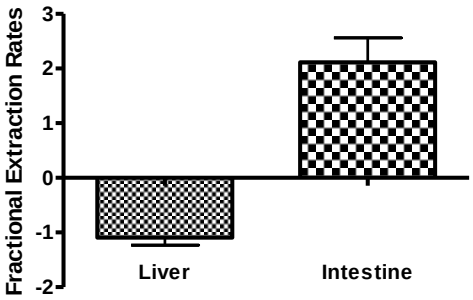

(b)

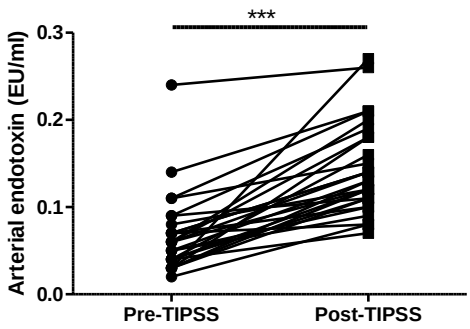

(c)

Figure 4.1(a) Endotoxin concentrations in portal and hepatic venous blood
Figure 4.1(b) Endotoxin Fractional extraction rates across liver and intestine
Figure 4.1(c) Arterial endotoxin levels pre- and 1 hour post-TIPSS insertion

*** denotes p<0.001

Pre-TIPSS intestinal fractional extraction of BPI (Bactericidal Permeability Increasing Protein) were found to be strongly positive at 12.40. Intestinal fractional extraction of LBP (Lipopolysaccharide binding protein) were also positive at 0.28. Negative

hepatic fractional extraction of BPI but positive hepatic fractional extraction of LBP were observed.

	Hepatic fractional extraction	Intestinal fractional extraction
BPI	-0.573 (0.07)	12.404 (6.7)
LBP	0.308 (0.21)	0.278 (0.15)

Figure 4.1 (d) Hepatic and Intestinal Fractional Extraction Rates of endotoxin-binding molecules

	Paired Differences					T	df	Sig.(2-tailed)
	Mean	SD	SEM	95% Confidence Interval of the Difference				
				Lower	Upper			
PV endotoxin	-.057	.065	.018	-.097	-.017	-3.134	12	.009

Figure 4.1 (e) Univariate analysis of portal venous endotoxin concentrations and mortality

Portal venous endotoxin concentrations were found to be predictive of survival in patients with variceal haemorrhage. No significant correlation was found with portal pressure gradient. Neither arterial nor hepatic venous endotoxin concentrations were found to be predictive of survival or portal pressure gradient.

4.3.3 Neutrophil Function

An intra-splanchnic difference in neutrophil function was observed in patients undergoing TIPSS insertion for variceal haemorrhage. A statistical significance in hepatic and portal venous neutrophil resting burst at 52.45±5.3% and 84.64±3.5% respectively ($p<0.0001$) was observed. Hepatic venous neutrophil resting burst was significantly increased from 52±5.3 to 78±4.5% after incubation with portal venous plasma ($p<0.0001$). Conversely, portal venous neutrophil resting burst was

significantly reduced from 85±3.5 to 60±5.3% ($p<0.0001$) after incubation with hepatic venous plasma.

Paralleling the observed increase in systemic endotoxaemia, peripheral neutrophil function was found to be significantly impaired following the insertion of TIPSS. Neutrophil phagocytic function was significantly reduced from 66±7.5% to 42±6.5% ($p=0.0004$) and resting burst increased from 62±5.6 to 87±2.8% ($p=0.0001$). Arterial neutrophil phagocytosis was found to be significantly lower 1 hour post-TIPSS insertion in patients with ACLF compared to those without ACLF in the context of refractory variceal haemorrhage (49.24$\pm$4.93 vs 31.00$\pm$2.71 % respectively $p<0.05$). Survival during follow-up was 67% in patients without ACLF and 27% in the ACLF group.

Portal venous neutrophil ROS production was found to significantly correlate with portal pressure gradient. No significant association with survival and neutrophil ROS (portal or hepatic venous) or arterial neutrophil phagocytosis was identified.

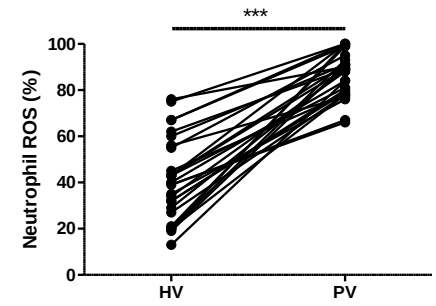

(a)

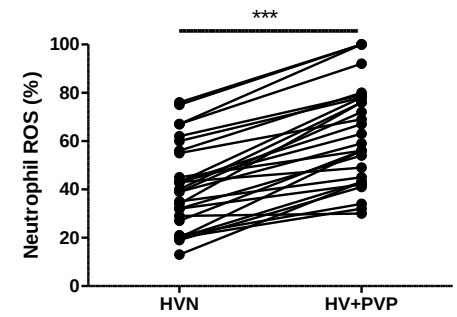

(b)

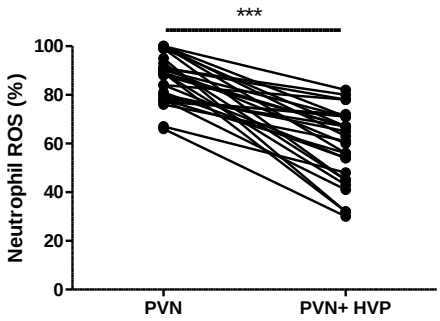

(c)

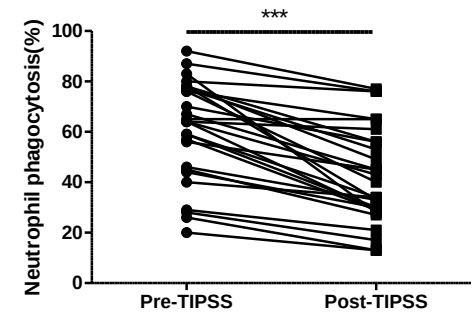

(d)

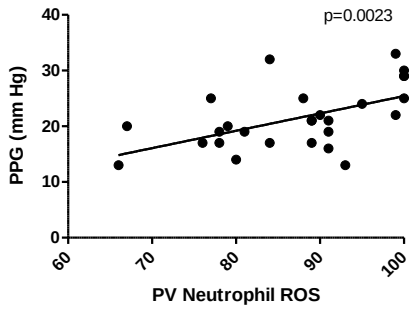

(e)

Figure 4.2(a) Neutrophil ROS production in hepatic venous (HV) and portal venous (PV) blood

Figure 4.2(b) Neutrophil ROS production in hepatic venous blood pre- and post-incubation with portal venous plasma (PVP)

Figure 4.2(c) Neutrophil ROS production in portal venous blood pre- and post-incubation with hepatic venous plasma (HVP)

Figure 4.2 (d) Arterial neutrophil phagocytosis pre- and post-TIPSS insertion

Figure 4.2 (e) Correlation between portal pressure gradient and portal venous neutrophil ROS production pre-TIPSS insertion (Pearson Coefficient R2 = 0.3058, Spearman Coefficient = 0.522)

* denotes $p<0.05$

*** denotes $p<0.001$

Table 4.2 Neutrophil Function (Non-ACLF vs ACLF)

	Non-ACLF		ACLF		
	Mean	SEM		SEM	p value
Arterial pre-TIPSS neutrophil phagocytosis	65.65	4.87	53.82	5.33	0.1
Arterial post-TIPSS neutrophil phagocytosis	**49.24**	**4.93**	**31**	**2.71**	**0.01**
HV neutrophil respiratory burst	45.94	4.19	34	5.09	0.06
PV neutrophil respiratory burst	86.29	2.67	87.73	2.45	0.92

Table 4.3 Univariate analysis of neutrophil function and mortality

	Paired Differences					t	df	Sig.(2-tailed)
	Mean	SD	SEM	95% Confidence Interval of the Difference				
				Lower	Upper			
PV neutrophil ROS	-3.231	13.211	3.664	-11.214	4.752	-.882	12	.395
HV neutrophil ROS	-11.692	21.708	6.021	-24.810	1.426	-1.942	12	.076
Arterial neutrophil phagocytosis	5.538	26.082	7.234	-10.223	21.300	.766	12	.459

4.3.4 Cytokine levels in splanchnic circulation pre-TIPSS insertion

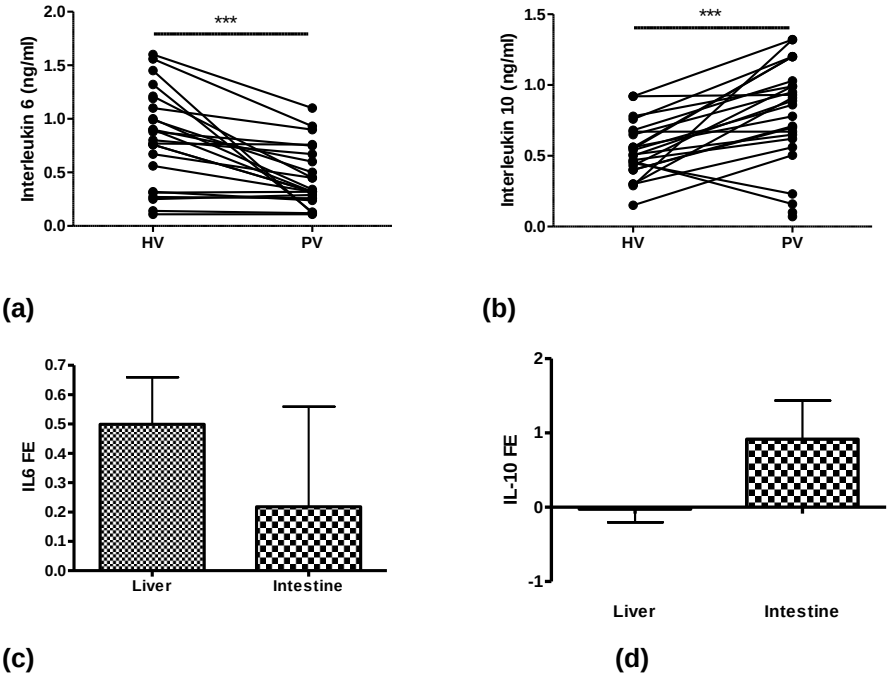

Figure 4.3(a) Interleukin 6 concentrations in hepatic and portal venous blood
Figure 4.3(b) Interleukin 10 concentrations in hepatic and portal venous blood
Figure 4.3(c) Fractional extraction of IL6 across liver and intestine
Figure 4.3(d) Fractional extraction of IL10 across liver and intestine

*** denotes p<0.001

	Non-ACLF		ACLF		
	Mean	SEM		SEM	p value
Arterial IL10	**0.50**	**0.09**	**0.77**	**0.08**	**0.03**
Hepatic venous IL10	0.52	0.06	0.55	0.06	0.9
Portal venous IL10	0.74	0.11	0.85	0.08	0.7
Arterial IL6	0.52	0.09	0.67	0.10	0.3
Hepatic venous IL6	0.78	0.13	0.88	0.12	0.49
Portal venous IL6	0.39	0.07	0.51	0.09	0.24

Table 4.4 Cytokine profile in patients with and without ACLF

		Paired Differences					t	df	Sig.(2-tailed)
		Mean	SD	SEM	95% Confidence Interval of the Difference				
					Lower	Upper			
	Arterial IL10	.036	.541	.163	-.327	.400	.223	10	.828
	HV IL10	.084	.306	.092	-.122	.289	.908	10	.385
	PV IL10	.110	.515	.155	-.235	.456	.711	10	.493
	Arterial IL6	**.283**	**.317**	**.100**	**.057**	**.509**	**2.827**	**9**	**.020**
	HV IL6	.215	.460	.145	-.114	.544	1.478	9	.174
	PV IL6	**.257**	**.273**	**.086**	**.062**	**.452**	**2.977**	**9**	**.016**

Table 4.5 Univariate analysis of cytokines and mortality

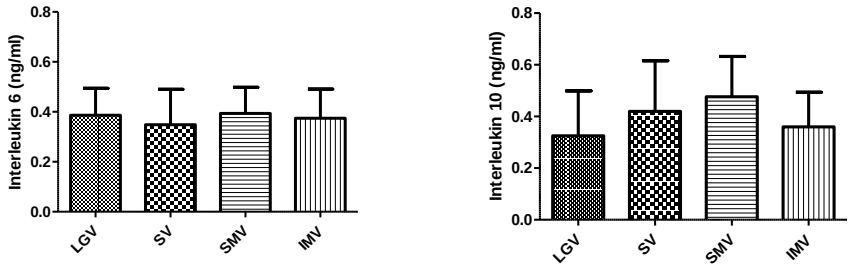

Figure 4.3 (e) Differential cytokine levels within splanchnic bed

Portal venous IL6 concentrations were found to be significantly lower than concentrations within the hepatic vein (0.44±0.28 vs 0.83±0.09 ng/ml) ($p<0.0001$). Conversely, portal venous IL10 levels were significantly higher in the portal vein compared to hepatic vein (0.78 ± 0.07 vs 0.53 ± 0.04 ng/ml) ($p=0.004$). IL6/IL10 ratios were significantly higher in the hepatic vein compared to portal vein.

Positive IL10 fractional extraction (FE) rates were observed across the intestine, however trans-hepatic IL10 FE rates were negligible. Positive IL6 FE rates were observed across the liver and intestine. No significant difference in IL-6 or IL-10 production was observed within the following portal vein tributaries: left gastric vein, splenic vein, superior mesenteric vein and inferior mesenteric vein.

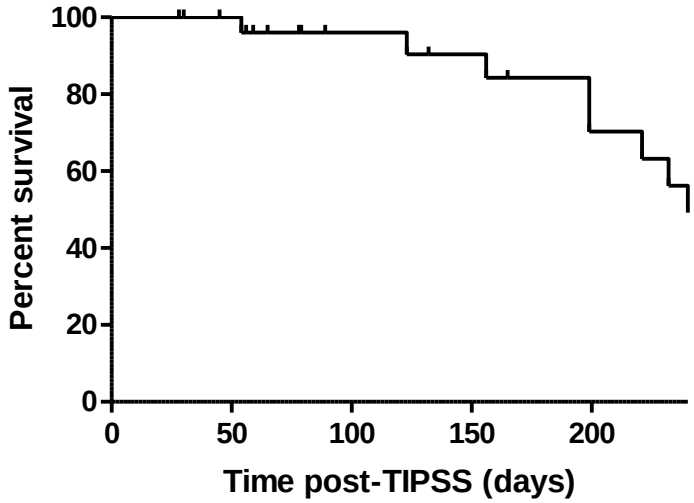

Figure 4.4 Kaplan-Meier Survival Curve post-TIPSS insertion

Arterial and portal venous IL6 was found to be predictive of survival. No significant association of IL10 with survival was identified. No significant association was identified with IL6 or IL10 and portal pressure gradient pre-TIPSS insertion in patients with variceal haemorrhage.

Neither MELD nor portal pressure gradient pre-TIPSS insertion in patients with variceal haemorrhage was found to be predictive of survival. Of conventional indices of liver function and outcome, only prothrombin time was identified as a predictor of survival in a univariate analysis.

4.4 Discussion

4.4.1 Differential intra-splanchnic endotoxin levels

Pre-TIPSS insertion, positive intestinal fractional extraction rates of endotoxin were observed, confirming a gut-derived origin for endotoxaemia consistent with bacterial translocation. Negative hepatic endotoxin fractional extraction was observed consistent with hepatic clearance of endotoxin. This is reflected in the significant difference between portal and hepatic venous endotoxin concentrations observed prior to TIPSS insertion demonstrating the integrity of hepatic endotoxin clearance mechanisms and portal compartmentalization of endotoxin despite advanced disease. Previous studies evaluating markers of bacterial translocation pre-TIPSS are conflicting possibly due to the heterogeneity of the patient cohort studied. Benten *et al* described a trans-hepatic endotoxin gradient in a cohort of 8 patients whereas Mortensen *et al* demonstrated no trans-hepatic bacterial DNA or cytokine gradient in patients undergoing TIPSS. In both instances however, the indications for TIPSS insertion were mixed with a majority of refractory ascites over refractory variceal haemorrhage. Previous studies have suggested that the immunopathology of acutely unwell cirrhotics is different from stable decompensated disease.

Portal venous endotoxin concentration was found to be a predictor of survival in variceal haemorrhage. In other studies, markers of bacterial translocation such as bacterial DNA and systemic endotoxin have been found to be predictors of survival. This may be of particular importance in TIPSS insertion as the portal venous endotoxin load is rendered systemic with the attendant risk of a SIRS response. Markers of bacterial translocation and associated dysregulatory response may be important additional biomarkers to predict survival. Strategies to diminish portal venous endotoxin load and SIRS response are important adjunctive measures to predict outcome in the context of refractory variceal haemorrhage.

Significant differences in endotoxin-binding molecules were also observed in variceal haemorrhage. Lipopolysaccharide binding protein (LBP) and Bactericidal/permeability-increasing protein (BPI) are endotoxin-binding molecules produced by hepatocytes and polymorphonuclear cells, mediating pro- and anti-inflammatory responses respectively. In this study, we observed high intestinal fractional extraction rates for BPI in concert with high portal endotoxaemia. LBP intestinal fraction extraction rates whilst positive were considerably lower. The mechanism of this increase in BPI is not clear but suggests that that endotoxin-induced neutrophil degranulation, that has been shown in this study as evidenced by an elevated neutrophil burst is also accompanied by release of BPI.

4.4.2 Differential intra-splanchnic neutrophil function

In parallel to the finding of a trans-hepatic endotoxin gradient, we observed a 'compartmentalization' of neutrophil dysfunction. Portal venous neutrophils were found to exhibit pathologically heightened respiratory burst, which was significantly elevated compared to hepatic venous neutrophils within a range known to be associated with excess mortality. This neutrophil defect could be conferred or abrogated by co-incubation of portal venous or hepatic venous plasma respectively. Previous studies in patients with alcoholic cirrhosis demonstrated that a humoral factor, endotoxin, is responsible for mediating neutrophil dysfunction.

Portal venous neutrophil ROS production was found to significantly correlate with portal pressure gradient in this patient cohort. This observation is consistent with the current understanding that there is an additional dynamic component of portal hypertension driven by inflammation which may precipitate variceal haemorrhage. It reinforces the importance of strategies such as antibiotics to reduce bacterial translocation to diminish clinically relevant end-points such as portal pressure and goes some way to explaining the observation of reduced re-bleeding rates in patients

receiving empirical antibiotic therapy. Mechanistically, reactive oxidant species are known to scavenge nitric oxide, contribute to endothelial dysfunction and thus raise portal pressures. This study reinforces the importance of the trafficking portal-derived innate immune cells in determining haemodynamic status.

4.4.3 Differential intra-splanchnic cytokine levels

Significant positive intestinal IL10 fractional extraction rates were observed pre-TIPSS insertion in patients with variceal haemorrhage consistent with intestinal generation of IL10. The most likely origin of portal-derived IL10 is from local innate immune populations and enterocytes. Production of IL-10 is a key strategy the lamina propria macrophages employ to induce an inhibitory, tolerising immunological phenotype in the gut in response to enterocyte stress. Trafficking neutrophils may further contribute and indeed have been also shown to be significant IL10 producers in the context of advanced cirrhosis. Metabolic stress is evident in intestinal mucosa even in the context of stable cirrhosis. Portal hypertension with splanchnic venous stasis and associated hypoxia is a likely driver of this. Dysbiosis, bacterial metabolites such as acetaldehyde and nutritional factors may further contribute.

In contrast to the intestine, the liver has a negligible role in IL10 production but is a significant source of IL6. IL6 is generated by many different cell types within the liver including stimulated monocytes, fibroblasts and endothelial cells. Hepatocytes may also be directly stimulated to produce IL6 by factors such as bacterial endotoxin. In addition to regulation of the acute phase response, IL6 results in activation of hepatoprotective pathways, promoting hepatocellular proliferation in response to high portal venous endotoxin levels such as in the context of variceal haemorrhage.

IL6/IL10 ratio has been described in the sepsis literature as a measure of the predominant phenotype of the inflammatory response. In this study, whilst hepatic

venous and arterial IL6/IL10 ratios are similar, ratios in portal venous blood are more skewed towards an anti-inflammatory response.

4.4.4. The effect of TIPSS insertion

Systemic neutrophil function was found to be impaired following the insertion of TIPSS. This was manifest as a significant reduction in neutrophil phagocytosis and increase in resting burst and mirrors the rise in systemic endotoxaemia post-TIPSS. These observations are consistent with previous studies demonstrating significant increases in arterial endotoxin levels following TIPSS insertion associated with a significant increase in induced neutrophil oxidative burst (Jalan et al).

Early TIPSS therapy has been proposed after the study by García-Pagán et al. Our data highlights the potential risks of early TIPSS intervention which must be considered when deciding on an optimal treatment strategy for the patient. In light of the data from this study, it may be appropriate to consider adjunctive therapy with endotoxin-binding strategies to diminish systemic endotoxin levels following TIPSS placement.

This study demonstrates that in the context of variceal haemorrhage, a trans-hepatic gradient of endotoxin and associated neutrophil function is observed. TIPSS insertion disturbs this compartmentalisation and is associated with a significant deterioration in neutrophil function. Markers of bacterial translocation and pro-inflammatory response were found to be predictive of mortality post-TIPSS insertion highlighting the clinical importance of bacterial translocation. The data from this study demonstrates that it is compromised gut barrier integrity rather than defective hepatic immune surveillance mechanisms which are responsible for systemic endotoxaemia in cirrhosis even in the context of advanced disease. The subject of subsequent studies was therefore

characterisation of the gut liver axis in a model of cirrhosis and evaluation of a novel strategy to modulate this process.

Chapter 5

In Vitro Adsorption of Biological Targets in Liver Disease

5.1 Introduction

Yaq-001 (TE7/8) is an a synthetic activated carbon produced from phenolic resin with a high surface area and tailored bimodal porosity conferring adsorptive properties appropriate for a range of biologically-relevant mediators. Yaq-001 has a high adsorptive capacity for both larger biologically relevant mediators such as bacterial toxins and cytokines, which bind to meso/small macropores (2-50nm) in addition to smaller molecules such as bacterial metabolites which bind in the smaller micropores (<2nm). The controlled production of these carbons by phase separation during resin curing, pyrolysis followed by secondary phase separation, allows for tight control of pore size and consistency of product. This is in contrast to many other activated carbons which have a more heterogenous pore distribution, typically within the more microporous range. Figure 5.1 (a) demonstrates the internal porous structure of a Yaq-001 bead comprising both microporous and larger meso/macroporous domains. Figure 5.1 (b) demonstrates the cut surface of the Yaq-001 bead.

(a) (b)

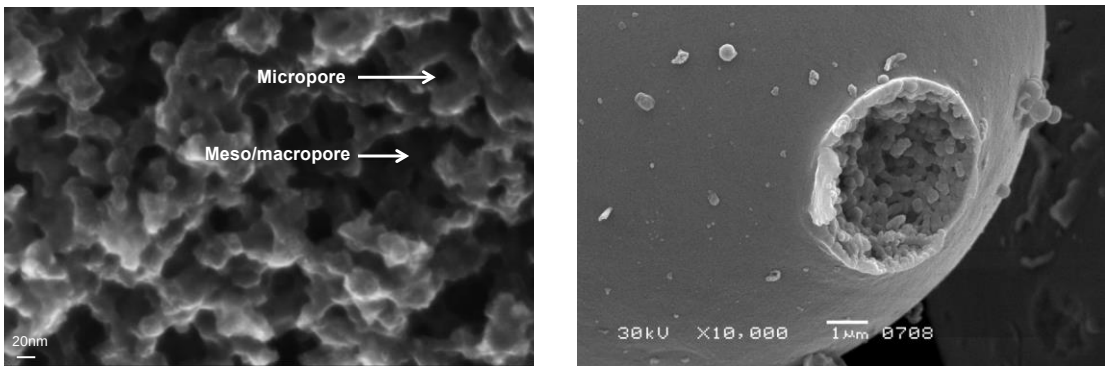

Figure 5.1 Electron micrograph images of Yaq-001 carbon beads (S Sandeman *et al* 2008)

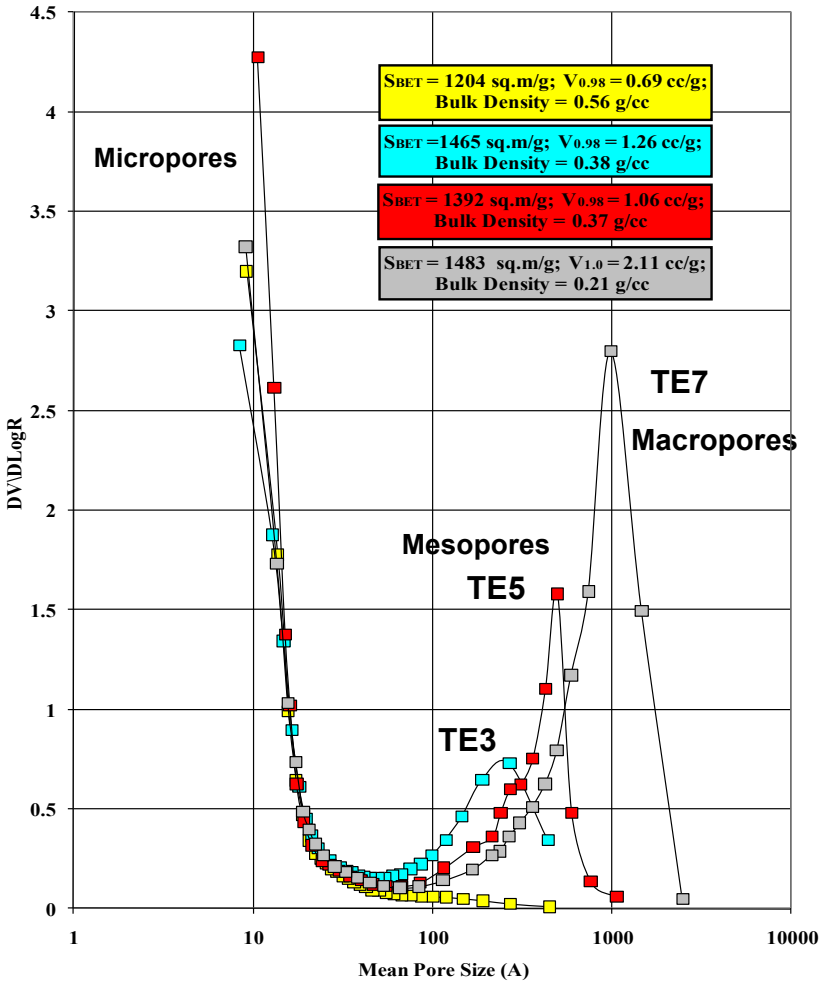

Figure 5.2 Pore size distribution of activated carbons TE3, TE5 and TE7 (Yaq-001)

5.2 Aims

The first objective of this study was to ascertain the optimal carbon porosity for *in vitro* adsorption of larger biologically relevant mediators for translation to *in vivo* studies. The second aim was to describe the adsorption kinetics of the selected carbon with endotoxin, cytokines and acetaldehyde. The third aim of this study was to ascertain whether Yaq-001 influenced the growth kinetics of gram positive and negative bacteria and thus exhibited an antibiotic-type effect.

5.3 Results

5.3.1 Studies to determine optimal carbon porosity for *in vivo* studies

Carbons of a range of pore sizes (TE1-9) were studied to determine their differential adsorptive properties for pro-inflammatory cytokines. The carbons ranged from the smallest pore sizes (microporous carbon TE1), through the medium sized or mesoporous carbons such as TE5 to the largest pore size, meso/macroporous carbon TE9. TE7/8 (Yaq-001) was found to have the best combination of high surface area and pore volume contributing to high adsorptive properties. Functionally, this translated to superior binding of TNFα and IL-6 removal by TE7 (Yaq-001) compared to beads of both larger and smaller pore sizes (figure 5.4 and 5.5). Figure 5.6 expresses the data as an adsorption isotherm demonstrating excellent TNFα adsorption by Yaq-001 from simulated intestinal fluid.

Sample	Bead Diameter (μm)	Surface Area S_{BET} (m^2g^{-1})	Pore Volume (cm^3g^{-1})	Bulk Density (g cm^{3-1})	Mean mesopore diameter (nm)
TE1	250-500	1204	0.69	0.56	microporous
TE3	250-500	1465	1.30	0.38	30
TE5	250-500	1493	1.75	0.27	70
TE7	250-500	1483	2.11	0.21	80
TE9	250-500	1236	1.61	0.18	120

Table 5.1 Physical properties of carbons TE1-9

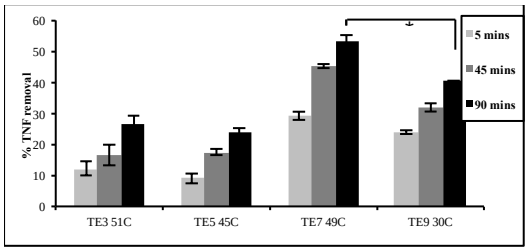

Figure 5.3 TNFα adsorption kinetics (n=3, Mean ± SEM)

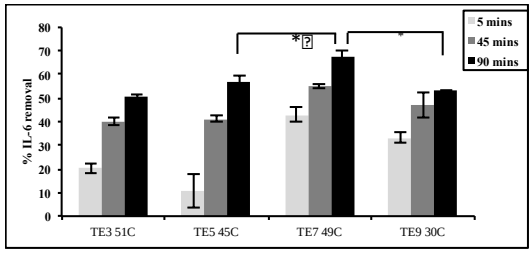

Figure 5.4 IL-6 adsorption kinetics (n=3, Mean ± SEM)

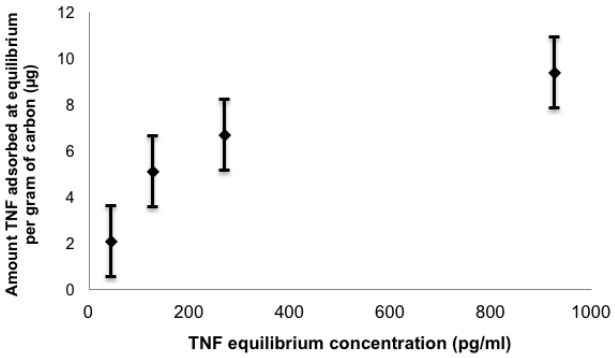

Figure 5.5 Adsorption isotherm showing carbon adsorption of TNFα from simulated intestinal fluid (n=4, Mean ± SEM) (S Sandeman et al, 2008)

5.3.2 Studies to determine adsorption kinetics of Endotoxin

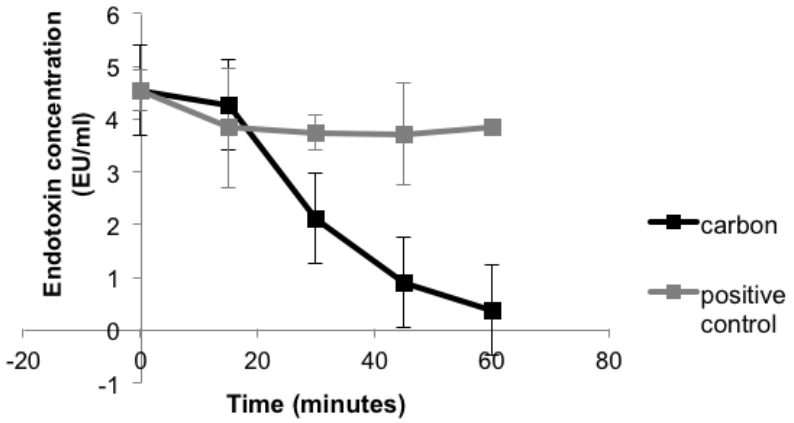

Figure 5.6 Adsorption kinetics of carbon for *E. coli* endotoxin (n=3, Mean ± SEM)

The concentration of endotoxin detected in the simulated intestinal fluid (SIF) solution initially spiked with 10 EU ml-1 declined from a detected value of 4.5 EU ml-1 at time 0 to 0.4 EU ml-1 following 60 minutes incubation with the TE7/8. The control solution maintained a steady 4.5 EU ml-1 concentration over time. These findings demonstrate rapid endotoxin adsorption kinetics.

5.3.3 Studies to determine adsorption kinetics of Acetaldehyde

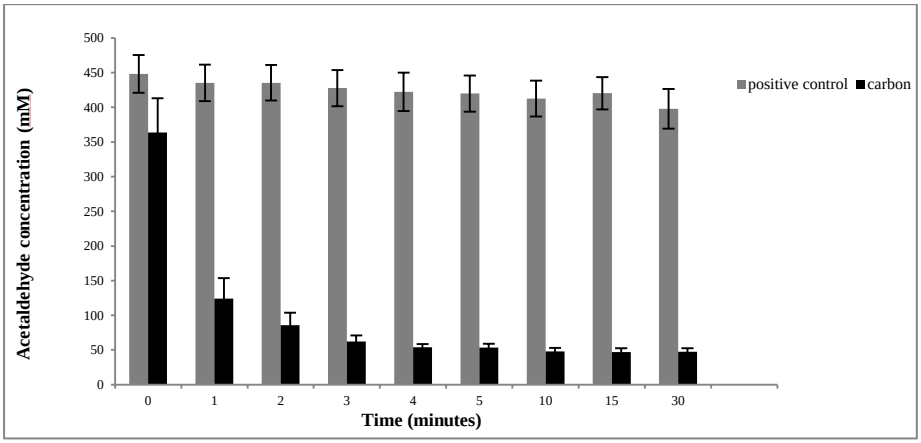

Figure 5.7 Acetaldehyde removal over time by TE8 carbon compared to no carbon control (n=3, Mean ± SEM)

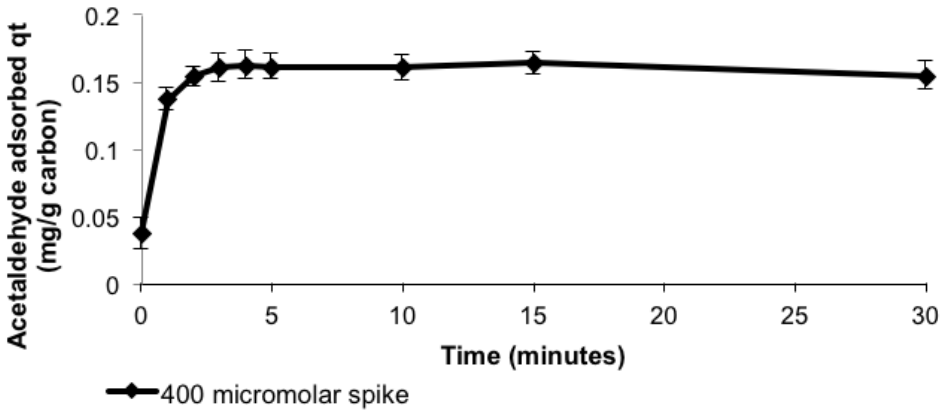

Figure 5.8 Carbon acetaldehyde adsorption kinetics expressed as quantity of acetaldehyde adsorbed (mg g^{-1}) with time (n=3, Mean ± SEM)

Rapid acetaldehyde adsorption kinetics were observed with TE8 (Yaq-001) carbon. The majority of the acetaldehyde was removed after an incubation time of 1 minute at room temperature following a spike of acetaldehyde in simulated intestinal fluid. By 3 minutes, incubation of carbon with acetaldehyde solution an equilibrium adsorptive capacity of 0.16g per gram of carbon was reached using a 400 □M acetaldehyde spike.

5.3.4 Studies to determine effects of carbon on bacterial growth kinetics

5.3.4.1 Investigating the effect of direct contact incubation of carbons on bacterial metabolism

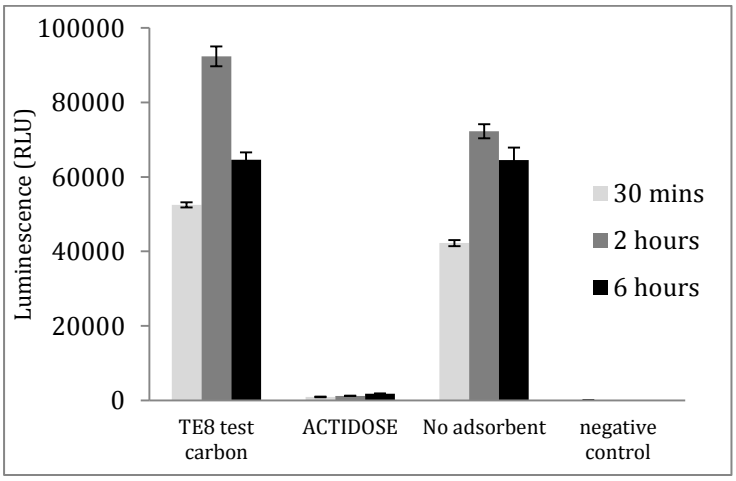

Figure 5.9 Effect of TE8 carbon on *E. coli* growth kinetics (BacTitre-Glo microbial cell viability assay) expressed as luminescence signal following direct contact with E. coli over time (innoculum $3.9x10^9$ bacteria ml^{-1}) (n=3 per group, Mean ± SEM)

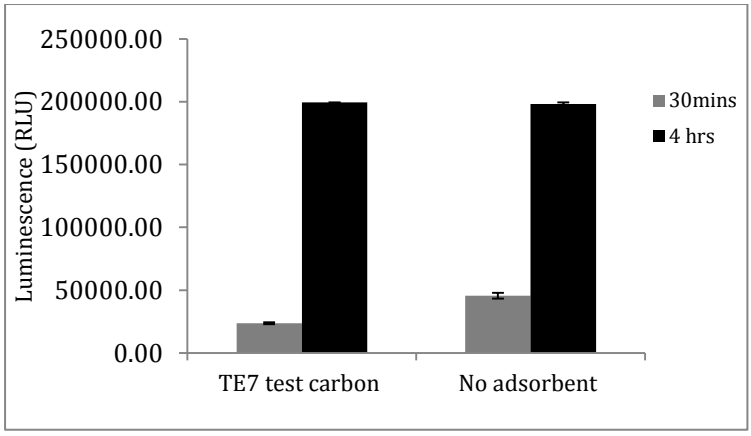

Figure 5.10 The effect of TE7 test carbon on *Staphylococcus aureus* bacterial growth kinetics (BacTiter-Glo microbial cell viability assay) expressed as luminescence signal following direct contact with *S. aureus* over time (Inoculum $7.5 x10^7$ bacteria ml^{-1}) (n=3, Mean ± SEM).

The luminescence measurement is an indirect measure of cell viability and cell number via the determination of bacterial ATP. Levels of luminescence, reflective of bacterial metabolism on sample contact, were comparable to the no adsorbent

control for both species over the time course of the experiment. Therefore the direct incubation of TE7/8 carbons with bacterial suspensions of either *E. coli* or *Staphylococcus aureus* in culture medium had no significant effect on bacterial growth kinetics following direct contact for 4 to 6 hours. In contrast, the control commercial oral carbon significantly reduced the luminescence signal following only 30 minutes incubation of bacteria with carbon.

5.3.4.2 Studies to determine the effect of carbon leachate on bacterial metabolism

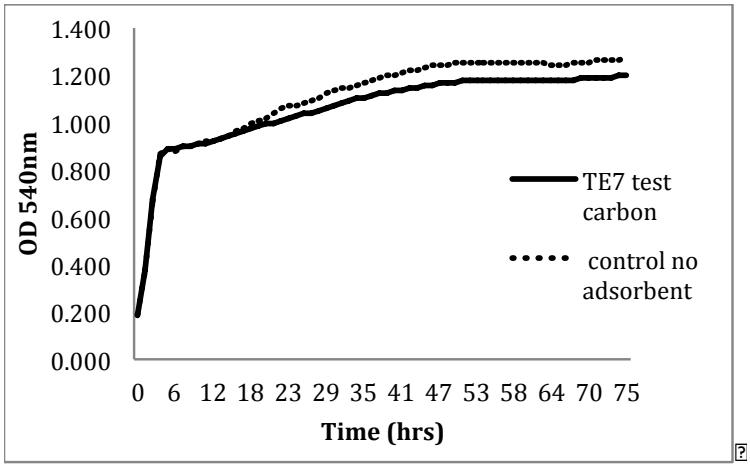

Figure 5.11 The effect of TE7 test carbon leachate on growth kinetics of *E. coli* over time as measured by Bioscreen turbidometric analyser (540nm) (n=4).

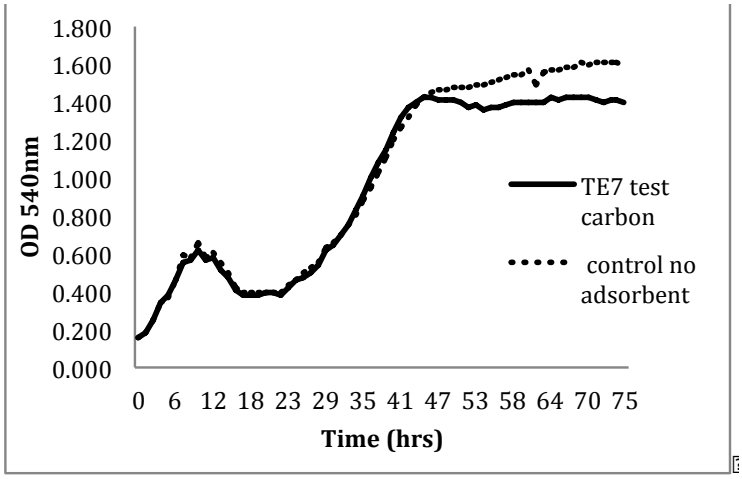

Figure 5.12 The effect of TE7 test carbon leachate on growth kinetics of *Bacillus subtilis* over time as measured by Bioscreen turbidometric analyser (540nm) (n=4).

The optical density (OD) measurement is an indirect measure of bacterial number. OD values for the TE7 sample were comparable to the no adsorbent control for both species over the time course of the experiment. The direct incubation of TE7 carbon leachate with bacterial suspensions of either *E. coli* or *Bacillus subtilis* in culture media for 72 hours therefore did not result in a significant difference in bacterial growth kinetics for either species.

5.4 Discussion

In summary, *in vitro* studies demonstrate that activated Yaq-001 carbons exhibit rapid adsorption kinetics for endotoxin, pro-inflammatory cytokines and acetaldehyde with no significant impact on bacterial growth kinetics. They therefore exhibit optimal properties of an oral strategy in liver disease ie binding of important intraluminal factors which drive pathogenesis without exerting an antibiotic effect on the resident bacterial flora with the attendant risks of dysbiosis. Furthermore, these carbon particles are non-absorbable and therefore mediate their effect locally at the gut-barrier interface.

These studies identified that TE7/8 carbons (hereafter termed Yaq-001) exhibit optimal adsorptive properties for binding both larger biologically relevant molecules such as endotoxin and cytokines together with other bacterial metabolites such as acetaldehyde. These carbons were therefore selected for further evaluation as an oral intervention in *in vivo* models of liver disease.

Chapter 6

Validation of the Bile Duct Ligated Rat model

6.1 Introduction

The bile duct ligated (BDL) rat model is an established surgical model of secondary biliary cirrhosis. It has been used widely in animal studies of cirrhosis and has features of portal hypertension at 4 weeks. Low dose intra-peritoneal administration of lipopolysaccharide (LPS) to 4 week BDL rats (BDL+LPS) has been considered as a model of acute-on-chronic liver failure (ACLF).

6.2 Aims

The aims of this study were to validate the 4 week bile duct ligated rat model as a model of cirrhosis, portal hypertension and bacterial translocation. A secondary objective was to characterise the 4 week bile duct ligated rat model with intraperitoneal lipolysaccharide as a model of acute on chronic liver failure.

6.3 Results

A significant increase in alanine transaminase was observed in bile duct ligated rats after 4 weeks (73.95 $\pm$4.10 IU/ml) compared to sham controls (48.45 $\pm$2.45 IU/ml) ($p<0.0001$). This was found to be associated with a significant decrease in albumin (BDL 24.63 $\pm$1.10 vs Sham 32.73 $\pm$ 1.20 g/dL) ($p<0.0001$) and a significant increase in alkaline phosphatase and bilirubin (BDL 230.60 $\pm$ 13.16 vs Sham 108.10 $\pm$ 17.65 IU/L) and (BDL 142.20 $\pm$ 6.00 vs Sham 1.3 $\pm$ 0.15 µmol/L) ($p<0.0001$) consistent with a surgical cholestatic model. A significant increase in plasma creatinine was observed in BDL rats compared to sham controls (BDL 32.01 $\pm$ 1.00 vs 28.33 µmol/L ($p=0.01$) although no significant increase in urea was observed.

6.3.1 Biochemical Profile

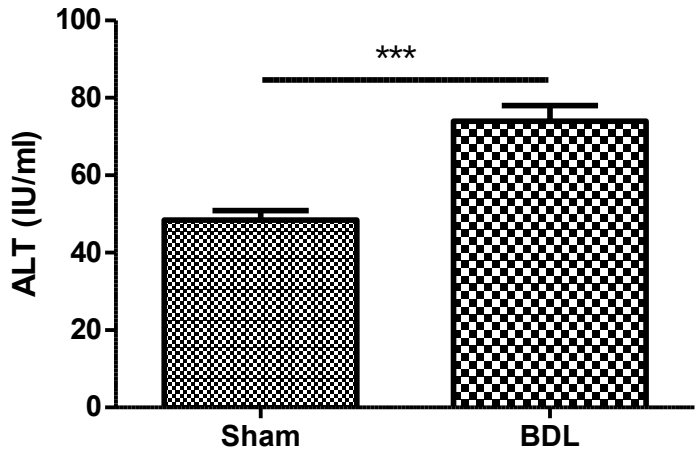

Figure 6.1 Biochemical evidence of liver injury in Sham vs BDL rats as evidenced by plasma alanine transaminase levels (Sham n=23, BDL n=25)
*** denotes p<0.001

(a)

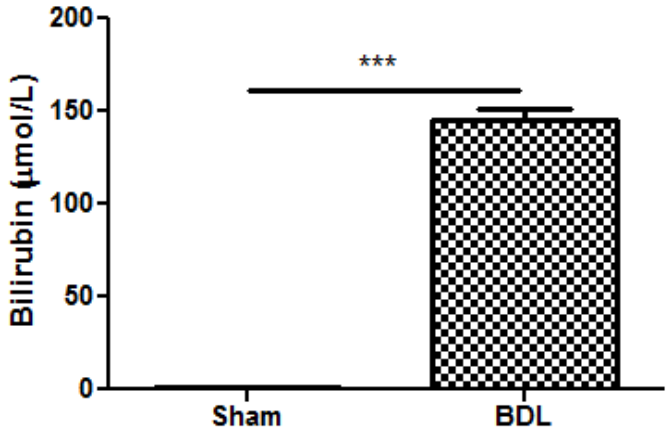

(b)

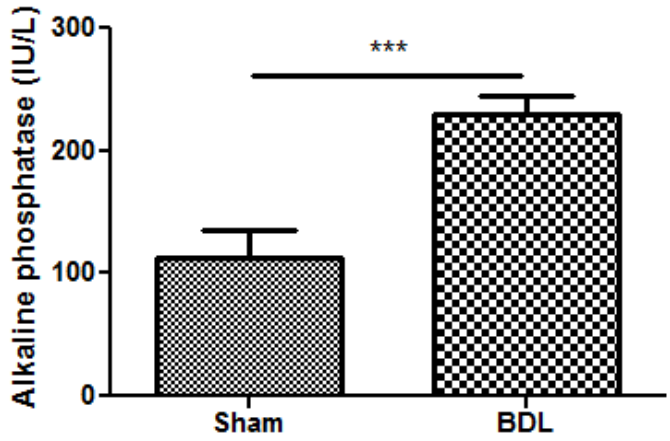

Figure 6.2 Biochemical evidence of cholestasis in Sham vs BDL rats as evidenced by (a) plasma bilirubin (Sham n=23, BDL n=25)

(b) alkaline phosphatase levels (Sham n=21, BDL n=25)
*** denotes p<0.001

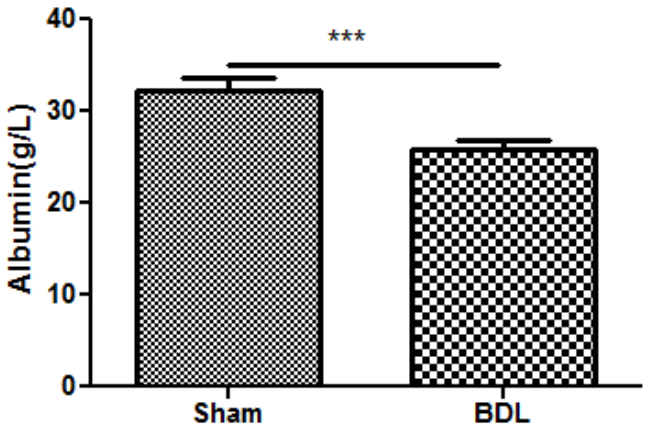

Figure 6.3 Biochemical evidence of liver synthetic function in Sham and BDL rats as evidenced by plasma albumin levels (Sham n= 22, BDL n=24)
*** denotes p<0.001

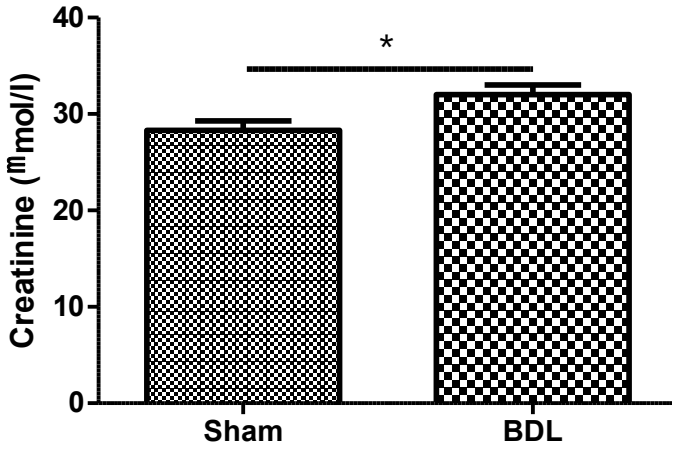

Figure 6.4 Biochemical evidence of renal function as evidenced by plasma creatinine in sham and BDL rats (Sham n=23, BDL n=22)
* denotes p<0.05

6.3.2 Histological Profile

Bile duct ligation was associated with a significant increase in collagen proportionate area quantified on digital image analysis (14.44 ± 4.38 vs 1.59 ± 0.00%). The increase in collagen deposition in bile duct ligated rats was associated with architectural disturbance evidenced by cholestasis, cholangiocyte proliferation and nodule formation. Such features were not evident on liver histology of sham-operated rats.

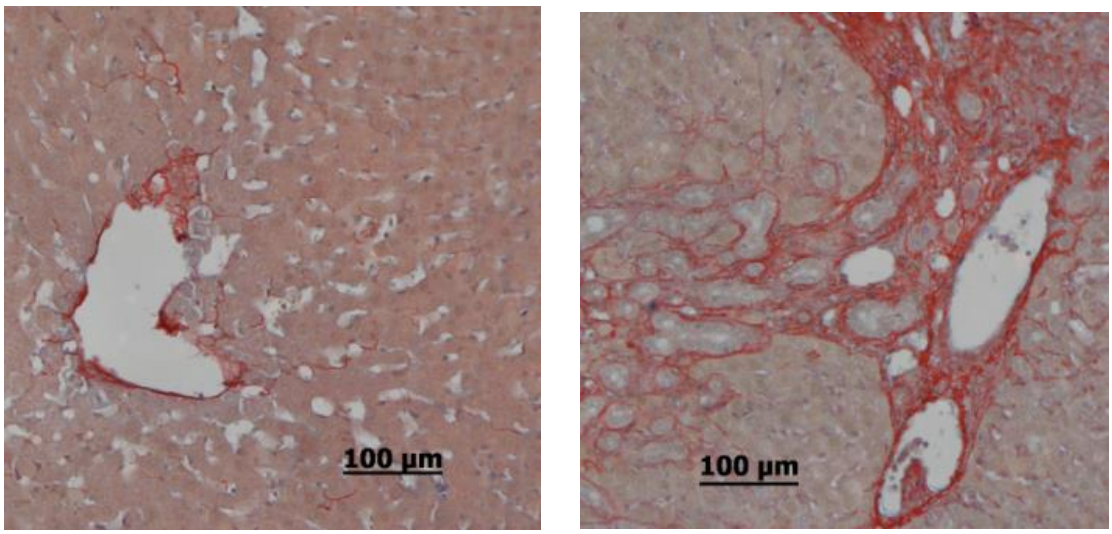

Figure 6.5 Collagen staining of liver tissue with Sirius Red stain in (a) sham and (b) BDL rats

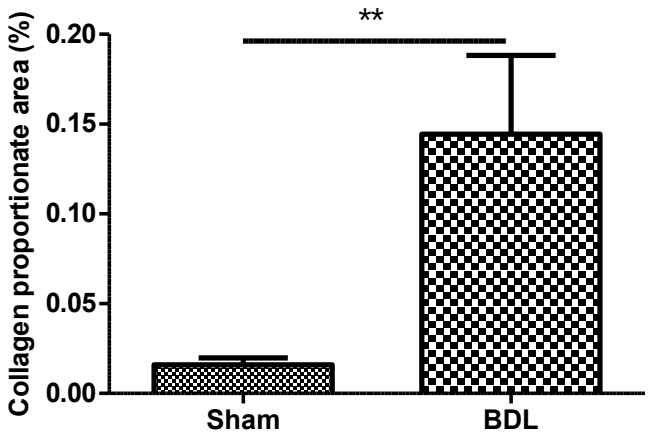

Figure 6.6 Quantification of collagen staining by digital image analysis of Sirius red stained liver histology in sham and BDL rats as a marker of liver fibrosis (Sham n=6, BDL n=8)
** denotes p<0.005

6.3.3 Haemodynamic Profile

Bile duct ligation was observed to be associated with a significant increase in portal pressure (BDL 11.86 ± 0.56 vs Sham 5.70 ± 0.38 mm Hg) (p<0.0001). A significant reduction in mean arterial pressure was also observed in BDL rats compared to sham controls (BDL 84.17 ± 5.76 vs Sham 112.70 ± 3.53 mm Hg) (p=0.0006).

Portal Pressure

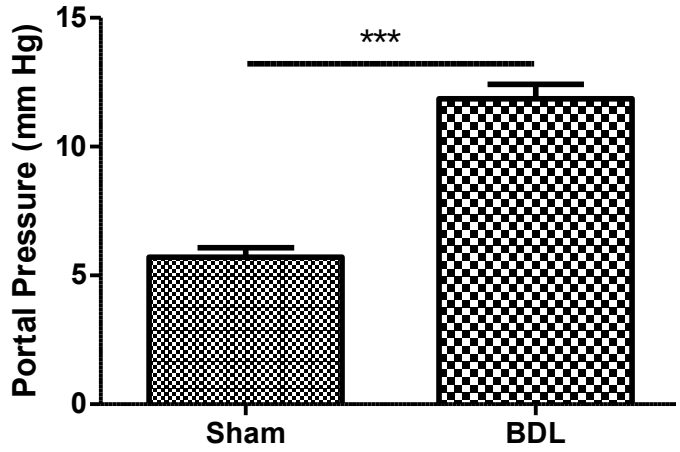

Figure 6.7 Portal haemodynamics in Sham and BDL rats at 4 weeks (Sham n=21, BDL n=15)
*** denotes p<0.001

Mean Arterial Pressure

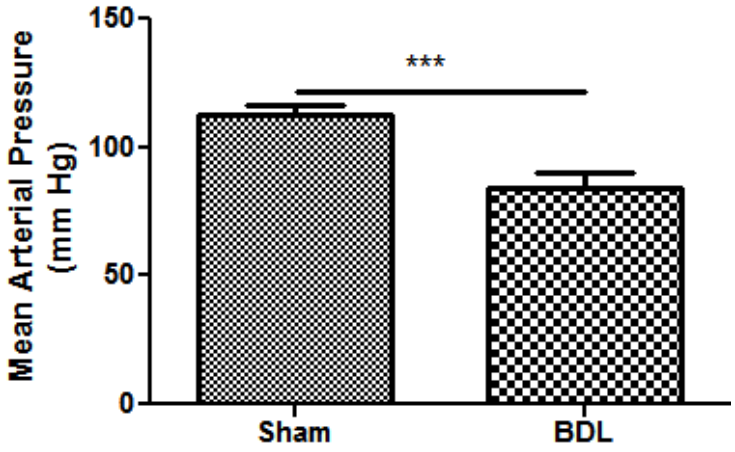

Figure 6.8 Systemic haemodynamics in Sham and BDL at 4 weeks (Sham n=13, BDL n=12) *** denotes p<0.001

6.3.4 Body weight

4 weeks post-surgery

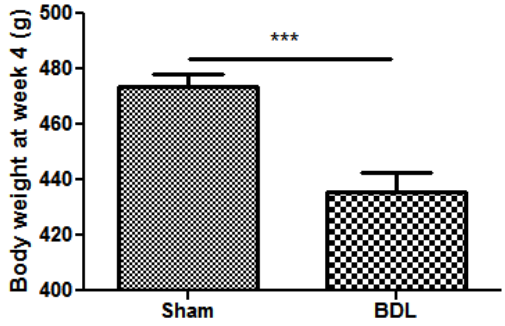

Figure 6.9 Final body weight (g) (Sham n=27, BDL n=27)
*** denotes p<0.001

Percentage body weight increase in 4 weeks post-surgery

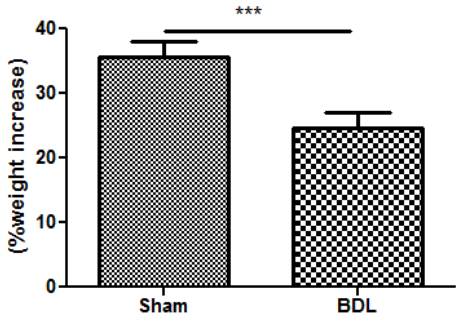

Figure 6.10 Percentage body weight increase in 4 weeks post-surgery (Sham n=27, BDL n=26)
*** denotes p<0.001

Bile duct ligation was associated with a significantly lower final body weight (BDL 435.6 $\pm$ 7.70 vs Sham 474.00 $\pm$ 5.46 g) (p=0.0003) and percentage body weight increase compared to sham controls (BDL 24.70 $\pm$ 2.30% vs Sham 35.56 $\pm$ 2.44) (p=0.0008). Of note, the rats were pair fed and of equivalent body weight (240-280g) at the time of surgery.

6.3.5 Markers of Bacterial Translocation

Endotoxin Levels (PVP)

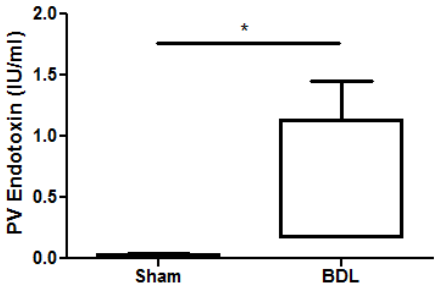

Presence of Bacterial DNA (PVP)

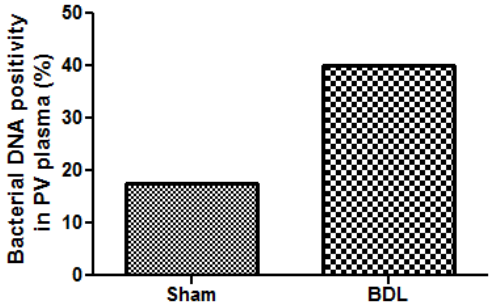

Figure 6.11 Quantification of portal venous endotoxin in sham vs BDL rats as determined by the chromogenic limulus amoebocyte lysate kinetic assay (Sham n=6, BDL n=4)

Figure 6.12 Bacterial DNA positivity in portal venous plasma in sham and BDL rats (Sham n=6, BDL n=5)

* denotes p<0.05
PVP = Portal venous plasma

Mesenteric Lymph Node Positivity

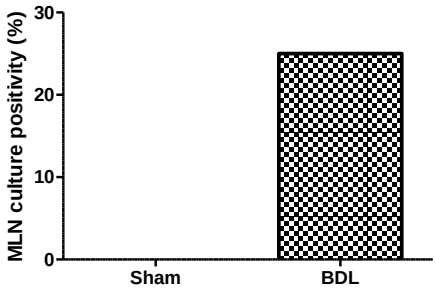

Figure 6.13 Mesenteric Lymph Node Culture Positivity in sham and BDL rats (n=4/group)

The four week bile duct ligation rat model was found to be associated with a significant increase in portal venous endotoxin (BDL 0.50 $\pm$ 0.32 vs Sham 0.01 $\pm$ 0.01 IU/ml) (p=0.01) and bacterial DNA positivity compared to sham controls (BDL 40% vs Sham 17.5%). Translocation of viable bacteria as determined by mesenteric lymph node culture was found to be 25% in BDL rats compared to 0% in sham controls.

6.3.6 Other metabolic parameters

Arterial Ammonia levels

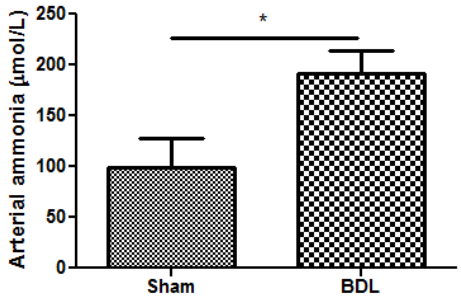

Glucose

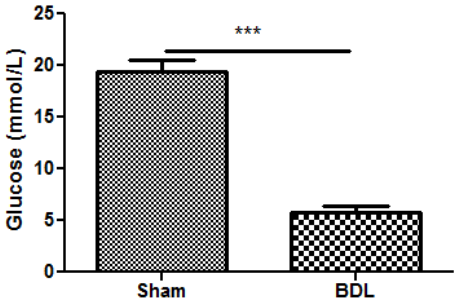

Figure 6.14 Arterial ammonia concentrations in BDL vs sham rats (Sham n=6, BDL n=15)
* denotes p<0.05

Figure 6.15 Plasma glucose concentrations in BDL vs sham rats (Sham n=11, BDL n=13)
*** denotes p<0.001

Lactate

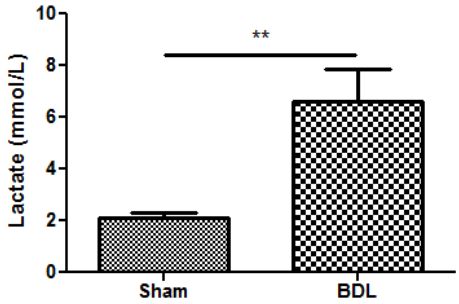

Figure 6.16 Plasma lactate concentrations in BDL vs sham rats (Sham n=8, BDL n=4)
** denotes p<0.005

Significantly higher arterial ammonia levels were observed in BDL rats compared to sham controls (BDL 170.10 $\pm$ 14.64 vs Sham 98.63 $\pm$ 28.73) (p=0.03). Plasma glucose concentrations were significantly lower in BDL rats compared to sham controls (BDL 5.70 $\pm$ 0.53 vs Sham 19.02 $\pm$ 1.15) (p<0.0001). Plasma lactate was significantly higher in BDL rats compared to sham controls (BDL 6.60 $\pm$ 1.26 vs Sham 2.12 $\pm$ 0.17 mmol/L) (p=0.004).

6.3.7 BDL + LPS Model

The BDL LPS model has been used as a model of acute on chronic liver failure. 4-5 week bile duct ligated rats undergo intra-peritoneal *Klebsiella pneumoniae* lipopolysaccharide injection 3.5 hours prior to sample collection. As evidenced by the results in figure 6.18, the BDL model is associated with a significant increase in organ injury as evidenced by a significant increase in ALT and creatinine. This is associated with a significant increase in portal pressure.

	Sham (Mean+SEM)	**Sham+LPS (Mean+SEM)**	**BDL (Mean+SEM)**	**BDL+LPS (Mean+SEM)**
ALT (IU/ml)	48.45±2.45	69.94±11.09	73.95±4.10	99.93±6.66
Creatinine (micmol/L)	28.33±0.96	24.29±1.44	32.01±1.00	40.77±3.88
Albumin (g/dL)	32.17±1.42	34.08±0.72	25.84±1.07	24.39±1.60
Alkaline phosphatase (IU/ml)	113.4±21.55	116.9±18.53	229.9±15.31	322.5±69.46
Portal pressure (mmHg)	5.70±0.38	8.48±0.96	11.86±0.56	15.86±1.05
Mean Arterial Pressure (mmHg)	112.70±3.53	102.70±5.11	84.17±5.76	102.4±5.73

	Sham vs BDL	**BDL vs BDLLPS**	**ShamLPS vs BDLLPS**	**Sham vs ShamLPS**
ALT (IU/ml)	p<0.0001	p=0.004	p=0.03	ns
Creatinine (micmol/L)	p=0.01	p=0.0495	p=0.004	p=0.03
Albumin (g/dL)	P<0.0001	ns	p=0.01	ns
Alkaline phosphatase (IU/ml)	p<0.0001	ns	p=0.01	ns
Portal pressure (mmHg)	p<0.0001	p=0.005	p=0.002	p=0.001
Mean Arterial Pressure (mmHg)	p=0.0006	p=0.07	ns	ns

Table 6.1 Biochemical and Haematological Profile (BDL+LPS Model)

Liver Histology

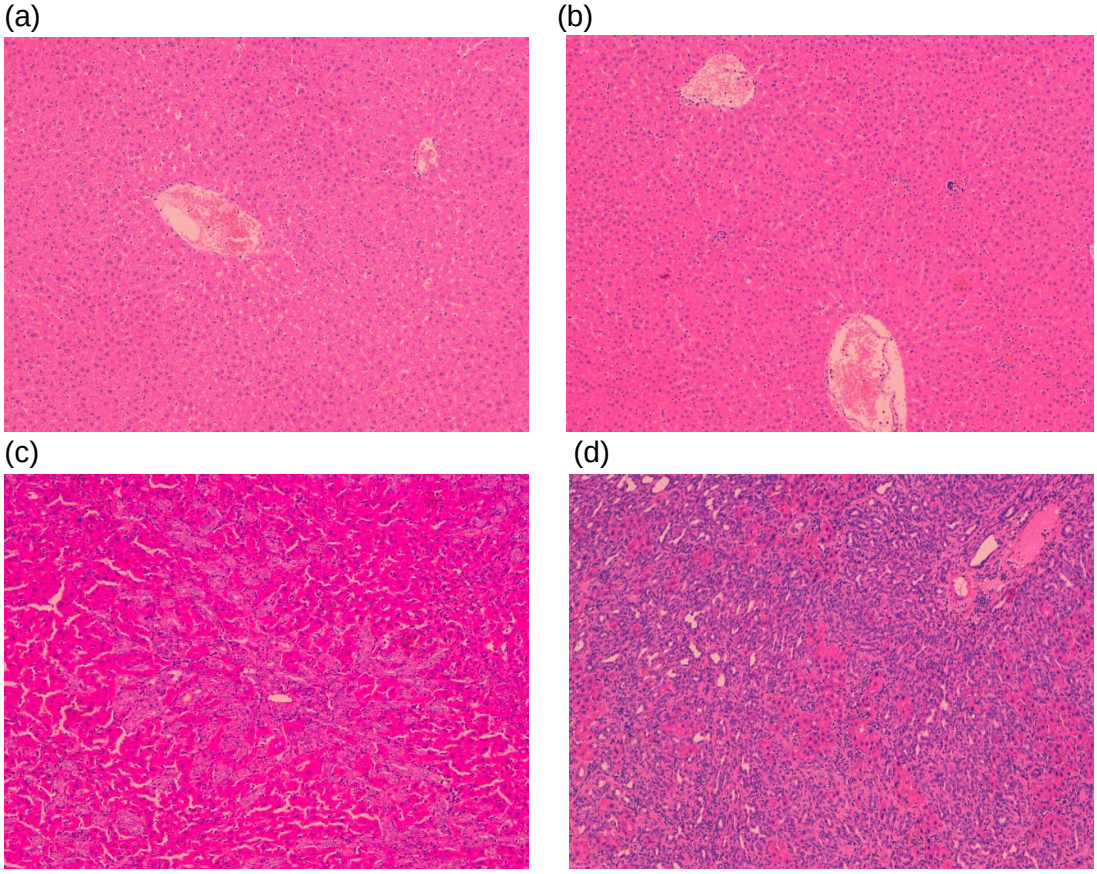

Figure 6.17 Liver histology (Haemaoxylin and Eosin)

(a) Sham (b) sham+LPS (c) BDL (d) BDL+LPS

Bile duct ligation is associated with cholangiocyte proliferation, nodule formation and inflammatory infiltrate. A marked increase in inflammatory infiltrate is observed in the BDL+LPS rats at 4 weeks compared to BDL alone.

These observations demonstrate that cirrhotic rats are exquisitely sensitive to endotoxin challenge and this is manifest by exacerbation of organ injury and portal pressure, clinically relevant biological determinants of outcome in cirrhotic patients.

6.4 Discussion

The 4 week bile duct ligated (BDL) rat model was associated with a significant increase in alanine transaminase (ALT) and bilirubin compared to sham controls indicative of cholestatic liver injury. A significant reduction in albumin was observed consistent with a reduction in liver synthetic function. A significant increase in plasma creatinine was observed in bile duct ligated rats compared to sham controls indicative of renal injury in the disease group.

BDL was also found to be associated with significant differences in both splanchnic and systemic haemodynamic status as compared to sham controls. A significant increase in portal pressure was observed in BDL rats associated with a significant reduction in mean arterial pressure. Degree of fibrosis was found to be significantly increased in BDL rats as quantified by digital image analysis of Sirius red stained liver tissue. A significant difference in nutritional status as evidenced by final body weight and percentage body weight increase was also observed. As the animals were pair fed, this discrepancy may be attributed to a heightened catabolic state in bile duct ligated rats.

BDL rats were found to have significantly higher markers of bacterial translocation. Phenotypically, Bile duct ligation was associated with heightened endotoxin-sensitivity *in vivo* with regards to organ injury and portal haemodynamic status. Taken together, the BDL model is one of bacterial translocation and a primed state to endotoxin challenge. The BDL+LPS model is associated with further increased inflammation, organ injury and portal pressure.

The features of this model which are of particular clinical relevance include portal hypertension, liver injury (both inflammatory and fibrotic) and gut barrier dysfunction. Subsequent studies were directed towards characterising the relative contribution of the three key factors promoting bacterial translocation, namely integrity of gut barrier, innate immune response and gut dysbiosis.

Chapter 7

Characterisation of the Gut-Liver axis in Bile Duct Ligated Rats

7.1 Introduction

Bacterial translocation rates are principally determined by three key factors: gut barrier integrity, bacterial overgrowth and immune status. The relative contribution of these factors is not clearly understood. A key early objective of this study was to determine the functional and structural integrity of the intestinal barrier in a model of cirrhosis and portal hypertension, the BDL rat and to complement these studies by characterisation of the microbiome and innate immune response along the gut-liver axis. The exact site of bacterial translocation remained unknown and so therefore all four regions of the small and large intestine were studied: duodenum, jejunum, terminal ileum and colon by light microscopy and duodenum and colon by electron microscopy. These studies were complemented by functional assessments.

7.2 Aims

The aims of this study were to characterize elements of the gut-liver axis which may contribute to bacterial translocation and disease progression. The three broad areas studied were integrity of the gut-barrier interface, innate immune phenotype and gut microbiota composition and function.

7.3 Results

7.3.1 Light microscopy

7.3.1.1 Duodenum

1 (a) 1 (b)

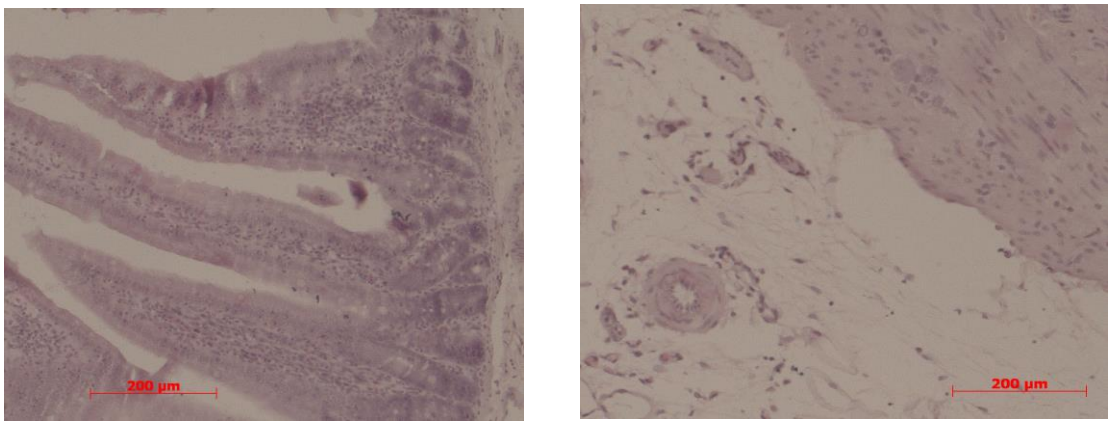

2 (a) 2 (b)

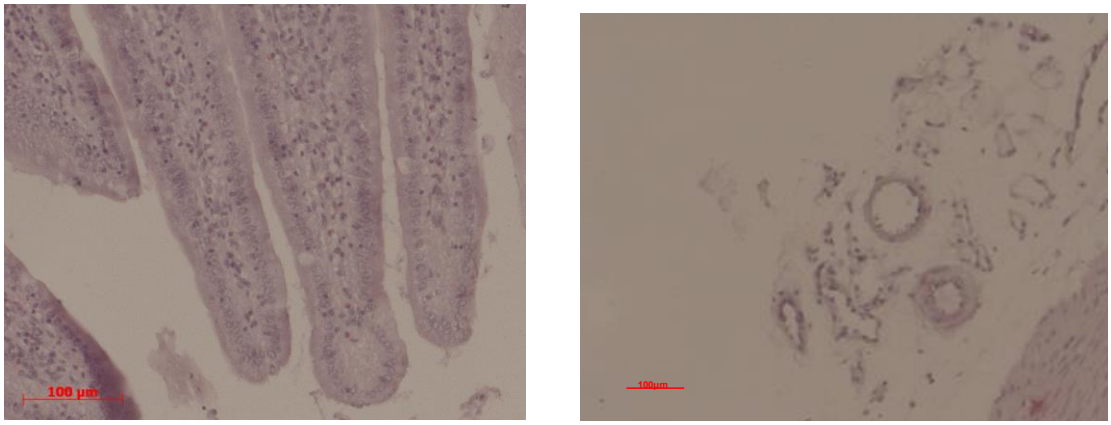

Figure 7.1 Light microscopy images of duodenum (H&E)

1 (a) Sham mucosa (b) Sham sub-mucosa and mesentery
2 (a) BDL mucosa (b) BDL sub-mucosa and mesentery

Normal appearances of duodenal villi, submucosa and mesentery with associated vasculature were observed on light microscopy in BDL rats compared to sham controls.

7.3.1.2 Jejunum

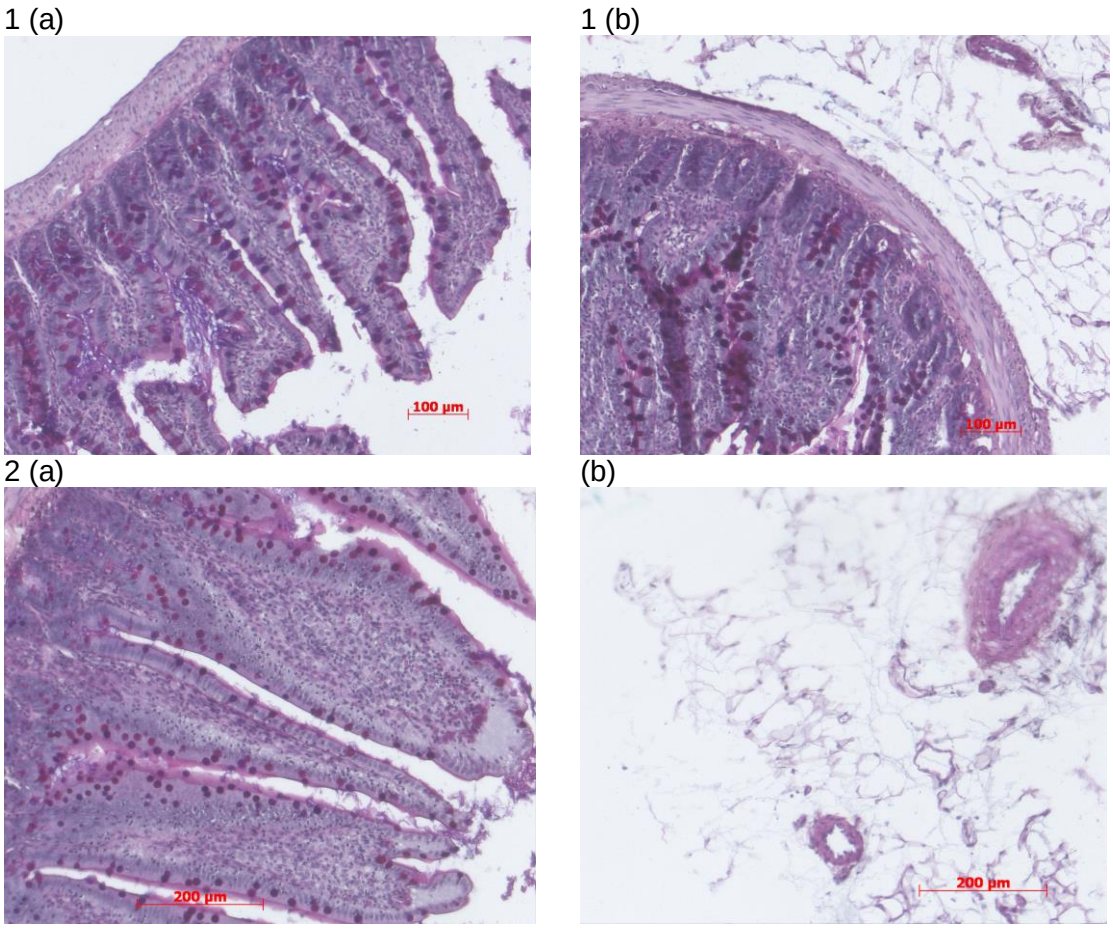

Figure 7.2

Light microscopy images of jejunum (H&E& Alcian blue)

1	(a) Sham mucosa	(b) Sham sub-mucosa and mesentery
2	(a) BDL mucosa	(b) BDL sub-mucosa and mesentery

Normal appearances of jejunal villi, submucosa and mesentery with associated vasculature were observed on light microscopy in BDL rats compared to sham controls.

7.3.1.3 Ileum

1 (a) 1 (b)

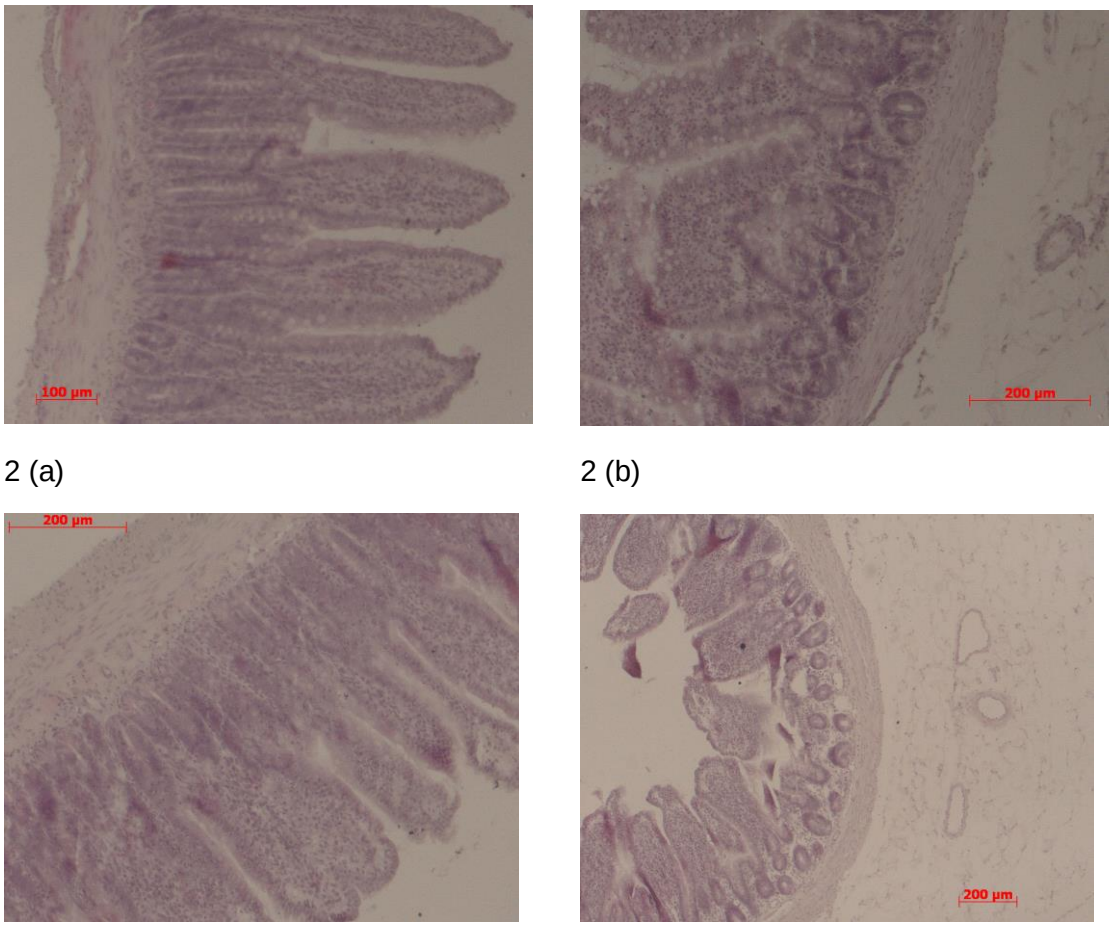

2 (a) 2 (b)

Figure 7.3 Light microscopy images of ileum (H&E)

1 (a) Sham mucosa (b) Sham sub-mucosa and mesentery
2 (a) BDL mucosa (b) BDL sub-mucosa and mesentery

Normal appearances of ileal villi, submucosa and mesentery with associated vasculature were observed on light microscopy in BDL rats compared to sham controls.

7.3.1.4 Colon

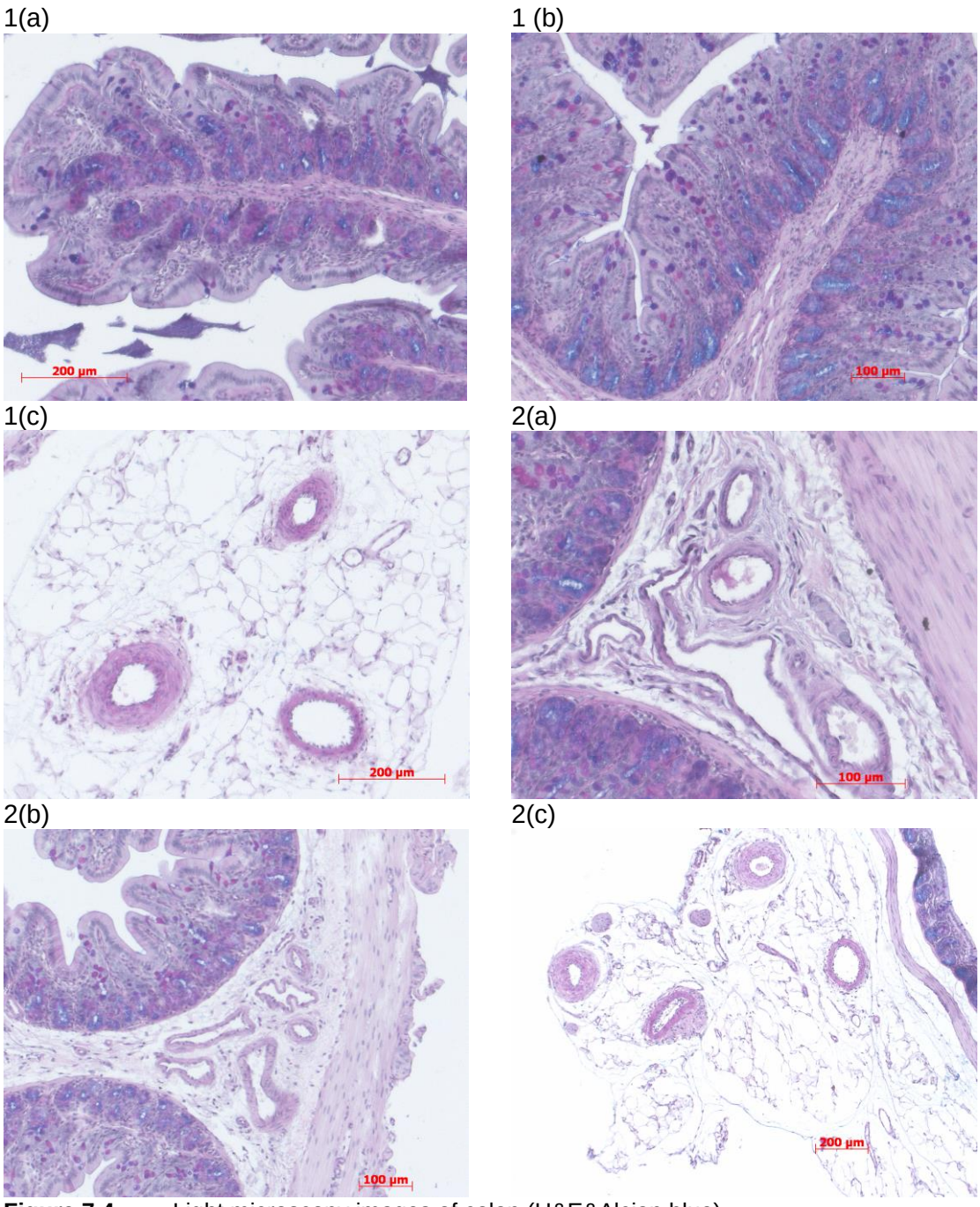

Figure 7.4 Light microscopy images of colon (H&E&Alcian blue)

1 (a) Sham mucosa (b) Sham sub-mucosa and mesentery (c) Sham mesentery
2 (a) BDL mucosa (b) BDL sub-mucosa and mesentery (c) BDL mesentery

Normal appearances of colonic villi was observed in BDL rats compared to sham controls. Slight tortuosity of the sub-mucosal vessels with perivascular inflammation in the smaller mesenteric vessels close to the peritoneal surface was observed in colonic tissue in BDL rats.

Light microscopy was performed on full thickness intestinal tissue at multiple sites along the gastrointestinal tract: duodenum, mid-jejunum, terminal ileum and colon. No significant mucosal abnormality was identified at any of these sites. With no clear breach in the mucosal surface, studies were conducted to evaluate ultra-structural features of the duodenal and colonic mucosa.

7.3.2 Electron microscopy

Qualitative analysis of electron microscopy images was performed by an independent expert histopathologist. No gross ultra-structural abnormalities were observed in the duodenum of cirrhotic compared to control rats although subtle changes were observed. These changes included widening of the inter-villus space was observed in the duodenum of BDL rats compared to sham controls (figures 7.6 and 7.5 respectively) and blunting of the microvilli (figures 7.8 vs 7.7). The sub-mucosa of duodenal tissue was more ragged in BDL rats (figure 7.10) compared to sham controls (figure 7.9). No ultra-structural abnormalities were observed in the colonic tissue of BDL or sham rats. Of note, microvilli and tight junctions remained intact suggestive that architectural disturbance is not a feature of this model.

7.3.2.1 Electron Microscopy of the Duodenum

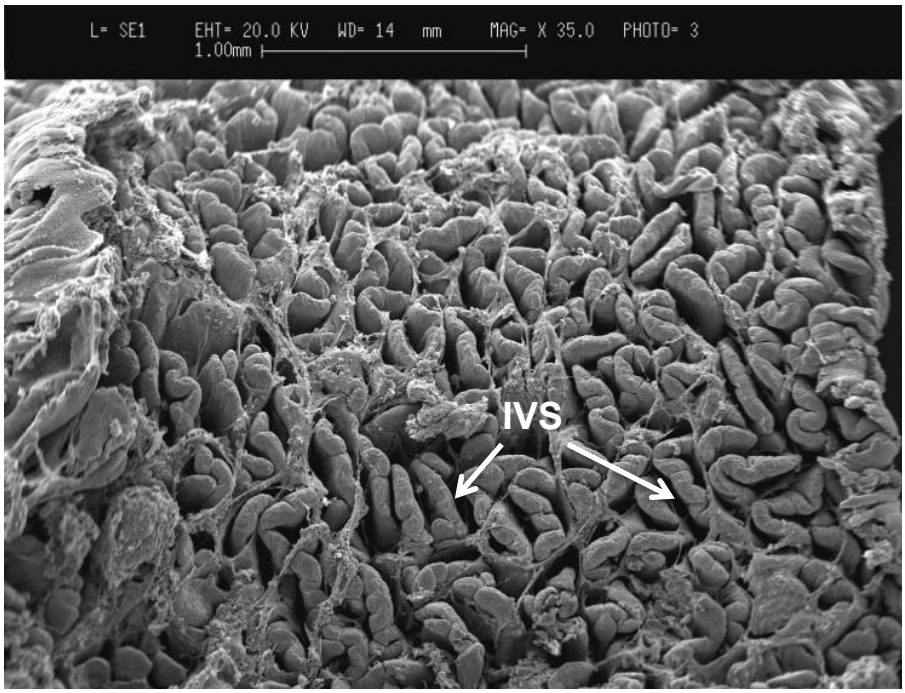

Figure 7.5 Electron micrograph of duodenal tissue in sham operated rats.

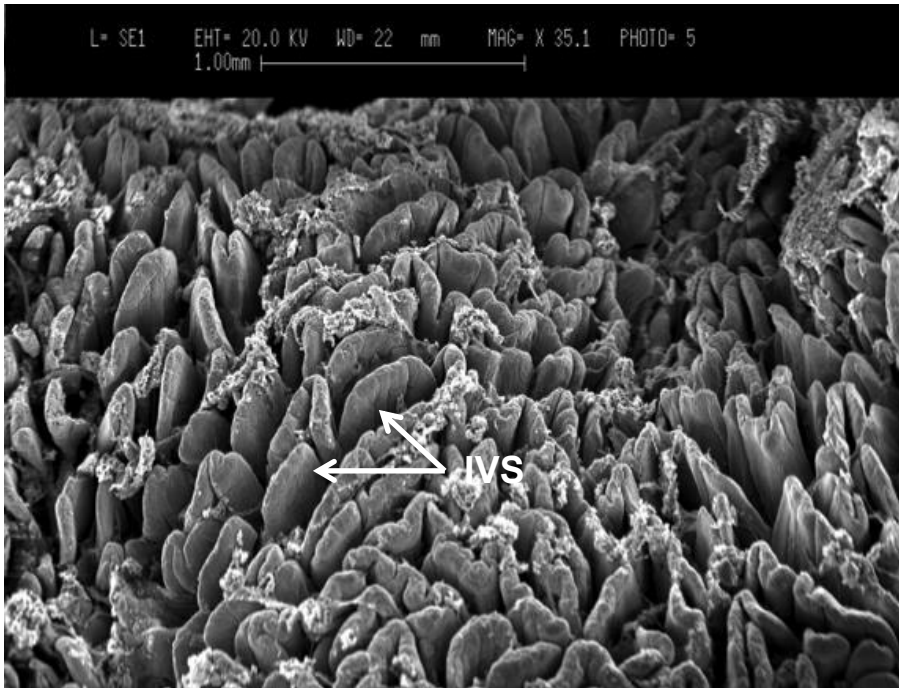

Figure 7.6 Electron micrograph of duodenal tissue in bile duct ligated rats.

IVS – Inter-villus space

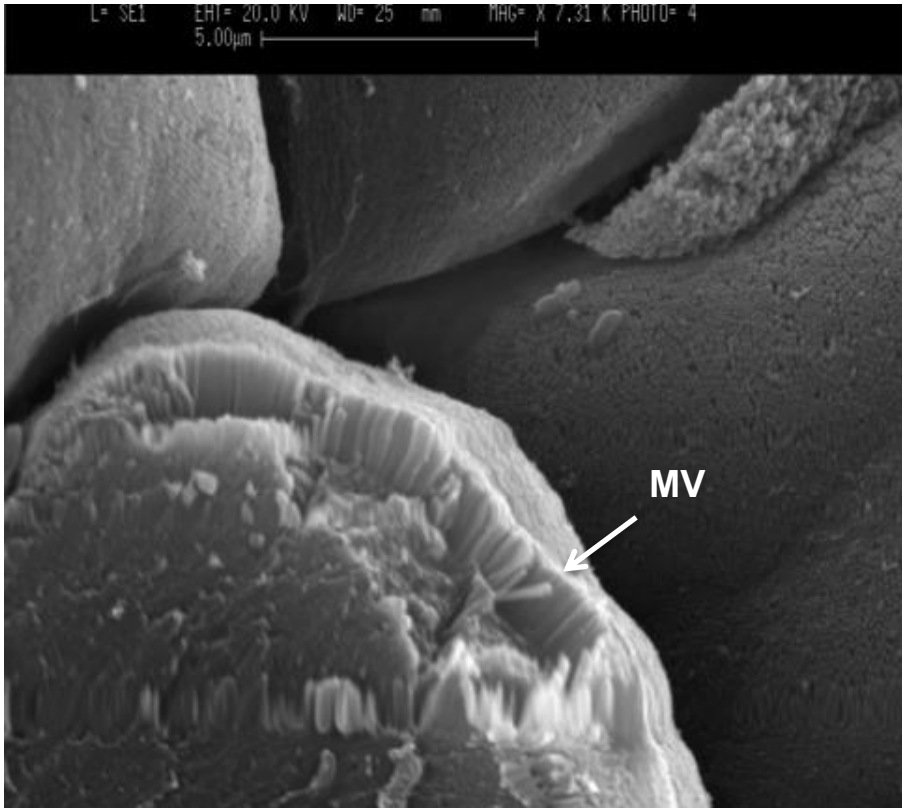

Figure 7.7 Electron micrograph of duodenal microvilli in sham-operated rats

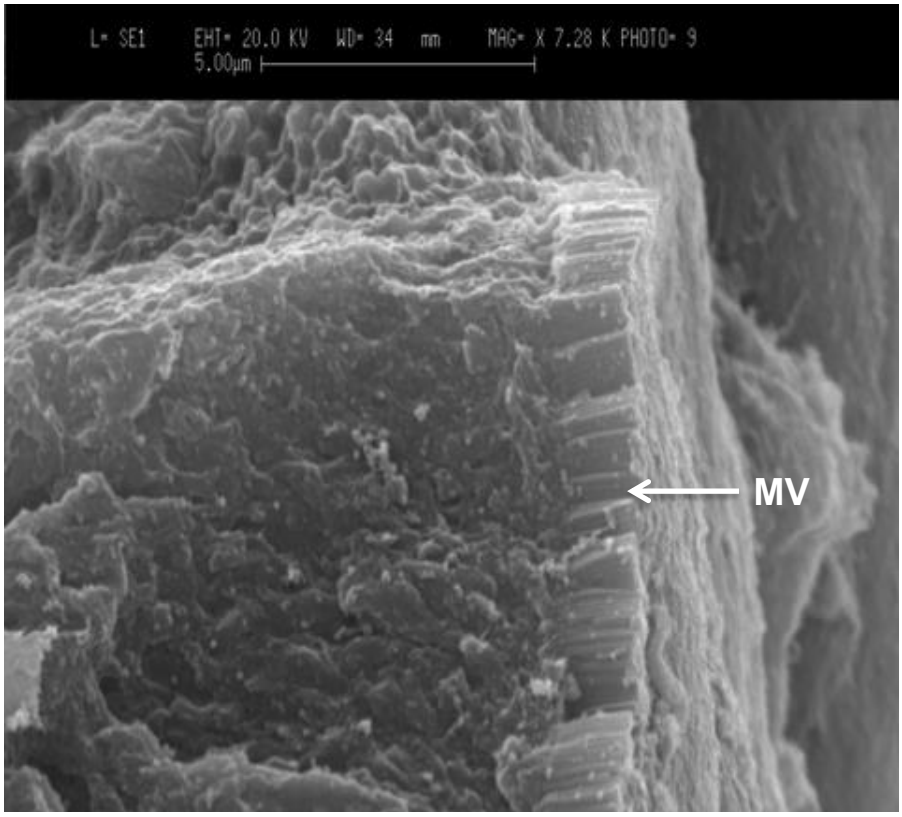

Figure 7.8 Electron micrograph of duodenal microvilli in BDL rats

MV - Microvilli

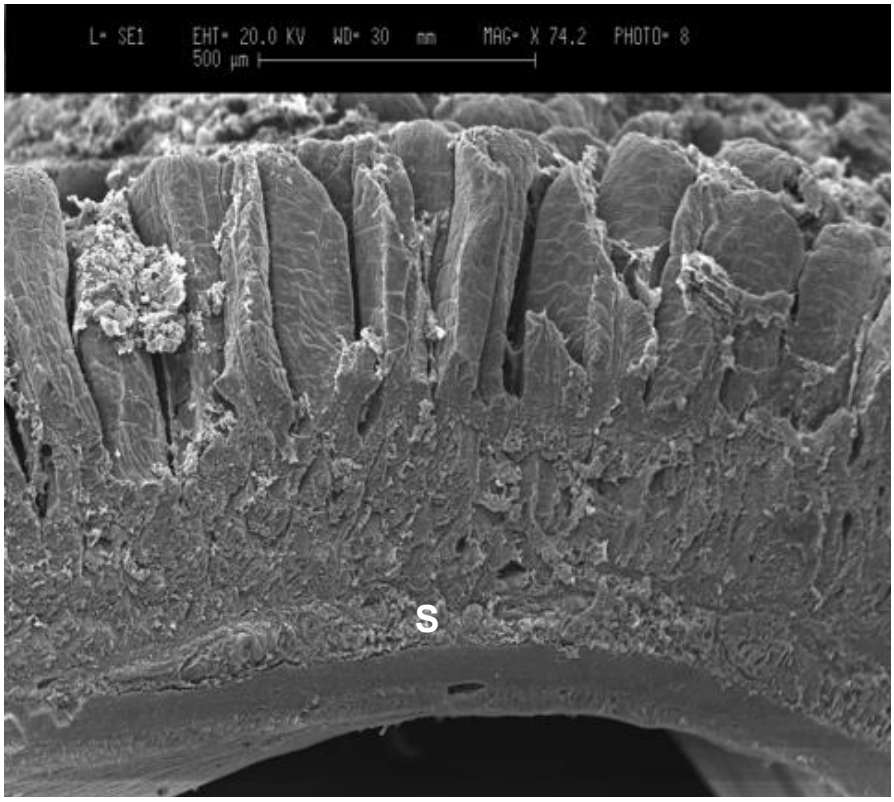

Figure 7.9 Electron micrograph of duodenal tissue in sham operated rats.

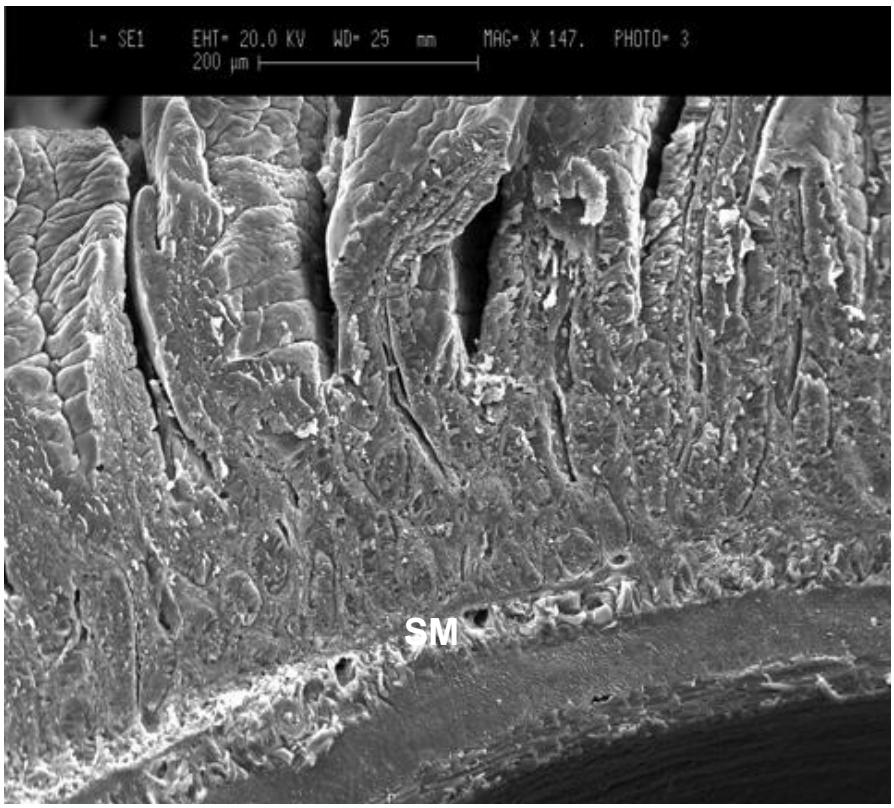

Figure 7.10 Electron micrograph of duodenal microvilli in BDL rats
SM - submucosa

7.3.2.2 Electron microscopy of the Colon

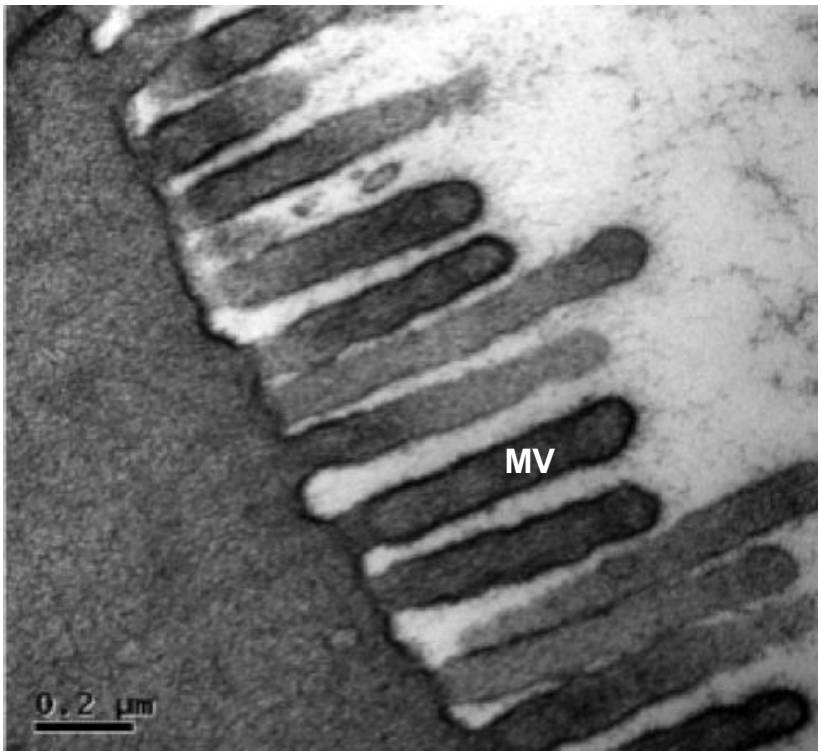

Figure 7.11 Electron micrograph of colonic tissue in sham operated rats

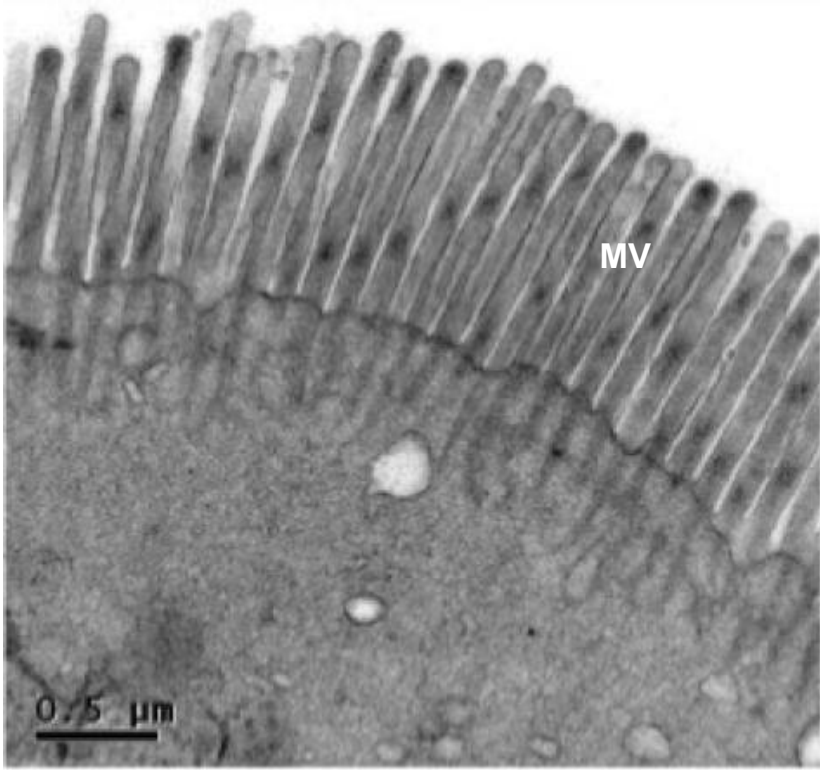

Figure 7.12 Electron micrograph of colonic tissue in bile duct ligated rats. MV - microvilli

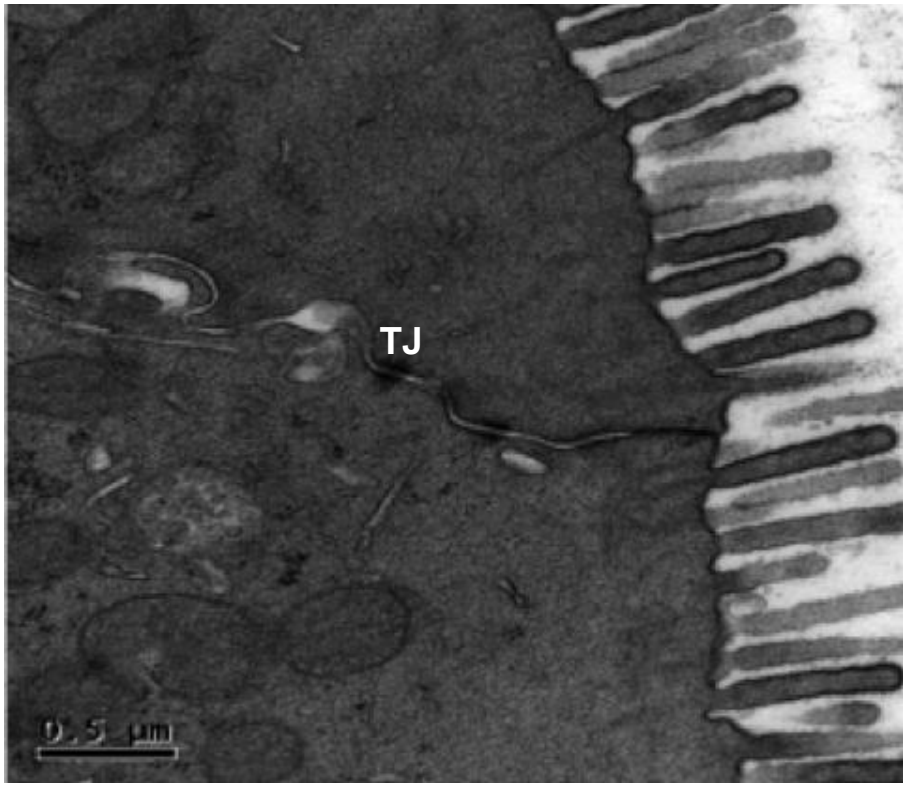

Figure 7.13 Electron micrograph of colonic tissue in sham operated rats.

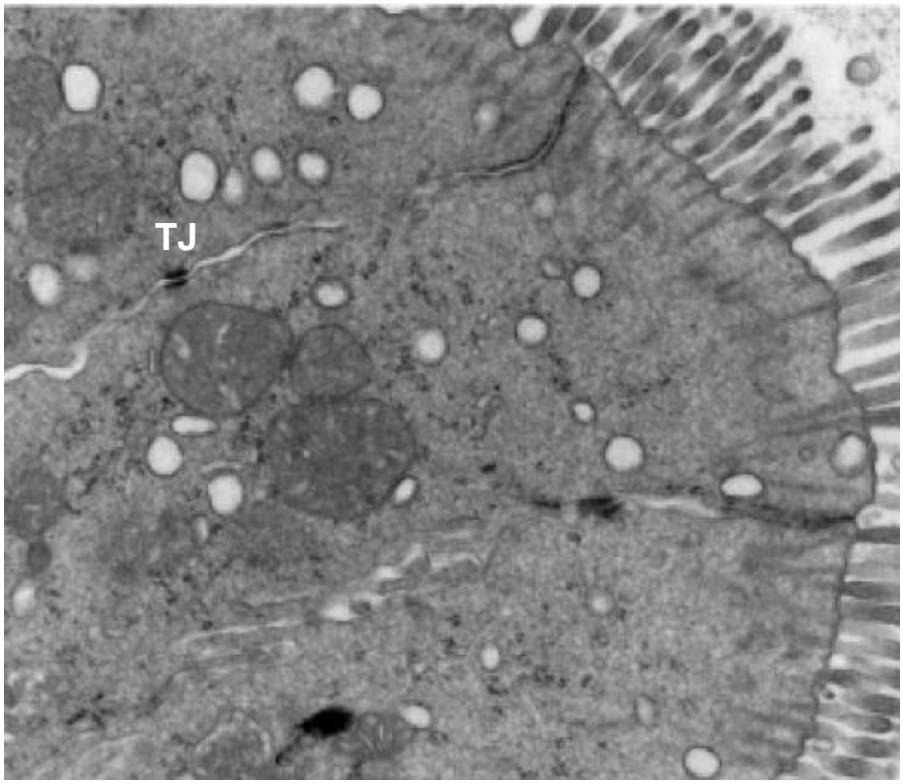

Figure 7.14 Electron micrograph of colonic tissue in bile duct ligated rats

TJ – Tight junction

7.3.3 Paneth Cell Function

Paneth cells play an important role in antimicrobial defence at the gut-barrier interface. Data exists to implicate them in rodent models of portal hypertension (CCL4 treated rats and portal vein ligated rats). No data exists as yet in a cholestatic model of cirrhosis. Gene expression studies were therefore conducted in terminal ileal tissue in sham operated and bile duct ligated rats to identify expression levels of Paneth cell antimicrobial factors.

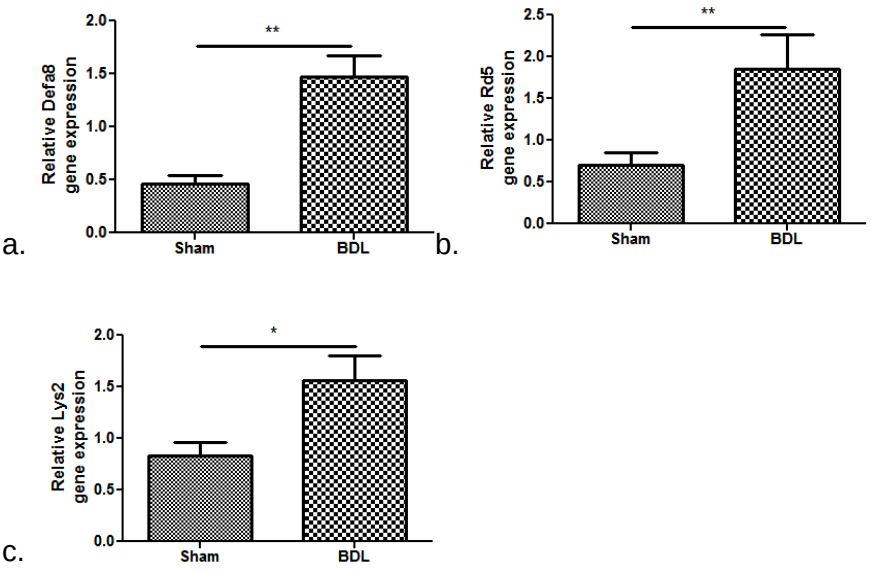

Figure 7.15 Relative gene expression in the terminal ileum of sham and BDL rats with regards to: *a.* defensin 8, b. defensin 5, c. lysozyme (n=4 per group)
* denotes p<0.05
** denotes p<0.005

A significant increase in the relative expression of alpha defensins 5 and 8 and lysozyme (standardised to expression of housekeeping genes *gapdh* and *actb*) was observed in the terminal ileal tissue of BDL rats as compared to sham. Previous studies in carbon tetrachloride-treated rats have demonstrated an opposite effect with a decrease in gene expression of alpha-defensins 5 and 7, most markedly in

animals with evidence of bacterial translocation. This was not observed in portal hypertensive rats without cirrhosis (portal vein ligation model) implicating liver cirrhosis rather than portal hypertension in pathogenesis. Why there is a discordance in alpha-defensin gene expression profile between BDL compared to CCl4 rats is unclear. It is known that alpha-defensin production is induced by microbial products such as endotoxin (Palazzo M et al 2007), therefore difference in microbiome composition between the two models may exert a differential effect on alpha-defensin gene expression. It may represent reactive change to a different microbial composition occurring as a consequence of chronic cholestasis in BDL rats with an increased representation of gram negative organisms with the propensity to stimulate defensin expression via TLR4-dependent mechanisms compared to CCl4 models. This however is speculative and warrants further studies.

7.3.4 Intestinal Permeability

a.

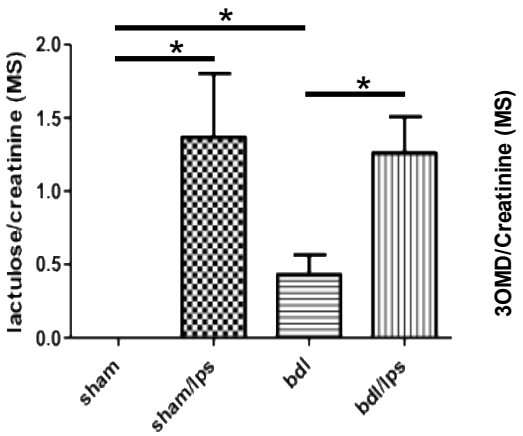

b.

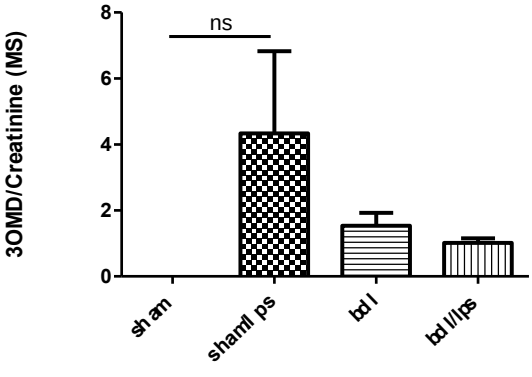

Figure 7.16 Urinary Lactulose/creatinine ratio (ESI-MS).

Figure 7.17 Urinary 3OMD/creatinine ratio (ESI-MS)

A significant increase in 5 hour urinary lactulose/creatinine was observed in BDL rats compared to sham controls suggesting an increase in intestinal paracellular permeability. Of note, intraperitoneal injection of lipopolysaccharide resulted in a significant increase in lactulose/creatinine ration in both sham and BDL models (Ruan Z et al 2014). Intraperitoneal LPS has been previously demonstrated to result in an increase in intestinal permeability as evidenced by increased lactulose/mannitol ratio consistent with our observations. This thought to be due to an effect on tight junction protein expression and function.

In contrast, the 3OMD/creatinine ratio was not significantly different between BDL and sham and BDL and BDL=LPS. 3OMD/creatinine is a measure of active transport. Taken together, this data suggests more of a pathological defect in paracellular permeability rather than active transport, potentially implicating tight junctions, the key regulators of paracellular permeability in pathogenesis.

7.3.5 Tight Junction Protein expression

Tight junctions are key regulators of paracellular permeability in the intestine. They are highly complex and comprise over 50 different subcomponent proteins. Claudin 3 is a sealant tight junction protein which has been shown to be downregulated in the duodenal biopsies of compensated cirrhotic patients (Piils KE et al 2014). Urinary claudin 3 concentrations have been found to be reciprocally elevated in rodent models of haemorrhage shock and also patients with active inflammatory bowel disease (Thuiils G et al 2010). This was the rationale for evaluating claudin 3 expression along the small and large intestine of BDL rats.

Claudin 3

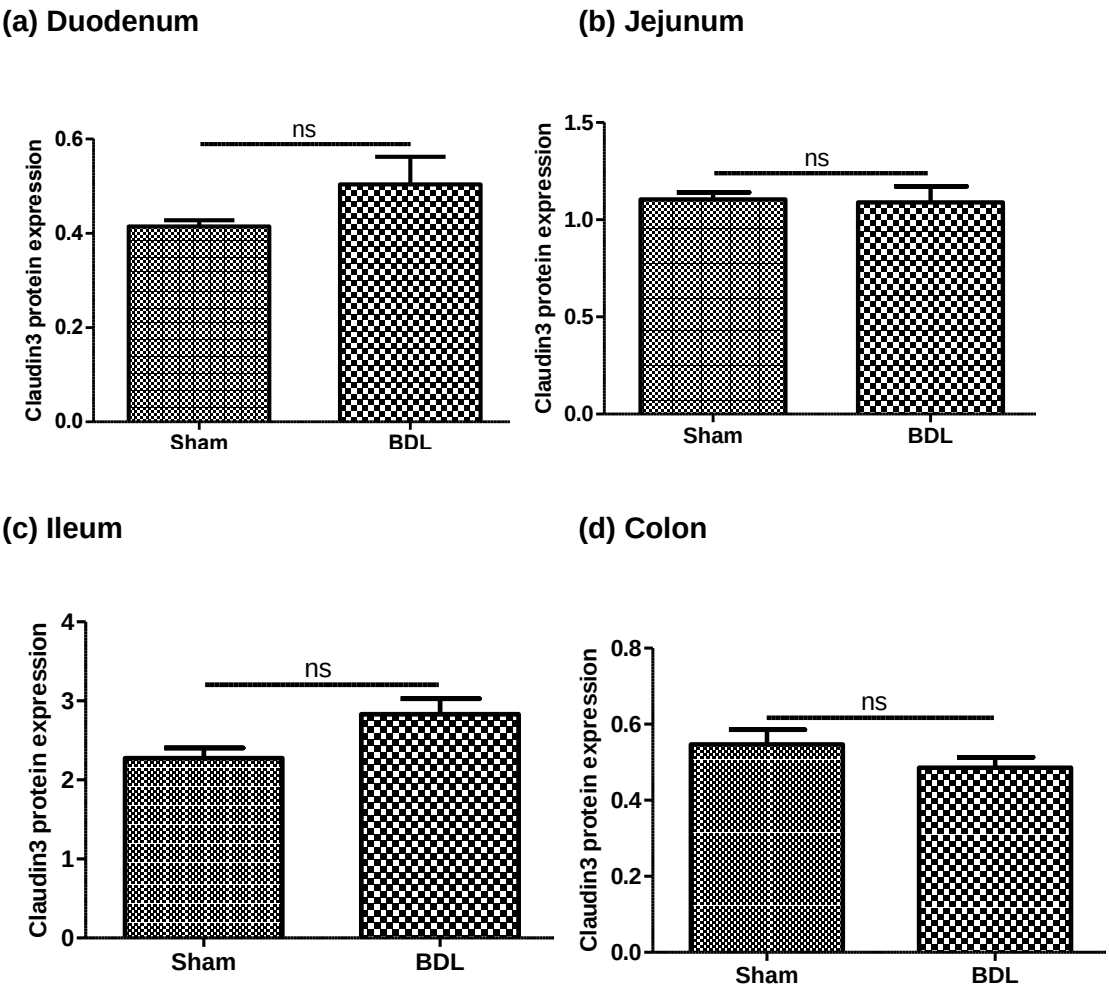

Figure 7.18 Relative protein expression of claudin-3 in mucosa of sham and BDL rats (Sham n=4, BDL n=6)

(a) Duodenum (b) Jejunum (c) Ileum (d) Colon

ns denotes non-significant

Zonula Occludens-1

Zonula Occludens proteins provide ZO-1 is the most widely studied zonula occludens and has been shown to be reduced in the ileum of carbon tetrachloride treated rats (Yang DH et al 2012). TLR-mediated pathways have been implicated in redistribution of ZO-1, an effect functionally associated with an increase in permeability as evidenced by transepithelial electrical resistance (Ulluwishewa D et al 2011).

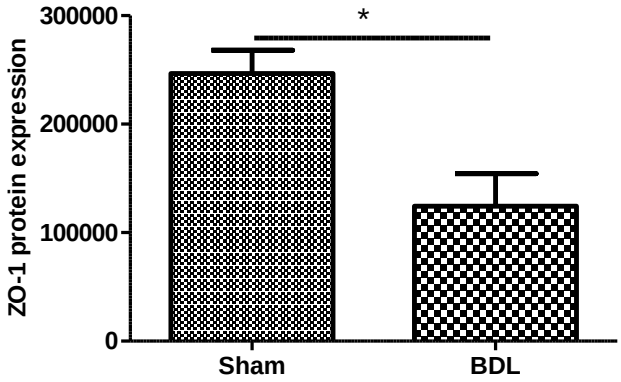

Figure 7.19 ZO-1 expression in full thickness colon (Sham n=4, BDL n=6)
* denotes p<0.05

Connexin-43

Connexin 43 is a gap junction protein which plays a key role in restitution of the intestinal epithelial layer by allowing inter-enterocyte communication of migrating epithelial cells (Leaphart CL et al 2007). Expression of Connexin-43 is therefore indicative of degree of restitution.

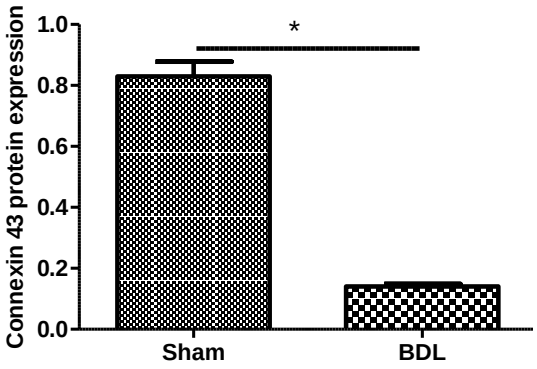

Figure 7.20 Connexin-43 protein expression in full thickness duodenum (Sham n=4, BDL n=6)
* denotes p<0.05

iNOS

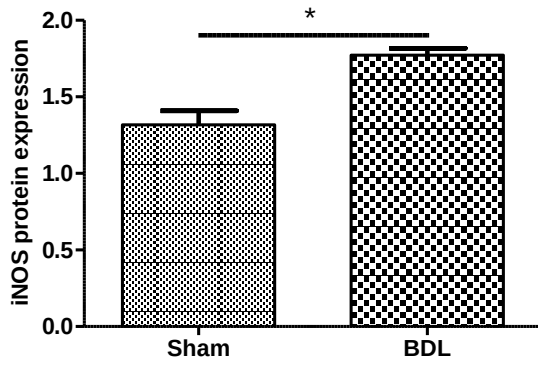

Figure 7.21 Duodenal iNOS expression in full thickness duodenum (Sham n=4, BDL n=6)
* denotes p<0.05

eNOS

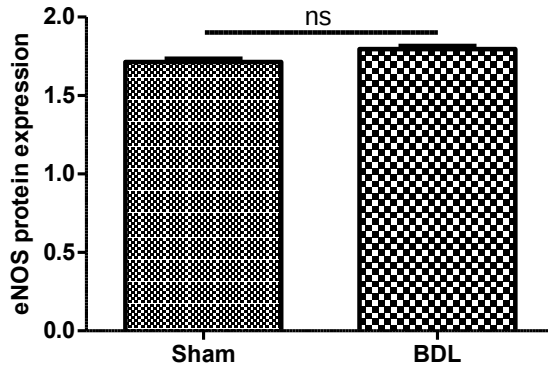

Figure 7.22 Duodenal eNOS expression in full thickness duodenum (Sham n=4, BDL n=6)
* denotes p<0.05

No significant difference in claudin-3 expression was observed along the length of the small and large bowel although a significant decrease in ZO-1 expression was observed in the colon of BDL rats. A significant reduction in gap junction connexion-43 was observed in full thickness duodenum in BDL rats compared to sham controls. A significant increase in full thickness duodenal iNOS protein expression was observed in BDL rats compared to sham controls. No significant difference in eNOS protein expression was observed.

7.3.6 Stool Microbiome Composition

7.3.6.1 Phyla Level

a **b**

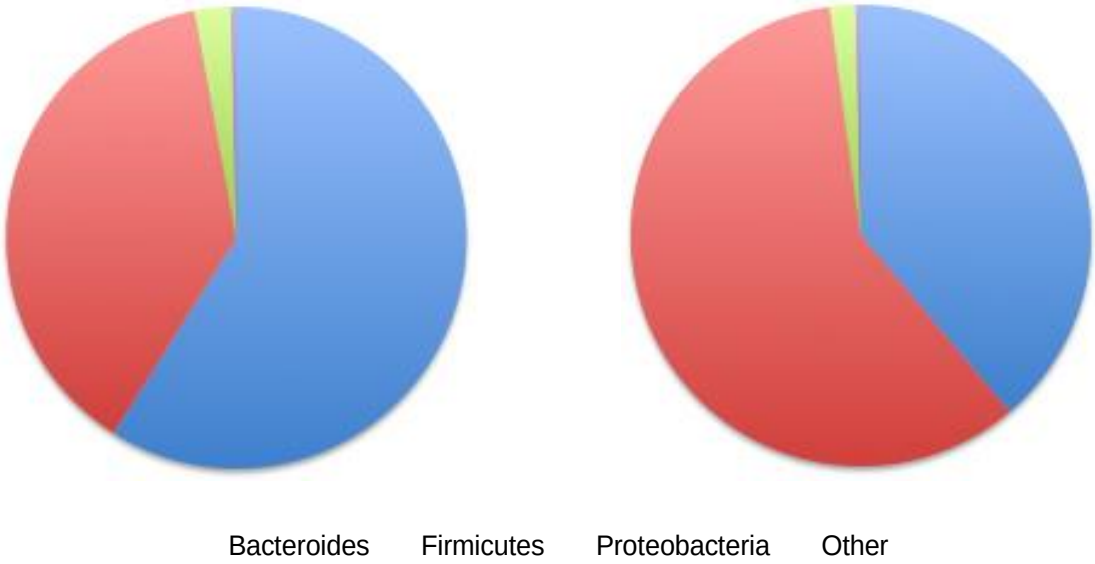

Figure 7.23 Microbiome composition of stool (phyla level) (n=6 both groups)

a) Sham rats b) Bile duct ligated rats

At a phyla level, bacteroides and firmicutes are the dominant phylae, comprising over 95% of stool microbiome. Bile duct ligation was associated with an expansion in the relative population of the Firmicutes phyla compared to sham rats (Sham 38.0±9.2% vs BDL 59.0±7.2%, $p>0.05$). A reciprocal reduction in the Bacteroides phyla was observed (Sham 59.0±9.6% vs BDL 39.0±7.3%, $p>0.05$).

7.3.6.2 Order level

a **b**

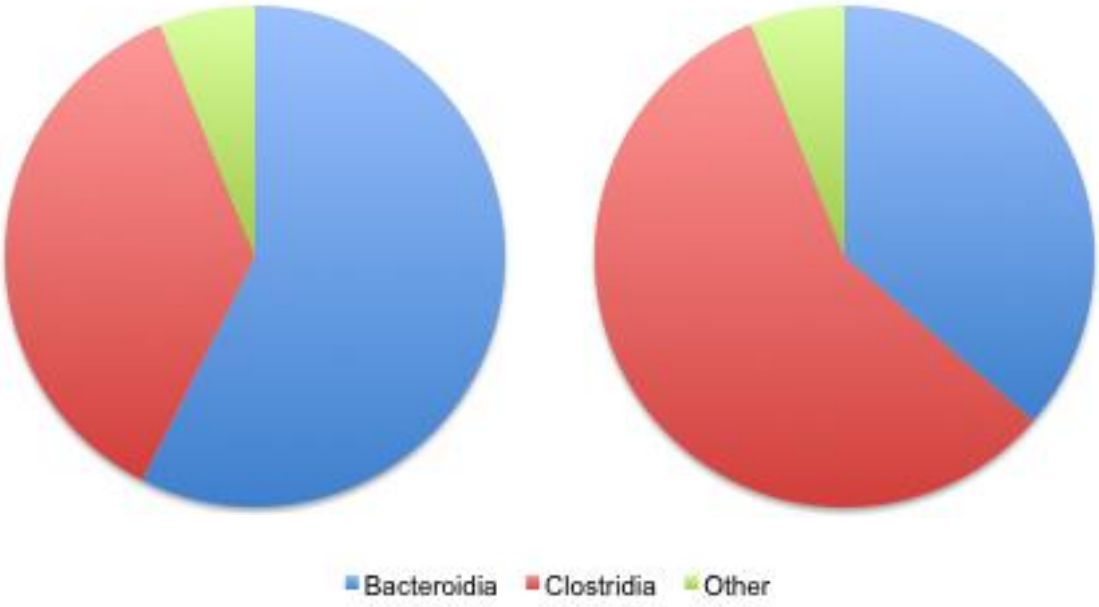

Figure 7.24 Microbiome composition of stool (order level) (n=6 both groups)

a) Sham rats untreated
b) Bile duct ligated rats untreated

Bacteroidia and clostridia were the dominant orders, comprising over 90% of stool microbiome. The expansion in the Firmicutes phyla was principally due to an expansion in the clostridia order (Sham 36.3±9.6% vs BDL 58.0±7.3%, p>0.05). A non-significant reduction in Bacteroidia was observed (Sham 57.5±9.7% vs BDL 36.3±7.1%, p>0.05).

7.3.6.3 Family level

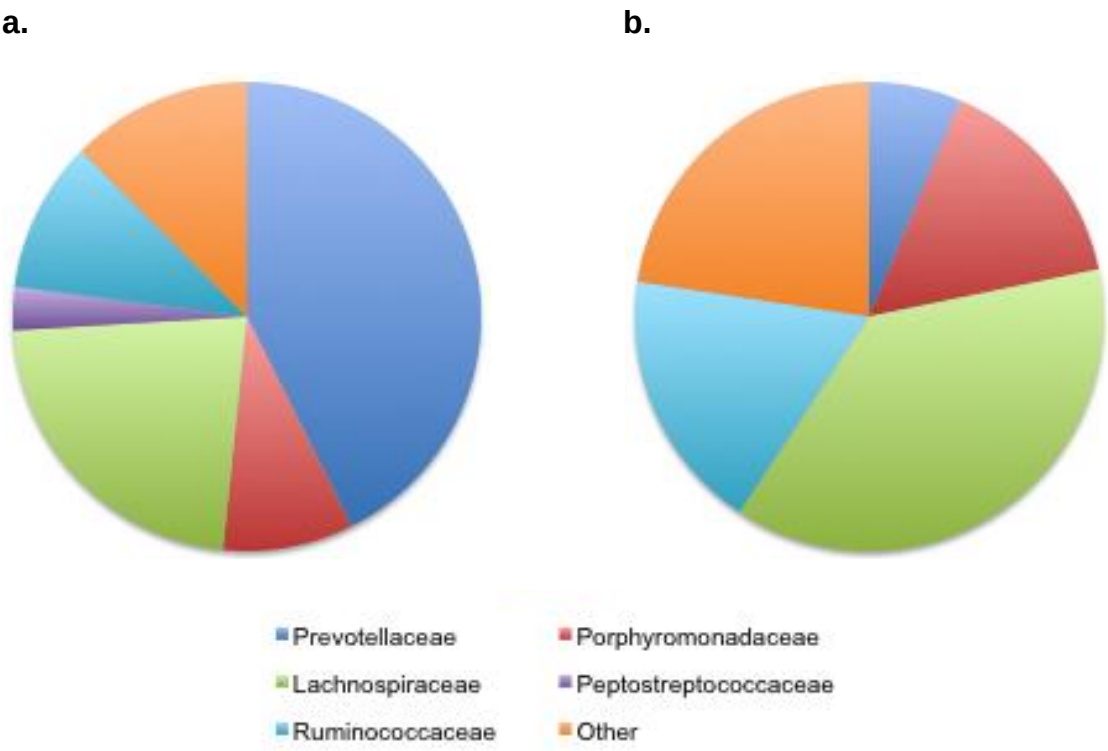

Figure 7.25 Microbiome composition of stool (family level) (n=6 both groups)

a) Sham rats b) Bile duct ligated rats

Bile duct ligation was associated with significant reductions in *Peptostreptococcaceae* (Sham 8.2±1.7% vs BDL 0±0%, p=0.005) and significant increases in *Porphyromonadaceae* (Sham 24.7±3.9% vs BDL 42.1±4.5%, p=0.004) compared to sham controls. *Prevotellaceae* was the dominant family in sham rats. A near significant reduction in *Prevotellaceae* and increase in *Ruminococcaceae* was observed in BDL rats compared to sham (Sham 42.6±12.9% vs BDL 6.3±1.8%, p=0.07 and Sham 28.5±9.8% vs BDL 49.3±6.6%, p=0.09 respectively).

7.3.6.4 Genus Level

a.

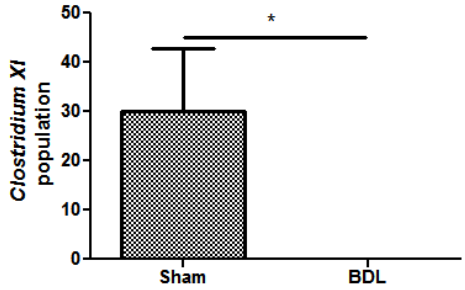

b.

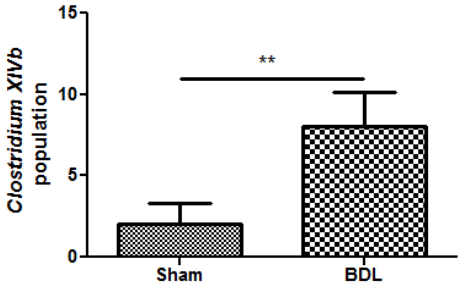

c.

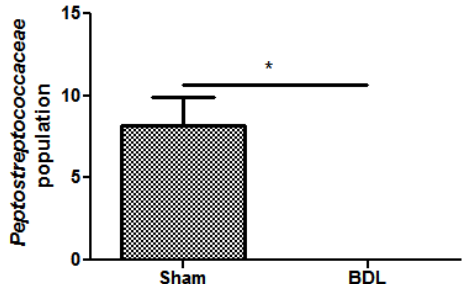

Figure 7.26 Geni in which significant differences between groups of sham and bile duct ligated rats were observed (n=6 both groups):

a) *Clostridium XI*
b) *Clostridium XIVb*
c) *Peptostreptococcaceae*
* denotes p<0.05
*** denotes p<0.001

BDL rats were found to have a collapse in *clostridium XI* and *peptostreptococcaceae* geni and expansion in *Clostridium XIVb.*

7.3.7 Metabolomic Profiling (urinary ^{1}NMR analysis)

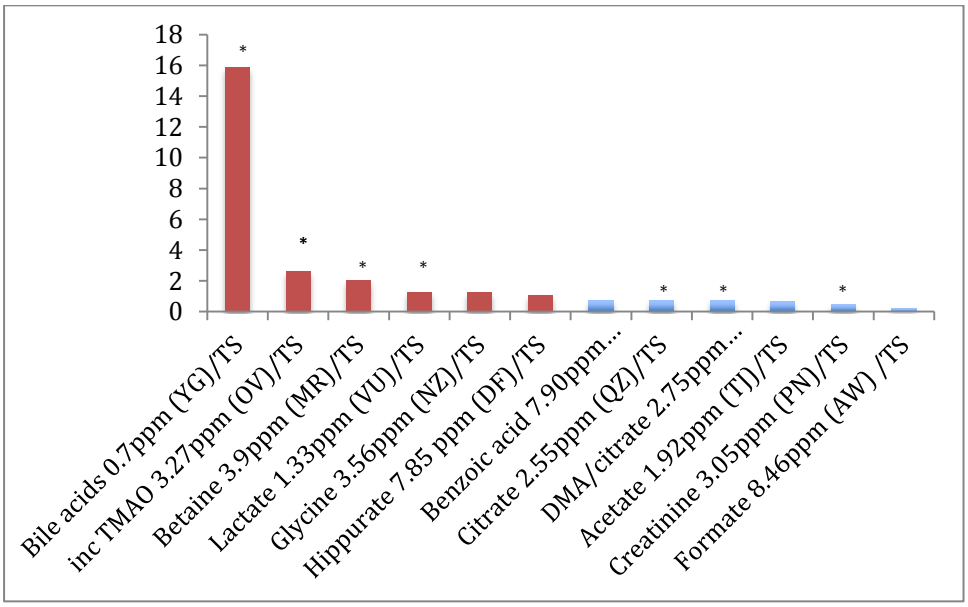

Figure 7.27 Relative urinary concentrations of metabolites in BDL compared to sham (n=6 both groups)

Bile duct ligation is associated with a distinct metabolomic profile as compared to sham controls. Significant increases in urinary bile acids, Trimethylamine oxidase (TMAO), betaine and lactate were and reductions in citrate, dimethylarginine (DMA) and creatinine were observed between BDL rats compared to sham controls.

7.3.8 Immunological Profiling

7.3.8.1 Population Studies

7.3.8.1.1 Liver

(a) Kupffer cell Populations

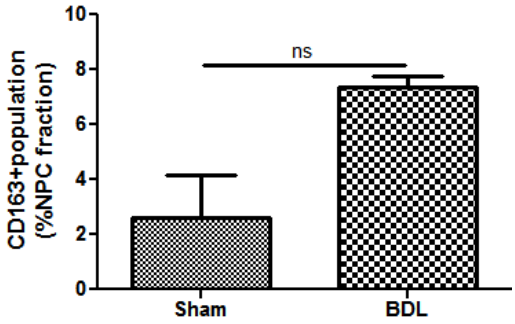

(b) Liver neutrophil Population

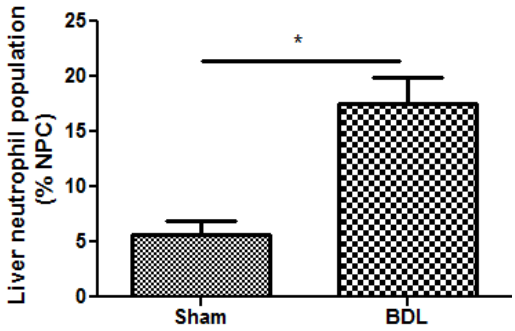

Figure 7.28 Hepatic neutrophil population was observed in bile duct ligated rats compared to sham controls (expressed as a percentage of non-parenchymal cell fraction). (n=4/group) * denotes $p<0.05$
(a) Kupffer cell populations
(b) Liver neutrophil populations

Bile duct ligation was is associated with an expansion in hepatic innate immune cell populations. In this study, a significant increase in hepatic neutrophil populations was observed in 4 week BDL rats associated with a trend towards an increase Kupffer cell populations.

7.3.8.1.2 Portal Venous/Arterial Blood

	Total WCC¥ (A)	Total WCC¥ (PV)	Neutrophil count¥ (A)	Neutrophil count¥ (PV)	Monocyte count¥ (A)	Monocyte count¥(PV)
Sham	1.2±0.1	1.5±0.04	0.3±0.1	0.3±0.5	0.1±0.03	0.1±0.02
BDL	8.9±1.5#	11.1±1.4#	2.6±0.4#	3.3±0.5#	2.9±0.9#	3.6±1.3#

¥(x10^7cells/ml); # P<0.05 (BDLvs sham)

Table 7.1 Absolute Leucocyte Populations in Sham and BDL rats (n=4/group)

A significant increase in both portal venous and arterial total leucocyte count, monocyte and neutrophil populations were observed in BDL rats compared to sham. Subpopulations of monocytes defined by relative CD43 expression were determined in both portal venous and arterial blood to ascertain whether phenotypic changes were associated with monocyte subpopulations. A significant reduction in CD43lo monocytes was observed in both portal venous and arterial blood. No difference was observed between these two compartments.

7.3.8.1.3 Mesenteric lymph node populations

(a) Absolute CD68+population **(b) Percentage CD68+ population**

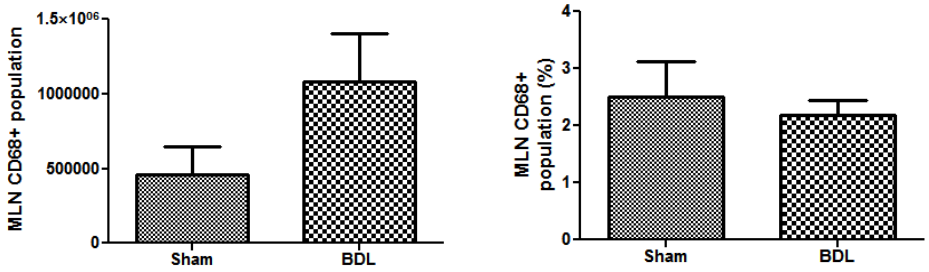

(c) Absolute CD68+/CD80+ population (d) Percentage CD68+/CD80+ population

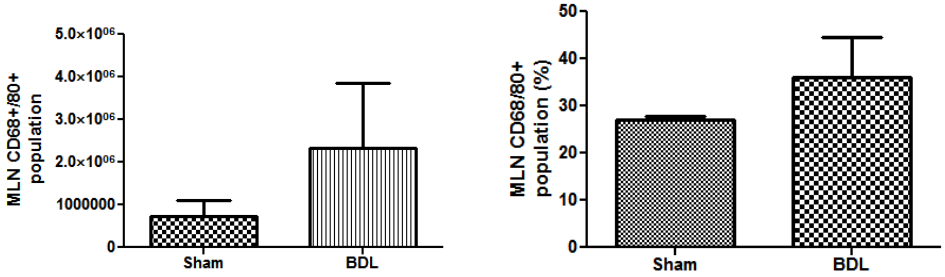

(e) Absolute CD163+ population **(f) Percentage CD163+ population**

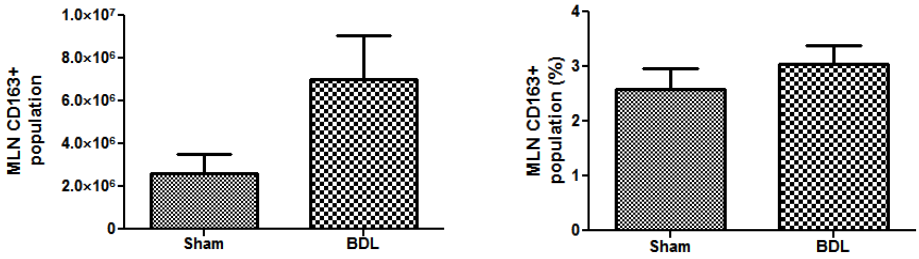

Figure 7.29 Mesenteric Lymph Node populations (n=4/group)

(a) Absolute CD68+ population
(b) PercentageCD68+ population
(c) Absolute CD68+/CD80+ population
(d) Percentage CD68+/CD80+ population
(e) Absolute CD163+ population
(f) Percentage CD163+ population

MLN population studies were performed using CD68, CD80 and CD163 staining. CD68 and CD80 are both more highly expressed in activated macrophages with a more pro-inflammatory, M1 phenotype. In contrast, CD163 is expressed on M2 macrophages with a more anti-inflammatory phenotype.

No significant differences in CD68+, CD163+ or CD80/68+ cells were observed between BDL and sham. A non-significant decrease in percentage population of CD68+ and CD163+ cells was observed in the mesenteric lymph nodes of bile duct ligated rat with an upward trend in CD80+CD68+ cells. When MLN populations were expressed as absolute counts, trends towards increases within the CD68+, CD68/80+, CD163+ populations were observed. This may represent expansion in macrophage populations but without a marked polarisation of macrophage phenotype. The studies are however small and warrant further validation.

7.3.8.2 Reactive Oxidant Species (ROS) Production

7.3.8.2.1 Liver

(a) Total Liver ROS

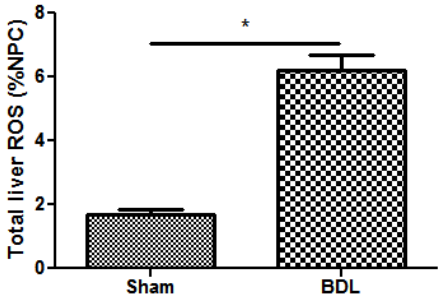

(b) Total Liver LPS ROS

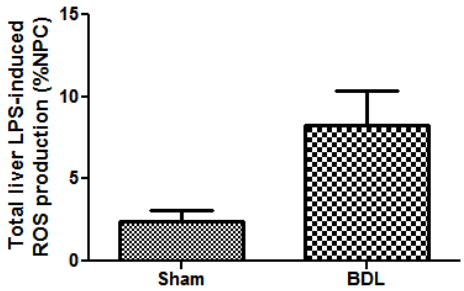

(c) Kupffer Cell ROS

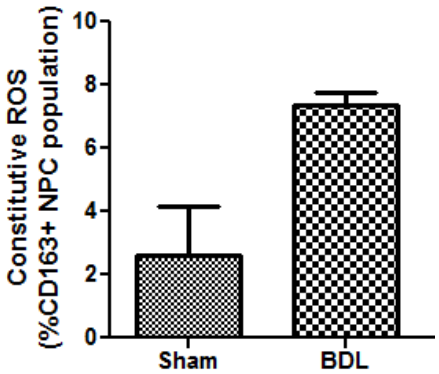

(d) Kupffer Cell LPS ROS

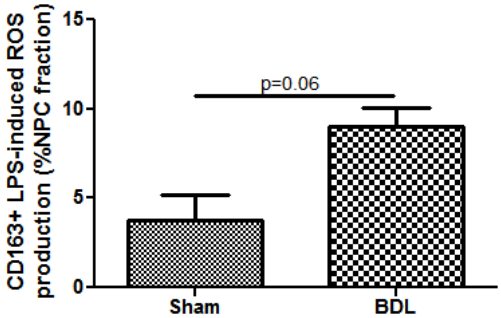

(e) Liver neutrophil ROS

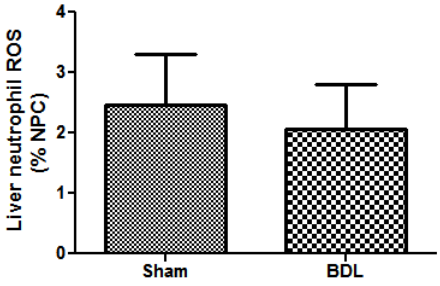

(f) Liver neutrophil LPS ROS

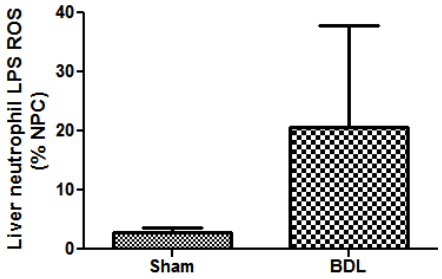

Figure 7.30 Hepatic ROS production (Sham n=4, BDL n=4)

(a) Total liver ROS production
(b) Total liver ROS production in response to ex-vivo LPS challenge
(c) Total Kupffer cell ROS production
(d) Total liver ROS production in response to ex-vivo LPS challenge
(e) Total hepatic neutrophil ROS production
(f) Total hepatic neutrophil ROS production in response to ex-vivo LPS challenge
* denotes p<0.05

7.3.8.2.2 Portal Venous Populations

7.3.8.2.2.1 Portal venous neutrophil ROS production

(a)

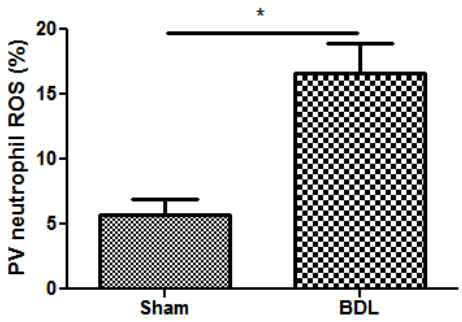

(b)

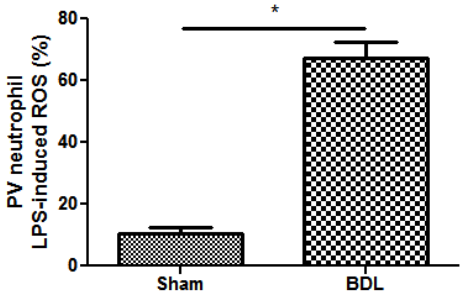

(c)

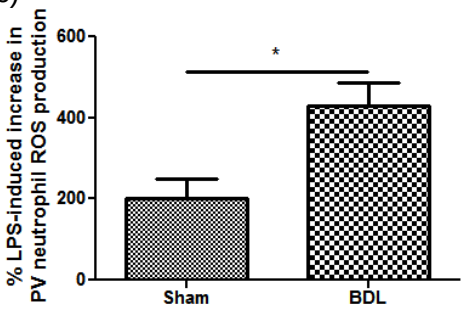

Figure 7.31

(a) Total Portal Venous Neutrophil ROS production
(b) Total Portal Venous Neutrophil ROS production in response to ex-vivo LPS challenge
(c) % Increase in Portal Venous Neutrophil ROS production as a marker of cellular priming to endotoxin challenge (n=4/group) * denotes p<0.05

7.3.8.2.2.2 Portal Venous Monocyte ROS production

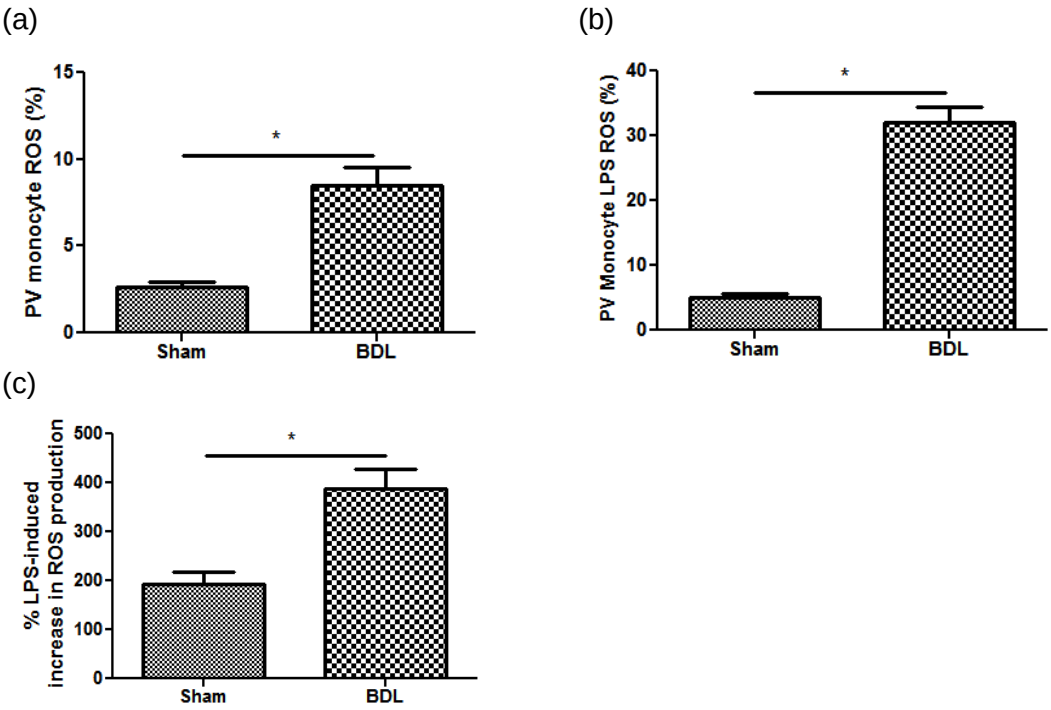

Figure 7.32

(a) Total Portal Venous Monocyte ROS production
(b) Total Portal Venous Monocyte ROS production in response to ex-vivo LPS challenge
(c) % Increase in Portal Venous Monocyte ROS production as a marker of cellular priming to endotoxin challenge (n=4/group) * denotes $p<0.05$

ROS production by Portal Venous Monocyte Subpopulations

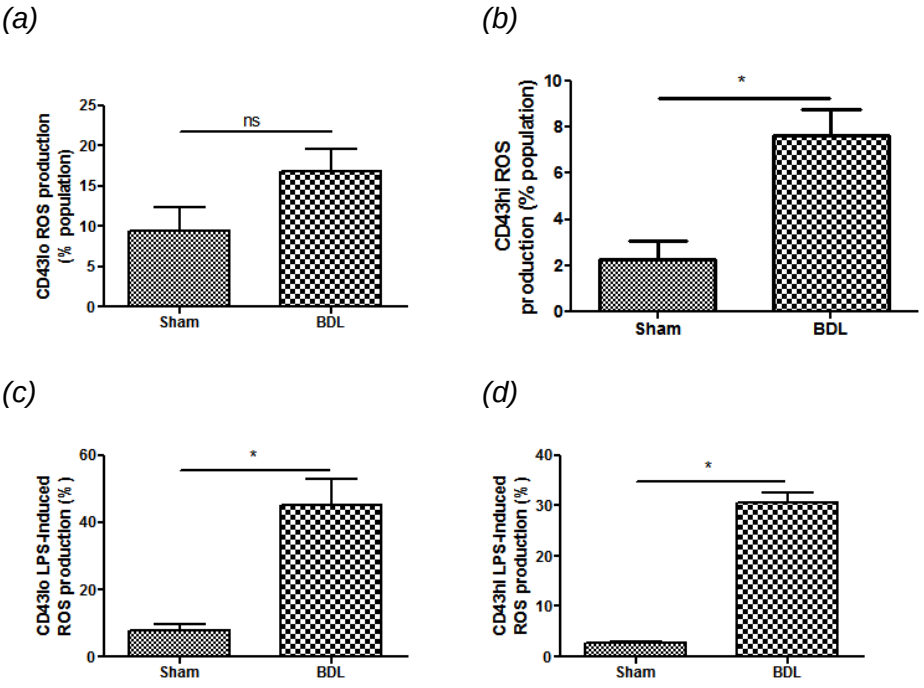

Figure 7.34

(a) Total Portal Venous CD43 hi Monocyte ROS production
(b) Total Portal Venous CD43hi Monocyte ROS production in response to ex-vivo LPS challenge
(c) Total Portal Venous CD43 lo Monocyte ROS production
(d) Total Portal Venous CD43lo Monocyte ROS production in response to ex-vivo LPS challenge (n=4/group) * denotes p<0.05

Bile duct ligation was associated with a significant increase in portal venous neutrophil and monocyte constitutive ROS and LPS-induced ROS production. When expressed as a ratio of LPS-induced ROS:constitutive ROS, a significant increase was observed suggestive of increased endotoxin sensitivity. Significant increases in LPS-induced ROS production were observed in both CD43 hi and lo monocyte subpopulations. Constitutive ROS was significantly raised in CD43hi with an upward trend observed with CD43lo monocyte constitutive ROS production.

7.3.8.3 Phagocytosis

(a) Kupffer Cell **(b) Liver Neutrophils**

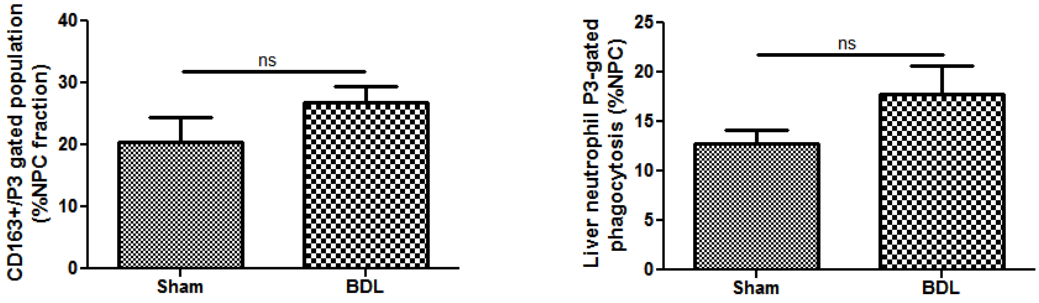

Figure 7.35 Percentage population actively phagocytosing a minimum of 3 particles (n=4/group)
(a) Kupffer cell
(b) Liver neutrophils

ROS production from the non-parenchymal fraction of liver-derived cells was found to be significantly raised in BDL rats compared to sham control. Of this fraction, both constitutive and LPS-ROS production from hepatic neutrophils were found to be

significantly raised in BDL rats compared to control. An upward trend in Kupffer cell ROS production was observed in BDL rats with borderline significance achieved with regards to LPS-induced ROS production. No significant difference in Kupffer cell or liver neutrophil phagocytosis was observed.

7.3.9 Portal Venous Cytokines

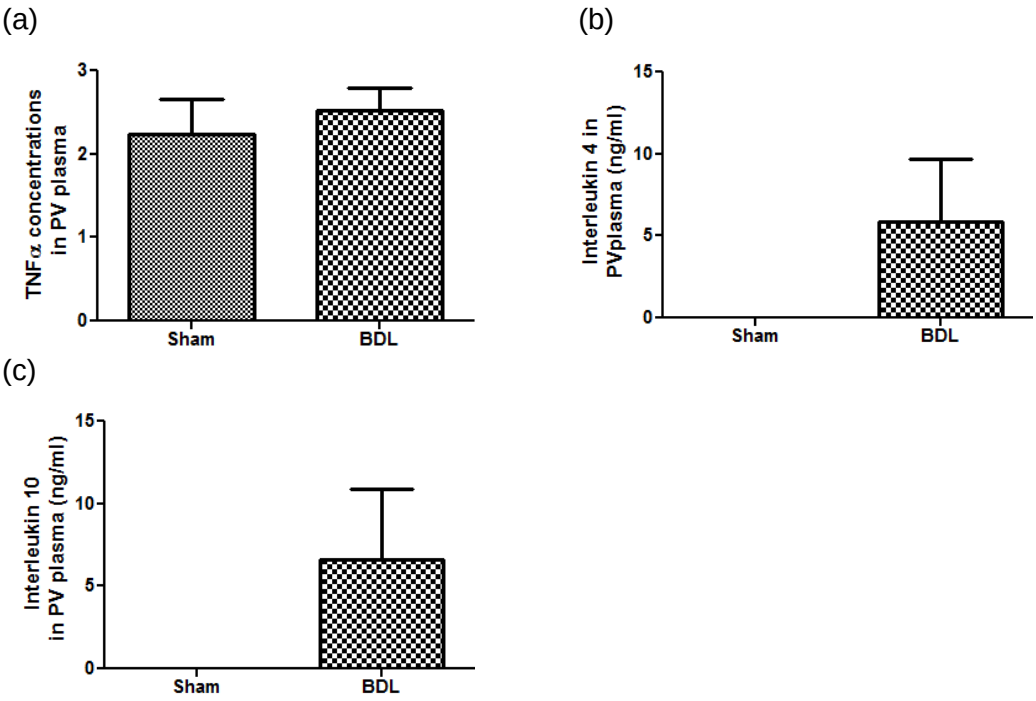

Figure 7.36

(a) Portal Venous plasma TNFα levels
(b) Portal Venous IL-4 levels
(c) Portal Venous IL-10 levels

(n=4/group)

No significant differences in portal venous TNFα, IL4 or IL10 concentrations were observed between sham and BDL. Upward trends were observed with IL4 and IL10 in BDL rats.

7.4 Discussion

7.4.1 Structural phenotype

Intestinal permeability is known to be increased in cirrhosis and an important factor promoting bacterial translocation. Despite this, the exact site of bacterial translocation remains poorly understood. Therefore, studies along the length of the small and large intestine in a model of cirrhosis were performed. The first study evaluated light microscopy appearances of duodenum, jejunum, ileum and colon with full thickness sections and associated mesentery. This was complemented by studies looking at tight junction and jap junction protein expression and correlated with functional studies to evaluate intestinal permeability using sugar probes studies. Mucosal integrity was preserved throughout the small and large intestine with subtle vascular changes at the level of the sub-mucosa in BDL rats. Perivascular inflammation was observed in the mesenteric vessels close to the peritoneal surface.

With no clear breach in the mucosal surface, studies were conducted to evaluate ultra-structural changes in the duodenal and colonic mucosa. At both sites, integrity of the epithelial barrier was observed. Tight junctions, responsible for modulating paracellular intestinal permeability, were intact. A slight reduction in mitochondrial density was observed in duodenal mucosa in BDL rats. The duodenal microvilli in BDL rats was found to be slightly blunted compare to control and a slight increase in inter-villus distance was observed in disease models.

Connexin-43 expression was found to be significantly increased in BDL rats. One potential explanation would be a required for increased enterocyte restitution. Certainly it is known that the oxidative stress in the gut of portal hypertensive rats is increased which is likely to result in heightened enterocyte turnover. For the time that restitution allows for compensation of any GI insult such as portal hypertension, apparent epithelial integrity is observed. It may be that in the context of more

advanced disease, this is not fully achieved and may contribute to the much higher rates of bacterial translocation observed in more advanced disease states.

A significant increase in the relative expression of defensins 5 and 8 and lysozyme was observed in the terminal ileal tissue of BDL rats as compared to sham. No significant difference in TNFα gene expression was observed. Antimicrobial peptides derived from Paneth cells play a key role in the maintenance of homeostasis with the intestinal flora at the gut barrier interface. Paneth cells have also been implicated in the process of bacterial translocation in rat models of cirrhosis in context of carbon tetrachloride-induced liver injury and portal venous ligation. This study evaluates the role of the paneth cell function in a cholestatic model of liver cirrhosis. The data suggests that there is an association with cirrhosis and increased production of antimicrobial peptide production from Paneth cells. Whether this is causal or consequential is unclear.

A significant increase in urinary lactulose excretion was observed in BDL rats compared to sham controls. Regrettably discrimination between rhamnose and 6-o-methyl-glucose on mass spectroscopy was not possible which may have been secondary to trace contamination in the original sugar probes. Urinary 5 hour lactulose excretion, a reflection of paracellular permeability, was standardised to creatinine levels to control for renal function. Without the rhamnose data, we were unable to standardise for other factors which may confound the results such as gastric emptying rates and intestinal transit times. It is a crude measure of intestinal permeability but is consistent with previously published data.

Finally, a significant increase in duodenal iNOS protein expression was observed in BDL rats compared to sham controls. No significant difference in eNOS protein expression was observed however. This is an interesting and novel observation and has since been confirmed in duodenal biopsy tissue from cirrhotic patients. iNOS is

produced by monocyte/macrophage populations as nitric oxide is a key factor in innate immune defence against bacteria. iNOS expression is largely induced rather than present constitutively and is responsive to IRF1 and NFkB-dependent signalling pathways. By this means, it produces nitric oxide, often in large quantities, in response to inflammatory cytokines often in the context of high oxidative stress. Nitric oxide itself can inhibit elements of the respiratory chain driving an increase in glycolysis. ATP depletion ultimately results in necrotic cell death. NO-mediated cell death requires first the production of peroxynitrite from NO and ROS with high cellular toxicity conferring potent anti-microbial properties but with the potential for host organ damage in the context of a dysregulated inflammatory response. Heightened reactive oxidant species derived from both circulating and tissue resident monocyte and macrophage populations is a cardinal feature of the disease state.

7.4.2 Gut Microbiota

A significant shift in microbiome composition is observed in BDL rats compared to sham controls associated with a distinct shift in urinary metabolomic profile. Bile salts are known to exert a differential bacteriostatic effect on the intestinal microflora and indeed bile salt deficiency secondary to cholestasis has been shown to be associated with dysbiosis. This shift in microbiome composition may be responsible for inducing the observed upregulation of paneth cell antimicrobial peptide production.

Urinary NMR analysis is a reflection of the combined metabolic status of both host and microbiota. The bile duct ligated rat model is a model of cholestasis and is associated with a significant increase in urinary bile acid level concentration compared to sham controls. A significant reduction in urinary creatinine was also observed in BDL rats indicative of reduced renal function.

A significant increase in urinary lactate is observed in BDL rats. This parallels the observed increase in plasma lactate indicative of increased anaerobic metabolism. A heightened catabolic state in BDL rats is suggested by low plasma glucose levels and significant weight loss in the context of pair feeding. This is further exacerbated by impaired hepatocellular mitochondrial metabolism known to occur in this model. Microbial origin lactate production is unlikely to be a major contributory source in context of the microbiome results

Trimethylamine oxidase (TMAO) and betaine are both breakdown products of dietary phosphatidylcholine. TMAO is formed from the oxidation of trimethylamine (TMA) and is a common metabolite in animals and humans. The key role of gut microflora in metabolism was demonstrated by a reduction in TMAO levels with selective gut decontamination with a quinolone. There has been considerable interest in TMAO as a pathogenic marker in atherosclerosis. This data highlights the importance in cirrhosis also. A significant rise in urinary betaine was observed in BDL rats. Betaine is a metabolic product of gut bacteria and is indicative of the increased dysbiosis evident in the BDL model.

A significant reduction in urinary citrate was observed in BDL rats compared to sham operated animals. Urinary citrate concentrations are influenced significantly by the integrity of the proximal convoluted tubules and degree of acidosis, both of which are observed in the BDL model.

7.4.3 Immunological Phenotype

The phenotype of the innate immune response in the BDL rat is one of a heightened primed state to endotoxin challenge most markedly with regards to ROS production. This phenotype is observed across the different vascular and tissue compartments. Total liver ROS production was increased in BDL rats compared to sham controls. Both Kupffer cell ($CD163^+$ gated non-parenchymal cells) and liver neutrophils exhibited a trend towards increased ROS production in BDL compared to sham but

no significant difference in phagocytosis. Portal venous monocytes and neutrophils exhibited a state of heightened endotoxin sensitivity with regards to ROS production. This may be due to a heightened primed state due to previous endotoxin exposure.

A significant increase in liver neutrophil population was observed with BDL compared to sham. In contrast, only an upward trend in Kupffer cell populations was observed with cirrhotic rats. This data suggests that infiltrating innate immune populations from the gut play a greater role in pathogenesis than tissue resident populations.

Phenotypically, the trafficking innate immune cell populations within the portal vein of BDL rats are characterised by an endotoxin-primed state resulting in a significant increase in ROS production. This effect is further compounded by the observation that the absolute populations of neutrophils and monocytes are significantly increased in the disease state compared to control. These cells are likely to have a significant impact on hepatocellular injury.

Mesenteric lymph node studies were conducted to evaluate the local innate immune response to determine whether the innate immune phenotype of heightened endotoxin sensitivity was conditioned at the gut-barrier interface or in more proximal lymphatics. A non-significant increase in CD80+/CD68+ populations were observed in mesenteric lymph node populations of BDL rats suggesting a skew toward the pro-inflammatory Th1 phenotype. This data suggests that the pro-inflammatory phenotype observed in BDL rats may be conditioned in part at the level of the gut.

In conclusion, multiple elements of the gut-liver axis are modulated in a model of cirrhosis. A phenotype of enhanced endotoxin sensitivity is observed in association with a shift in microbiome composition and metabolomic profile. Subsequent work will focus on the biological effects of modulating the gut liver axis with Yaq-001, a powerful non-absorbable endotoxin and bacterial metabolite adsorbant in a model of cirrhosis and non-alcoholic fatty liver disease.

Chapter 8

Biological Effects of Oral Administration of Yaq-001 Carbon Therapy in Bile Duct Ligated Rats

8.1 Introduction

Bacterial translocation plays a key role in the pathogenesis of liver disease. Modulation of the gut microflora with oral antibiotics has been shown to improve outcome but attendant risks of resistance and super-infection limits their role. Yaq-001 is a non-absorbable activated carbon with a tailored bimodal porosity conferring optimal adsorptive properties to bind pathologically relevant gut-derived factors including endotoxin and bacterial metabolites. These in vitro properties render oral Yaq-001 a good candidate to modulate clinically relevant end-points in cirrhosis.

8.2 Aims

The aim of this study was to characterise the biological effects of oral administration of Yaq-001 in bile duct ligated rats. The primary end-points were reduction in organ injury and portal pressure. The secondary end points were improvement in gut barrier function and attenuation in primed innate immune phenotype. Microbiome composition and function was evaluated to ascertain whether the carbons, despite not exhibiting an antibiotic effect in vitro, were able to shape the microbiome composition and function towards a more autocthonous phenotype.

8.3 Results

8.3.1 Biochemical Profile

As previously described, bile duct ligation was observed to be associated with a significant increase in ALT, a biochemical marker of liver injury. A significant reduction in alanine transaminase (ALT) was observed in the carbon treated BDL and BDL+LPS groups compared to untreated groups. Carbon treatment was associated with a reduction in ALT from 73.95 $\pm$ 4.10 IU/ml to 61.02 $\pm$ 3.71U/ml ($p<0.05$) in BDL rats.

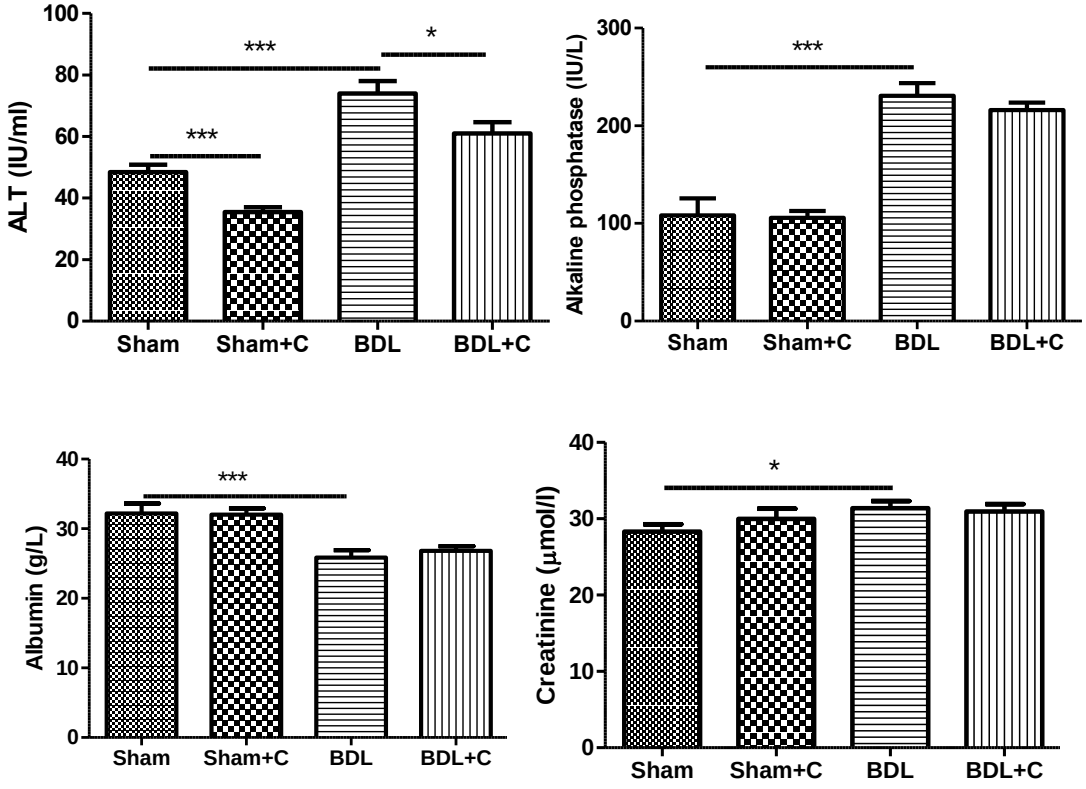

Figure 8.1 Biochemical response to oral Yaq-001 carbon therapy

(a) Alanine transaminase (Sham n=23, Sham+C n=19, BDL n=25, BDL+C n=25)
(b) Alkaline phosphatase (Sham n=21, Sham+C n=16, BDL n=25, BDL+C n=26)
(c) Albumin (Sham n=22, Sham+C n=16, BDL n=24, BDL+C n=25)
(d) Creatinine (Sham n=23, Sham+C n=18, BDL n=24, BDL+C n=25)

* denotes $p<0.05$

*** denotes $p<0.001$

8.3.2 Haemodynamic Profile

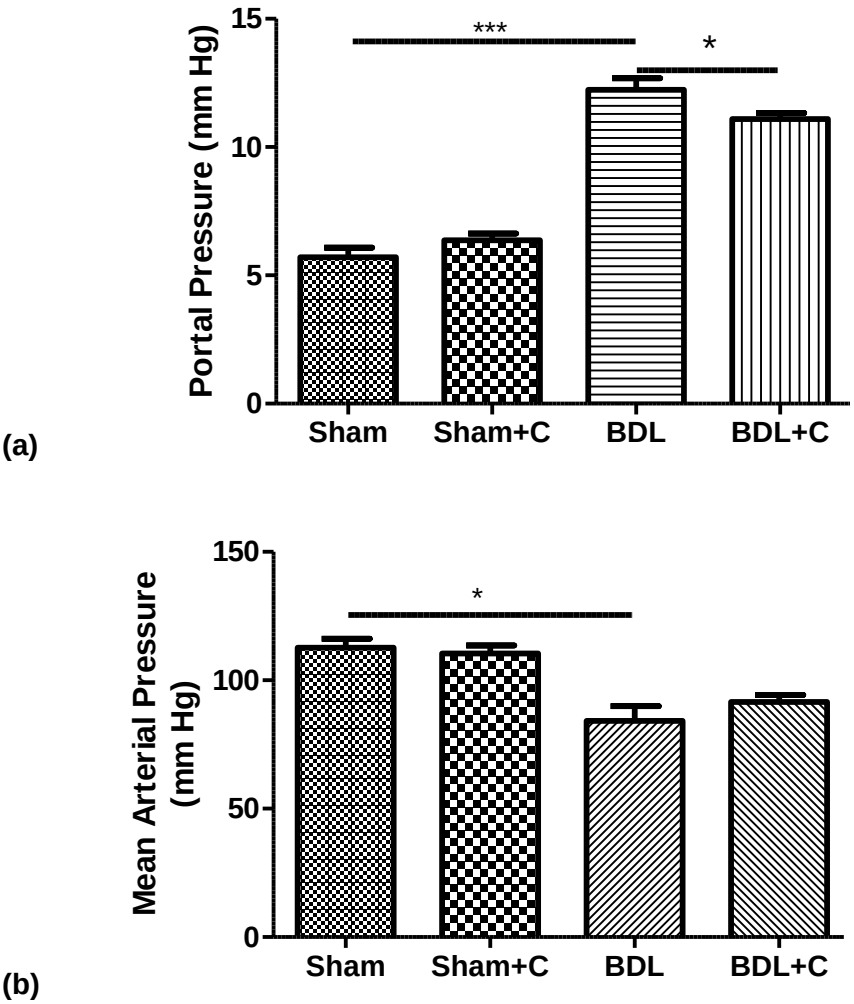

Figure 8.2 Haemodynamic Response to oral Yaq-001carbon therapy

(a) Portal Pressure (Sham n=21, Sham+C n=22, BDL n=14, BDL+C n=25)
(b) Mean Arterial Pressure (Sham n=13, Sham+C n=15, BDL n=12, BDL+C n=14) * denotes $p<0.05$ *** denotes $p<0.001$

A significant reduction in portal pressure was observed in BDL rats from 12.23 $\pm$ 0.45 mmHg untreated to 11.10 $\pm$ 0.23 mmHg with carbon, $p<0.05$) groups following carbon treatment. No significant change in mean arterial pressure was observed.

The effect size, as evidenced by Cohen's d, is 0.996 and therefore represents a large biological effect of Yaq-001 in this context.

8.3.3 Immunological Phenotype

8.3.3.1 Population studies

8.3.3.1.1 Liver

Kupffer cell population

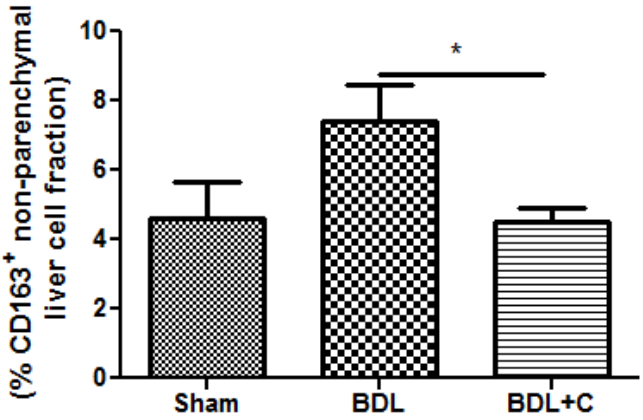

Figure 8.3 CD163^{+} gated liver non-parenchymal cell fraction as expressed as a percentage of the parent population in sham, bile duct ligated and carbon treated bile duct ligated rats (n=4/group) * denotes $p<0.05$

Liver Neutrophil Population

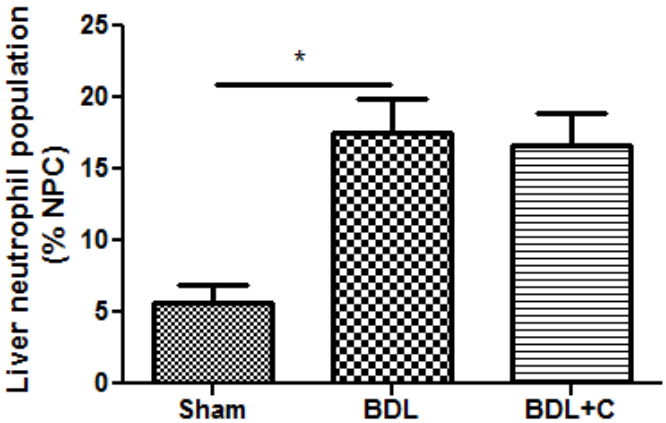

Figure 8.4 Liver neutrophil populations as expressed as a percentage of the parent liver non-parenchymal cell population in sham, bile duct ligated and carbon treated bile duct ligated rats. (n=4/group) * denotes $p<0.05$

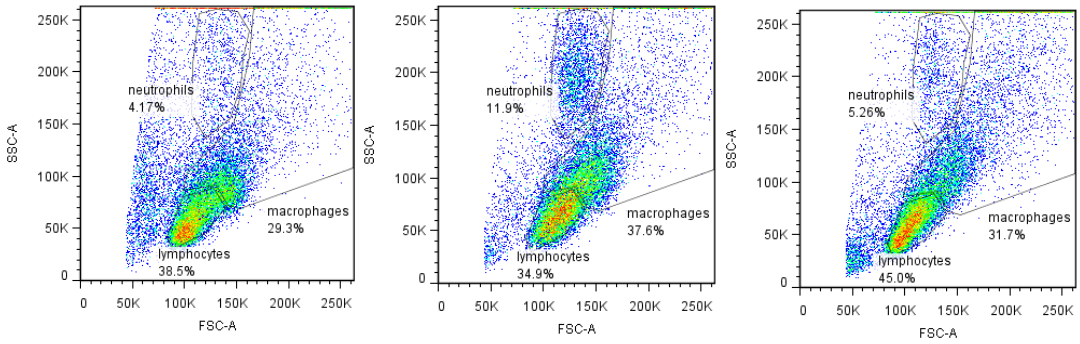

Figure 8.5 Plots demonstrating gating strategy for populations of liver non-parenchymal cells in sham, bile duct ligated and carbon treated bile duct ligated rats

Bile duct ligation was associated with a significant increase in liver neutrophil population with an upward trend in Kupffer cell (CD163+) populations. Oral Yaq-001 therapy resulted in a significant reduction in CD163+ populations in BDL rats with no impact on liver neutrophil populations.

8.3.3.1.2 Arterial and Portal Venous blood populations

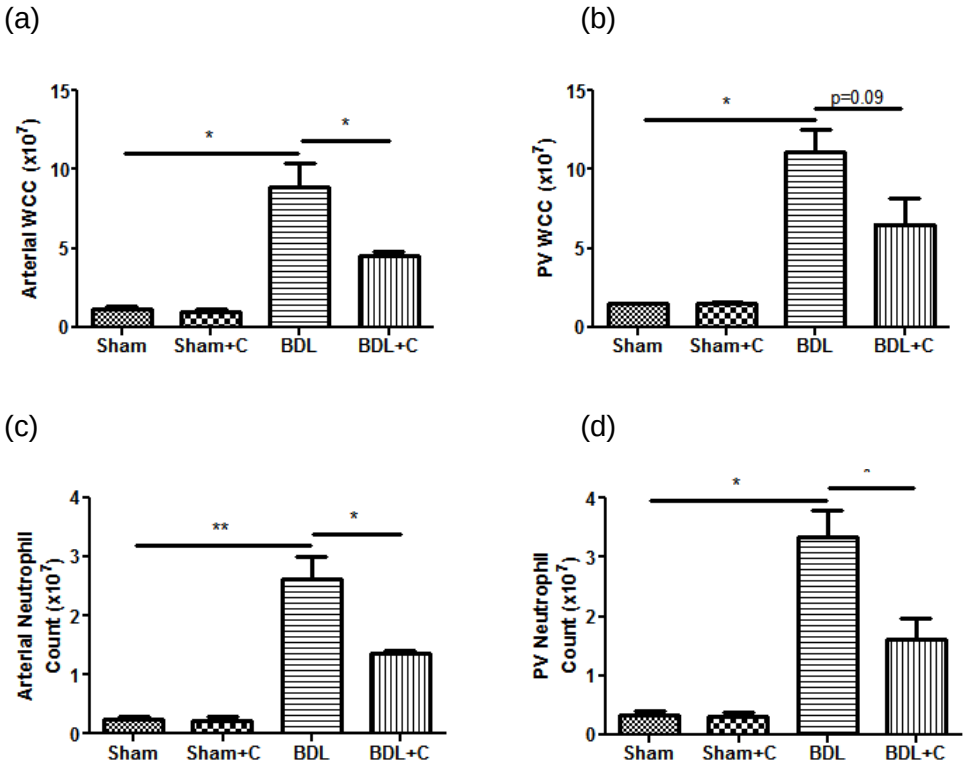

(e) (f)

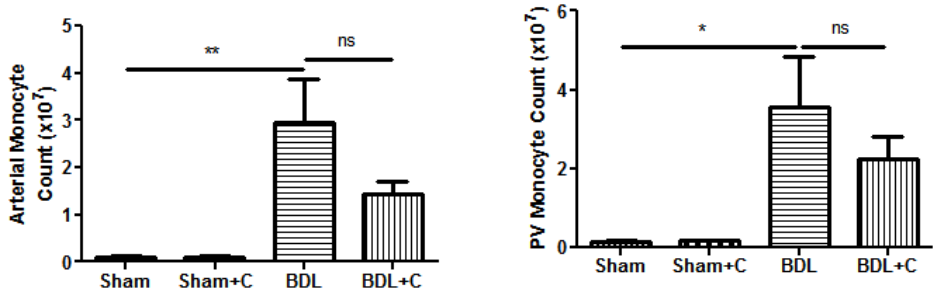

Figure 8.6 Absolute arterial and portal venous total, neutrophil and monocyte populations in sham, carbon treated sham, bile duct ligated and carbon treated bile duct ligated rats(n=4/group) * denotes $p<0.05$

a) Absolute leucocyte count in arterial blood (x10^7 cells/ml)
b) Absolute leucocyte count in portal venous blood (x10^7 cells/ml)
c) Absolute neutrophil count in arterial blood (x10^7 cells/ml)
d) Absolute neutrophil count in portal venous blood (x10^7 cells/ml)
e) Absolute monocyte count in arterial blood (x10^7 cells/ml)
f) Absolute monocyte count in portal venous blood (x10^7 cells/ml)

Monocyte subpopulations

(a) (b)

(c) (d)

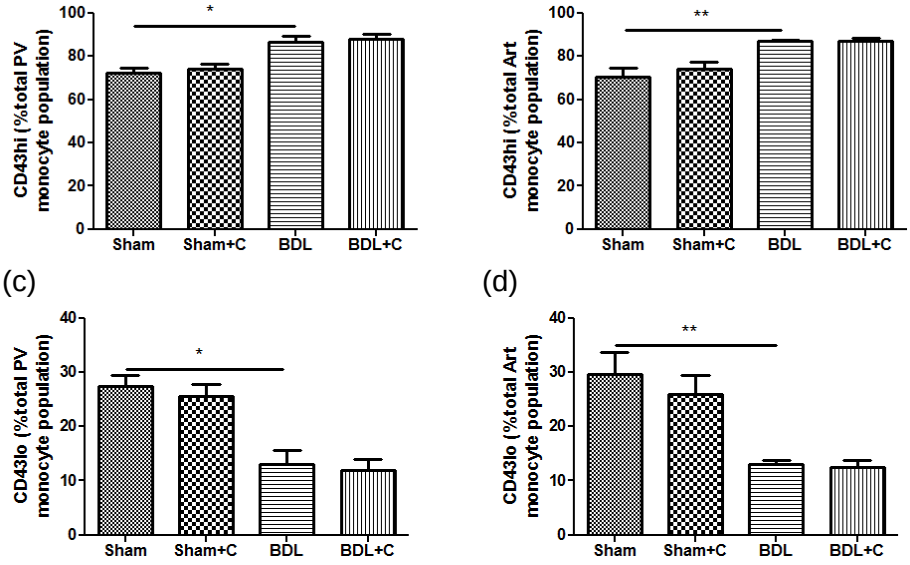

Figure 8.7 Arterial and portal venous monocyte subpopulations as expressed as a percentage of total monocyte count in sham, carbon treated sham, bile duct ligated and carbon treated bile duct ligated rats. (n=4/group) * denotes $p<0.05$

a) Portal venous CD43^{hi} monocyte populations
b) Arterial CD43^{hi} monocyte populations
c) Portal venous CD43^{lo} monocyte populations
d) Arterial CD43^{lo} monocyte populations

Significant expansions in total leucocyte, neutrophil and monocyte counts were observed with BDL rats compared to sham controls. Oral carbon therapy resulted in a significant reduction in neutrophil count with non-significant downward trends observed with total leucocyte and monocyte counts. No significant differences in total leucocyte, neutrophil or monocyte populations were observed between arterial and portal venous blood.

Monocyte subpopulations were evaluated to determine whether bile duct ligation resulted in polarisation of monocyte subpopulations and if so, whether carbon therapy could modulate this. Bile duct ligation was associated with a significant increase in the $CD43^{hi}$ sub-population at the expense of $CD43^{lo}$. Carbon therapy had no significant effect on the composition of monocyte subpopulations.

8.3.3.2.3 Mesenteric Lymph Node populations

(a) Mesenteric Lymph Node CD68$^+$ population

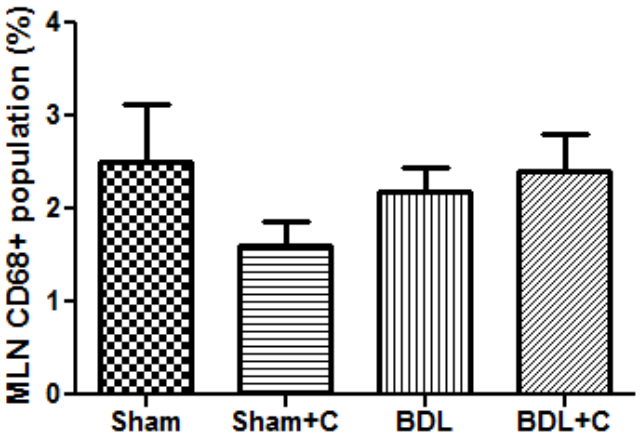

(b) Mesenteric Lymph Node CD68$^+$ absolute population

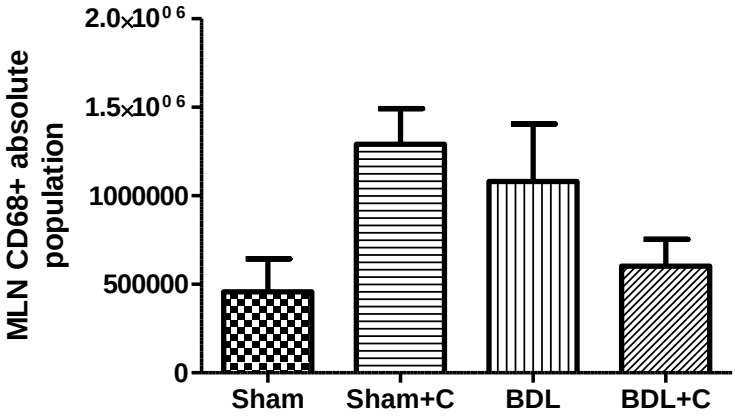

Figure 8.8 CD68$^+$ gated mesenteric lymph node populations in sham, carbon treated sham, bile duct ligated and carbon treated bile duct ligated rats

a) Relative populations (%total mesenteric lymph node cells)
b) Absolute populations (cells/ml)

(a) Mesenteric Lymph Node $CD68^+CD80^+$ population

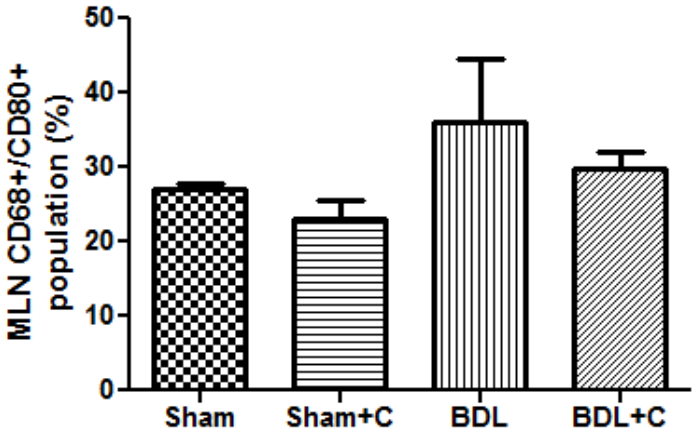

(b) Mesenteric Lymph Node absolute $CD68^+CD80^+$ populations

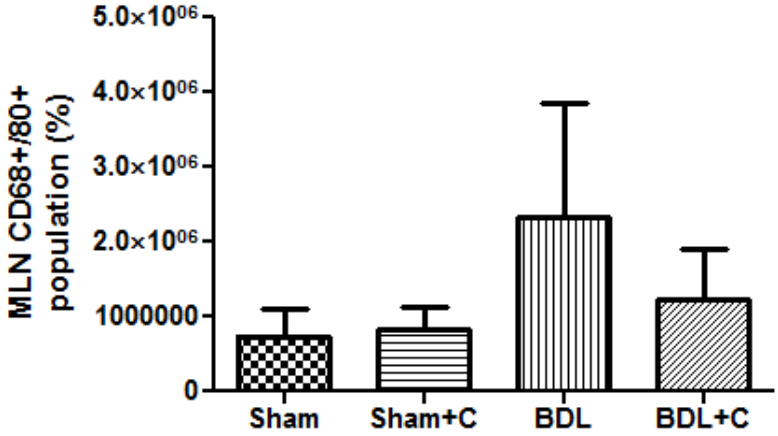

Figure 8.9 $CD68^+/CD80^+$ gated mesenteric lymph node populations in sham, carbon treated sham, bile duct ligated and carbon treated bile duct ligated rats. (n=4/group) * denotes $p<0.05$

a) Relative populations (%total mesenteric lymph node cells)
b) Absolute populations (cells/ml)

(a) Mesenteric Lymph Node CD163$^+$ population

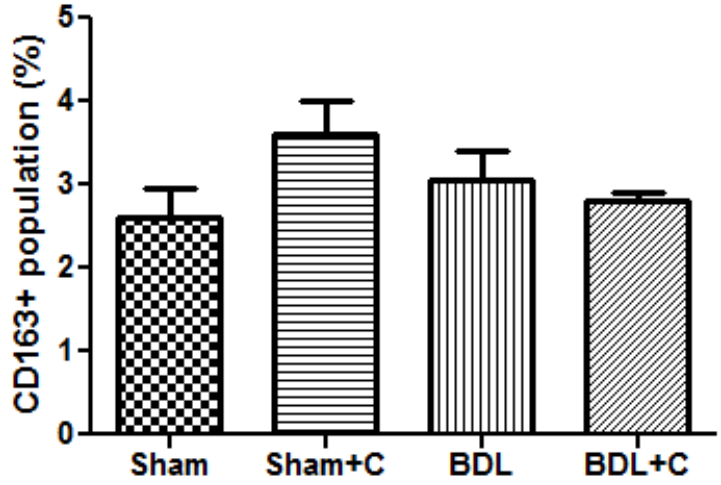

(b) Mesenteric Lymph Node absolute CD163$^+$ population

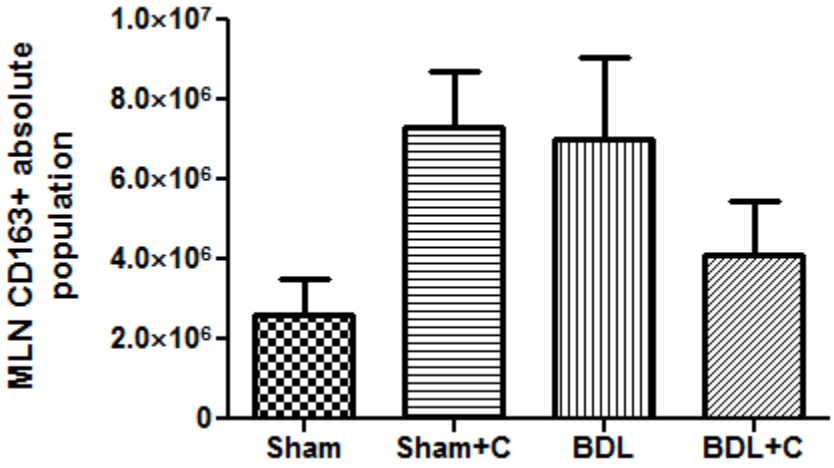

Figure 8.10 CD163$^+$ gated mesenteric lymph node populations in sham, carbon treated sham, bile duct ligated and carbon treated bile duct ligated rats. (n=4/group)

* denotes $p<0.05$

a) Relative populations (%total mesenteric lymph node cells)
b) Absolute populations (cells/ml)

No significant shifts in mesenteric lymph node populations were observed although bile duct ligation does appear to be associated with an upward trend in absolute CD163+ and CD68+ population. Carbon therapy appears to result in a downward trend in absolute CD163+ CD68+ mesenteric lymph node populations in BDL rats towards untreated sham controls.

8.3.3.2 ROS production

8.3.3.2.1 Liver

Total Liver ROS

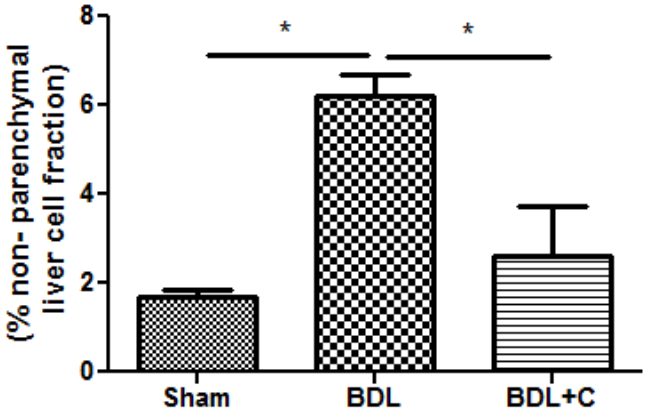

Figure 8.11 Total reactive oxidant species production in liver non-parenchymal cell fraction as expressed as a percentage of the parent population in sham, bile duct ligated and carbon treated bile duct ligated rats. (n=4/group) * denotes p<0.05

Kupffer cell ROS production

Constitutive ROS

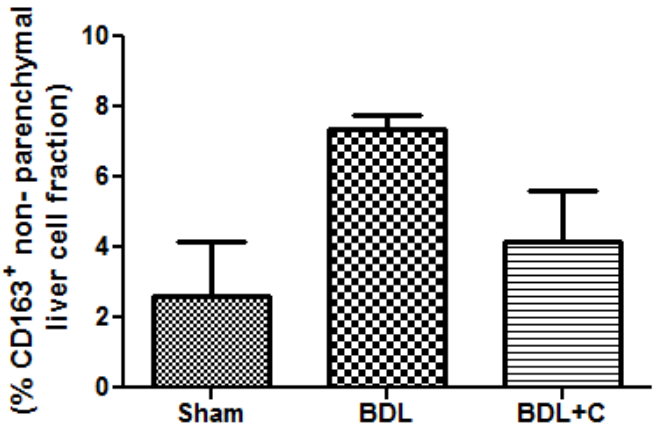

Figure 8.12 Constitutive reactive oxidant species production in CD163+-gated liver non-parenchymal cell fraction as expressed as a percentage of the parent population in sham, bile duct ligated and carbon treated bile duct ligated rats. (n=4/group)

* denotes p<0.05

LPS-induced ROS production

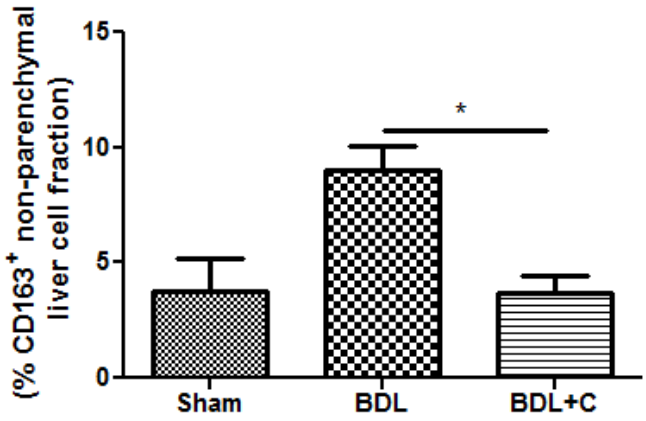

Figure 8.13 Lipopolysaccharide-induced reactive oxidant species production in CD163+-gated liver non-parenchymal cell fraction as expressed as a percentage of the parent population in sham, bile duct ligated and carbon treated bile duct ligated rats (n=4/group). * denotes $p<0.05$

Liver neutrophil ROS production

Constitutive ROS production

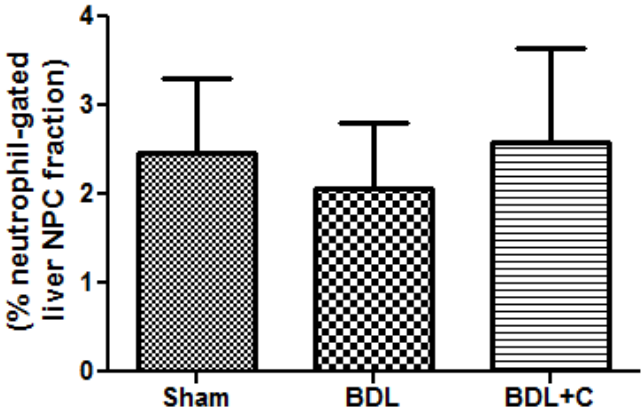

Figure 8.14 Constitutive reactive oxidant species production in neutrophil-gated liver non-parenchymal cell fraction as expressed as a percentage of the parent population in sham, bile duct ligated and carbon treated bile duct ligated rats. (n=4/group)

LPS-induced ROS production

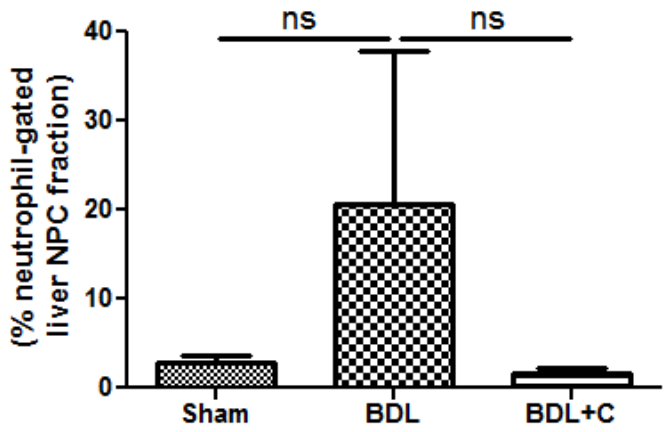

Figure 8.15 Lipopolysaccharide-induced reactive oxidant species production in neutrophil-gated liver non-parenchymal cell fraction as expressed as a percentage of the parent population in sham, bile duct ligated and carbon treated bile duct ligated rats. (n=4/group) * denotes $p<0.05$

Bile duct ligation was found to be associated with a significant increase in total ROS production within the liver total non-parenchymal cell (NPC) fraction with an upward trend in constitutive ROS production in CD163+-gated non-parenchymal cells. Oral carbon therapy was associated with a significant attenuation in constitutive ROS production in the NPC fraction of BDL rats. Whilst a downward trend in constitutive ROS was observed in CD163+-gated populations, this did not achieve statistical significance. No significant differences were observed in liver neutrophil constitutive ROS. The discordance may be accounted for by non-parenchymal liver cell populations other than Kupffer cells and neutrophils. These include stellate cells, cholangiocytes, sinusoidal endothelial cells and intrahepatic lymphocytes.

Despite these observations, Yaq-001 therapy was associated with a significant reduction in LPS-induced ROS production in BDL rats. This is suggestive that the carbon therapy has a particular effect on LPS-sensitivity, diminishing the primed state observed in BDL rats. No significant differences were observed in LPS-induced neutrophil ROS between sham and BDL and untreated and Yaq-001-treated BDL

rats. Marked heterogeneity in neutrophil LPS-induced ROS production were observed in BDL rats contributing to the broad standard error values. In the light of such heterogeneity and small group numbers, statistical significance was not observed.

8.3.3.2.2 ROS production (Portal Venous blood)

Monocyte populations

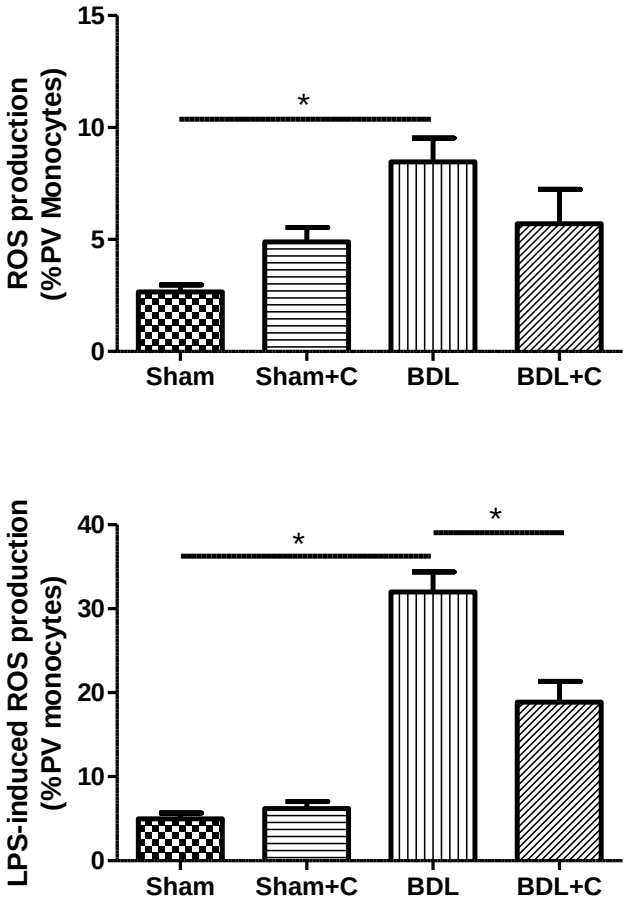

Figure 8.16 Constitutive and lipopolysaccharide-induced reactive oxidant species production in portal venous monocytes as expressed as a percentage of total monocyte count in sham, carbon treated sham, bile duct ligated and carbon treated bile duct ligated rats. (n=4/group) * denotes $p<0.05$

Monocyte subpopulations

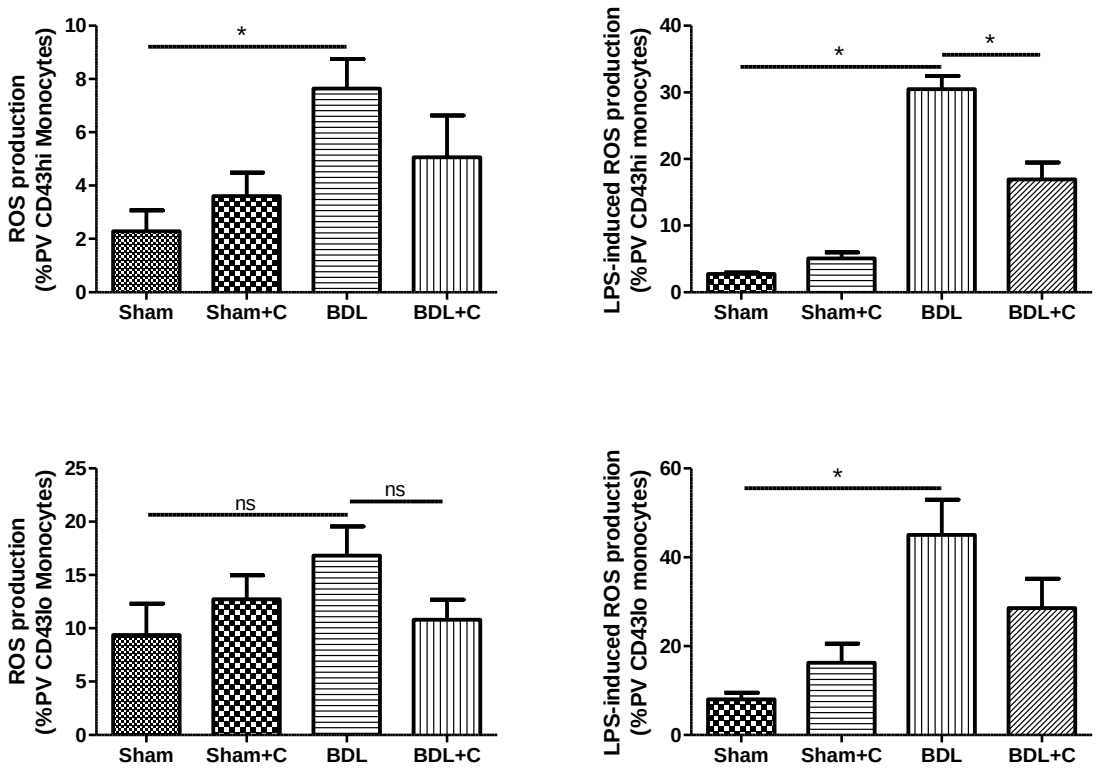

Figure 8.17 Constitutive and lipopolysaccharide-induced reactive oxidant species production in portal venous monocyte subpopulations as expressed as a percentage of total monocyte count in sham, carbon treated sham, bile duct ligated and carbon treated bile duct ligated rats. (n=4/group) * denotes $p<0.05$

Neutrophil populations

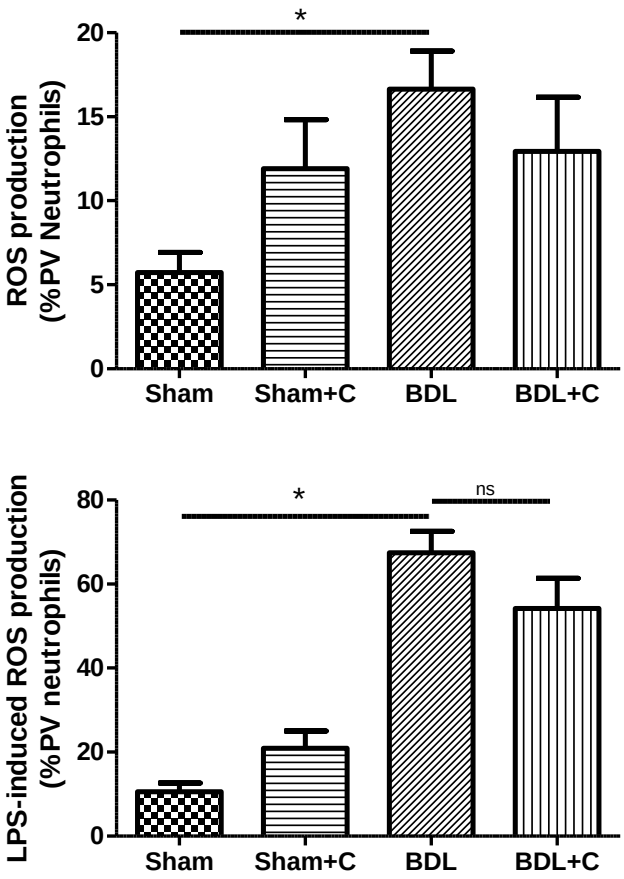

Figure 8.18 Constitutive and lipopolysaccharide-induced reactive oxidant species production in portal venous neutrophils as expressed as a percentage of total monocyte count in sham, carbon treated sham, bile duct ligated and carbon treated bile duct ligated rats. (n=4/group) * denotes $p<0.05$

Functionally, bile duct ligation was associated with a significant increase in constitutive and LPS-induced ROS production from portal venous monocytes and neutrophils. Carbon therapy resulted in a significant attenuation of portal venous monocyte LPS-induced ROS production in BDL rats suggestive of a diminished primed state to endotoxin challenge. This effect was observed within the $CD43^{hi}$ monocyte sub populations. In contrast, no significant differences in portal venous neutrophil phenotype were observed with carbon therapy in BDL rats although downward trends towards sham controls were observed. Regulation of endotoxin sensitivity is regulated most stringently in monocyte/macrophage populations. They

are considered the cellular mediators of endotoxin tolerance and phenotype most responsive to changes in endotoxin concentrations. This may account for the differential effect of Yaq-001 on LPS-induced ROS production in portal venous blood.

8.3.3.2.3 Phagocytosis

Kupffer Cell Phagocytosis

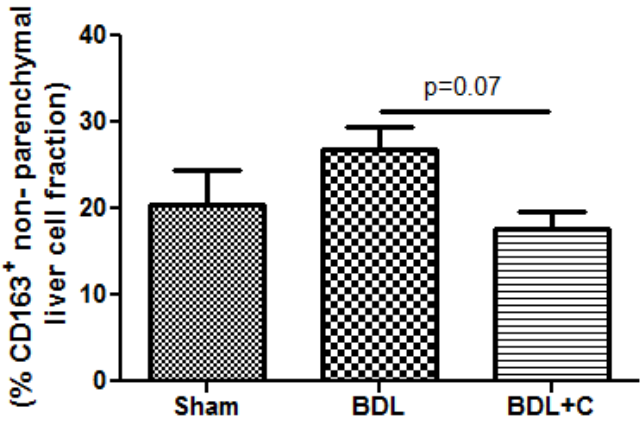

Figure 8.19 Phagocytosis of bead particles in CD163+-gated liver non-parenchymal cell fraction as expressed as a percentage of the parent population in sham, bile duct ligated and carbon treated bile duct ligated rats. (n=4/group)

Liver Neutrophil Phagocytosis

P3-gated

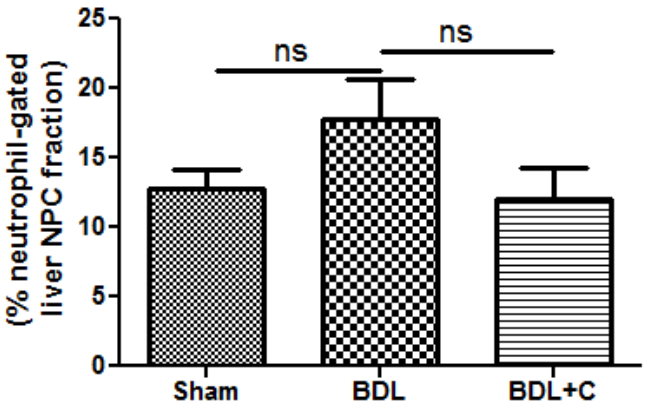

Figure 8.20 Phagocytosis of bead particles (P3-gated) in neutrophil-gated liver non-parenchymal cell fraction as expressed as a percentage of the parent population in sham, bile duct ligated and carbon treated bile duct ligated rats. P3=phagocytosis of 3 or more beads. (n=4/group)

Total Phagocytosis

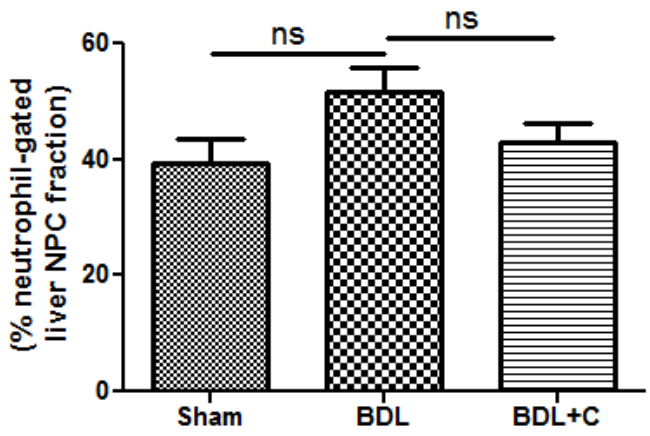

Figure 8.21 Phagocytosis of bead particles in neutrophil-gated liver non-parenchymal cell fraction as expressed as a percentage of the parent population in sham, bile duct ligated and carbon treated bile duct ligated rats. (n=4/group)

No significant differences in phagocytosis were observed between sham , BDL and carbon-treated BDL rats. A downward trend towards sham control values were observed with carbon-treated BDL rats.

Gating strategy for phagocytosis assays

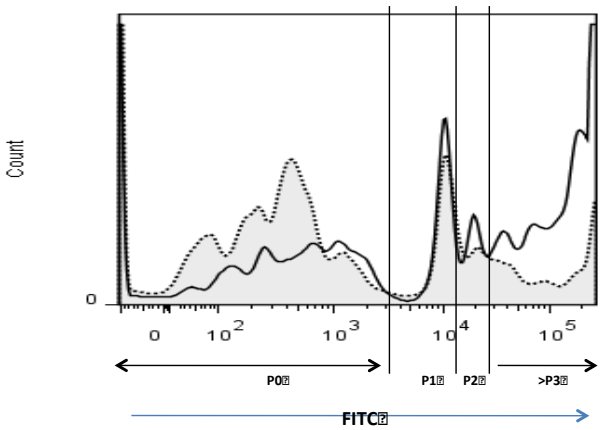

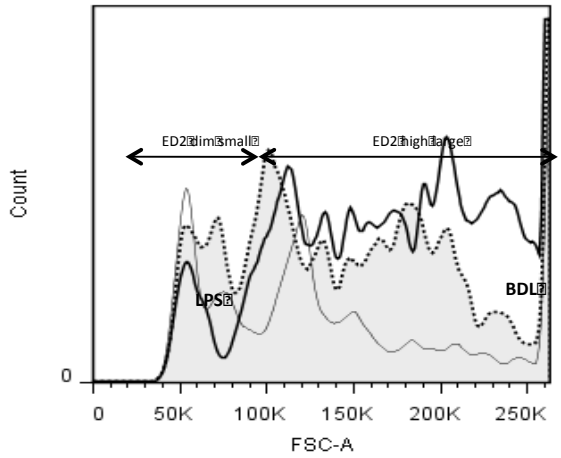
Count
0
0
50K
100K
150K
200K
250K
FSC-A
LPS
BDL

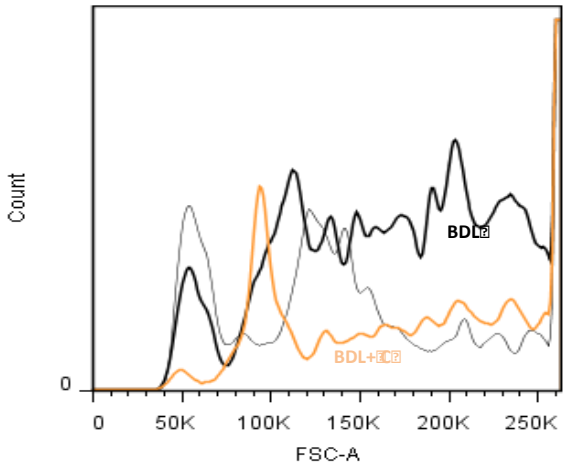
Count
0
0
50K
100K
150K
200K
250K
FSC-A
BDL

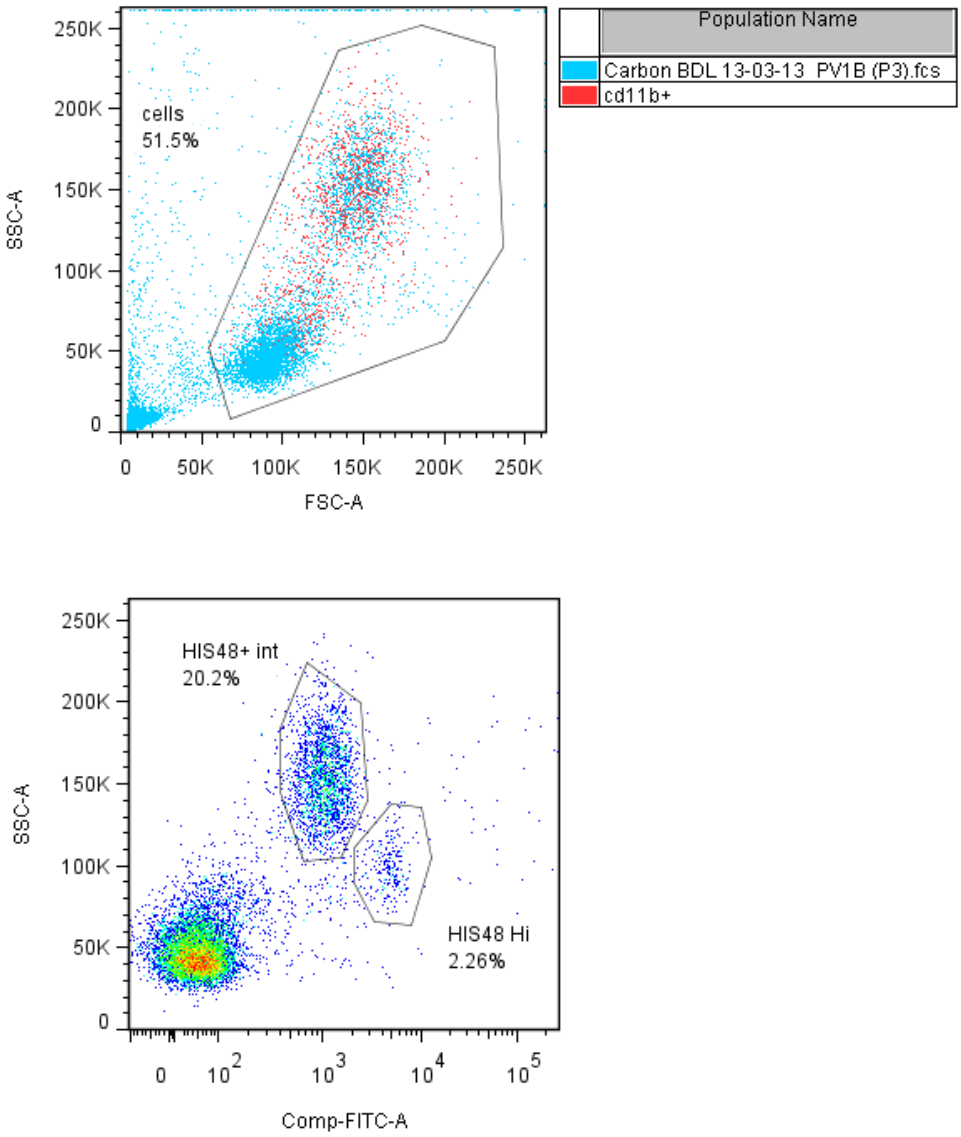

Figure 8.22 Plots demonstrating gating strategy for populations of whole blood in sham, carbon treated sham, bile duct ligated and carbon treated bile duct ligated rats

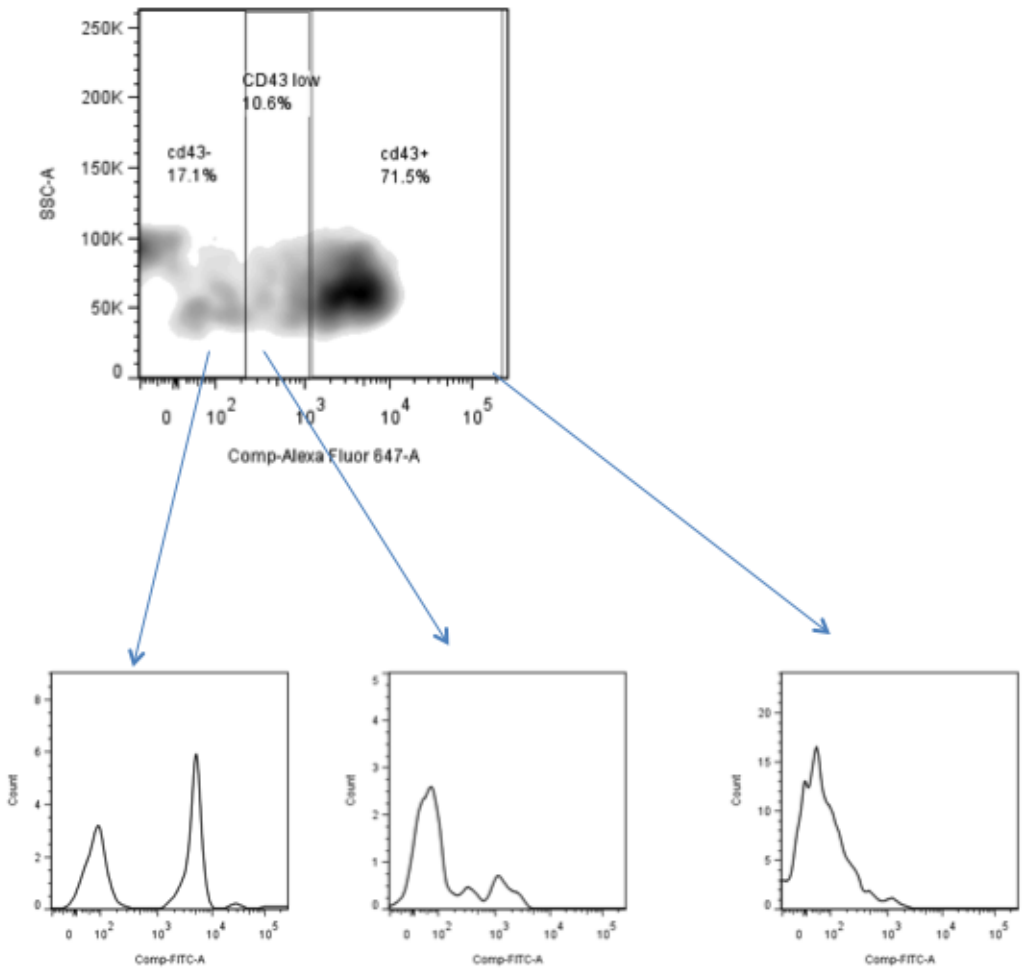

Figure 8.23 Histograms demonstrating gating strategy for populations of whole blood in sham, carbon treated sham, bile duct ligated and carbon treated bile duct ligated rats

8.3.3.4 Inflammasome activation

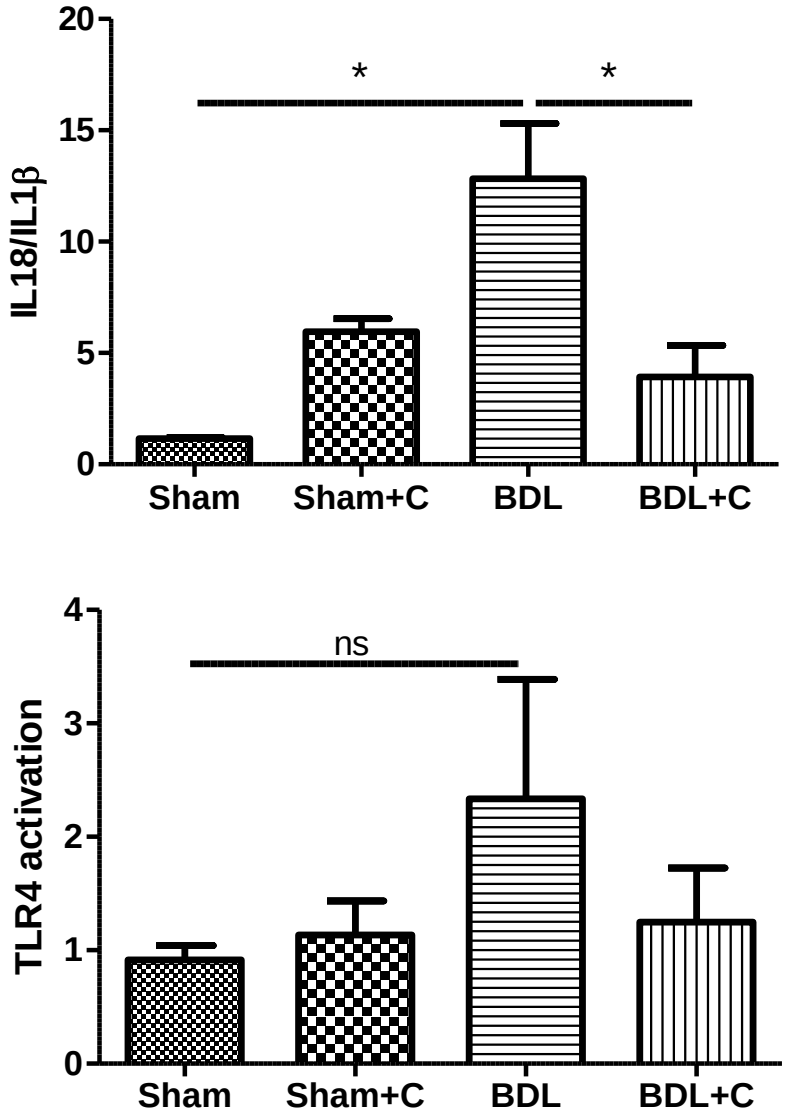

Figure 8.24 (a) Inflammasome activation with arterial plasma in HEK reporter cells (b) TLR4 activation with arterial plasma in HEK reporter cells (n=4/group) * denotes $p<0.05$

Bile duct ligation was associated with a significant increase in inflammasome activation which was attenuated with carbon therapy. Similar trends were observed with TLR4 reporter cell lines but did not achieve statistical significance.

8.3.3.5 Terminal Ileal TNFα gene expression

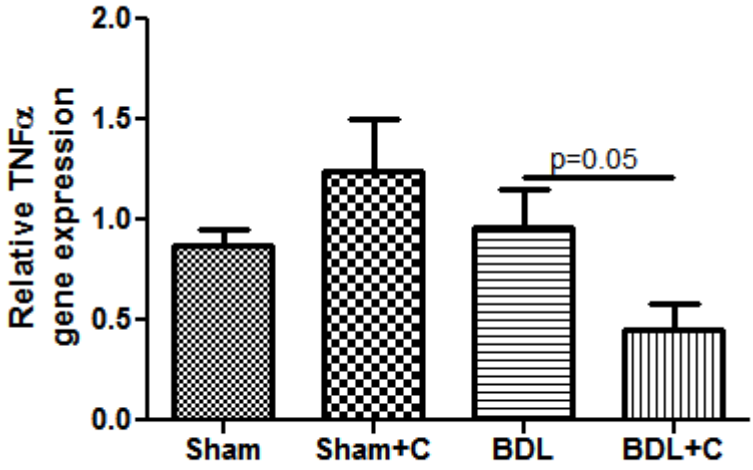

Figure 8.25 Relative expression of TNFα in terminal ileal tissue of sham, sham+ carbon, BDL, BDL+carbon (n=4/group) * denotes p<0.05

No significant increase in terminal ileal TNFα gene expression was observed. Carbon therapy resulted in a borderline significant reduction increase in terminal ileal TNFα gene expression.

8.3.4 Gut Barrier Integrity

8.3.4.1 Intestinal Permeability Assays

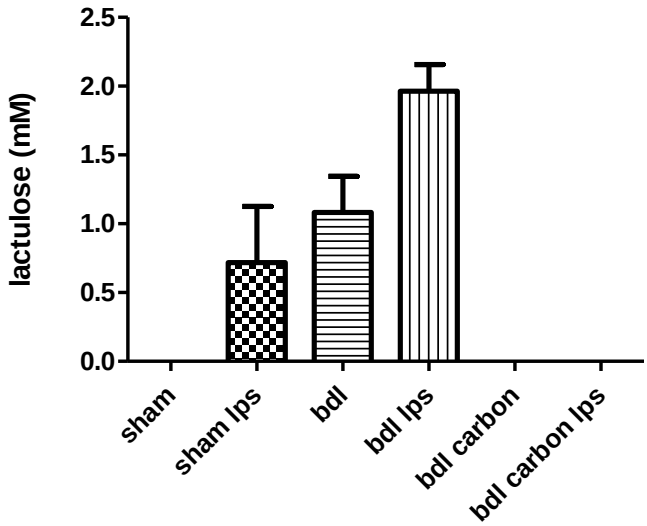

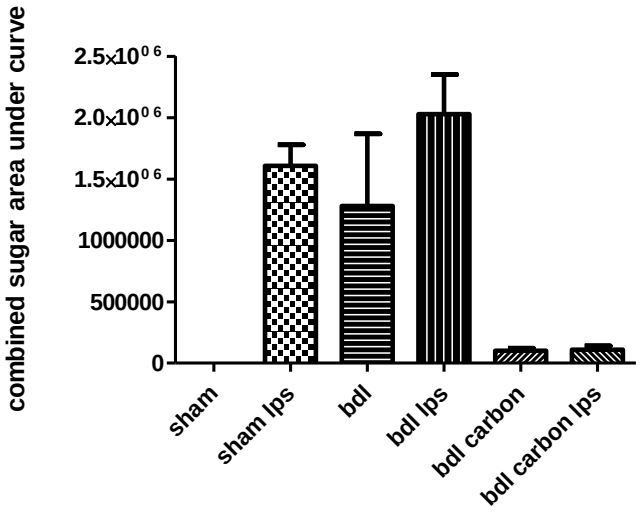

Figure 8.26 5 hour urinary excretion of lactulose, rhamnose and 6-OMG in sham, sham+LPS, BDL, BDL+LPS, BDL+carbon, BDL+LPS+carbon. (n=4/group)

* denotes<0.05

Progressive increases in intestinal permeability as evidenced by increased excretion of lactulose, rhamnose and 6-o-methyl-glucose is observed with bile duct ligation and BDL with intraperitoneal LPS challenge. Carbon therapy resulted in a significant reduction in urinary excretion of lactulose, rhamnose and 6-o-methyl-glucose. Yaq-001 exhibits preferential adsorption for hydrophobic compounds. In principal therefore, Yaq-001 should not bind the sugar probes in this study.

8.3.4.2 Paneth Cell Gene Expression Data

(a)

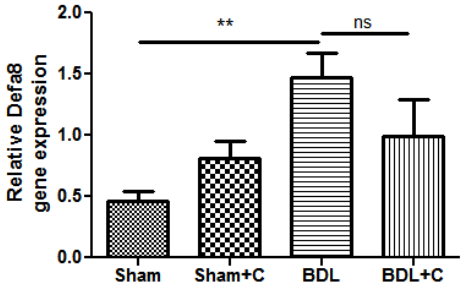

(b)

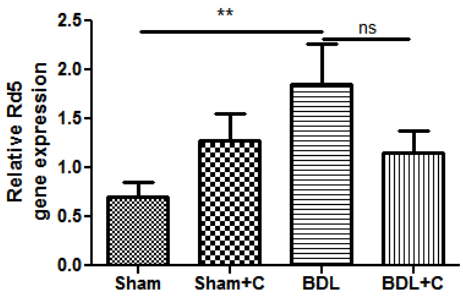

(c)

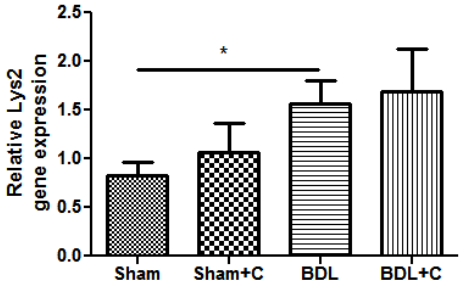

Figure 8.27 Relative gene expression in the terminal ileum of sham and BDL rats with and without carbon therapy regards to:

a. defensin 8
b. defensin 5
c. lysozyme 2

Significant increases in gene expression Paneth cell markers defensins 5,8 and lysozyme 2 was observed in terminal ileal tissue of BDL rats compared to sham controls. Downward trends in defensin 5 and 8 gene expression were observed with carbon-treated BDL rats although no significant changes were observed with lysozyme expression.

8.3.4.3 Nutrition

8.3.4.3.1 Weight

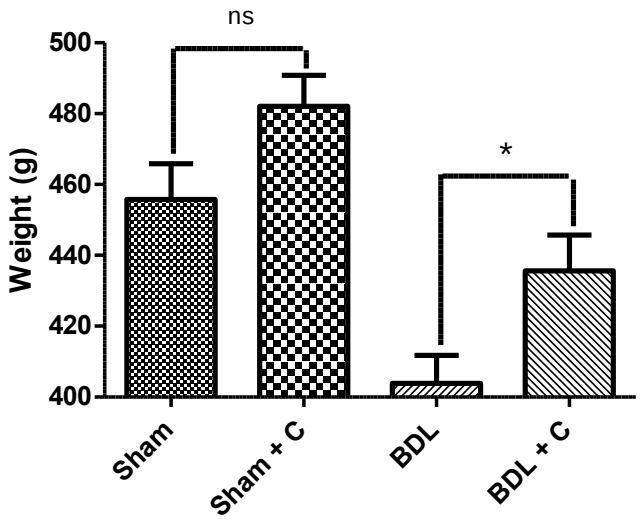

Figure 8.28 Final body weight in sham, carbon treated sham, bile duct ligated and carbon treated bile duct ligated rats. . (n=4/group) * denotes<0.05

8.3.4.3.2 Micronutrients and electrolytes

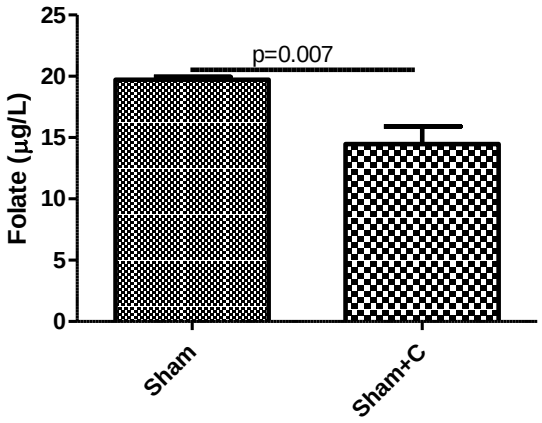

Figure 8.29 Plasma folate concentrations in sham and carbon treated sham rats (n=6/group) * denotes<0.05

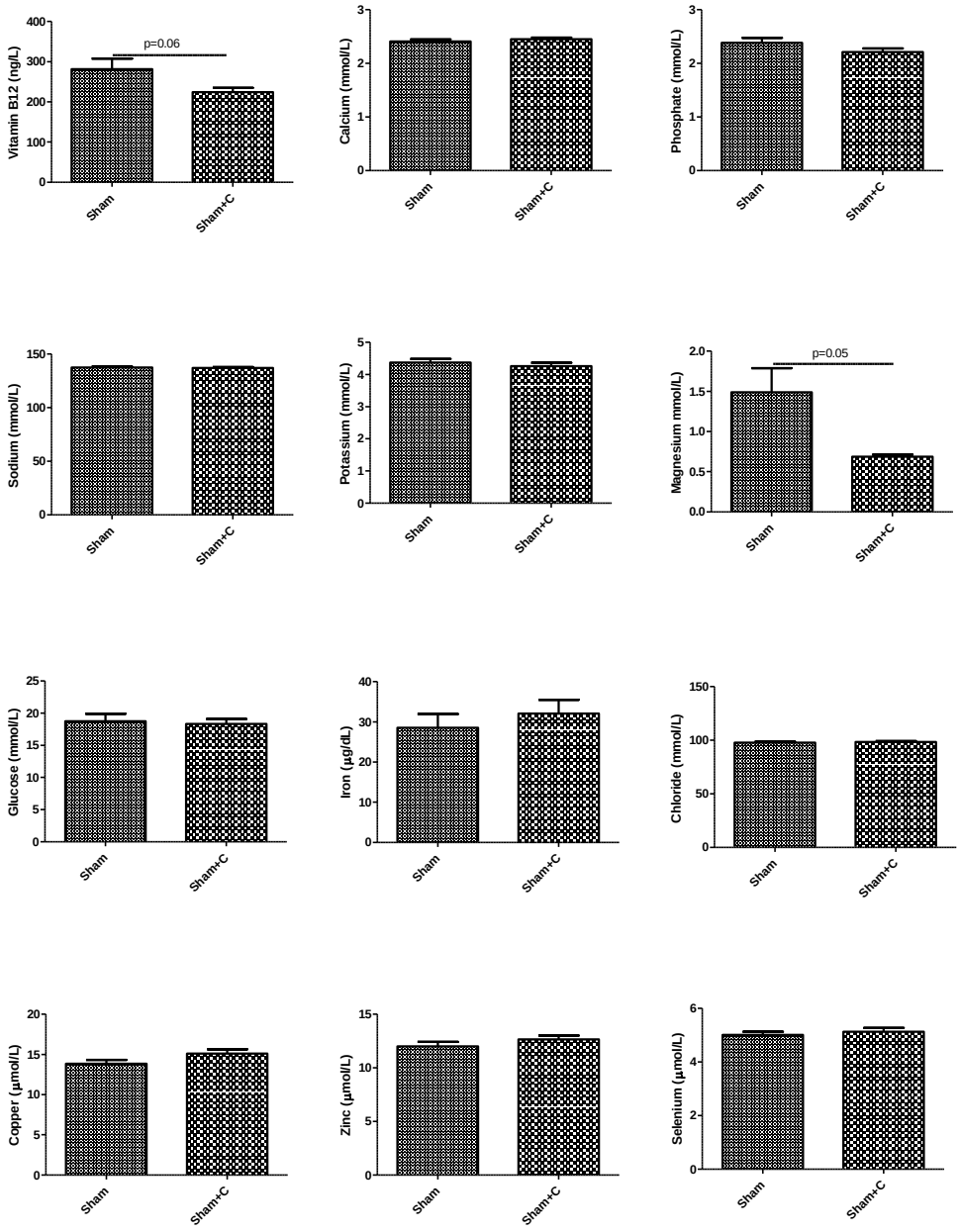

Figure 8.30 Plasma micronutrient and electrolyte concentrations in sham and carbon treated sham rats (n=6/group) * denotes<0.05

Bile duct ligation was associated with a significant reduction in final body weight. Carbon treatment results in a significant improvement in 4 week body weight. No significant effect on micronutrient and electrolyte profile was observed with the exception of folate.

8.3.4.3.2 Primary Bile acid profile

Cholic acid

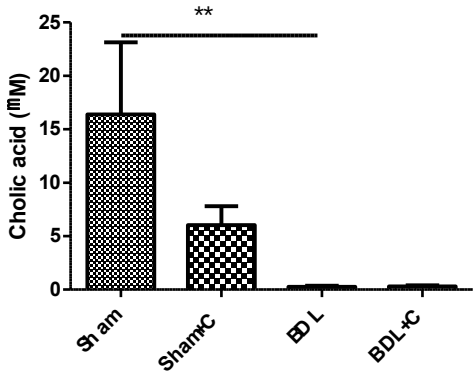

Glycocholic acid

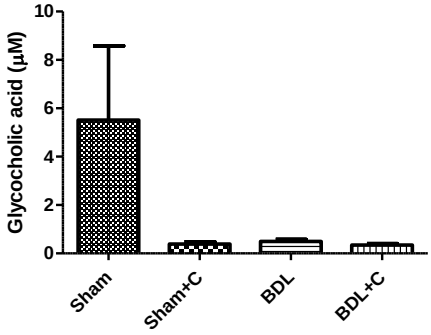

Taurocholic acid

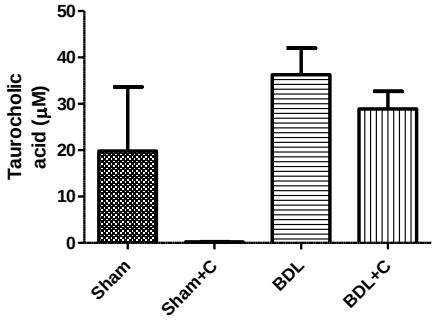

Figure 8.31 Arterial concentrations of cholic acid and derivatives in sham, carbon treated sham, BDL and BDL+carbon rats at 4 weeks post-surgery (n=6/group)

* denotes<0.05

a) Cholic acid
b) Glycocholic acid
c) Taurocholic acid

Chenodeoxycholic acid

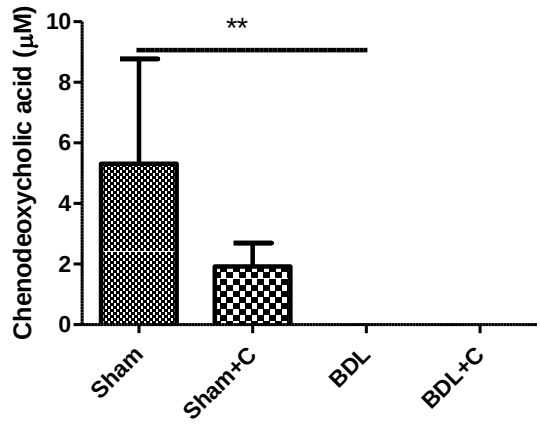

Glycochenodeoxycholic acid

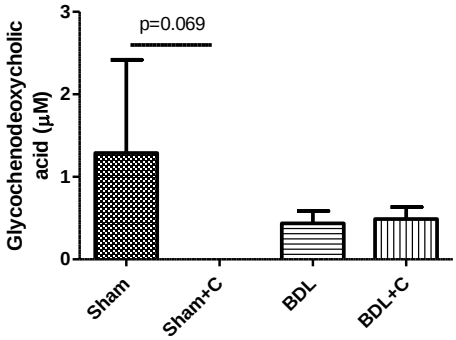

Taurochenodeoxycholic acid

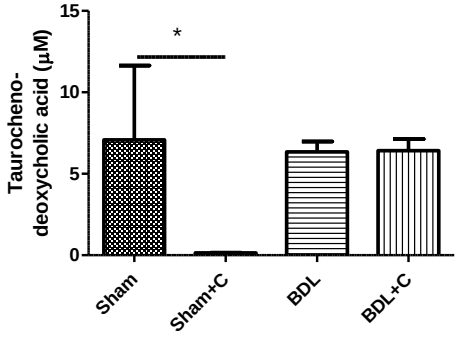

Figure 8.32 Arterial concentrations of chenodeoxycholic acid and derivatives in sham, carbon treated sham, BDL and BDL+carbon rats at 4 weeks post-surgery (n=6/group) * denotes<0.05

a) Chenodeoxycholic acid
b) Glycochenodeoxycholic acid
c) Taurochenodeoxycholic acid

Secondary Bile acids

Deoxycholic Acid

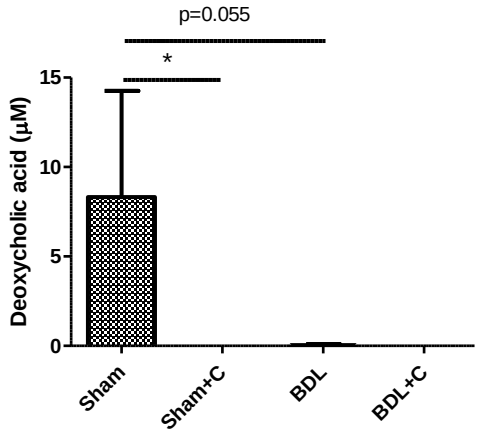

Glycodeoxycholic acid

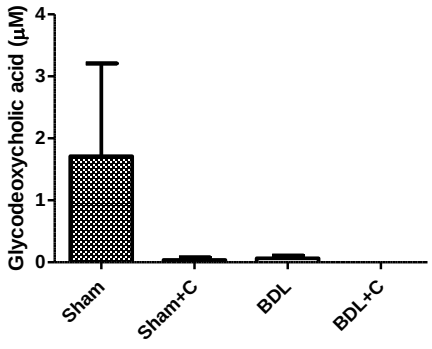

Taurodeoxycholic acid

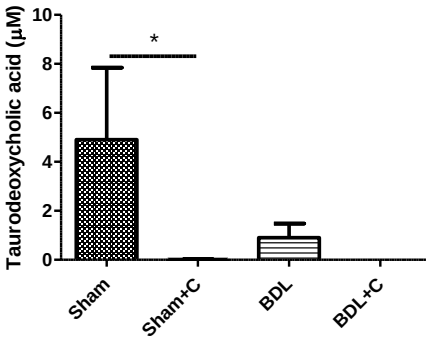

Figure 8.33 Arterial concentrations of deoxycholic acid and derivatives in sham, carbon treated sham, BDL and BDL+carbon rats at 4 weeks post-surgery (n=6/group) * denotes<0.05

a) Deoxycholic acid
b) Glycodeoxycholic acid
c) Taurodeoxycholic acid

Lithocholic acid

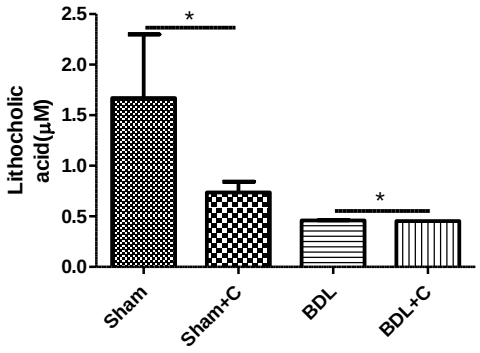

Glycolithocholic acid

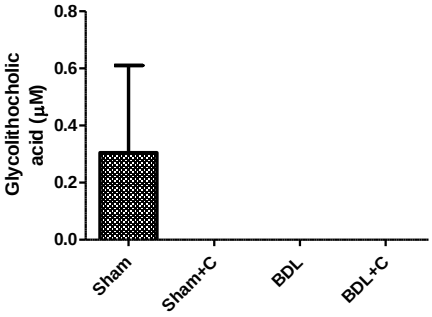

Taurolithocholic acid

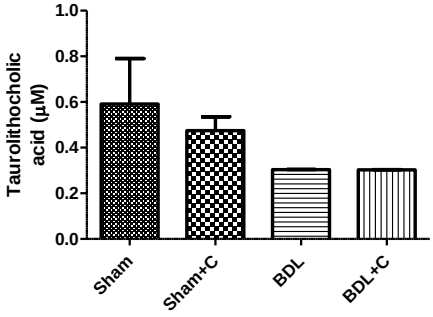

Figure 8.34 Arterial concentrations of lithocholic acid and derivatives in sham, carbon treated sham, BDL and BDL+carbon rats at 4 weeks post-surgery (n=6/group) * denotes<0.05

a) Lithocholic acid
b) Glycolithocholic acid
c) Taurolithocholic acid

Ursodeoxycholic acid

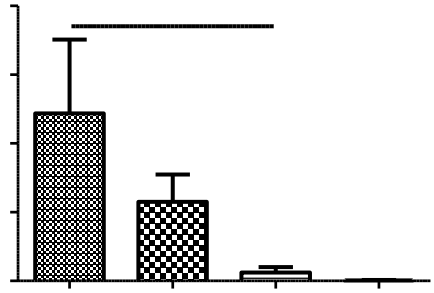

Glycoursodeoxycholic acid

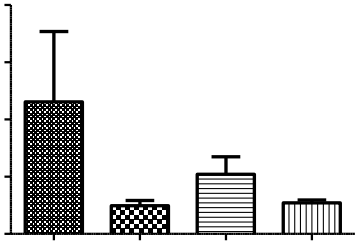

Tauroursodeoxycholic acid

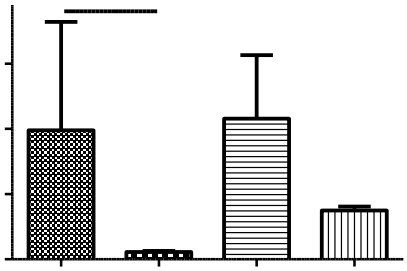

Figure 8.35 Arterial concentrations of ursodeoxycholic acid and derivatives in sham, carbon treated sham, BDL and BDL+carbon rats at 4 weeks post-surgery (n=6/group) * denotes<0.05

a) Ursodeoxycholic acid
b) Glycoursodeoxycholic acid
c) Tauroursodeoxycholic acid

Muricholic acid

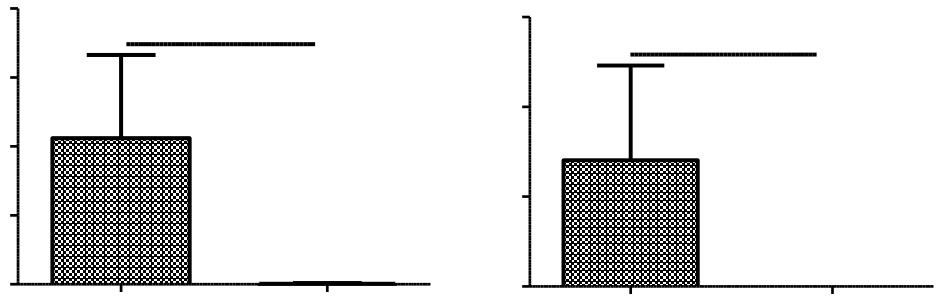

Figure 8.36 Arterial concentrations of muricholic acid in sham, carbon treated sham, BDL and BDL+carbon rats at 4 weeks post-surgery (n=6/group)
* denotes<0.05

Bile duct ligation was found to be associated with a marked reduction in several unconjugated plasma bile acids. Significant reductions were observed with primary bile acids cholic acid, chenodeoxycholic acid and secondary bile acids ursodeoxycholic acid, lithocholic acid and a near significant reduction with deoxycholic acid (p=0.05). Alpha muricholic acid, a rodent FXR antagonist was also found to be significantly depleted with bile duct ligation as compared to sham.

A significant reduction in deoxycholic acid was observed in carbon-treated sham rats compared to untreated controls. Non-significant downward trends in several bile acids were observed in carbon-treated sham rats compared to sham controls (albeit in context of wide standard error margins).

A significant 16 fold increase in urinary bile acids was observed with bile duct ligated rats compared to sham controls. No significant increases were observed with carbon treated sham or BDL compared to untreated controls.

One potential explanation for differential bile acid adsorption is that Yaq-001 has preferential adsorption for hydrophobic compounds. Bile acids differ in their hydrophobicity as illustrated in figure x with more hydrophobic compounds implicated in hepatotoxicity, cholestasis, necrosis and apoptosis of hepatocytes. We did observe significant reductions in arterial secondary bile acids LCA, DCA but not total primary bile acids CA and CDCA in sham operated rats. Against this argument is the observation that Yaq-001 did also bind the more hydrophilic bile acids aMCA and b-MCA. More hydrophilic compounds are generally hepatoprotective and hydrophobic more hepatotoxic. The net effect on liver injury is a function of the combination and size of the bile acid pool. FXR signaling is an important component of the gut-liver axis. Adsorption of bile acids has the potential to alter this however, biochemically a net improvement in liver injury is observed with Yaq-001 which is the most important

end point. Further studies are required to determine the effect of Yaq-001 on FXR pathways and total bile acid pool.

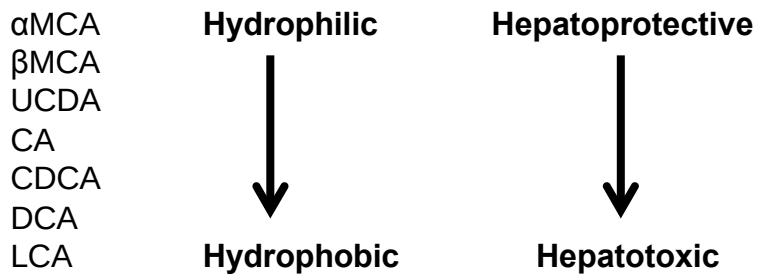

Figure 8.37 Hydrophobicity Index of Bile Acids

8.3.5 Stool Microbiome (Phylogenic Studies)

8.3.5.1 Phyla Level

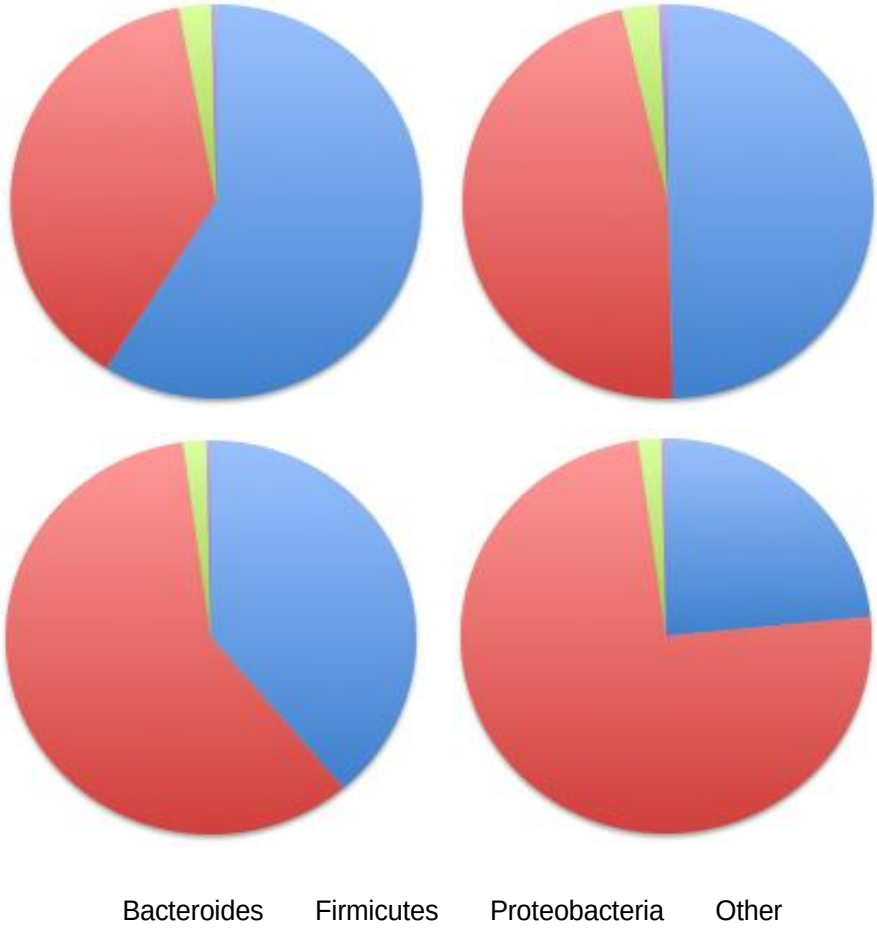

Figure 8.37 Phylogenic profile of stool (phyla level)
a) Sham rats untreated
b) Bile duct ligated rats untreated
c) Sham rats with carbon treatment
d) Bile duct ligated rats with carbon treatment

Bile duct ligation was associated with an expansion in the relative population of the Firmicutes phyla compared to sham rats (Sham 38.0±9.2% vs BDL 59.0±7.2%, p>0.05). A reciprocal reduction in the Bacteroides phyla was observed (Sham 59.0±9.6% vs BDL 39.0±7.3%, p>0.05). Yaq-001 treatment was associated with near significant increases in Firmicutes (BDLC 74.3±4.4% vs BDL 59.0±7.2%, p=0.05) and reductions in Bacteroides (BDLC 23.4±4.0% vs BDL 39.0±7.3%, p=0.07) in BDL rats. No effect was observed with Yaq-001 in sham controls.

8.3.5.2 Order level

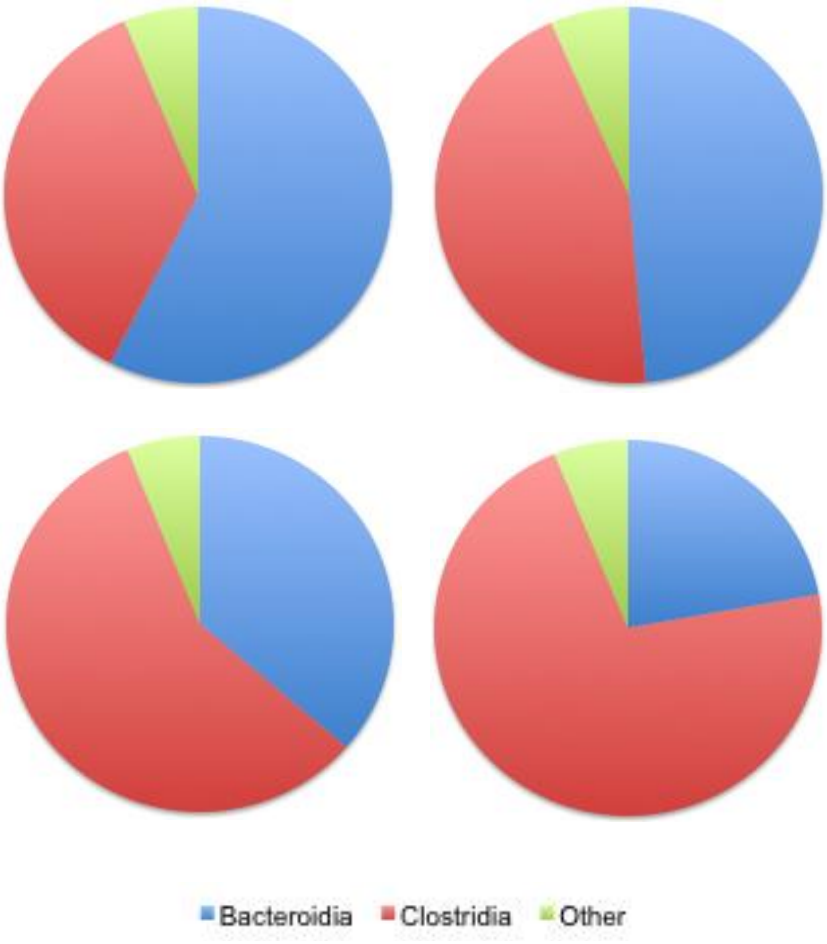

Figure 8.38 Phylogenic profile of stool (order level)

a) Sham rats untreated
b) Bile duct ligated rats untreated
c) Sham rats with carbon treatment
d) Bile duct ligated rats with carbon treatment

Yaq-001 treatment was associated with significantly lower Bacteroidia populations in BDL rats (BDLC 22.1±3.9% vs BDL 36.4±7.1% p=0.049). No significant difference in Bacteroidia populations was observed with carbon-treated sham rats (ShamC 48.6±11.4 vs Sham 57.5±9.7%, p>0.05). Yaq-001 treatment was not associated with any significant differences in BDL or Sham rats (BDLC 71.6±4.7% vs BDL 57.5±7.3, p>0.05), (ShamC 36.3±9.5 vs Sham 36.3±9.6, p>0.05).

8.3.5.3 Family level

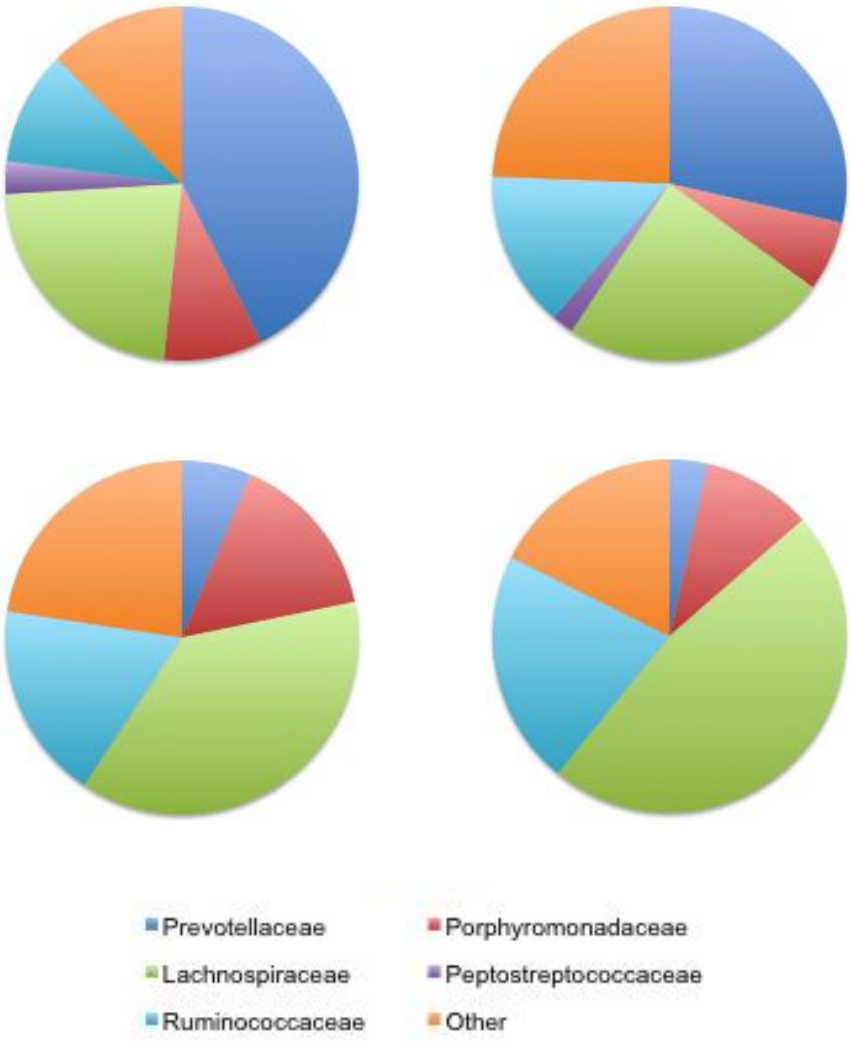

Figure 8.39 Phylogenic profile of stool (family level)

a) Sham rats untreated
b) Bile duct ligated rats untreated
c) Sham rats with carbon treatment
d) Bile duct ligated rats with carbon treatment

Bile duct ligated rats were found to have significantly higher populations of Porphyromonadaceae compared to sham controls (BDL 15.4±1.7% vs Sham 9.0±1.4%, p=0.004). Yaq-001 significantly lowered the Porphyromonadaceae populations in BDL rats compared to untreated controls (BDLC 10.1±3.5% vs BDL 15.4±1.7%, p=0.02). A downward trend towards reduction in Prevotellaceae and increase in Ruminococcaceae populations were observed in BDL compared to sham

rats (Sham 42.6±12.9% vs BDL 6.3±1.8%, p=0.07 and Sham 28.5±9.8% vs BDL 49.3±6.6%, p=0.09 respectively) but no significant changes with Yaq-001 in either sham or BDL rats were observed. No significant differences in Lachnospiraceae populations were observed between BDL and sham rats, Yaq-001-treated and untreated BDL or sham rats. Peptostreptococcaceae populations collapsed in BDL rats compared to sham controls (BDL 0±0% vs Sham 8.2±1.7%, p=0.005). No significant differences were observed with Yaq-001 treatment in either BDL or sham rats.

8.3.5.4 Genus Level

a.

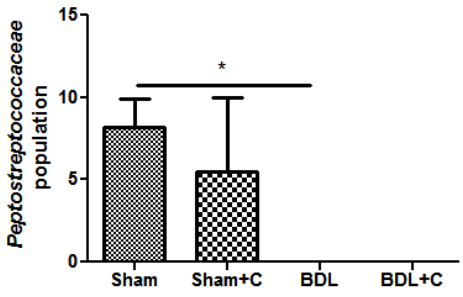

b.

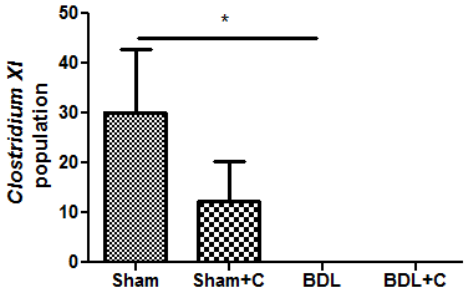

c.

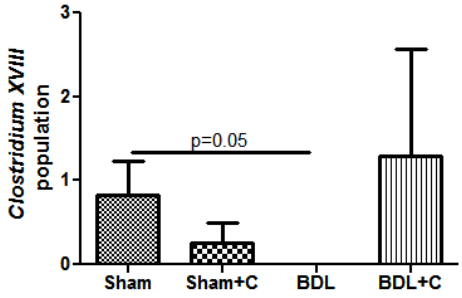

d.

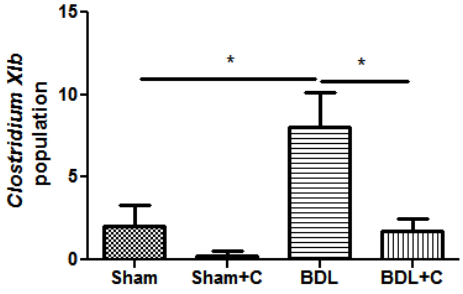

e.

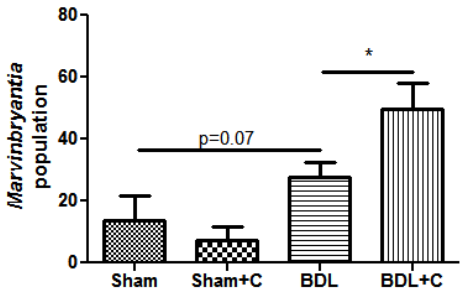

Figure 8.40 Geni in which significant differences between groups (sham, sham carbon treated, bile duct ligated and carbon treated bile duct ligated rats) were observed:

a) *Peptostreptococcaceae*
b) *Clostridium XI*
c) *Clostridium XVIII*
d) *Clostridium XIVb*
e) *Marvinbryantia*

Bile duct ligation is associated with a relative expansion in firmicutes at the expense of bacteroides populations. Carbon treatment in context of both sham and BDL is associated with a further expansion of firmicutes populations. At order level, bile duct ligation is associated with an increase in clostridia at the expense of bacteroidia. This is further increased with sham and most markedly in BDL carbon treated rats. At family level, untreated BDL, carbon treated sham and BDL rats are observed to have a collapse of prevotellaceae. BDL is associated with an expansion in bacteroidaceae and autochthonous lachnospiraceae and ruminococcaceae populations. The latter two families predominate in carbon treated BDL rats at the expense of bacteroidaceae. BDL was found to be associated with a significant collapse in peptostreptococcaceae, clostridium XI and XIVb populations. Near significant changes were observed at the level of the clostridium XVIII genus (p=0.05) and marvinbryantia (p=0.07). Carbon therapy was associated with significant shifts in marvinbryantia and clostridium XIVb populations.

8.3.6 Urinary ^{1}NMR analysis

Principal Component Analysis

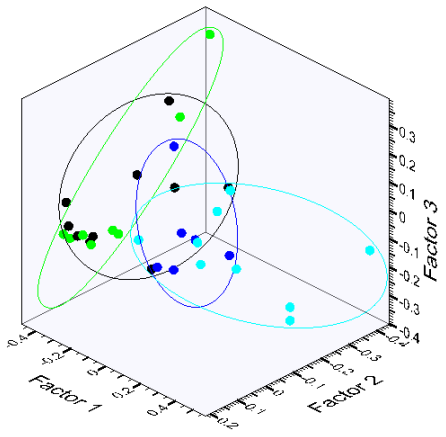

	Sham	Sham+Carbon	BDL	BDL+Carbon
Sham		0.79	1.71	1.20
Sham+Carbon	0.79		1.36	1.64
BDL	1.71	1.36		0.12
BDL+Carbon	1.20	1.64	0.12	

Figure 8.41 Principal Component Analysis

BDL/Sham

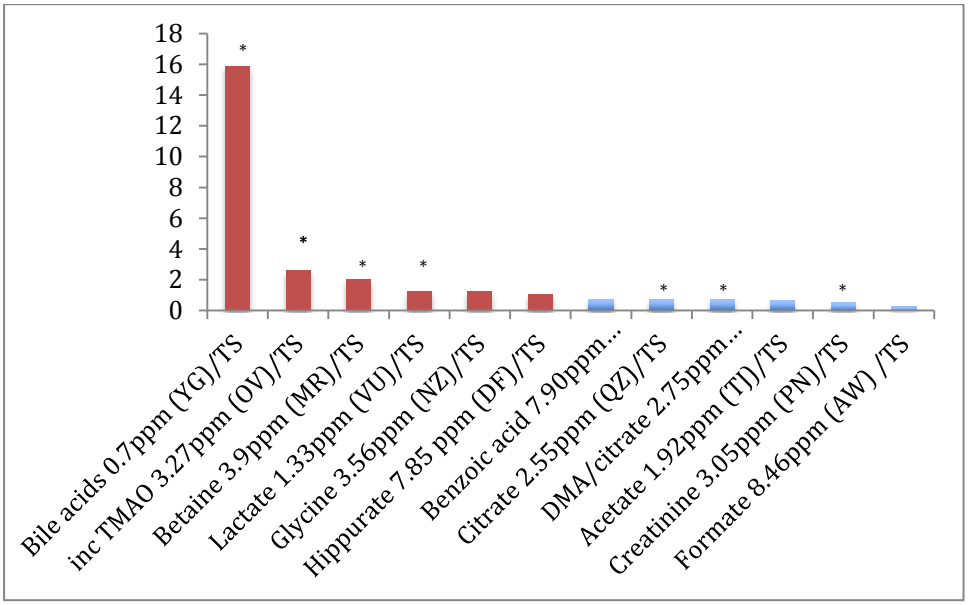

Figure 8.42 Relative urinary concentrations of metabolites in BDL compared to sham (n=6/group)**.** Red columns denote higher concentrations in BDL vs sham**.** Blue columns denote lower concentrations in BDL vs sham * denotes statistically significant difference between BDL and sham

Carbon treated BDL/BDL

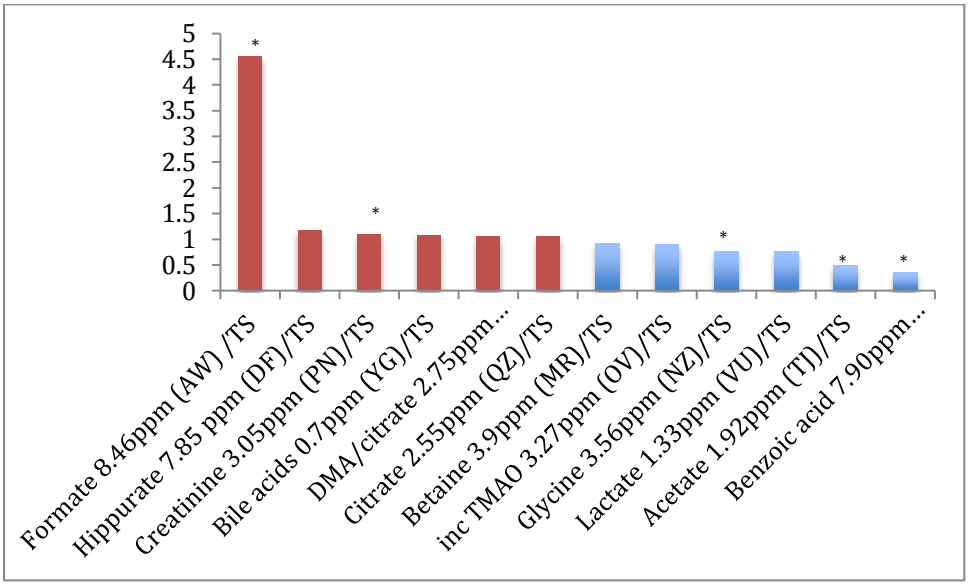

Figure 8.43 Relative urinary concentrations of metabolites in BDL+C compared to BDL (n=6/group). Red columns denote higher concentrations in BDLC vs BDL Blue columns denote lower concentrations in BDLC vs BDL denotes statistically significant difference between BDLC and BDL

Carbon treated sham/Sham

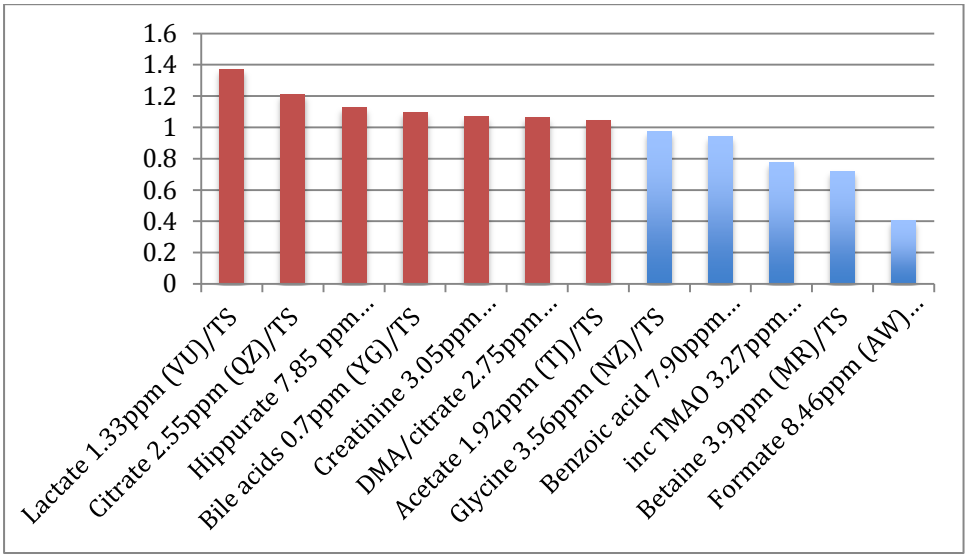

Figure 8.44 Relative urinary concentrations of metabolites in Sham= carbon compared to sham (n=6/group). Red columns denote higher concentrations in ShamC vs sham. Blue columns denote lower concentrations in ShamC vs sham
* denotes statistically significant difference between ShamC and sham

Carbon therapy is associated with a significant increase in urinary formate and creatinine with significant reductions in glycine, benzoate and acetate. No significant differences in urinary metabolomic profile between untreated and carbon-treated sham rats were observed.

8.3.7 Markers of Bacterial Translocation

(a)

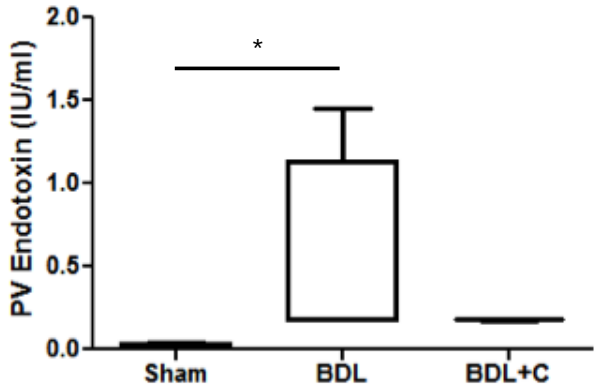

(b)

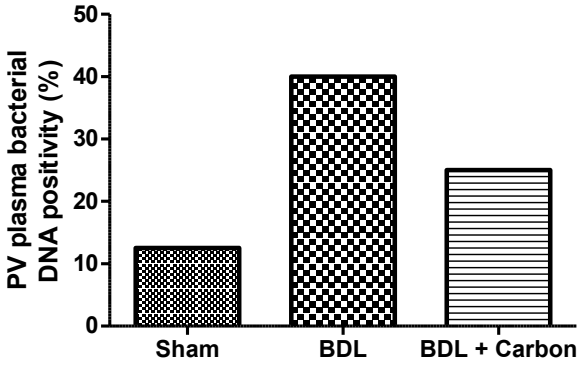

(c)

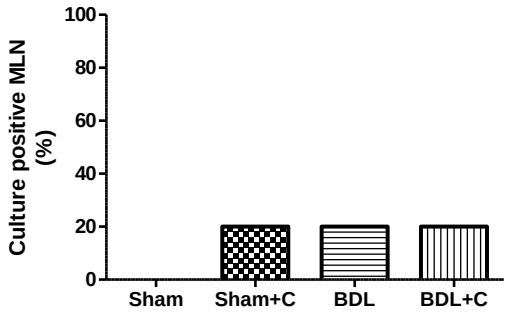

Figure 8.45
(a) Portal venous endotoxin (LAL assay) (n=4/group)
(b) Bacterial DNA positivity in portal venous plasma (n=4/group)
(c) Mesenteric lymph node culture positivity (n=5/group)

Oral Yaq-001 administration is associated with a reduction in portal venous endotoxin, portal venous plasma bacterial DNA positivity but no significant difference in mesenteric lymph node culture. This is consistent with the known in vitro properties of carbon in which bacterial ligands are adsorbed but no significant effect on bacterial growth kinetics is observed.

8.3.8 ACLF Data

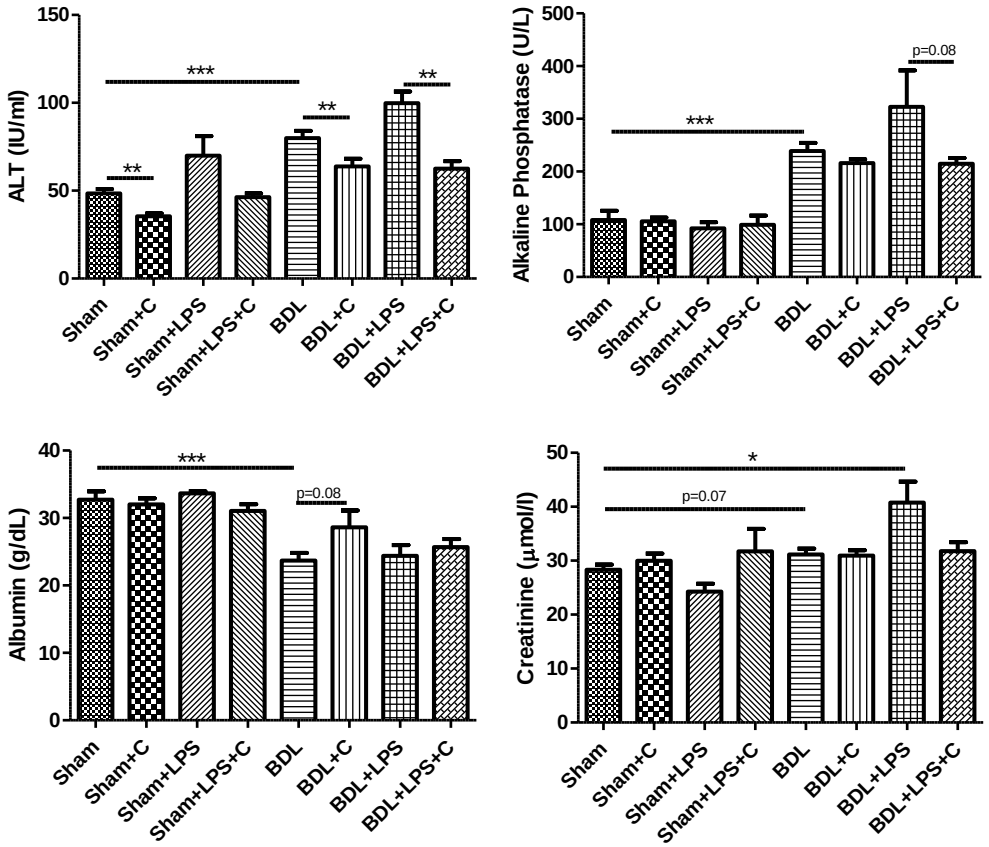

Figure 8.46 Biochemical response to oral Yaq-001 carbon therapy
(a) Alanine transaminase (Sham n=13, Sham+C n=15, Sham+LPS n=8, Sham+LPS+C n=10, BDL n=12, BDL+C n=14, BDL+LPS n=10, BDL+LPS+C n=10)
(b) Alkaline phosphatase (Sham n=21, Sham+C n=16, BDL n=25, BDL+C n=26)
(c) Albumin (Sham n=22, Sham+C n=16, BDL n=24, BDL+C n=25)
(d) Creatinine (Sham n=23, Sham+C n=18, Sham+LPS n=8, Sham+LPS+C n=4,BDL n=22, BDL+C n=25, BDL+LPS n=12, BDL+LPS+C n=9)
* denotes $p<0.05$ *** denotes $p<0.001$

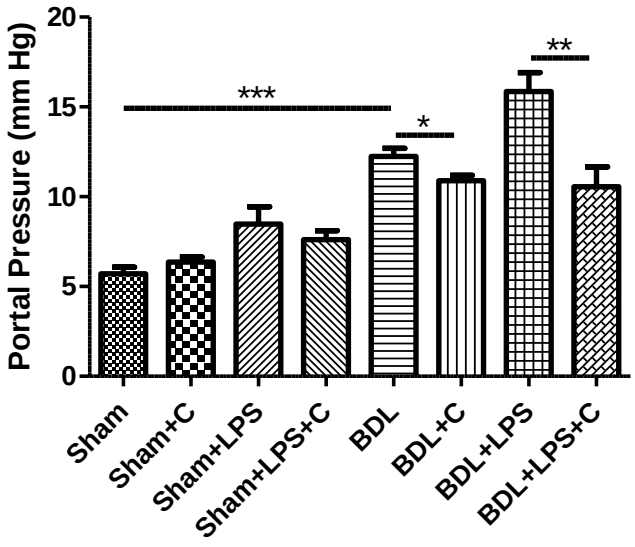

Figure 8.47 Portal Pressure (mm Hg)

(Sham n=21, Sham+C n=22, Sham+LPS n=8, Sham+LPS+C n=10, BDL n=15, BDL+C n=26, BDL+LPS n=9, BDL+LPS+C n=9)

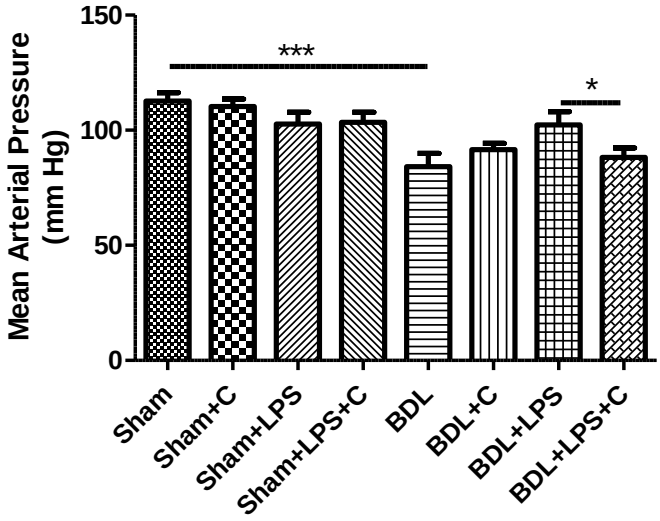

Figure 8.48 Mean Arterial Pressure

(Sham n=13, Sham+C n=15, Sham+LPS n=8, Sham+LPS+C n=10, BDL n=12, BDL+C n=14, BDL+LPS n=10, BDL+LPS+C n=10)

Liver Histology

Bile duct ligation was associated with nodule formation, cholangiocyte proliferation and inflammatory infiltrate. Yaq-001 therapy did not significantly alter fibrosis as evidenced by surrogate collagen proportionate area as described in section 6.3. This suggests that the effect of Yaq-001 on portal pressure is at the level of the inflammatory component of portal hypertension. Intraperitoneal LPS challenge was associated with an exacerbation of the inflammatory infiltrate in BDL rats, an effect attenuated with Yaq-001 therapy.

(a) (b)

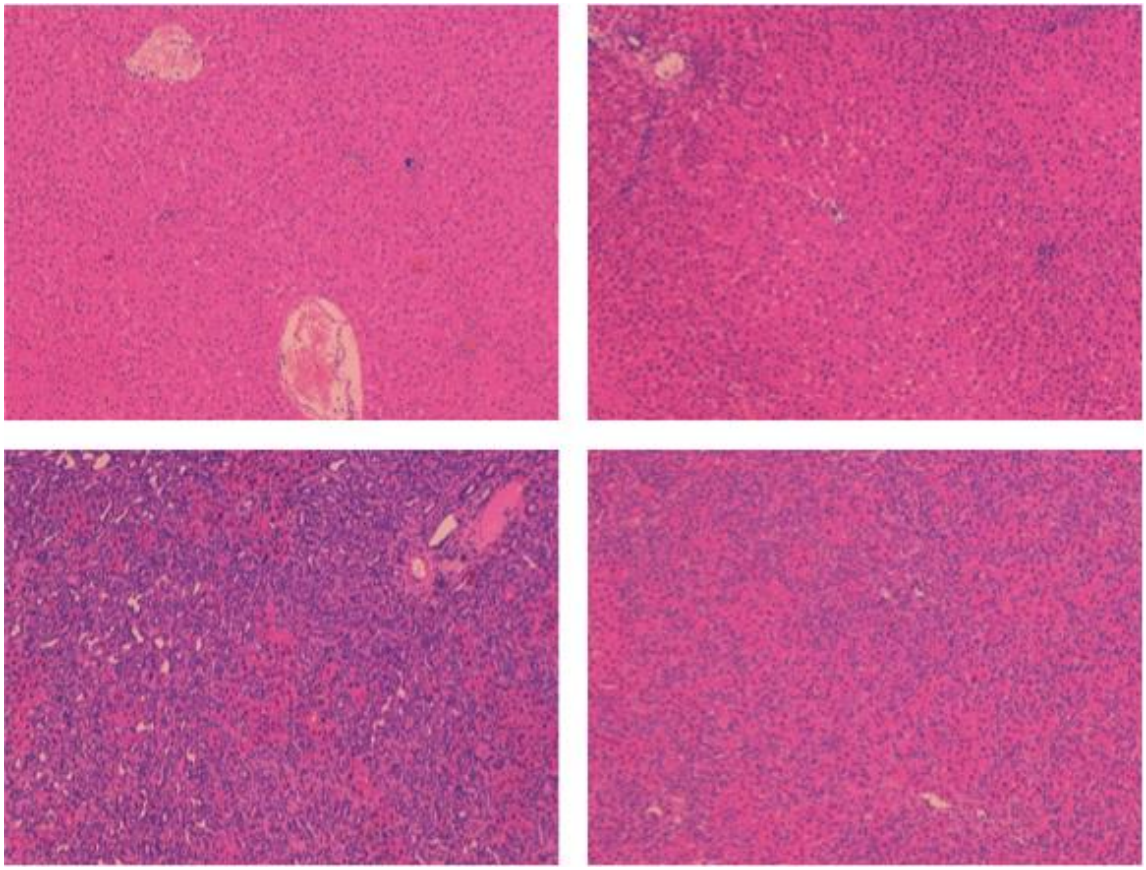

(c) (d)

Figure 8.49 Liver histology (Haemaoxylin and Eosin)

(a) Sham+LPS (b) sham+LPS+Yaq-001 (c) BDL+LPS (d) BDL+LPS+Yaq-001

Oral administration of Yaq-001 in a model of ACLF is associated with a significant reduction in organ injury and improvement in portal pressure, important prognostic determinants in the clinical context. The BDL+LPS model assesses in vivo endotoxin sensitivity and therefore the observed improvement with carbon therapy is indicative of a diminished primed state to endotoxin challenge. This is an identical phenotype to that observed in in vitro studies of circulating and tissue resident innate immune populations.

8.4 Discussion

The primary aim of this study was to evaluate the efficacy of oral administration of Yaq-001 in the bile duct ligated model of cirrhosis particularly with regards to clinically relevant end-points such as markers of organ injury, portal haemodynamics and innate immune function.

Two weeks of oral Yaq-001 therapy was found to be associated with a significant reduction in alanine transaminase as a marker of hepatocellular liver injury in bile duct ligated rats. The most marked effects were observed with BDL +LPS rats suggesting a reduction in in vivo endotoxin sensitivity conferred by the carbon.

A significant reduction in portal pressure in BDL and BDL+LPS rats was observed following oral administration of Yaq-001 carbon. Carbon therapy however had no significant impact on mean arterial pressure demonstrating that the haemodynamic effects are confined locally within the portal circulation. Collagen proportionate area as a measure of fibrosis was not found to be significantly different following carbon treatment suggestive that the effects of Yaq-001 were exerted at the level of the dynamic modifiable component of portal hypertension driven by inflammation rather than a modulation of fibrosis and fixed intrahepatic resistance.

Kupffer cells play a key role in regulation of endotoxin-sensitivity and thus are a key cell type responsible for integration of inflammatory and portal haemodynamic signals. Kupffer cell population and function were observed to be modulated by carbon-treatment. Normalisation of Kupffer cell populations towards sham levels was observed in carbon-treated BDL rats. A significant reduction in LPS-induced Kupffer cell ROS activity was observed with Yaq-001 suggestive that Kupffer cells in carbon-treated BDL rats are less primed to subsequent endotoxin challenge. Biochemically this finding was paralleled by a significant reduction in alanine transaminase suggesting diminished ROS-induced liver injury.

An important consideration in the study was determining the relative contribution of trafficking portal venous monocyte and neutrophil populations within the portal vein to total liver ROS and subsequent organ injury and portal hypertension. A significant increase in absolute neutrophil count and population in both portal venous and arterial blood was observed in bile duct ligated rats compared to sham control. Phenotypically, bile duct ligation was associated increase in portal venous constitutive ROS and LPS-induced ROS production. Yaq-001 therapy resulted in a significant reduction in portal venous monocyte LPS-induced ROS production, most markedly within the CD43hi subpopulation. Significant reductions in total leucocyte and neutrophil counts were observed with carbon therapy with trends towards reduction in monocyte populations.

No significant shifts in mesenteric lymph node populations were observed with carbon therapy albeit in context of a small sample size. Expansions in CD68+ and CD163+ populations observed with bile duct ligated rat mesenteric lymph nodes appear to be non-statistically reduced with carbon therapy. Further studies are required to augment this dataset to ascertain whether this is significant observation.

In light of the observation of diminished endotoxin sensitivity with carbon therapy, evaluation of TLR4 and inflammasome activation was performed using rodent plasma co-incubated with HEK reporter cell lines. A significant increase in inflammasome activation was observed with BDL rats which was significantly attenuated with carbon therapy. Similar but non-significant trends were observed with the TLR4 reporter cell lines. Of note only small numbers were used for this experiment. This data suggests a strong inflammasome activation associated with cellular ROS production both in the portal vein, liver and arterial monocyte/ macrophage populations. TLR4 signalling may be playing a contributory role and warrants further evaluation in larger studies although endotoxin sensitivity is not a solely mediated via TLR4 expression. Furthermore, the reporter cell line is an artificial and does not account for preconditioning of these pathways by weeks of endotoxin exposure in the animal model system. Cell sorting and gene expression data would serve to complement this data set well and further determine the molecular mechanisms of action of the carbons, most markedly on the monocyte / macrophage cell lines of the gut-liver axis.

Sugar probe-based assays were used to evaluate intestinal permeability in BDL rats. Progressive increases in intestinal permeability were observed with progressive disease. In contrast, carbon therapy was associated with a significant improvement in intestinal permeability. Technical limitations in ability to discriminate 6-o-methyl-glucose and rhamnose resulted in urinary concentrations of these sugars as a composite figure. This compromises the evaluation of intestinal permeability to smaller solutes but interestingly follows the same trend as the lactulose/creatinine ratios. Replication of the studies using lactulose and rhamnose only represents the best next step to assess this further.

Paneth cell gene expression has been implicated in susceptibility to bacterial translocation in a CCl4 model of cirrhosis. Bile duct ligation was associated with a

significant increase in defensin 5 and 8 and lysozyme gene expression within terminal ileal tissue. Carbon therapy has no significant impact on Paneth cell gene expression data although downward trends were observed with defensins 5 and 8. Of note a borderline significant reduction in TNFα gene expression was observed with carbon therapy in context of bile duct ligation. Augmentation of this dataset is required to further validate these observations. Of note, TNFα and defensins act synergistically and so the biological effect of these observations may be functionally more significant than evidenced by the single datasets.

Bile duct ligation was found to be associated with a marked reduction in several unconjugated plasma bile acids. Significant reductions were observed with both primary bile acids cholic acid, chenodeoxycholic acid and secondary bile acids ursodeoxycholic acid, lithocholic acid and a near significant reduction with deoxycholic acid. Alpha muricholic acid an FXR antagonists in rodents was also found to be significantly depleted with bile duct ligation as compared to sham.

Whilst the bile duct ligated rat model is one of extra-hepatic cholestasis, this data suggests that by week 4, there is a significant depletion of the total bile acid pool associated with an increase in urinary bile acid excretion. The increased urinary bile acids may therefore be the mechanism by which the total bile pool is depleted over the course of 4 weeks. BDL mice have been shown to have an increased renal expression of MRP4, a bile acid export protein in the proximal convoluted tubule. Renal excretion of bile acids may be a protective mechanism in context of bile duct ligation to minimize toxicity of high levels of circulating unconjugated bile acids in context of cholestasis.

A significant reduction in deoxycholic acid was observed in carbon-treated sham rats compared to untreated controls. Non-significant downward trends in several bile acids were observed in carbon-treated sham rats compared to sham controls (albeit

in context of wide standard errors). No significant differences in renal excretion of total bile acids was observed with carbon treated compared to non-carbon treated sham rats. This suggests that the intraluminal adsorption of carbon rather than enhanced renal excretion of bile acids underlies the observations.

One potential explanation for differential adsorption of bile acids by Yaq-001 may be a preferential adsorption of hydrophobic compounds. The only significant difference in bile acid concentration was observed with deoxycholic acid which is relatively more hydrophobic. In vitro studies are also required to ascertain differential adsorption kinetics of carbon for individual bile acids.

A significant reduction in lithocholic acid and chenodeoxycholic acid was observed with carbon treatment of bile duct ligated rats. It must be noted however, that despite the statistical significance identified, the percentage reduction with carbon therapy was very low. Urinary bile acid excretion was not found to be significantly increased in carbon-treated BDL rats as compared to untreated BDL controls. This suggests the site of action is likely in the intestine rather than promotion of renal excretion but further studies are warranted to augment the dataset and determine differential urinary bile acid profile.

Oral carbon therapy in sham animals did not significantly influence arterial concentrations of standard electrolytes and micronutrients. A significant reduction in folate levels were however observed. This may be a function of intraluminal carbon adsorption or due to a shift in microbiome composition with carbon treated sham animals.

A significant improvement in final body weight was observed in carbon-treated compared to untreated BDL rats. No significant difference in final body was observed between the sham groups. Weight loss in cirrhosis is attributed to an increased catabolic state particularly in the context of systemic inflammatory response. The

animals in this experiment were pair-fed and it seems likely that the weight gain in the BDL rats is due to a reduction in the systemic inflammatory response observed and an improvement in organ injury.

Significant shifts in stool microbiome composition were observed with carbon therapy both in context of sham or bile duct ligated carbon-fed rats despite the apparent lack of impact on bacterial growth kinetics. Carbon therapy both in contact of sham rats and bile duct ligated rats results in a relative expansion of firmicutes phyla and a reciprocal contraction in bacteroides populations. The predominant shifts in firmicutes phyla are due to an expansion in clostridia populations and reduction in bacteroides. Carbon therapy resulted in similar shifts in a progressive manner with sham and subsequently BDL rats.

Analysis at genus level is perhaps more informative still. BDL is associated with a collapse of peptostreptococcaceae, clostridium XI and XVIII. Bile duct ligation is significantly associated with an expansion of clostridium XIVb and upward trend in marvinbryantia. Given the small sample size, it is suggestive that the signal change with disease and carbon therapy is strong.

Urinary NMR analysis is a reflection of the combined metabolic status of both host and microbiota. Carbon treatment was associated with a distinct shift in metabolomic profile in BDL rats. In contrast, no significant differences were observed in urinary metabolomic profile with carbon treatment in sham rats. The most marked difference in profile was a significant increase in urinary formate with a near two-fold increase in concentration. Formate together with lactate, acetate and succinate are products generated by mixed acid fermentation (MAF) typically by bacteria such as enterobacter. MAF is not the preferred metabolic pathway for facultative anaerobes and may be indicative that enterobacter populations may be under conditions of

metabolic stress in carbon treated BDL. Given these are the type of bacteria which are often pathogenic in cirrhosis with a heightened propensity to translocate, this may represent a beneficial change. Formate itself exhibits antibacterial properties and has been used in feed to diminish carriage of facultative anaerobes such as salmonella in poultry. This may further shape the microbial population.

A significant increase in urinary creatinine was observed in carbon-treated BDL rats compared to untreated BDL. This may be indicative of an improvement in renal function as evidenced by a significant reduction in plasma creatinine in these animals. Significant reductions in urinary glycine and benzoate were observed with carbon treatment. Benzoic acid is a fungistatic compound produced by bacteria as a byproduct of phenylalanine and polyphenol metabolism. It is conjugated to glycine in the liver and excreted as hippuric acid. Significant reductions in urinary benzoate and glycine were observed with carbon treatment although hippurate levels were not significantly different. Further analysis is required to determine the relative contribution of host and microbial metabolism to these observations.

In summary, oral administration of Yaq-001 to cirrhotic rats is associated with a significant reduction in organ injury and improvement in portal pressure, important clinical prognostic determinants. Carbon therapy attenuates the heightened endotoxin sensitivity observed in the BDL model and is associated with a normalisation of population and functional status in tissue resident and trafficking innate immune populations in the gut-liver axis with diminished inflammasome activation. These changes are associated with a distinct shift in metabolomic phenotype associated with an improvement in body weight and expansion of autochthonous bacterial populations in the microbiome. Further studies are required to more fully ascertain the mechanisms of action of Yaq-001 in more detail but the

observed changes in vivo demonstrate that the carbon is safe and efficacious and is a good candidate for translation to clinical studies.

Chapter 9

Oral nanoporous carbons attenuate disease pathogenesis in models of Non-alcoholic fatty liver disease

9.1 Introduction

Non-alcoholic fatty liver disease (NAFLD) is an important cause of cirrhosis and hepatocellular carcinoma. Exponential rises in prevalence have been observed affecting 15% of the developed population, attributed to a worldwide increase in obesity. Emerging evidence however has implicated the gut as a driver of disordered lipid metabolism in NAFLD a target for which there is no effective interventional strategy.

Gut-derived endotoxin has been shown to be an important pathogenic factor driving progression to steatohepatitis, cirrhosis and hepatocellular carcinoma. Intraluminal acetaldehyde derived from gut bacteria causes mucosal injury and increased portal endotoxaemia. This results in Kupffer cell activation, ROS and TNFα production promoting liver injury, stellate cell activation and fibrosis. Removal of these intraluminal gut-derived factors represent an unmet clinical need with the potential to impact significantly on disease progression, morbidity and mortality.

Having established that oral administration of Yaq-001 results in an improvement in organ inury, haemodynamic profile and normalisation of populations and phenotype of innate immune function in a model of cirrhosis, the final and exploratory stage of the project was to determine efficacy of oral Yaq-001 therapy in model systems of non-alcoholic fatty liver disease in particular as Yaq-001 has a high adsorptive for acetaldehyde in addition to endotoxin. Several models of non-alcoholic fatty liver disease utilise dietary methods such as high fat high carbohydrate compositions. As

Yaq-001 carbons are non-selective adsorbants with the possibility of removing a dietary insult, the models studied were the dietary deficient and knock-out models of leptin deficient and methionine choline deficient mice.

9.2 Aims

The aim of this pilot study were to establish whether oral administration of Yaq-001 carbon therapy was associated with a significant attenuation of liver injury in two complementary models of non-alcoholic fatty liver disease.

9.3 Leptin deficient mice (obob$^{-/-}$)

9.3.1 Markers of liver Injury

Male genetically leptin deficient (ob/ob) obese mice were randomized to receive standard powdered chow with or without carbon supplementation for four weeks. Heterozygote mice were used as the control population and also randomized to receive standard powdered chow with or without carbon supplementation for four weeks.

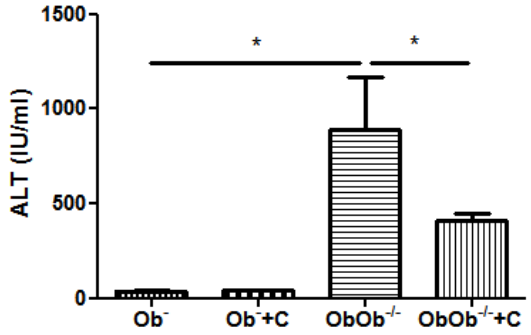

Figure 9.1 Plasma alanine transaminase levels at 4 weeks (n=5/group)
* denotes p<0.05

In accordance with previous literature, the leptin deficient mouse model was associated with a significant deterioration in liver biochemistry as evidenced by an increase in alanine transaminase from 38± 2.83 IU/ml in heterozygote control animals to 889 IU/ml in ob/ob mice. 4 weeks of carbon therapy was found to be associated with a significantly lower ALT in Yaq-001-treated compared to untreated ob/ob mice with values of 889 IU/ml (+/-280) and 408 IU/ml (+/-42) respectively. This is indicative of an abrogation of liver injury in obese mice by Yaq-001.

Figure 9.2 Liver histology (Haematoxylin & Eosin) (40x)

(a) Ob- heterozygote untreated

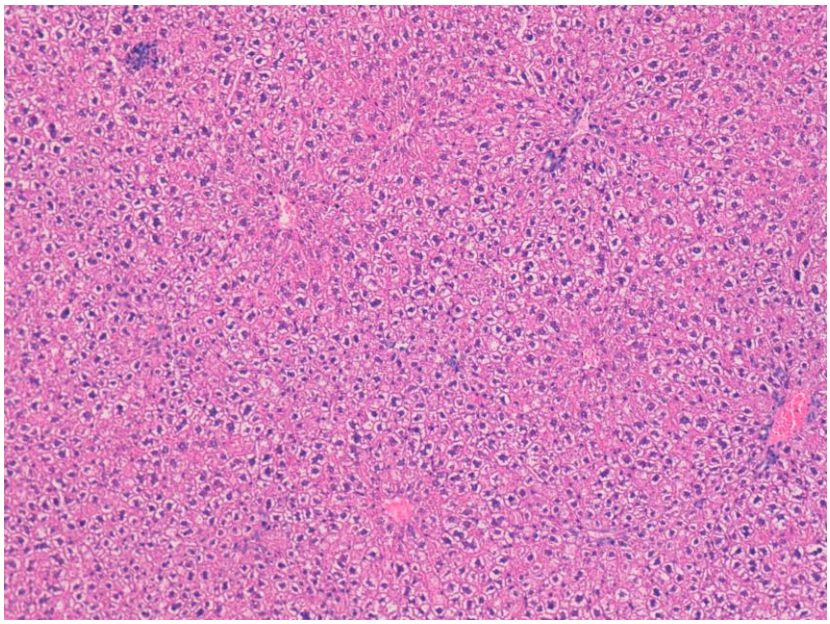

(b) Ob- heterozygote + carbon

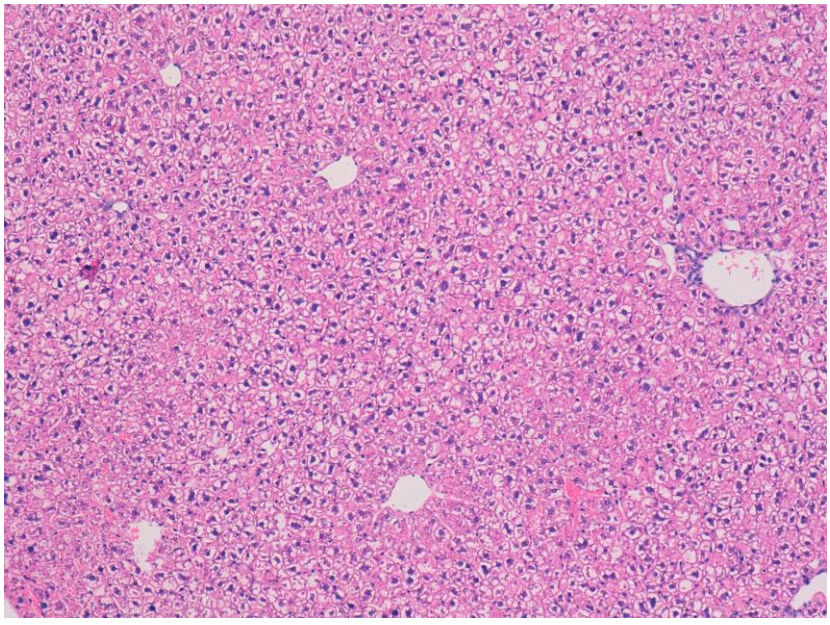

(c) Ob-/Ob- untreated

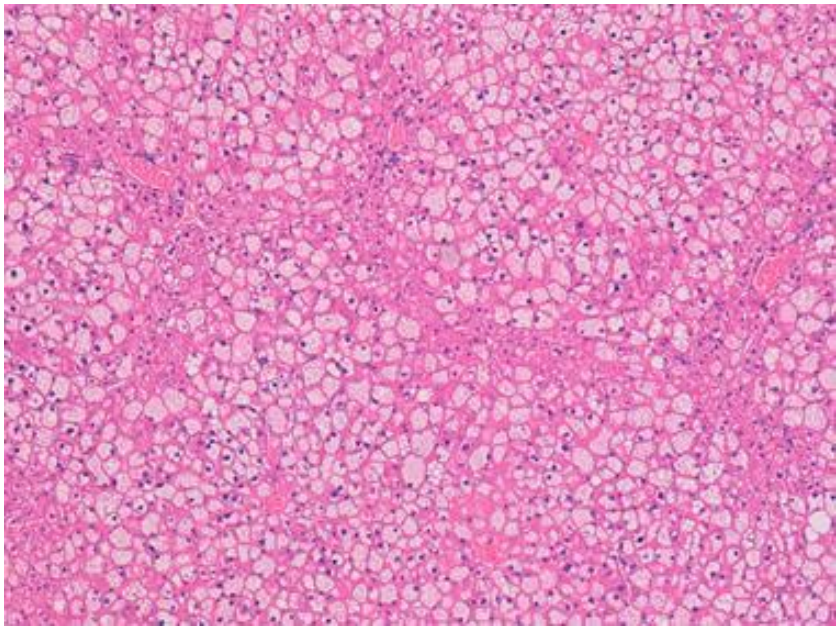

(d) Ob-Ob- + carbon

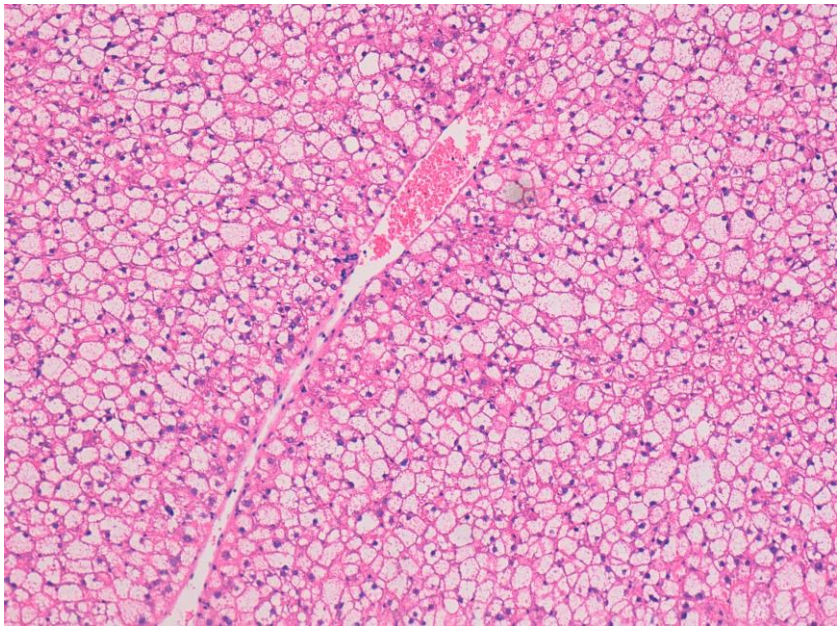

Marked steatosis was evident in both untreated and treated leptin-deficient mice. Inflammatory infiltration was also evident in both groups but less marked in Yaq-001 treated ob-ob- mice.

9.3.2 Kupffer Cell Populations

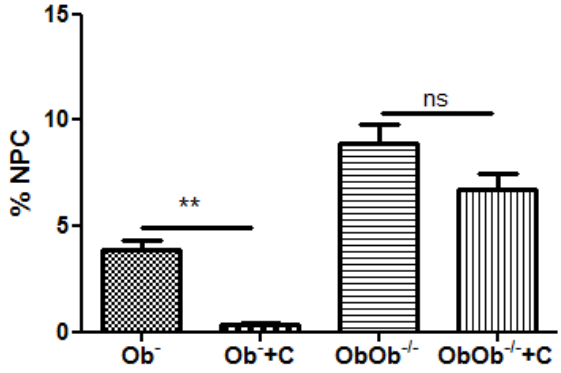

Figure 9.3 Kupffer cell populations in leptin deficient mice as determined by F4/80^{+}-gated non-parenchymal cell fraction (n=5/group) ** denotes p<0.005

Kupffer cell populations were determined using F4/80+-gated liver non-parenchymal cell fraction. A significant increase in F4/80+ cell population (expressed as a fraction of total non-parenchymal cell fraction) was observed between untreated heterozygote controls and untreated ob/ob mice. Carbon therapy was associated with a significant reduction in this population in heterozygote controls but not ob/ob mice.

(a)

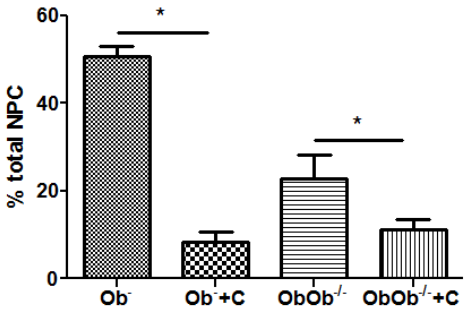

(b)

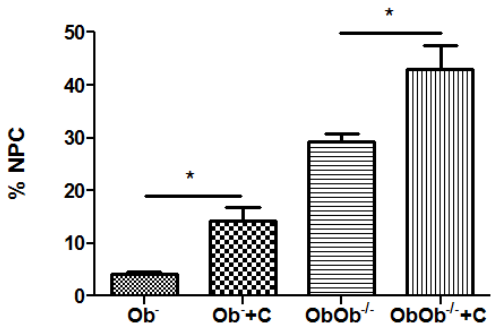

(c)

(d)

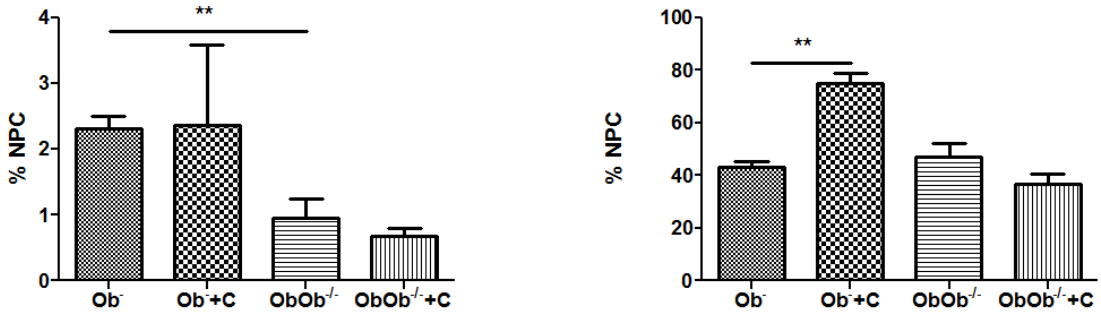

Figure 9.4 Kupffer cell (F4/80+) subpopulations (n=5/group)
(a) $CD11b^{+}CD68^{-}$ populations
(b) $CD11b^{-}CD68^{+}$ populations
(c) $CD11b^{+}CD68^{+}$ populations
(d) $CD11b^{-}CD68^{-}$ populations

Kupffer cell subpopulations were determined by CD11b and CD68 surface expression. Previous studies demonstrate that F4/80+/CD11b+ populations produce higher TNFα in response to TLR2 and 9 ligand exposure with the capacity to differentiate to CD68+/CD11b+ cells (Nakashima et al). F4/80+/CD68+/CD11b+ populations typically represent a small percentage of the non-parenchymal cell liver fraction and differentiate from F4/80+/CD11b+ cells in response to endotoxin exposure. Clearly there are significant shifts in Kupffer cell sub-populations with carbon therapy in which there appears to be an expansion in CD68+ Kupffer cell populations at the expense of CD11b+ subpopulations perhaps suggesting a shift away from a more pro-inflammatory phenotype. Current understanding regarding the role of these sub-populations of Kupffer cells is limited and therefore correlation with phenotype is important.

9.3.3 Kupffer cell ROS production

(a) (b)

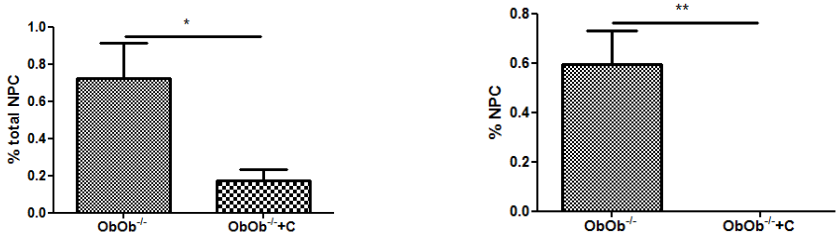

Figure 9.5 Kupffer cell (F4/80+) ROS production

(a) Constitutive ROS production
(b) LPS-induced ROS production

Analysis of Kupffer cell ROS production was technically limited by Kupffer cell yield in the heterozygote control populations in which liver size was considerably smaller than the ob/ob groups. A significant reduction in LPS-induced ROS production was observed in carbon treated compared to untreated ob/ob mice. This phenotype is identical to carbon treated BDL kupffer cell populations suggesting that the mechanisms are similar in both model systems. This diminished primed state to endotoxin challenge provides a potential explanation for the observed improvement in liver biochemistry despite small sample size.

9.3.4 Urinary NMR Profiling

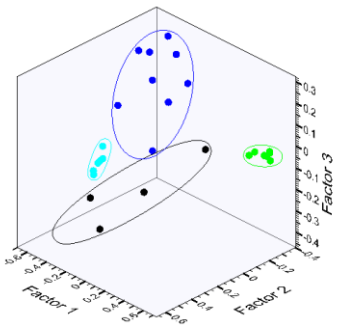

glucose	acetate	lactate+acetate	TMA
	2.94	6.13	18.77
2.94		2.12	1.76
6.13	2.12		6.01
18.77	1.76	6.01	

Figure 9.6 Principal Component Analysis (n=6/group)

(Black =ob+Yaq-001; Dark blue =obob+Yaq-001; Light blue ob untreated; Green = ob/ob untreated)

With regards to urinary metabolomic profile, ob/ob mice were characterized by a glycosuria, a typical phenotype of metabolic syndrome. In contrast, carbon treatment resulted in a significant metabolic shift in leptin-deficient mice resulting in a predominant lactate and acetate spikes in carbon treated leptin-deficient mice. Ob-heterozygote controls were characterized by TMA whereas carbon treated heterozygote controls were characterised by a predominant acetate spike.

9.3.5 Body Weight

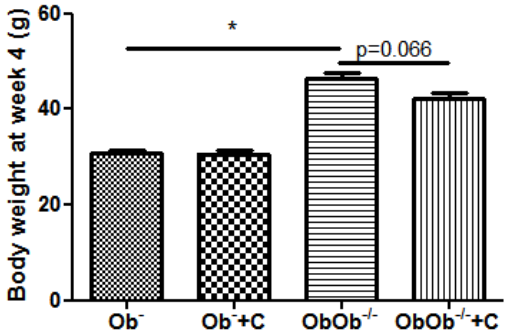

Figure 9.7 Final body weight (n=5/group)

A trend towards reduction in final body weight was observed in carbon treated ob/ob (42.28 ± 1.24 g) mice compared to untreated control (46.34 ± 1.39 g) ($p=0.066$) whereas no significant effects were observed with heterozygote mice. This is in contrast to the significant weight increase in BDL mice. Of note, the group sizes were small (n=5) and the study was underpowered. Further studies are required to validate these findings and augment the dataset.

9.4 Methionine choline deficient mice

The effects of oral carbon therapy methionine choline deficient mouse model was also evaluated in methionine choline deficient mice. Whilst lacking some features of the full metabolic syndrome, it is a good model of hepatic oxidative stress with marked inflammatory phenotype and therefore was a good complementary model to evaluate the efficacy of Yaq-001.

Female C57/B mice were randomized to receive a diet of control powdered chow or powdered chow deficient in methionine choline (IPS Irradiated Baker Amino Acid Diet without Choline or Methionine (578B – 1811438) for 4 weeks. These feeds were randomized to be supplemented with carbon or not. The carbon was administered at a dose of 0.4g/100g body weight per day. The diet and treatment was continued for 4 weeks.

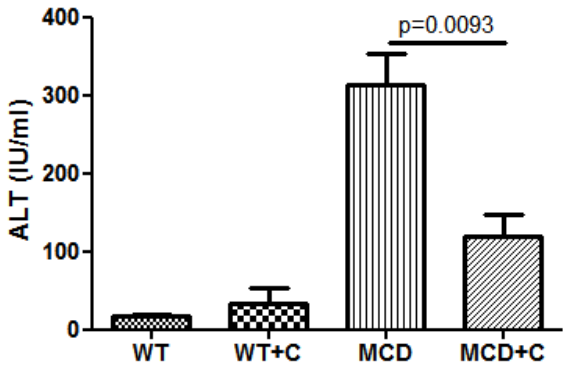

Figure 9.8 Plasma alanine transaminase
(Wild type/Wild type+carbon n=5)
(MDC/MCD+carbon, n=8)

Group	WT (Mean)	SEM	WT+C (Mean)	SEM	MCD (Mean)	SEM	MCD+C (Mean)	SEM
ALT (IU/ml)	16.94	1.4	32.66	20.08	313.5	38.96	119.51	28.59
AST (IU/ml)	74.14	19.45	93	36.12	286.83	26.78	139.56	23.71
Bilirubin (µmol/L)	3.96	0.58	5.56	2.5	23.8	5.72	17.58	4.77
ALP (IU/L)	55.46	3.17	92	23.93	75.48	4.32	70.91	9.41
Albumin (g/L)	25.93	1.12	28.15	1.16	19.72	2.89	22.67	3.74
Creatinine (µmol/L)	9.38	0.26	8.02	0.57	8.86	0.93	9.81	0.68

Table 9.1 Plasma biochemistry
(Wild type/Wild type+carbon n=5)
(MDC/MCD+carbon, n=8)

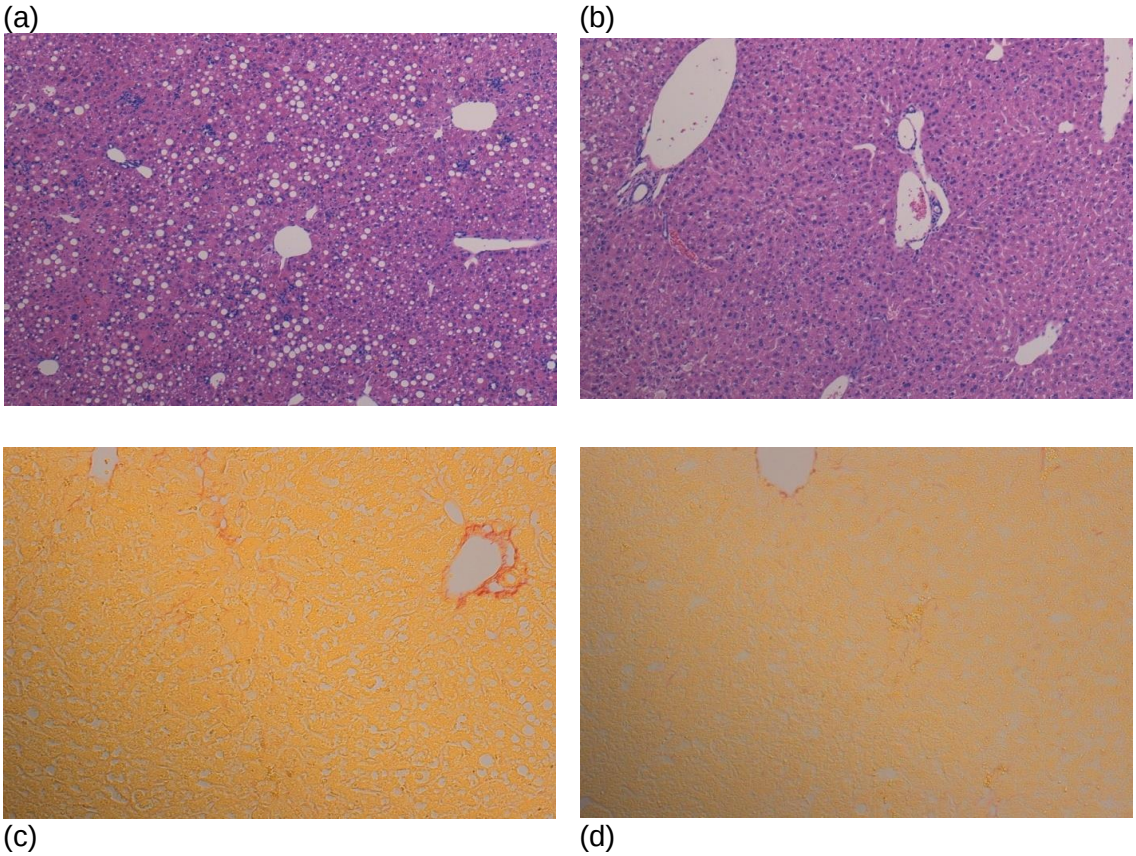

Figure 9.9 Liver histology (H&E)
(a) MCD fed mice
(b) MCD+carbon fed mice

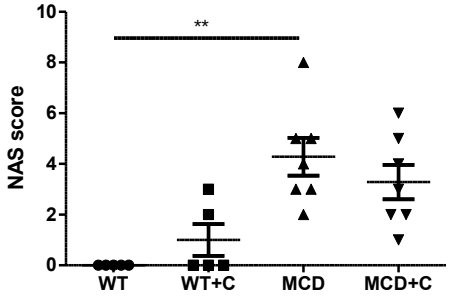

Figure 9.10 NAS score
(Wild type/Wild type+carbon n=5)
(MDC/MCD+carbon, n=8)

A highly significant near three-fold reduction in alanine transaminase were observed with carbon therapy in MCD mice. MCD mice had a non-significantly lower NAS score than untreated MCD mice. This may reflect the significantly lower ALT in Yaq-001 treated mice but further studies are required to ascertain the mechanisms of action of Yaq-001 in this model.

9.5 Discussion

Oral Yaq-001 therapy is associated with a significant improvement in liver biochemistry in two complementary models of non-alcoholic fatty liver disease. This is associated with a significant attenuation in Kupffer cell ROS production in

response to LPS challenge indicative of a diminished endotoxin-primed state. An identical phenotype was observed with carbon therapy in cirrhotic rats suggestive of common mechanisms of action of the carbon in both model systems. Furthermore, carbon therapy significantly altered the Kupffer cell total populations and subpopulations both in ob/ob mice and heterozygote controls. The most significant reduction in liver injury was observed in methionine choline deficient mice, a model characterized by oxidative stress and pro-inflammatory phenotype. This suggests that Yaq-001 therapy results in an attenuation of oxidative stress and inflammation, consistent with the current flow cytometry data. Further work is required to characterise these mechanisms.

Oral carbon therapy was also associated with a distinct shift in metabolomic phenotype in ob/ob and heterozygote control populations. Reductions in final body weight were also observed in carbon-treated leptin-deficient mice with no significant effects on heterozygote controls. Further work is required to ascertain the mechanisms of action with a particular emphasis on stool microbiome analysis.

Future studies will be conducted on more physiologically relevant NAFLD models with longitudinal analysis of metabolomic profile and stool microbiome metagenomic studies. Liver, terminal ileum and colon tissue microarrays will be performed to characterise the relative local and distant effects of carbon therapy, of particular importance given the non-selective adsorptive properties of Yaq-001. Of particular interest will be the effects on TLR4-dependent pathways and markers of fibrosis.

Chapter 10

Conclusions

The gut-liver axis plays a central role in disease progression in cirrhosis. Bacterial translocation plays an important role in the pathogenesis of complications of cirrhosis and, in particular, ACLF, associated with multi-organ failure and a high mortality. This study describes the contribution of the gut-liver axis to the clinical phenotype in cirrhosis and describes the associated dysfunctional innate immune response. Characterisation of changes at the gut-barrier interface and innate immune populations along the gut-liver axis were described in a model of ACLF. Evaluation of the effiicacy of Yaq-001, a non-absorbable endotoxin adsorbant in a model of cirrhosis and NAFLD was determined.

Data from the clinical study described the differential endotoxin concentrations and associated innate immune response within the splanchnic territories in patients with refractory variceal haemorrhage undergoing TIPSS insertion. In so doing, the relative contribution of the gut and liver to systemic endotoxin concentrations and innate immune response was determined. Portal-derived endotoxaemia and associated neutrophil dysfunction was observed with apparent preserved integrity of endotoxin surveillance mechanisms within the liver despite advanced disease. This trans-hepatic gradient of endotoxin, neutrophil dysfunction and cytokine profile was found to be disrupted upon TIPSS insertion.

Neutrophil function has previously been identified as of prognostic worth in patients with cirrhosis and alcoholic hepatitis. In this study, neutrophil dysfunction was significantly worse in patients who developed ACLF compared uncomplicated acute decompensation. The presence of ACLF in this context was found to be associated

with a significantly worse prognosis. Portal venous neutrophil ROS was found to significantly correlate with portal pressure reinforcing the importance of the dynamic inflammatory-driven component of portal hypertension in this context.

To further evaluate characterise the mechanisms underlying the observed high bacterial translocation rates clinically, the bile duct ligated rat model, a model of cirrhosis was studied. The BDL rat model is one of increased liver injury, portal hypertension with a pro-inflammatory phenotype. Data from this project has demonstrated in the bile duct ligation model that a significant difference in phenotype at the gut-barrier interface, innate immune function along the gut-liver axis and portal haemodynamic status is observed. This is associated with a distinct alteration in microbiome composition and function. Phenotypically this is associated with a significant increase in endotoxin sensitivity both *in vivo* and *in vitro*.

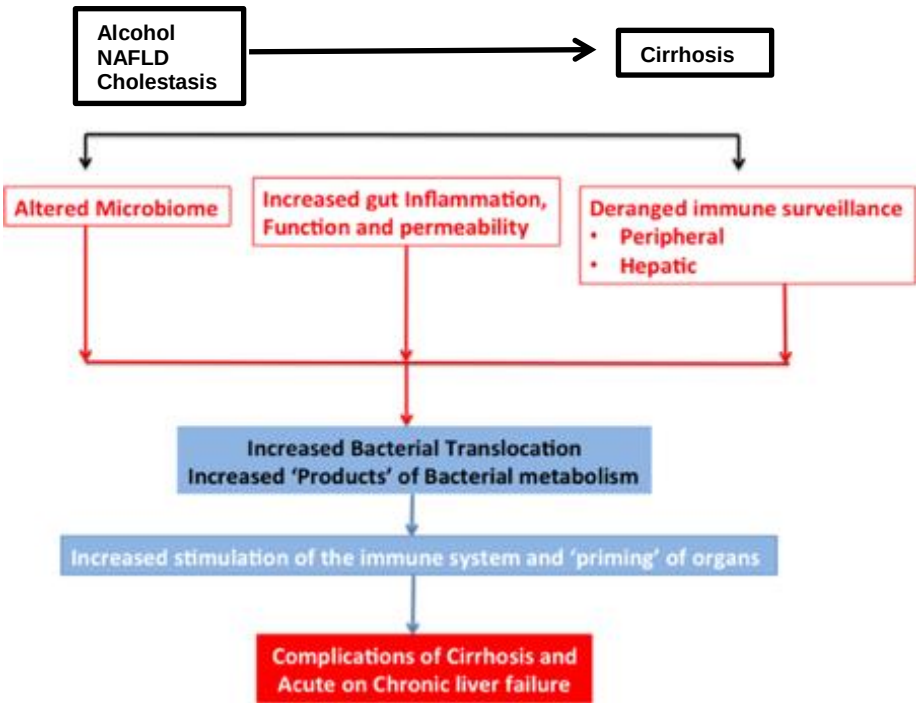

Figure 10.1 Pathogenesis of bacterial translocation and role in the natural history of cirrhosis

Modulation of the gut liver axis remains an unmet clinical need. Selective intestinal decontamination is the only strategy currently in clinical practice which impacts on this process but antibiotic resistance and superinfection limits their role. Yaq-001, an activated carbon with tailored bimodal porosity has been shown to exhibit favourable adsorption kinetics *in vitro* with regards to intraluminal bacterial factors such as endotoxin and acetaldehyde without exerting an effect on bacterial growth kinetics.

Oral administration of Yaq-001 therapy is associated with a significant reduction in liver and renal injury associated with a significant improvement in portal haemodynamic status. Locally, carbon therapy results in an improvement in gut barrier function as evidenced by intestinal permeability and nutritional status.

Despite the lack of effects on bacterial growth kinetics, oral carbon therapy was found to be associated with a distinct shift in microbiome composition and function. This is paralleled by a significant normalization in both tissue resident and circulating innate immune populations and phenotype characterised by a reduction in oxidative stress. HPLC data suggests that these carbons are capable of binding bile acids and influencing folate availability which may be a function of microbiome composition or may be a function of adsorption. Despite this most other nutritional factors such as common electrolytes and trace elements remain unchanged.

Preliminary work in complementary models of non-alcoholic fatty liver disease suggest that a similar phenotype of diminished organ injury and oxidative stress is observed with oral administration of carbons of bimodal porosity. There is some suggestion of potential to impact on elements of the metabolic syndrome but further work is required to further characterize these effects in more physiologically relevant model systems.

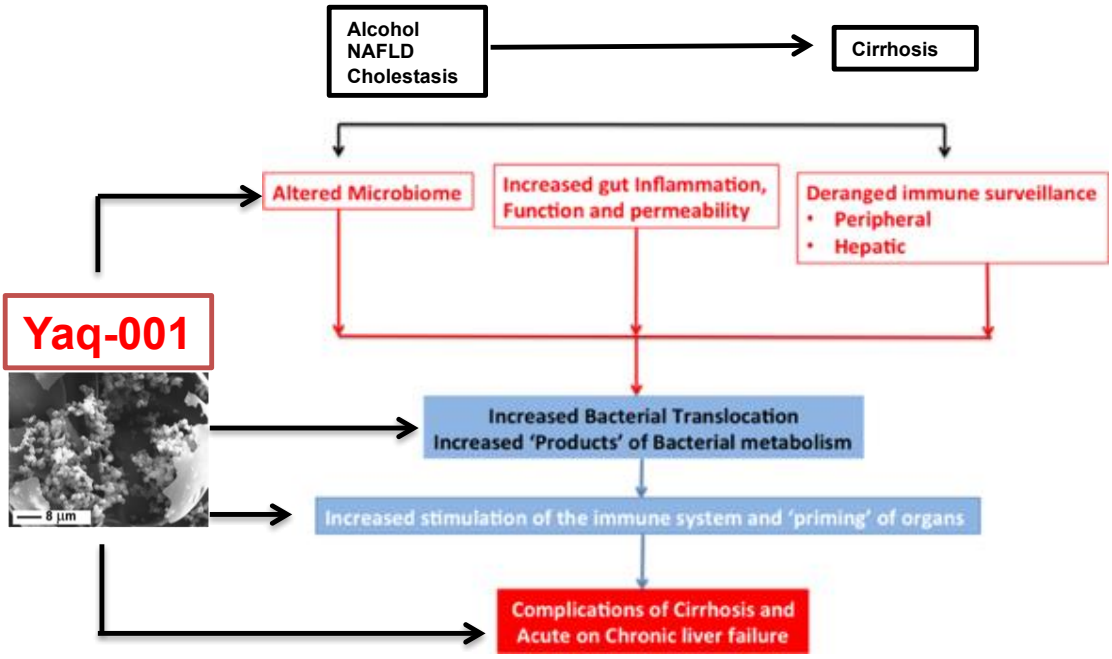

Figure 10.2 Effects of Yaq-001 on pathogenesis of cirrhosis

Future pre-clinical experiments will be conducted to ascertain the underlying cellular mechanisms of action of Yaq-001 in models of liver disease. The nature of the underlying liver injury and cell death requires further characterisation. Further work will be conducted to determine whether Yaq-001 carbons confer a protective effect via reduction in apoptosis, autophagy or necrosis. Markers of endoplasmic reticulum, mitochondrial and oxidative stress will be performed on liver, terminal ileal and colonic tissue. Further characterisation of nutritional profile including fat soluble vitamins is required together with an assessment of the effects of carbon on nutritional uptake. Further assessment of mechanisms of reduced endotoxin sensitivity will be conducted assessing TLR4 pathways in liver, intestine, kidney and brain using gene and protein expression. Phylogenic studies of caecal luminal microbiome composition will be complemented by metagenomic studies to assess a functional shift in the microbiome. Microbiome composition will also be evaluated in caecal mucosal associated microflora populations.

Activated carbon Yaq-001 therefore exhibits many favourable adsorptive properties which makes it an excellent candidate product for translation to clinical studies. Consideration of a colonic release preparation will help obviate concerns regarding bile salt absorption and potential drug interactions. Nonetheless, this technology represents a novel interventional strategy to modulate the gut-liver axis without being associated with any of the attendant risks of oral antibiotics. In these series of experiments, we demonstrate that Yaq-001 has the ability to impact on many clinically relevant end-points both in cirrhotic and non-cirrhotic models. Whilst further studies are required to more fully ascertain all of the molecular pathways influenced by the carbons, considerable potential has been shown in the experiments described in this thesis. Translational clinical studies to evaluate efficacy in NAFLD and cirrhotic patients are scheduled with the potential to impact on natural history of a disease process with a currently unacceptable mortality with an otherwise unmet clinical need.

References

AGRAWAL A, SHARMA BC, SHARMA P. 2012. Secondary prophylaxis of hepatic encephalopathy in cirrhosis: an open-label, randomized controlled trial of lactulose, probiotics, and no therapy. Am J Gastroenterol., 107,1043-50.

ALBILLOS A, HERA AD ADE L, REYES E et al. 2004. Tumour necrosis factor-alpha expression by activated monocytes and altered T-cell homeostasis in ascitic alcoholic cirrhosis: amelioration with norfloxacin. J Hepatol, 40, 624-31.

ALBILLOS A. DE LA HERA A, GONZÁLEZ M et al. 2003. Increased lipopolysaccharide binding protein in cirrhotic patients with marked immune and hemodynamic derangement. Hepatology, 37, 208-17.

ALDEMIR M, GEYIK MF, KÖKOĞLU OF et al. 2003. Effects of ursodeoxycholic acid, glutamine and polyclonal immunoglobulins on bacterial translocation in common bile duct ligated rats. ANZ J Surg., 73, 722-6.

ALEXOPOULOU A, PAPADOPOULOS N, ELIOPOULOS DG et al. 2013. Increasing frequency of gram-positive cocci and gram-negative multidrug-resistant bacteria in spontaneous bacterial peritonitis. Liver Int., 33, 975-81.

APPENRODT B, GRÜNHAGE F, GENTEMANN MG et al. 2010. Nucleotide-binding oligomerization domain containing 2 (NOD2) variants are genetic risk factors for death and spontaneous bacterial peritonitis in liver cirrhosis. Hepatology, 51,1327-33.

ATKINSON KJ AND RAO RK. 2001. Role of protein tyrosine phosphorylation in acetaldehyde-induced disruption of epithelial tight junctions. Am.J.Physiol Gastrointest.Liver Physiol , 280, G1280-G1288.

ATTERBURY CE, MADDREY WC, CONN HO. 1978. Neomycin-sorbitol and lactulose in the treatment of acute portal-systemic encephalopathy. A controlled, double-blind clinical trial. Am J Dig Dis., 23, 398-406.

BAJAJ JS, BETRAPALLY NS, HYLEMON PB et al. 2015. Salivary Microbiota Reflects Changes in Gut Microbiota in Cirrhosis with Hepatic Encephalopathy. Hepatology, 62, 1260-71.

BAJAJ JS, COX IJ, BETRAPALLY NS et al. 2014. Systems biology analysis of omeprazole therapy in cirrhosis demonstrates significant shifts in gut microbiota composition and function. Am J Physiol Gastrointest Liver Physiol., 307, G951-7.

BAJAJ JS, HEUMAN DM, HYLEMON PB et al. 2014. Altered profile of human gut microbiome is associated with cirrhosis and its complications. J Hepatol., 60, 940-7.

BAJAJ JS, HEUMAN DM, HYLEMON PB et al. 2014. Randomised clinical trial: Lactobacillus GG modulates gut microbiome, metabolome and endotoxemia in patients with cirrhosis. Aliment Pharmacol Ther., 39, 1113–1125.

BAJAJ JS, HEUMAN DM, SANYAL AJ et al. 2013. Modulation of the Metabiome by Rifaximin in Patients with Cirrhosis and Minimal Hepatic Encephalopathy. PLoS One., 8, e60042.

BAJAJ JS, HYLEMON PB, RIDLON JM et al. 2012. Colonic mucosal microbiome differs from stool microbiome in cirrhosis and hepatic encephalopathy and is linked to cognition and inflammation. Am J Physiol Gastrointest Liver Physiol., 303, G675–G685.

BAJAJ JS, RIDLON JM, HYLEMON PB et al. 2012. Linkage of gut microbiome with cognition in hepatic encephalopathy. Am J Physiol Gastrointest Liver Physiol., 302:G168-G175.

BAJAJ JS, SHEIKH MY, CHOJKIER M et al. 2013. AST-120 (Spherical Carbon Adsorbent) in Covert Hepatic Encephalopathy: Results of the Astute Trial. Gastroenterology, 144, S-997.

BALA S, MARCOS M, GATTU A et al. 2014. Acute binge drinking increases serum endotoxin and bacterial DNA levels in healthy individuals. PLoS One, 9, e96864.

BALAKRISHNAN A, MARA*THE SA, JOGLEKAR M et al. 2013.*
Bactericidal/permeability increasing protein: a multifaceted protein with functions beyond LPS neutralization. Innate Immun.,19, 339-47*.*

BANAN A, FIELDS JZ, DECKER H et al. 2000. Nitric oxide and its metabolites mediate ethanol-induced microtubule disruption and intestinal barrier dysfunction. J.Pharmacol.Exp.Ther, 294, 997-1008.

BAÑARES R, NEVENS F, LARSEN FS et al. RELIEF STUDY GROUP. 2013. Extracorporeal albumin dialysis with the molecular adsorbent recirculating system in acute-on-chronic liver failure: the RELIEF trial. Hepatology., 57, 1153-62.

BASS NM, MULLEN KD, SANYAL A et al. 2010. Rifaximin treatment in hepatic encephalopathy. N Engl J Med., 362, 1071-81.

BASUROY S, SHETH P, MANSBACH CM et al. 2005. Acetaldehyde disrupts tight junctions and adherens junctions in human colonic mucosa: protection by EGF and L-glutamine. Am.J.Physiol Gastrointest.Liver Physiol., 289, G367-G375.

BEESLEY RC. 1986. Ethanol inhibits Na+-gradient-dependent uptake of L-amino acids into intestinal brush border membrane vesicles. Dig.Dis.Sci.,31, 987-92.

BERG RD, GARLINGTON AW. 1979. Translocation of certain indigenous bacteria from the gastrointestinal tract to the mesenteric lymph nodes and other organs in a gnotobiotic mouse model. Infect Immun., 23, 403-11.

BERNARD B, GRANGÉ JD, KHAC EN et al. 1999. Antibiotic prophylaxis for the prevention of bacterial infections in cirrhotic patients with gastrointestinal bleeding: a meta-analysis. Hepatology, 29, 1655-1661.

BERRES ML, SCHNYDER B, YAGMUR E et al. 2009. Longitudinal monocyte human leukocyte antigen-DR expression is a prognostic marker in critically ill patients with decompensated liver cirrhosis. Liver Int., 29, 536-43.

BHONCHAL S. NAIN CK, PRASAD KK et al. 2008. Functional and morphological alterations in small intestine mucosa of chronic alcoholics. J.Gastroenterol.Hepatol. , 23, e43-e48.

BILZER M, ROGGEL F, GERBES AL. 2006. Role of Kupffer cells in host defense and liver disease. Liver Int., 26, 1175-86.

BODE JC, BODE C, HEIDELBACH R et al. 1984. Jejunal microflora in patients with chronic alcohol abuse. Hepatogastroenterology., 31, 30-4.

BONE RC, BALK RA, CERRA FB et al. 1992. Definitions for sepsis and organ failure and guidelines for the use of innovative therapies in sepsis. The ACCP/SCCM Consensus Conference Committee. American College of Chest Physicians/Society of Critical Care Medicine. Chest, 101, 1644-55.

BOSOI CR, PARENT-ROBITAILLE C, ANDERSON K et al. 1995. AST-120 (spherical carbon adsorbent) lowers ammonia levels and attenuates brain edema in bile duct-ligated rats. Hepatology, 53, 1995-2002.

BRUNS T, PETER J, REUKEN P A et al. 2012. NOD2 gene variants are a risk factor for culture-positive spontaneous bacterial peritonitis and monomicrobial bacterascites in cirrhosis. Liver Int., 32, 223-30.

BUCCI L, PALMIERI GC. 1993. Double-blind, double-dummy comparison between treatment with rifaximin and lactulose in patients with medium to severe degree hepatic encephalopathy. Curr Med Res Opin., 13, 109-18.

BUTTERWORTH RF. 2013. The liver-brain axis in liver failure: neuroinflammation and encephalopathy. Nat Rev Gastroenterol Hepatol., 10;522-8.

CARIELLO R, FEDERICO A, SAPONE A et al. 2010. Intestinal permeability in patients with chronic liver diseases: Its relationship with the aetiology and the entity of liver damage. Dig Liver Dis., 42, 200-04.

CHANG CS, CHEN GH, LIEN HC et al. 1998. Small intestine dysmotility and bacterial overgrowth in cirrhotic patients with spontaneous bacterial peritonitis. Hepatology, 28, 1187-90.

CHANG CS, CHEN GH, LIEN HC et al. 1998. Small intestine dysmotility and bacterial overgrowth in cirrhotic patients with spontaneous bacterial peritonitis. Hepatology, 28, 1187-90.

CHEN Y, GUO J, QIAN G et al. 2015. Gut dysbiosis in acute-on-chronic liver failure and its predictive value for mortality. J Gastroenterol Hepatol., 30, 1429-37.

CHEN Y, YANG F, LU H et al. 2011. Characterization of fecal microbial communities in patients with liver cirrhosis. Hepatology, 54, 562-72

CHINNARATHA MA, CHAUDHARY S, DOOGUE M et al. 2015. Prevalence of hepatic osteodystrophy and vitamin D deficiency in cirrhosis. Intern Med J., 45,1230-5.

CHU CJ, LEE FY, WANG SS et al. 2000. Splanchnic endotoxin levels in cirrhotic rats induced by carbon tetrachloride. Zhonghua Yi Xue Za Zhi, 63, 196-204.

CORDOBA J, VENTURA-COTS M, SIMÓN-TALERO M et al. 2014. Characteristics, risk factors, and mortality of cirrhotic patients hospitalized for hepatic encephalopathy with and without acute-on-chronic liver failure (ACLF). J Hepatol., 60, 275-81.

COPE K, RISBY T, DIEHL AM. 2000. Increased gastrointestinal ethanol production in obese mice: implications for fatty liver disease pathogenesis. Gastroenterology, 119, 1340-7.

CROWLEY SD, RUDEMILLER NP. 2017. Immunologic Effects of the Renin-Angiotensin System. J Am Soc Nephrol. Feb 1.

CSAK T, VELAYUDHAM A, HRITZ I et al. 2011. Deficiency in myeloid differentiation factor-2 and toll-like receptor 4 expression attenuates nonalcoholic steatohepatitis and fibrosis in mice. Am J Physiol Gastrointest Liver Physiol. 300, G433-41.

DAWSON AM, MCLAREN J AND SHERLOCK S. 1957. Neomycin in the treatment of hepatic coma. Lancet, 273, 1262-68.

DE OCA MM, SHAH N, DHAR DK et al. 2010. Evidence of dendritic cell dysfunction in cirrhosis and its restoration by toll-like receptor 4 antagonism. Hepatology, 52, 1018A.

DEGIROLAMO C, RAINALDI S, BOVENGA F et al. 2014. Microbiota modification with probiotics induces hepatic bile acid synthesis via downregulation of the Fxr-Fgf15 axis in mice. Cell Rep., 7, 12-8.

DESHPANDE A, PASUPULETI V, THOTA P et al. 2013. Acid-suppressive therapy is associated with spontaneous bacterial peritonitis in cirrhotic patients: A meta-analysis. Journal of Gastroenterology and Hepatology, 28, 235–242.

DHIMAN RK, SAWHNEY MS, CHAWLA YK et al. 2000. Efficacy of lactulose in cirrhotic patients with subclinical hepatic encephalopathy. Dig Dis Sci., 45, 1549-52.

DING JW, ANDERSSON R, SOLTESZ V et al. 1993. The role of bile and bile acids in bacterial translocation in obstructive jaundice in rats. Eur Surg Res., 25, 11-9.

EL KEBIR D, JÓZSEF L, FILEP JG. 2008. Neutrophil recognition of bacterial DNA and Toll-like receptor 9-dependent and -independent regulation of neutrophil function. Arch Immunol Ther Exp, 56, 41-53.

ELKINGTON SG, FLOCH MH AND CONN OH.1969. Lactulose in the Treatment of Chronic Portal-Systemic Encephalopathy — A Double-Blind Clinical Trial. N Engl J Med, 281, 408-412.

FERNÁNDEZ J, NAVASA M, PLANAS R et al. 2007. Primary prophylaxis of spontaneous bacterial peritonitis delays hepatorenal syndrome and improves survival in cirrhosis. Gastroenterology, 133, 818-24.

FERNÁNDEZ J, RUIZ DEL ARBOL L, GÓMEZ C et al. 2006. Norfloxacin vs ceftriaxone in the prophylaxis of infections in patients with advanced cirrhosis and hemorrhage. Gastroenterology, 131, 1049-56.

FERRIER L, BÉRARD F, DEBRAUWER L et al. 2006. Impairment of the intestinal barrier by ethanol involves enteric microflora and mast cell activation in rodents. Am J Pathol., 168, 1148-54.

FINKELMEIER F, KRONENBERGER B, ZEUZEM S et al. 2015. Low 25-Hydroxyvitamin D Levels Are Associated with Infections and Mortality in Patients with Cirrhosis. PLoS One., 10, e0132119.

FIUZA C, SALCEDO M, CLEMENTE G et al. 2000. In vivo neutrophil dysfunction in cirrhotic patients with advanced liver disease. J Infect Dis., 182, 526-33.

FRANCÉS R, MUÑOZ C, ZAPATER P et al. 2004. Bacterial DNA activates cell mediated immune response and nitric oxide overproduction in peritoneal macrophages from patients with cirrhosis and ascites. Gut, 53, 860-864.

GAO B, SEKI E, BRENNER DA et al. 2011. Innate immunity in alcoholic liver disease. Am J Physiol Gastrointest Liver Physiol., 300, G516-25.

GINÉS P, RIMOLA A, PLANAS R et al. 1990. Norfloxacin prevents spontaneous bacterial peritonitis recurrence in cirrhosis: results of a double-blind, placebo-controlled trial. Hepatology, 12, 716-24.

GIOFRÉ MR, MEDURI G, PALLIO S et al. 2000. Gastric permeability to sucrose is increased in portal hypertensive gastropathy. Eur J Gastroenterol Hepatol., 12, 529-33.

GONZÁLEZ-NAVAJAS JM, FRANCÉS R, SUCH J. 2007. Bacterial DNA in patients with cirrhosis and sterile ascites. Its role as a marker of bacterial translocation and prognostic tool. Rev Esp Enferm Dig., 99, 599-603.

GRANOWITZ EV, PORAT R, MIER JW et al. 1993. Intravenous endotoxin suppresses the cytokine response of peripheral blood mononuclear cells of healthy humans. J Immunol., 151: 1637-45.

GUNNARSDOTTIR SA, SADIK R, SHEV S et al. 2003. Small intestinal motility disturbances and bacterial overgrowth in patients with liver cirrhosis and portal hypertension. Am J Gastroenterol., 98, 1362-70.

GUPTA N, KUMAR A, SHARMA P et al. 2013. Effects of the adjunctive probiotic VSL#3 on portal haemodynamics in patients with cirrhosis and large varices: a randomized trial. Liver Int., 33, 1148-57.

GUSTOT T, FERNANDEZ J, GARCIA E et al. 2015. Clinical Course of acute-on-chronic liver failure syndrome and effects on prognosis. Hepatology, 62, 243-52.

HENAO-MEJIA J, ELINAV E, JIN C et al. 2012. Inflammasome-mediated dysbiosis regulates progression of NAFLD and obesity. Nature, 482, 179-85.

HEREDIA D, CABALLERIA J, ARROYO V et al. 1987. Lactitol versus lactulose in the treatment of acute portal systemic encephalopathy (PSE). A controlled trial. J Hepatol., 4, 293-8.

HORSMANS Y, SOLBREUX PM, DAENENS C et al. 1997. Lactulose improves psychometric testing in cirrhotic patients with subclinical encephalopathy. Aliment Pharmacol Ther., 11, 165-70.

HOTCHKISS RS, COOPERSMITH CM, MCDUNN JE et al. 2009. The sepsis seesaw: tilting toward immunosuppression. Nat Med., 15, 496-7.

HOU MC, LIN HC, LIU TT et al. 2004. Antibiotic prophylaxis after endoscopic therapy prevents re-bleeding in acute variceal hemorrhage: a randomized trial. Hepatology, 39, 746-53.

HOWELL CA, SANDEMAN SR, PHILLIPS GJ et al. 2013. Nanoporous activated carbon beads and monolithic columns as effective hemoadsorbents for inflammatory cytokines. Int J Artif Organs., 36, 624-32.

HU X, BONDE Y, EGGERTSEN G et al. 2014. Muricholic bile acids are potent regulators of bile acid synthesis via a positive feedback mechanism. J Intern Med., 275, 27-38.

IWAKIRI, Y. 2007. The molecules: mechanisms of arterial vasodilatation observed in the splanchnic and systemic circulation in portal hypertension. J.Clin.Gastroenterol., 41, S288-S294.

JALAN R, STADLBAUER V, SEN S et al. 2012. Role of predisposition, injury, response and organ failure in the prognosis of patients with acute-on-chronic liver failure: a prospective cohort study. Crit Care,16, R227.

JUURLINK DN, GOSSELIN S, KIELSTEIN JT et al. 2015. Extracorporeal Treatment for Salicylate Poisoning: Systematic Review and Recommendations From the EXTRIP Workgroup. Ann Emerg Med., 66, 165-81.

KAKIYAMA G, PANDAK WM, GILLEVET PM et al. 2013. Modulation of the fecal bile acid profile by gut microbiota in cirrhosis. J Hepatol., 58, 949-55.

KEMP W, COLMAN J, THOMPSON K. 2009. Norfloxacin treatment for clinically significant portal hypertension: results of a randomised double-blind placebo-controlled crossover trial. Liver Int., 29, 427-33.

KESHAVARZIAN A, HOLMES EW, PATEL M et al. 1999. Leaky gut in alcoholic cirrhosis: a possible mechanism for alcohol-induced liver damage. Am.J.Gastroenterol., 94, 200-07.

KWON JH, SEONG-JOON K, WON K et al. 2014. Mortality associated with proton pump inhibitors in cirrhotic patients with spontaneous bacterial peritonitis. Journal of Gastroenterology and Hepatology, 29, 775–781.

LATA J, JURÁNKOVÁ J, PRÍBRAMSKÁ V et al. 2006. Effect of administration of Escherichia coli Nissle (Mutaflor) on intestinal colonisation, endotoxemia, liver function and minimal hepatic encephalopathy in patients with liver cirrhosis. Vnitr Lek., 52, 215-9.

LE ROY T, LLOPIS M, LEPAGE P et al. 2013. Intestinal microbiota determines development of non-alcoholic fatty liver disease in mice. Gut, 62, 1787-1794.

LEAPHART CL, QURESHI F, CETIN S et al. 2007. Interferon-gamma inhibits intestinal restitution by preventing gap junction communication between enterocytes. Gastroenterology,132, 2395-411.

LEY RE, BÄCKHED F, TURNBAUGH P et al. 2005. Obesity alters gut microbial ecology. Proc Natl Acad Sci U S A., 102, 11070-5.

LIN CY, TSAI IF, HO YP et al. 2007. Endotoxemia contributes to the immune paralysis in patients with cirrhosis. J Hepatol, 46, 816-26.

LIU J, WU D, AHMED A et al. 2012. Comparison of the gut microbe profiles and numbers between patients with liver cirrhosis and healthy individuals. Curr Microbiol., 65, 7-13.

LIU Q, DUAN ZP, HA DK et al. 1995. Synbiotic Modulation of Gut Flora: Effect on Minimal Hepatic Encephalopathy in Patients With Cirrhosis. Hepatology, 39, 1441-9.

LOGUERCIO C, ABBIATI R, RINALDI M et al. 1995. Long-term effects of Enterococcus faecium SF68 versus lactulose in the treatment of patients with cirrhosis and grade 1-2 hepatic encephalopathy. J Hepatol., 23, 39-46.

LORENZO-ZÚÑIGA V, BARTOLÍ R, PLANAS R et al. 2003. Oral bile acids reduce bacterial overgrowth, bacterial translocation, and endotoxemia in cirrhotic rats. Hepatology, 37, 551-7.

LU H, WU Z, XU W et al. 2011. Intestinal microbiota was assessed in cirrhotic patients with hepatitis B virus infection. Intestinal microbiota of HBV cirrhotic patients. Microb Ecol., 61, 693-703.

LUNIA MK, SHARMA BC, SHARMA P et al. 2014. Probiotics Prevent Hepatic Encephalopathy in Patients With Cirrhosis: A Randomized Controlled Trial. Clinical Gastroenterology and Hepatology, 12, 1003–1008.

MACNAUGHTAN J, DAVIES N, STADLBAUER V et al. 2010. Evidence for compartmentalised endotoxaemia and its effect on neutrophil function in the portal circulation in cirrhosis Hepatology, 52:46.

MACNAUGHTAN J, STADLBAUER V, MOOKERJEE RP et al. 2011. SIRS, Bacterial Infections, and Alterations of the Immune System. Clinical Gastroenterology, 219-238.

MACNAUGHTAN, SOEDA J, MOURALIDARANE A et al. 2012. Gut Decontamination using Nanoporous Carbons reduces portal pressure and prevents liver failure in bile-duct ligated cirrhotic animals by reducing Kupffer cell activation. J Hep., 56, S230.

MAIWALL R, CHANDEL SS, WANI Z et al. 2016. SIRS at Admission Is a Predictor of AKI Development and Mortality in Hospitalized Patients with Severe Alcoholic Hepatitis. Dig Dis Sci., 61, 920-9.

MALAGUARNERA M, GRECO F, BARONE G. 2007. Bifidobacterium longum with fructo-oligosaccharide (FOS) treatment in minimal hepatic encephalopathy: a randomized, double-blind, placebo-controlled study. Dig Dis Sci, 52, 3259-65.

MANN ER, LANDY JD, BERNARDO D et al. 2013. Intestinal dendritic cells: their role in intestinal inflammation, manipulation by the gut microbiota and differences between mice and men. Immunol Lett. 150, 30-40.

MARGARITIS VG, FILOS KS, MICHALAKI MA et al. 2005. Effect of oral glutamine administration on bacterial tanslocation, endotoxemia, liver and ileal morphology, and apoptosis in rats with obstructive jaundice. World J.Surg., 29, 1329-34.

MÁRQUEZ M, FERNÁNDEZ-GUTIÉRREZ C, MONTES-DE-OCA M et al. 2009. Chronic antigenic stimuli as a possible explanation for the immunodepression caused by liver cirrhosis. Clin Exp Immunol., 158, 219-29.

MAS A, RODÉS J, SUNYER L et al. 2003. Comparison of rifaximin and lactitol in the treatment of acute hepatic encephalopathy: results of a randomized, double-blind, double-dummy, controlled clinical trial. J Hepatol., 38, 51-8.

MENCIN A, KLUWE J, SCHWABE RF. 2009. Toll-like receptors as targets in chronic liver diseases. Gut, 58, 704-20.

MIELE L, VALENZA V, LA TORRE G et al. 2009. Increased intestinal permeability and tight junction alterations in nonalcoholic fatty liver disease. Hepatology, 49, 1877-87.

MITTAL VV, SHARMA BC, SHARMA P et al. 2011. A randomized controlled trial comparing lactulose, probiotics, and L-ornithine L-aspartate in treatment of minimal hepatic encephalopathy. Eur J Gastroenterol Hepatol., 23, 725-32.

MOHAMMAD MK, ZHOU Z, CAVE M et al. 2012. Zinc and liver disease. Nutr.Clin.Pract., 27, 8-20.

MOOKERJEE RP, PAVESI M, THOMSEN KL et al. 2016. Treatment with non-selective beta blockers is associated with reduced severity of systemic inflammation and improved survival of patients with acute-on-chronic liver failure. J Hepatol. ,64, 574-82.

MOOKERJEE RP, STADLBAUER V, LIDDER S et al. 2007. Neutrophil dysfunction in alcoholic hepatitis superimposed on cirrhosis is reversible and predicts the outcome. Hepatology, 46, 831-40.

MOOKERJEE RP, TILG H, WILLIAMS R, JALAN R. 2004. Infliximab and alcoholic hepatitis. Hepatology, 40, 499-500.

MOREAU R, JALAN R, GINES P et al. 2013. Acute-on-chronic liver failure is a distinct syndrome that develops in patients with acute decompensation of cirrhosis. Gastroenterology, 144, 1426-37.

MORENCOS FC, DE LAS HERAS CASTAÑO G, MARTÍN RAMOS L et al. 1995. Small bowel bacterial overgrowth in patients with alcoholic cirrhosis. Dig Dis Sci., 40, 1252-6.

MORGAN MH, READ AE AND SPELLER DC.1982. Treatment of hepatic encephalopathy with metronidazole. Gut, 23,1-7.

MORGAN MY, HAWLEY KE, STAMBUK D. 1987. Lactitol versus lactulose in the treatment of chronic hepatic encephalopathy. A double-blind, randomised, cross-over study. J Hepatol., 4, 236-44.

MORRIS MC, GILLIAM EA, LI L. 2015. Innate immune programing by endotoxin and its pathological consequences. Front Immunol., 6, 680.

MUÑOZ L, ALBILLOS A, NIETO M et al. 2005. Mesenteric Th1 polarization and monocyte TNF-alpha production: first steps to systemic inflammation in rats with cirrhosis. Hepatology, 42, 411-19.

NAIR S, COPE K, RISBY TH et al. 2001. Obesity and female gender increase breath ethanol concentration: potential implications for the pathogenesis of nonalcoholic steatohepatitis. Am J Gastroenterol., 96, 1200-4.

NAKAO A, TAKI S, YASUI M et al. 1994. The fate of intravenously injected endotoxin in normal rats and in rats with liver failure. Hepatology. 19, 1251-6.

NAVEAU S, CHOLLET-MARTIN S, DHARANCY S et al. 2004. A double-blind randomized controlled trial of infliximab associated with prednisolone in acute alcoholic hepatitis. Hepatology, 39,1390-1397.

NG SC, HART AL, KAMM MA et al. 2009. Mechanisms of action of probiotics: recent advances. Inflamm Bowel Dis., 15, 300-10.

NISCHALKE HD, BERGER C, ALDENHOFF K et al. 2011. Toll-like receptor (TLR) 2 promoter and intron 2 polymorphisms are associated with increased risk for spontaneous bacterial peritonitis in liver cirrhosis. J.Hepatol., 55, 1010-16.

NIWA T. 2016. The role of carbon adsorbent in the conservative management of chronic kidney disease.. Panminerva Med. [Epub ahead of print]

OGATA Y, NISHI M, NAKAYAMA H et al. 2003. Role of bile in intestinal barrier function and its inhibitory effect on bacterial translocation in obstructive jaundice in rats. J Surg Res., 115, 18-23.

ORLANDI F, FREDDARA U, CANDELARESI MT et al. 1981. Comparison between neomycin and lactulose in 173 patients with hepatic encephalopathy: a randomized clinical study. Dig Dis Sci., 26, 498-506.

PALAZZO M, BALSARI A, ROSSINI A et al. 2007. Activation of enteroendocrine cells via TLRs induces hormone, chemokine, and defensin secretion. J Immunol., 178, 4296-303.

PARKS RW, STUART CAMERON CH, GANNON CD et al. 2000. Changes in gastrointestinal morphology associated with obstructive jaundice. J.Pathol., 192, 526-32.

PEREG D, KOTLIROFF A, GADOTH N et al. 2011. Probiotics for patients with compensated liver cirrhosis: a double-blind placebo-controlled study. Nutrition, 27, 177-81.

PETER J, FREY O, STALLMACH A et al. 2013. Attenuated antigen-specific T cell responses in cirrhosis are accompanied by elevated serum interleukin-10 levels and down-regulation of HLA-DR on monocytes. BMC Gastroenterol., 13, 37.

PIJLS KE, KOEK GH, ELAMIN EE et al. 2014. Large intestine permeability is increased in patients with compensated liver cirrhosis. Am J Physiol Gastrointest Liver Physiol. 306, G147-53.

QI ZX, YU SX, HAO HS et al. 2011. The analysis of IL-10 and its methylation in the patients with acute on chronic liver failure. Zhonghua Shi Yan He Lin Chuang Bing Du Xue Za Zhi., 25, 99-101.

QIN N, YANG F, LI A et al. 2014. Alterations of the human gut microbiome in liver cirrhosis. Nature, 513, 59-64.

RABILLER A, NUNES H, LEBREC D et al. 2002. Prevention of gram-negative translocation reduces the severity of hepatopulmonary syndrome. Am J Respir Crit Care Med., 166, 514-7.

RABOT S, MEMBREZ M, BRUNEAU A et al. 2010. Germ-free C57BL/6J mice are resistant to high-fat-diet-induced insulin resistance and have altered cholesterol metabolism. FASEB J., 24, 4948-59.

RESCIGNO M, ROTTA G, VALZASINA B et al. 2001. Dendritic cells shuttle microbes across gut epithelial monolayers. Immunobiology, 204, 572-81.

RIDLON JM, ALVES JM, HYLEMON PB et al. 2013. Cirrhosis, bile acids and gut microbiota. Unraveling a complex relationship. Gut Microbes, 4, 382–387.

RIDLON JM, KANG DJ, HYLEMON PB, BAJAJ JS. 2014. Bile acids and the gut microbiome. Curr Opin Gastroenterol., 30, 332-8.

RIORDAN SM AND WILLIAMS R. 2006. The intestinal flora and bacterial infection in cirrhosis. J Hepatol., 45, 744-57.

RIORDAN SM AND WILLIAMS R. 2010. Gut flora and hepatic encephalopathy in patients with cirrhosis. N Engl J Med., 362, 1140-42.

RIORDAN SM, SKINNER N, NAGREE A et al. 2003. Peripheral blood mononuclear cell expression of toll-like receptors and relation to cytokine levels in cirrhosis. Hepatology, 37, 1154-64.

RIVERA CA, ADEGBOYEGA P, VAN ROOIJEN N et al. 2007. Toll-like receptor-4 signaling and Kupffer cells play pivotal roles in the pathogenesis of non-alcoholic steatohepatitis. J Hepatol., 47, 571-9.

RUAN Z, LIU S, ZHOU Y et al. 2014. Chlorogenic acid decreases intestinal permeability and increases expression of intestinal tight junction proteins in weaned rats challenged with LPS. PLoS One, 9, e97815.

SABATÉ JM, JOUËT P, HARNOIS F et al. 2008. High prevalence of small intestinal bacterial overgrowth in patients with morbid obesity: a contributor to severe hepatic steatosis. Obes Surg., 18, 371-7.

SAJI S, KUMAR S AND THOMAS V. 2011. A randomized double blind placebo controlled trial of probiotics in minimal hepatic encephalopathy. Trop Gastroenterol., 32, 128-32.

SALASPURO M. 1996. Bacteriocolonic pathway for ethanol oxidation: characteristics and implications. Ann Med, 28,195-200.

SANDEMAN SR, HOWELL CA, MIKHALOVSKY SV et al. 2008. Inflammatory cytokine removal by an activated carbon device in a flowing system. Biomaterials, 29, 1638-44.

SAYIN SI, WAHLSTRÖM A, FELIN J et al. 2013. Gut microbiota regulates bile acid metabolism by reducing the levels of tauro-beta-muricholic acid, a naturally occurring FXR antagonist. Cell Metab., 17, 225-35.

SCARPELLINI E, VALENZA V, GABRIELLI M et al. 2010. Intestinal permeability in cirrhotic patients with and without spontaneous bacterial peritonitis: is the ring closed? Am J Gastroenterol., 105, 323-7.

SCHIMPL G, PESENDORFER P, STEINWENDER G et al. 1996. Allopurinol and glutamine attenuate bacterial translocation in chronic portal hypertensive and common bile duct ligated growing rats. Gut, 39, 48-53.

SCHIMPL G, PESENDORFER P, STEINWENDER G et al. 1996. Allopurinol reduces bacterial translocation, intestinal mucosal lipid peroxidation, and neutrophil-derived myeloperoxidase activity in chronic portal hypertensive and common bile duct-ligated growing rats. Pediatr.Res., 40, 422-28.

SEKI E, DE MINICIS S, OSTERREICHER CH et al. 2007. TLR4 enhances TGF-beta signaling and hepatic fibrosis. Nat Med., 13, 1324-32.

SEMBA RD. 1994. Vitamin A, immunity, and infection. Clin Infect Dis., 19, 489-99.

SENZOLO M, CHOLONGITAS E, BURRA P et al. 2009. Beta-Blockers protect against spontaneous bacterial peritonitis in cirrhotic patients: a meta-analysis. Liver Int., 29, 1189-93.

SENZOLO M, FRIES W, BUDA A et al. 2009. Oral propranolol decreases intestinal permeability in patients with cirrhosis: another protective mechanism against bleeding? Am J Gastroenterol., 104, 3115-16.

SERINO M, LUCHE E, GRES S et al. 2012. Metabolic adaptation to a high-fat diet is associated with a change in the gut microbiota. Gut, 61, 543-53.

SHAH N, DHAR D, EL ZAHRAA MOHAMMED F et al. 2012. Prevention of acute kidney injury in a rodent model of cirrhosis following selective gut decontamination is associated with reduced renal TLR4 expression. J Hepatol., 56:1047-53

SHANAB AA, SCULLY P, CROSBIE O et al. 2011. Small intestinal bacterial overgrowth in nonalcoholic steatohepatitis: association with toll-like receptor 4 expression and plasma levels of interleukin 8. Dig Dis Sci., 56, 1524-34.

SHARMA BC, SHARMA P, LUNIA MK. 2013. A randomized, double-blind, controlled trial comparing rifaximin plus lactulose with lactulose alone in treatment of overt hepatic encephalopathy. Am J Gastroenterol., 108, 1458-63.

SHAWCROSS DL, DAVIES NA, WILLIAMS R et al. 2004. Systemic inflammatory response exacerbates the neuropsychological effects of induced hyperammonemia in cirrhosis. J.Hepatol., 40, 247-54.

SHAWCROSS, DL, SHABBIR SS, TAYLOR NJ et al. 2010. Ammonia and the neutrophil in the pathogenesis of hepatic encephalopathy in cirrhosis. Hepatology, 51: 1062-69.

SORIANO G, GUARNER C, TOMÁS A et al. 1992. Norfloxacin prevents bacterial infection in cirrhotics with gastrointestinal hemorrhage. Gastroenterology, 103, 1267-72.

SPAHR L, RUBBIA-BRANDT L, FROSSARD JL *et al*. 2002. Combination of steroids with infliximab or placebo in severe alcoholic hepatitis: a randomized controlled pilot study. J Hepatol,.37,448-455.

STADLBAUER V, MOOKERJEE RP, WRIGHT GA et al. 2009. Role of Toll-like receptors 2, 4, and 9 in mediating neutrophil dysfunction in alcoholic hepatitis. Am J Physiol Gastrointest Liver Physiol., 296, G15-G22.

STENMAN LK, HOLMA R, EGGERT A et al. 2013. A novel mechanism for gut barrier dysfunction by dietary fat: epithelial disruption by hydrophobic bile acids. Am J Physiol Gastrointest Liver Physiol., 304, G227- 34.

STEPHENSEN CB, MOLDOVEANU Z, GANGOPADHYAY NN. 1996. Vitamin A deficiency diminishes the salivary immunoglobulin A response and enhances the serum immunoglobulin G response to influenza A virus infection in BALB/c mice. J Nutr., 126, 94-102.

SZTRYMF B, LIBERT JM, MOUGEOT C et al. 2005. Cirrhotic rats with bacterial translocation have higher incidence and severity of hepatopulmonary syndrome. J Gastroenterol Hepatol.,20, 1538-44.

TANG Y, FORSYTH CB, FARHADI A et al. 2009. Nitric oxide-mediated intestinal injury is required for alcohol-induced gut leakiness and liver damage. Alcohol Clin.Exp.Res., 33, 1220-30.

TANOUE S, CHANG LY, LI Y, KAPLAN DE. 2015. Monocyte-derived dendritic cells from cirrhotic patients retain similar capacity for maturation/activation and antigen presentation as those from healthy subjects. Cell Immunol., 295, 36-45.

TERG R, CASCIATO P, GARBE C et al. 2015. Proton pump inhibitor therapy does not increase the incidence of spontaneous bacterial peritonitis in cirrhosis: A multicenter prospective study. J Hepatol., 62, 1056–1060.

TESTRO AG, VISVANATHAN K. 2009. Toll-like receptors and their role in gastrointestinal disease. J Gastroenterol Hepatol., 249, 43-54.

THABUT D, MASSARD J, GANGLOFF A et al. 2007. Model for end-stage liver disease score and systemic inflammatory response are major prognostic factors in patients with cirrhosis and acute functional renal failure. Hepatology, 46, 1872-82.

THALHEIMER U, TRIANTOS CK, SAMONAKIS DN et al. 2005. Infection, coagulation, and variceal bleeding in cirrhosis. Gut, 54, 556-63.

THUIJLS G, DERIKX JP, DE HAAN JJ et al. 2010. Urine-based detection of intestinal tight junction loss. J Clin Gastroenterol., 44, e14-9.

TILG, H. 2010. Obesity, metabolic syndrome, and microbiota: multiple interactions. J Clin Gastroenterol., 44, S16-S18.

TISO M, SCHECHTER AN. 2015. Nitrate Reduction to Nitrite, Nitric Oxide and Ammonia by Gut Bacteria under Physiological Conditions. PLoS One, 10, e0119712.

TRITTO G, BECHLIS Z, STADLBAUER V et al. 2011. Evidence of neutrophil functional defect despite inflammation in stable cirrhosis. J Hepatol., 55, 574-81.

TUOMISTO S, PESSI T, COLLIN P et al. 2014. Changes in gut bacterial populations and their translocation into liver and ascites in alcoholic liver cirrhotics. BMC Gastroenterol., 14, 40.

TURNBAUGH PJ, LEY RE, MAHOWALD MA et al. 2006. An obesity-associated gut microbiome with increased capacity for energy harvest. Nature, 444, 1027-31.

UKLEJA A, SCOLAPIO JS, MCCONNELL JP et al. 2002. Nutritional assessment of serum and hepatic vitamin A levels in patients with cirrhosis. J Parenter Enteral Nutr., 26, 184-8.

ULLUWISHEWA D, ANDERSON RC, MCNABB WC et al. 2011. Regulation of tight junction permeability by intestinal bacteria and dietary components. J Nutr. 141, 769-76.

VELAYUDHAM A, DOLGANIUC A, ELLIS M et al. 2009. VSL#3 probiotic treatment attenuates fibrosis without changes in steatohepatitis in a diet-induced nonalcoholic steatohepatitis model in mice. Hepatology, 49, 989-97.

VLACHOGIANNAKOS J, VIAZIS N, VASIANOPOULOU P et al.2013. Long-term administration of rifaximin improves the prognosis of patients with decompensated alcoholic cirrhosis. J Gastroenterol Hepatol., 28, 450-5.

WASMUTH HE, KUNZ D, YAGMUR E et al. 2005. Patients with acute on chronic liver failure display "sepsis-like" immune paralysis. J Hepatol., 42, 195-201.

WATANABE A, SAKAI T, SATO S et al. 1997. Clinical efficacy of lactulose in cirrhotic patients with and without subclinical hepatic encephalopathy. Hepatology, 26, 1410-4.

WEI X, YAN X, ZOU D et al. 2013. Abnormal fecal microbiota community and functions in patients with hepatitis B liver cirrhosis as revealed by a metagenomic approach. BMC Gastroenterology, 13, 175-82.

WIEDERMANN U, TARKOWSKI A, BREMELL T et al. 1996. Vitamin A deficiency predisposes to Staphylococcus aureus infection. Infect Immun., 64, 209-14.

WILLIAMS R, ASPINALL R, BELLIS M et al. 2014. Addressing liver disease in the UK: a blueprint for attaining excellence in health care and reducing premature

mortality from lifestyle issues of excess consumption of alcohol, obesity, and viral hepatitis. Lancet, 384, 1953-97.

WORLICEK M, KNEBEL K, LINDE HJ et al. 2010. Splanchnic sympathectomy prevents translocation and spreading of E coli but not S aureus in liver cirrhosis. Gut, 59, 1127-34.

WRIGHT G, DAVIES NA, SHAWCROSS DL et al. 2007. Endotoxemia produces coma and brain swelling in bile duct ligated rats. Hepatology, 45: 1517-26.

XING T, LI L, CAO H, HUANG J. 2007. Altered immune function of monocytes in different stages of patients with acute on chronic liver failure. Clin Exp Immunol., 147, 184-8.

XU WH, WU XJ, AND LI JS. 2002. Influence of portal pressure change on intestinal permeability in patients with portal hypertension. Hepatobiliary.Pancreat.Dis.Int.,1, 510-14.

YANG DH, YE ZY, XIE YJ et al. 2012. Effect of salvianolate on intestinal epithelium tight junction protein zonula occludens protein 1 in cirrhotic rats. World J Gastroenterol., 18, 7040-7.

YANG SQ, LIN HZ, LANE MD et al. 1997. Obesity increases sensitivity to endotoxin liver injury: implications for the pathogenesis of steatohepatitis. Proc Natl Acad Sci U S A., 94, 2557-62.

YOUNGSTER I, RUSSELL GH, PINDAR C. 2014. Oral,capsulized, frozen fecal microbiota transplantation for relapsing Clostridium difficile infection. JAMA, 312, 1772-8.

ZENG R, ODERUP C, YUAN R et al. 2013. Retinoic acid regulates the development of a gut-homing precursor for intestinal dendritic cells. Mucosal Immunol., 6, 847-56.

ZHANG C, ZHAO L, MA L et al. 2012. Vitamin D status and expression of vitamin D receptor and LL-37 in patients with spontaneous bacterial peritonitis. Dig Dis Sci., 57,182-8.

ZHANG Z, ZHAI H, GENG J et al. 2013. Large-Scale Survey of Gut Microbiota Associated With MHE Via 16S rRNA-Based Pyrosequencing. Am J Gastroenterol., 108,1601-11.

ZHAO HY, WANG HJ, LU Z et al. 2004. Intestinal microflora in patients with liver cirrhosis. Chin J Dig Dis. 5, 64-67.

ZHU Q, ZOU L, JAGAVELU K et al. 2012. Intestinal decontamination inhibits TLR4 dependent fibronectin-mediated cross-talk between stellate cells and endothelial cells in liver fibrosis in mice. J Hepatol., 56, 893-99.

ZUCKERMAN MJ, MENZIES IS, HO H et al. 2004. Assessment of intestinal permeability and absorption in cirrhotic patients with ascites using combined sugar probes. Dig.Dis.Sci., 49, 621-26.